



UNIVERSITY OF LEEDS

**A Chemical Proteomic Approach to Reveal the
Cellular Targets of Anti-Protozoan Unnatural
Products.**

Jack Stewart White

Submitted in accordance with the requirements the degree of Doctor of Philosophy

The University of Leeds
School of Chemistry
Faculty of Engineering and Physical Sciences

December 2022

The candidate confirms that the work submitted is his own and that appropriate credit has been given where reference has been made to the work of others.

This copy has been supplied on the understanding that it is copyright material and that no quotation from the thesis may be published without proper acknowledgement.

The right of Jack Stewart White to be identified as Author of this work has been asserted by him in accordance with the Copyright, Designs and Patents Act 1988.

© 2022 The University of Leeds and Jack Stewart White.

Acknowledgments

Firstly, I'd like to give a big thank you to Megan and Adam! I couldn't have asked two better supervisors through my PhD; they were both super supportive and encouraging as I've developed through my studies and through the rocky road that was the last four years, I am extremely grateful for all they've done for me. I'd also like to thank Terry and Will up in St. Andrews for their collaboration on this project and will always be sorry for our first in real life encounter! A special shout out to Will for all of his hard work that made my project possible, too our WhatsApp chat filled with science questions (and hopefully some answers), we have done some really great work together.

I Thank all of the members of lab 1.49 and G.56 for all the fun we had, and I guess for some of the science too, from Ryan and Johnny to Jacob and Julian, thank you all. A Particular thanks Sam Griggs and Andrew Gomm, for all of their help working on this project together, for all the advice and troubleshooting chats, helping me to navigate the treacherous road that is chemistry. A thank you to Emily Faulkner and Hannah Askey for their help with the substate scope and design of the photoredox library. Also, a thank you to the master's students I worked with over the years, to Callum, Sanya, and Alfie, for helping to piece together some of this story. My final special shoutout is to Jeanine Williams, for all of her help over the years with the HPLC and MS, for helping me isolate so many compounds for the library, but more importantly for the chats around the machines to brighten up a dark day of purifications!

To the friends we made along the way, thank you Laia and Kristian, for the cinema trips and the four-pint limit. I am very grateful to call you both my friends, Laia you are truly a ray of sunshine in my life, and Kristian I will always well up when you tell literally any story. Also, to the whole team, Alexandra, Pablo, and Tam for all of our Leeds adventures, and those still to come! Thank you to Jaime for all the coffees, all the stories and all the science complaints she's had to listen to. To my pals for keeping me sane, Kiran, Tonicha, Aisha, Faye, Callum. To Alicia for her friendship and support those few months you spent in Leeds were some of my favourite Leeds memories. To Sophie, my bestie, for all the calls, the constant ongoing Messenger conversation, all the vines, and eating well for less.

A final thanks to my family for always being there for me, to mum, dad, and Amanda for their complete support and to Stu for the family we gain along the way. To Nana and Grandad, remembering those we lost, love you all.

Abstract

Electrophilic inhibitors have, until recently, been underutilised in drug design. But there has been a growing recognition for their utility as powerful tools for exploring biological mechanisms. The irreversible covalent interactions formed make identifying targets of compounds in cells more straight-forward than for non-covalent inhibitors, as chemical proteomics approaches can be utilised to isolate and identify interacting proteins. This is particularly attractive for phenotypic screening approaches, where the mode of action and protein targets are unknown.

Generation of these electrophilic screening libraries typically uses a limited synthetic toolkit, resulting in libraries with poor diversity that do not efficiently explore biologically relevant chemical space. Therefore, we aimed to develop a workflow that moves from the creation of a library of electrophilic compounds through to inhibitor discovery and profiling biological mechanisms in cells using chemical proteomics. Building a structurally diverse compound library using an iridium catalysed dehydrogenative coupling based around sulfonyl fluoride warheads, to exploit their reactivity and stability under physiological conditions, and their reactive promiscuity to several protein amino acid side chains, aiming to reveal novel protein targets not accessible to traditional synthetic design.

Working in collaboration with the Smith group at the University of St. Andrews, the sulfonyl fluoride-based library was then screened in phenotypic assays against the human African trypanosomiasis parasite *T. brucei*, obtaining several active compounds with sub-micromolar potency with significant selectivity over human HeLa cells. We then designed chemical probes, analogous compounds containing an alkyne tag to directly explore the protein targets and mode of action of the active compounds using chemical proteomics methods. Initial work was undertaken to visualise these protein-probe interactions by SDS-PAGE from in-gel fluorescence. From here, future work should focus on the identification of these reactive proteins by mass spectrometry.

Table of Contents

Acknowledgments	iii
Abstract	iv
List of Figures	viii
List of Tables	x
List of Abbreviations	xi
1. Introduction	1
1.1. Trypanosoma Kinetoplastid Parasites	1
1.1.1. Introduction to Trypanosoma kinetoplastids.....	1
1.1.2. Phenotypic vs. Target-Based Screening of Trypanosoma Kinetoplasts	6
1.2. Exploring Diversity Generating Synthetic Strategies	8
1.2.1. The Medicinal Chemistry Toolkit.....	8
1.2.2. Introduction to Photoredox-Mediated Dehydrogenative Couplings	9
1.3. Covalent Inhibitor Discovery	15
1.3.1. An Introduction to Covalent Inhibitors	15
1.3.2. Reactive Electrophilic Warheads	18
1.4. Chemical Proteomics	25
1.4.1. Chemical Probes	25
1.4.2. Mass Spectrometry in Chemical Proteomics	32
1.4.3. Functionalising Trypanocidal Compounds for Target Identification	33
1.5. Project Outline	36
1.5.1. Design and Synthesis of a Library of Covalent Inhibitors.....	36
1.5.2. Phenotypic Discovery of Anti-trypanosomal Activity.....	37
1.5.3. Synthesis of Functionalised Electrophilic Probes	37
2. Design and Synthesis of a Diverse Library of Electrophilic Ligands	39
2.1. Generating a Library of Electrophilic Ligands	39
2.1.1. Selection and Synthesis of Functionalised Hetarenes.....	39
2.1.2. Identification of Viable Hetarene Substrates	40
2.1.3. Identification of Viable Hetarene and Hydrogen Donor Combinations	45
2.2. Compound Screening Against Trypanosome Kinetoplasts.....	52
2.2.1. Initial Identification of Active Compounds	52

2.2.2.	Validation of Potential Hit Compounds	54
2.2.3.	Potential α -Nitrile Electrophiles, a Second Covalent Warhead.....	57
2.3.	Conclusion of Covalent Library Generation	58
3.	Chemical Proteomics for Anti-Trypanosomal Target Identification	61
3.1.	Profiling the Reactivity of the Electrophilic Ligand Library	61
3.1.1.	Synthesis of Broad-Spectrum Sulfonyl Fluoride probes.....	61
3.1.2.	Competitive Profiling Against Sulfonyl Fluoride Probes	67
3.1.3.	Competitive Profiling Against a Fluorophosphonate Probe	69
3.2.	Competitive Identification of Protein Targets.....	74
3.2.1.	Serine Hydrolases as Potential Anti-Trypanosomal Targets	74
3.2.2.	Competitive Profiling of α -Nitrile Protein Targets.....	78
3.3.	Identification of Reactive Protein Targets with Chemical Probes	80
3.3.1.	Generation of Anti-Trypanosomal Electrophilic Probes.....	80
3.3.2.	Validation of Chemical Probe's Anti-Trypanosomal Activity	85
3.3.3.	Visualisation of Anti-Trypanosomal Protein Targets	87
3.4.	Conclusion of A Chemical Proteomics Investigation into Protein Targets	92
4.	Conclusions and Future Work.....	94
4.1.	Generation of an Electrophile Library	94
4.2.	Phenotypic Screening for Anti-Trypanosomal Activity	95
4.3.	Synthesis of Electrophilic Probes	95
4.4.	Identifying α -Nitriles as A Second Reactive Warhead.....	96
4.4.1.	Identifying Protein Targets Using Chemical Proteomics.....	97
5.	Experimental Procedures	99
5.1.	General Information	99
5.2.	General Procedures for Chemical Synthesis	101
5.2.1.	Synthesis of Sulfonyl Fluoride Hetarenes.....	101
5.2.2.	Synthesis of Photoredox Mediated Dehydrogenative Coupling Array	101
5.3.	General Procedures for Cell Culture	103
5.3.1.	General Procedure for HeLa Cell Culture.....	103
5.3.2.	General Procedure for <i>Trypanosoma brucei</i> Cell Culture	104
5.4.	General Procedures for Gel-Based Imaging	106
5.4.1.	Buffer Preparation.....	106

5.4.2. Protein Labelling with Alkyne Containing Probes	106
5.4.3. Competitive Profiling of Electrophilic Compounds	107
5.4.4. Visualisation of Probe Labelling.....	107
Click Reaction:.....	107
Protein Precipitation:.....	108
Preparation of SDS-PAGE gels:	108
Running SDS-PAGE Gels and Imaging:	108
5.5. Experimental Details of Isolated Compounds.....	109
References	179
Appendices	190

List of Figures

Figure 1.1: Morphology of trypanosoma kinetoplastid parasites.....	1
Figure 1.2: Life cycle of trypanosoma Kinetoplastid parasites.....	2
Figure 1.3: Alternative treatments of <i>T. brucei gambiense</i>	5
Figure 1.4: Illustrative example of an electrophilic fragment library	8
Figure 1.5: An example of a dehydrogenative coupling reaction	9
Figure 1.6: Dehydrogenative photo-coupling reaction cycle	10
Figure 1.7: Scope of compatible dehydrogenative coupling substrates	12
Figure 1.8: Isolated compounds from a dehydrogenative coupling array.....	13
Figure 1.9: EC ₅₀ values of active compounds against <i>T. brucei brucei</i>	14
Figure 1.10: A schematic representation of covalent drug inhibition	15
Figure 1.11: Covalent inhibition ornithine decarboxylase for treating gHAT.....	17
Figure 1.12: The anti-trypanosomal compound PMSF, an alkyl sulfonyl fluoride	22
Figure 1.13: The reactivity of sulfonyl fluorides with amino acid side chains.....	23
Figure 1.14: α -Nitriles as reversible electrophilic warheads	24
Figure 1.15: The key components of a chemical probe	25
Figure 1.16: Photoreactive groups used to label proteins	27
Figure 1.17: Workflow of chemical proteomics	28
Figure 1.18: Bioorthogonal click reactions used in chemical proteomics	30
Figure 1.19: Reaction cycle of the copper catalysed click reaction	31
Figure 1.20: A bottom-up workflow of LC-MS/MS.....	32
Figure 1.21: Exploring the mode of action of potent <i>T. brucei</i> inhibitors	34
Figure 1.22: Schematic representation of the photo-redox reaction	36
Figure 1.23: Schematic representation of the resazurin-based viability assay.....	37
Figure 1.24: An illustrative example of chemical probe design	38
Figure 2.1: Reaction conditions to synthesise sulfonyl fluorides	39
Figure 2.2: Screening to identify hetarenes compatible with photoredox chemistry.....	40
Figure 2.3: Variability in fluorine shift in the ¹⁹ F NMR.....	42
Figure 2.4: Isolated compounds from the test screen of hetaryl sulfonyl fluorides	43
Figure 2.5: The Substrates used for the synthesis of the electrophilic library	45
Figure 2.6: Preparation of the hydrogen donor substrates	46
Figure 2.7: The synthesised covalent library of 40 compounds.....	51
Figure 2.8: EC ₅₀ values of the hetarene cores screened against <i>T. brucei brucei</i>	52

Figure 2.9: Initial screening data of the compound library against <i>T. brucei brucei</i>	53
Figure 2.10: Comparing the toxicity of 3-1 against <i>T. brucei</i> and HeLa cells.....	54
Figure 2.11: Full screening data of the 12 active compounds.....	55
Figure 2.12: Plotting molecular properties of the compound library	56
Figure 2.13: Exploring the importance of α -nitriles for anti-trypanosomal activity	58
Figure 2.14: The five active compounds identified in the library screening	60
Figure 3.1: Synthesis of broad-spectrum sulfonyl fluoride reactive probes	63
Figure 3.2: Comparative gel of broad-spectrum sulfonyl fluoride probes.....	65
Figure 3.3: Illustrative example of competitive reactivity profiling	67
Figure 3.4: Competitive labelling of the broad-spectrum sulfonyl fluoride probes.....	68
Figure 3.5: Competitive profiling against a serine selective fluorophosphate.....	70
Figure 3.6: Competitive profiling of the reactive library against FP-RH	72
Figure 3.7: Competitive profiling of the 12 active compounds against FP-RH.....	75
Figure 3.8: Competitive profiling of the compound 3-1 in dilution against FP-RH.....	76
Figure 3.9: Comparison of the 3-1 competitive profile against inactive analogues.....	77
Figure 3.10: Competitive profiling of α -nitriles to identify amino acid selectivity.....	79
Figure 3.11: Potential alkyne containing analogues of hits compounds	81
Figure 3.12: Preparation of hydrogen donor analogues containing alkynes	82
Figure 3.13: Alternative route to synthesising sulfonyl fluoride probe analogues	84
Figure 3.14: Synthesis of α -nitrile probes.....	85
Figure 3.15: Comparing the activities of alkyne analogues and parent compounds ...	86
Figure 3.16: Labelling profile of the sulfonyl fluoride probe, 3-1 Alkyne	88
Figure 3.17: Assessing the stability of α -nitrile-protein adducts in-gel.....	89
Figure 3.18: Labelling profile of the three α -nitrile based probes.....	90

List of Tables

<i>Table 1.1:</i> Diseases caused by Trypanosomal parasites	3
<i>Table 1.2:</i> Current drug treatments for African Sleeping Sickness	4
<i>Table 1.3:</i> Optimisation of the dehydrogenative photocoupling reaction	11
<i>Table 1.4:</i> Common commercially available covalent drugs.....	16
<i>Table 1.5:</i> Examples of electrophilic covalent warheads.....	19
<i>Table 2.1:</i> Screening of compatible electrophilic warhead-containing hetarenes	44
<i>Table 2.2:</i> Summary of analysis and purifications of the compound library	48
<i>Table 2.3:</i> Summary of hydrogen donor reactivity for building the compound library.	50

List of Abbreviations

AEBSF	4-(2-Aminoethyl)benzenesulfonyl fluoride
Boc	<i>tert</i> -Butyloxycarbonyl
CLogP	Calculated Partition Coefficient
CuAAc	Copper(I)-catalysed azide alkyne cycloaddition
DCM	Dichloromethane
DIC	N,N'-Di-isopropyl carbodiimide
DIPEA	Di-isopropyl amine
DMAP	4-Dimethylaminopyridine
DMF	Dimethyl Formamide
DMSO	Dimethyl Sulfoxide
DNA	Deoxyribonucleic Acid
EC50	Half Maximal Effective Concentration
ESI	Electron Spray Ionisation
EWG	Electron Withdrawing Group
flu	Fluorescein
FP	Fluorophosphonate
gHAT	<i>Trypanosoma brucei gambiense</i> , West African Sleeping Sickness
HA	Heteroarene
HD	Hydrogen Donor
HPLC	High Performance Liquid Chromatography
IA	Iodoacetamide
IC50	Half Maximal Inhibitory Concentration
L.	<i>Leishmania</i>
LC	Liquid Chromatography
m/z	Mass/Charge Ratio
Mal	Maleimide
MeOH	Methanol
MHz	Mega Hertz
MS	Mass Spectrometry
MS/MS	Tandem Mass Spectrometry
NMR	Nuclear Magnetic Resonance
PAGE	Polyacrylamide Gel Electrophoresis

PBD	Protein Data Bank
PBS	Phosphate Buffered Saline
PEC50	Negative Log of EC50
PEG	Polyethylene Glycol
PMSF	Phenyl Methyl Sulfonyl Fluoride
Poc	Propargyloxycarbonyl
ppm	Parts Per Million
RH	Rhodamine
rHAT	<i>Trypanosoma brucei rhodesiensis</i> , East African Sleeping Sickness
SAR	Structure Activity Relationship
SDS	Sodium Dodecyl Sulfate
SF	Sulfonyl Fluoride
SLB	Sample Loading Buffer
S_N(AR)	Nucleophilic Aromatic Substitution
SUFEX	Sulfonyl Fluoride Exchange
T.	<i>Trypanosoma</i>
TBTA	Tris(benzyltriazolylmethyl)amine
TCEP	Tris(2-carboxyethyl)phosphine
TFA	Trifluoroacetic acid
TG	Targeting Group
UV	Ultraviolet
WHO	World Health Organisation

1. Introduction

1.1. Trypanosoma Kinetoplastid Parasites

Parasites are organisms which live on or in a host to gain food and nutrients at their expense. Parasites can cause or transmit many diseases to host organisms; including animals, humans and plants¹. This project focuses on trypanosoma kinetoplastids, a subset of protozoan parasites, mastigophora.

1.1.1. Introduction to Trypanosoma kinetoplastids

Trypanosoma Kinetoplastids are characterised by their single flagellum, used to propel the organism, as well as their kinetoplasts, a network of DNA, arranged in an irregular, circular disk like structure^{2,3}. The trypanosomes are able to change morphology during their life cycle (*Figure 1.1*), allowing for cell division and transportation, enabling the parasite to infect a host organism⁴.

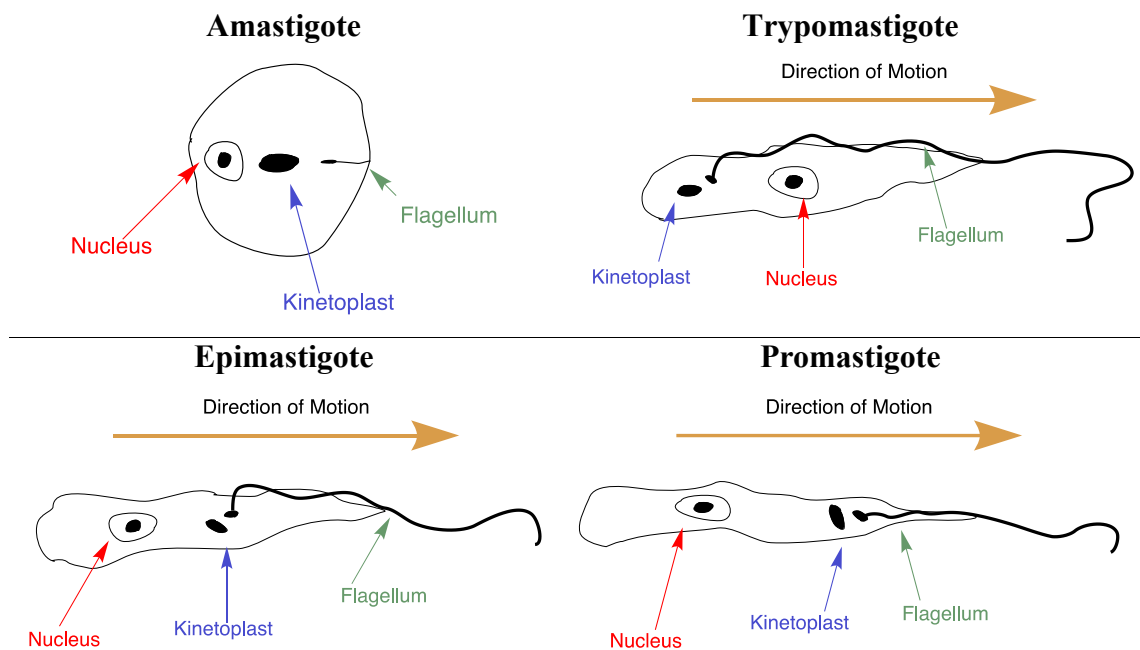


Figure 1.1: Morphology of trypanosoma kinetoplastid parasites. Their morphological changes enable infection of a host. Figure adapted from sources ⁴ and ⁵.

Trypanosomes can infect humans and other animals through insect bites. The specific carrier of the disease is dependent on the parasite species and its geographical location. For example, African Sleeping Sickness is transmitted by tsetse flies, found throughout central Africa⁶, while Chagas disease is spread by ‘kissing bugs’ typically located in South America⁷.

Figure 1.2 shows the typical life cycle of trypanosoma parasites and how they are spread. The parasites are found in the saliva of infected insects and are injected into the blood of mammals when the insect takes a blood meal (1). The trypomastigote parasites penetrate blood cells and differentiate as amastigotes via binary fission (2,3). Once the parasite has multiplied within the cell, it ruptures, allowing metacyclic trypomastigotes to spread, infecting other cells (4). The parasite can spread if the host is bitten by another insect (5) which ingests the parasites where they multiply in the gut as epimastigotes (6) before transporting through mucosal membranes back into the insects' saliva (7) to infect another host on its next meal^{8,9}.

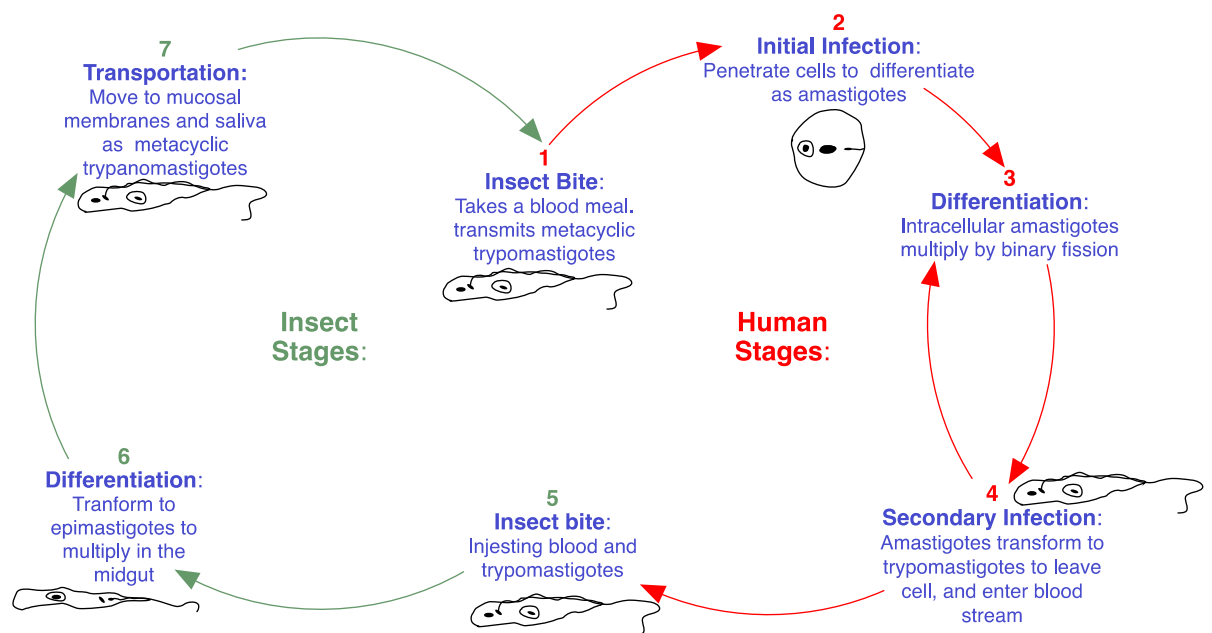


Figure 1.2: Life cycle of trypanosoma Kinetoplastid parasites, highlighting the infection and transmission from insect to human. Figure adapted from source ⁹.

The trypanosomes include two main species, trypanosoma and leishmania, both of which cause a range of diseases affecting humans and other mammals (**Table 1.1**). Of the diseases caused by trypanosoma parasites, three are found on the CDC's list of Neglected tropical Diseases; African Sleeping Sickness, Chagas Disease and Leishmaniasis. These diseases affect hundreds of millions of people but are generally not typically addressed by pharmaceutical companies¹⁰.

Table 1.1: Diseases caused by Trypanosomal parasites, divided by the sub-sets of trypanosoma and leishmania. Highlighting the three neglected tropical diseases affecting humans (Blue)^{11,12}.

Trypanosoma

Species	Disease	Host	Region	
<i>T. brucei</i>	<i>brucei</i>	Nagana	Cattle, Horses, Game	Africa
	<i>rhodesiensis</i>	East African Sleeping sickness (Severe)	Humans, Pigs, Game	East Africa
	<i>gambiensis</i>	West African Sleeping Sickness (Mild)	Humans, Game	West/ Central Africa
	<i>evansi</i>	Surra	Horses, Camels, Buffaloes	South/ Central America, Asia, Europe, Africa
	<i>equiperdum</i>	Dourine	Horses, Donkeys, Camels	South/ Central America, Asia, Europe, Africa
<i>T. cruzi</i>		Chagas'	Humans, Wild Animals	South/ Central America
<i>T. cogolense</i>		Trypanosomiasis	Horses, Donkeys Camels.	Africa

Leishmania

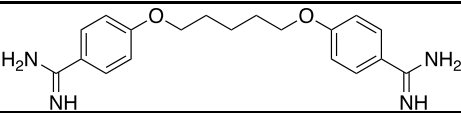
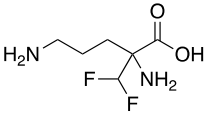
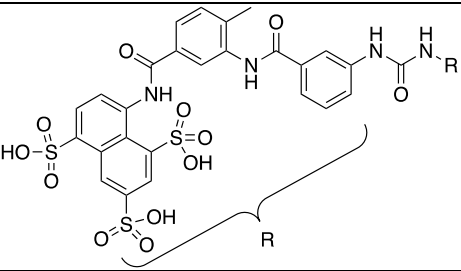
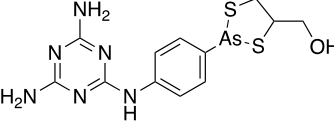
Species	Disease	Host	Region
<i>L. braziliensis</i>	Mucocutaneous Leishmaniasis	Humans, Rodents	South America
<i>L. mexicana</i>	Visceral Leishmaniasis	Humans, Rodents	Central America
<i>L. donovani</i>	Sleeping Sickness (mild)	Humans, Dogs	Africa, Asia, Europe
<i>L. major</i>	Cutaneous Leishmaniasis (Wet)	Humans, Rodents	Africa, Asia
<i>L. tropica</i>	Cutaneous Leishmaniasis (Dry)	Humans, Hyrax	Africa, Asia Europe
<i>L. infantum</i>	Visceral Leishmaniasis	Humans, Dogs	Africa, Europe, South America
<i>Phytomonas</i>	Hartrodt Disease	Coconut, Oil palms	Central/ South America

African Sleeping Sickness, or Human African Trypanosomiasis (HAT), is caused by the *T. brucei* subspecies. Specifically, two parasites cause the disease; *T. brucei rhodesiensis*, which causes East African Sleeping Sickness (*r*HAT), the less common, but more severe form, and *T. brucei gambiensis*, causing West African Sleeping Sickness (*g*HAT)⁹. In its early stages, the *gambiensis* parasite causes fevers, rashes, swelling of the lymph nodes and joints and an enlargement of the liver. As the disease progresses, the parasite infects the central nervous system as the parasite is able to penetrate the blood-brain barrier,

causing physical and mental deterioration, comas and eventually death⁹. Both forms of the disease are transmitted by the tsetse fly bite and exhibit the same symptoms but differ in the rate of infection. The infection of *r*HAT is more rapid and patients often die before exhibiting inflammation in the brain⁸. This often causes a misdiagnosis of the disease.

Over 60 million people live within the tsetse fly habitat, so are at risk of infection. In 1995, it was estimated that 300,000 people were infected with HAT, but less than 30,000 of these cases were actually treated as a result of limited access to health care. In 2014, the number of estimated cases dropped to 15,000 with 3,796 reported cases¹⁰ thanks to increased support to rural communities by WHO⁶. Previously, there were four main treatments for African Sleeping Sickness, depending on the type of infection and severity (**Table 1.2**). Although they appear to treat the disease successfully, they have many adverse effects associated with them, highlighting the need for safer alternatives.

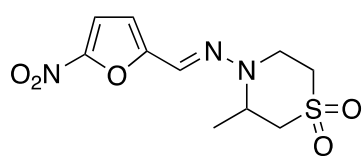
Table 1.2: Current drug treatments for African Sleeping Sickness¹³.

Drug	Structure	Treatment	Adverse Effects
Pentamidine ¹⁴		<i>T. brucei gambiensis</i> (Early stage)	Hypoglycaemia, diarrhoea, nausea
Eflornithine ⁹		<i>T. brucei gambiensis</i> (Late stage)	Bone marrow suppression, gastrointestinal issues.
Suramin ⁸		<i>T. brucei rhodesiensis</i> (Early stage)	Rash, nephrotoxicity, peripheral neuropathy, hypersensitivity (rare)
Melarsoprol ¹⁴		<i>T. brucei rhodesiensis</i> (Late stage)	Brain damage (5-10% risk) which is fatal in 50% cases

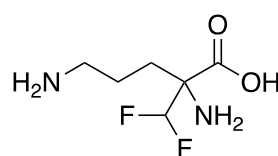
In 2009, a Nifurtimox-Eflornithine Combination Therapy (NECT) was shown to successfully treat last stage *T. brucei gambiensis* (**Figure 1.3a**). Treatment requires 10 days of oral Nifurtimox to be taken, followed by 7 days of intravenous eflornithine. NECT had a much higher efficacy and selectivity than an eflornithine monotreatment, with a cure rate of around 97%¹⁵. It also reduces the number of intravenous treatments from 56

to 14¹⁶. As of 2018, fexinidazole is the first orally bioavailable drug for treating West African Sleeping sickness (**Figure 1.3b**)¹⁷ and is the first new drug approved for treating HAT in nearly 40 years¹⁸. Originally identified as a broad spectrum anti-microbial, fexinidazole was found to be active against HAT from a screening library of existing anti-microbials against a range of parasitic targets¹⁸. Further testing showed no toxicity or genotoxicity¹⁹ and had an activity, comparable with the NECT treatment²⁰. Fexinidazole is converted *in vivo* into two active metabolites, a sulfone, and a sulfoxide (**Figure 1.3c**), both are shown to be equally as active as the parent molecule and also show increased permeability of the blood-brain barrier *in vivo* models²¹. As of 2021, there were 805 reported cases of HAT, with only 55 *r*HAT, showing a significant reduction, resulting from advances in treatment and increased access to reliable healthcare for patients²².

a)

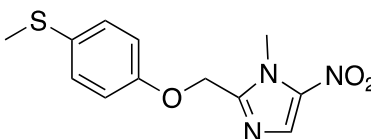


Nifurtimox: EC₅₀ = 2.4 μM



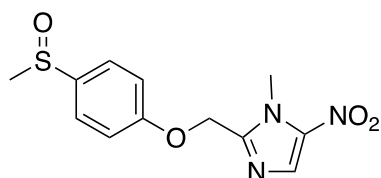
Eflornithine: EC₅₀ = 16.4 μM

b)

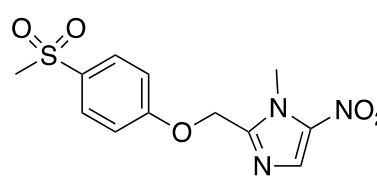


Fexinidazole: EC₅₀ = 1.0 μM

c)



Fexinidazole Sulfone: EC₅₀ = 0.6 μM



Fexinidazole sulfoxide: EC₅₀ = 1.4 μM

Figure 1.3: Alternative treatments of *T. brucei gambiensis*, including a combination therapy, NECT, of nifurtimox and eflornithine (a) with increased efficacy compared to the monotherapies shown¹⁶, as well as the first orally bioavailability treatment fexinidazole (b) along with the active metabolites (c) highlighting their potency *in vivo* mouse models¹⁵.

1.1.2. Phenotypic vs. Target-Based Screening of Trypanosoma Kinetoplasts

There are many examples of both phenotypic^{23,24} and target-based screening^{25,26} approaches being used to develop novel inhibitors of trypanosomes²⁷. Target-based screening aims to disrupt a specific protein function that is essential to the parasite to have a therapeutic effect. The protein target is initially identified from genomic data and the isolated, recombinant protein can be assayed using high-throughput screening to rapidly find active compounds for this interaction. Limitations of this method are caused by reproducibility of results *in vivo*. For an initially potent inhibitor to be taken forward as a lead compound, the compound must also have high selectivity to the parasite without affecting the host. The inhibitor must additionally be cell permeable and remain stable to the metabolism of the host and parasite cells^{28,29}. This information cannot be gained from the *in vitro* assay on the target protein, so secondary studies are needed to validate the compound as a potential lead compound for further optimisation³⁰.

In comparison, phenotypic screening allows for a full cell analysis of potential inhibitors, identifying active compounds that meet drug-like requirements such as being cell permeable and metabolically stable. These screens often results in a low hit rate, as the compounds need to exhibit all of these properties to produce a phenotypic effect^{31,32}. Phenotypic screening can be used to discover new druggable protein targets, by using a structurally diverse compound libraries that better explore 3D chemical space, identifying novel reactive scaffolds with drug-like properties. This also reduces the hit rate as the library would need to be target agnostic and not influenced by existing inhibitors³³. A hit identified from an *in vitro* phenotypic screen will require further testing to investigate the compounds selectivity and broad-spectrum toxicity profiles against other cell lines to build a picture of the compounds efficacy as a potential drug candidate³¹. Optimisation of these active compounds requires the target site to be identified to aid design³⁴. This can be achieved with chemical proteomics by functionalising the compound to pull-out the protein targets of interest³⁵, or by functionalising the inhibitors to form reactive chemical probes³⁶.

In parasite-based phenotypic screens, the main limitation arises from the changing morphology of parasites during their life cycle^{28,29}. Inhibitors may not maintain their activity against different forms of the parasite. For example, in a study to identify novel *Leishmania* inhibitors, only 4% of compounds active against promastigotes maintained their activity against intracellular amastigotes found in the host³⁷. *In vivo*, the amastigotes

penetrate the granular cells of the host, protecting them from the drug molecule making them harder to treat, the molecule must enter the host cell before it can interact with the parasite³⁸. The intracellular amastigotes are the most clinically relevant stage of the parasites life cycle but are also more difficult to identify active inhibitors³⁹.

Using a target-agnostic approach in phenotypic screening, novel anti-trypanosomal compounds can be created without the influence of existing inhibitors. Aiming to discovery new protein targets when combined with chemical proteomics. Understanding these compound-protein binding interactions can guide further optimisation of the active compounds, such as exploring their structure-activity relationship (SAR) to improve potency and selectivity of the compounds³⁴⁻³⁶.

1.2. Exploring Diversity Generating Synthetic Strategies

Typically, compound libraries are designed and synthesised using a limited synthetic toolkit, creating libraries that only explore a small portion of drug-like chemical space⁴⁰. In this work, diversity generating chemistry is utilised to build complex libraries from simple starting materials for use in phenotypic screens. This approach leads to the discovery of novel active compounds that would not be accessible through traditional synthetic methods⁴¹.

1.2.1. The Medicinal Chemistry Toolkit

Traditional methods of drug design, using lead discovery⁴², identify hits by screening a large library of compounds against a variety of different targets. Hits are then optimised by synthesising analogues of those active molecules, aiming to improve their potency and pharmacological properties⁴³. This method consistently uses reliable chemical reactions that produce limited libraries of possible drug leads⁴⁰. The ‘typical’ synthesis of drug design produces large, flat, and achiral molecules, which often results in lead molecules with poor drug-like properties. In medicinal chemistry, the top 10 most used chemical processes in organic synthesis account for over 60% of the total reactions carried out in small scale drug design⁴⁴. This shows the reductive and repetitive nature of traditional drug discovery, where reactions produce single and predictable products, highlighting the need for alternative techniques to better explore biologically-relevant chemical space⁴⁵.

This methodology is also commonly applied to the discovery of electrophilic ligands^{46,47}. Often functionalising substrates with reactive warheads via safe and reliable chemistries such as amide bond formations, between amines and carboxylic acids or acid chlorides⁴⁸, to create limited libraries (**Figure 1.4**). These libraries also tend to focus on cysteine reactive warheads including acrylamides, or α -halo acetamides⁴⁶, which further reduces the scope of protein targets that can be explored.

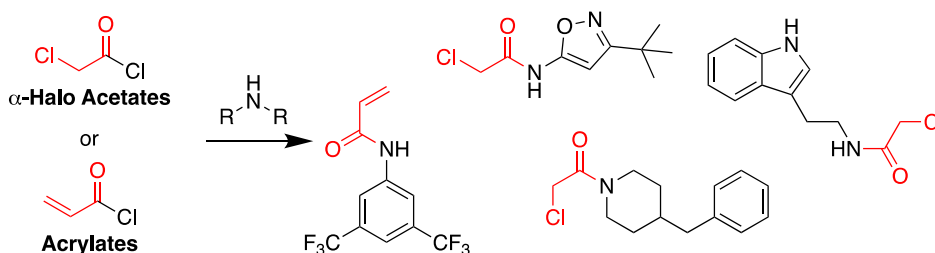


Figure 1.4: Illustrative example of an electrophilic fragment library containing cysteine reactive α -halo acetamides and acrylamide warheads synthesised via amide bond formation⁴⁶.

This work aims to utilise diversity generating chemistry and using electrophilic warheads selective for non-cysteine residues to move away from using typical chemistry, with the aim of better exploring chemical space, and identify novel, druggable targets that are not accessible to traditional discovery.

1.2.2. Introduction to Photoredox-Mediated Dehydrogenative Couplings

Photoreactive dehydrogenative cross-couplings can be used to functionalise two substrates by inserting into C–H bonds, resulting in a formal loss of H₂ via a single electron transfer cascade. Functionalisation of both substrates creates the potential for several unique products to form. The reactions are facilitated by photocatalysts, activated by light. These catalysts include transition metal complexes and organic dyes capable of absorbing UV light, exciting the catalyst to a redox-active state. In this form, by oxidising and reducing the reagents and substrates, the catalyst initiates these radical-mediated reactions^{41,49,50}.

An example of a dehydrogenative coupling is shown between an electron-deficient heteroarene and a hydrogen donor, such as a saturated nitrogen heterocycle (**Figure 1.5**)⁴¹. This outlines an illustrative reaction between the benzothiazole heteroarene (blue) reacting with the hydrogen donor *N*-Boc-pyrrolidine (purple) to form the cross-coupled product. The reactions proceed under non-inert conditions using stable reagents and have been shown to be compatible with a range of electron deficient heteroarene and donors. These couplings do not require pre-functionalised substrates to drive the formation of reactive radical precursors, such as borates and silicates previously used in these reactions, increasing the scope of compatible donors^{41,49–51}.

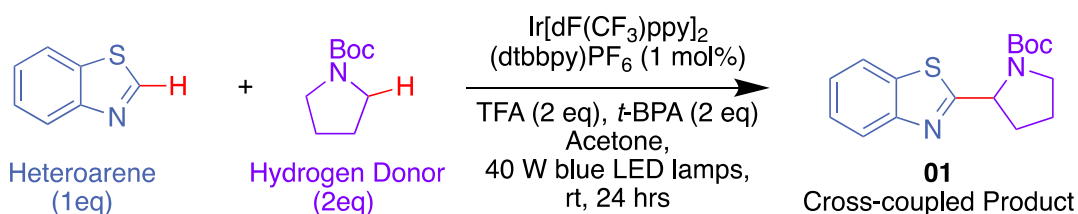


Figure 1.5: An example of a dehydrogenative coupling reaction between benzothiazole (blue) and *N*-Boc-pyrrolidine (purple), highlighting the sites of reactivity in red⁴¹.

This photo-coupling proceeds in a Minisci-type reaction, using either an iridium-based catalyst, $[\text{Ir}(\text{dF}(\text{CF}_3)\text{ppy})_2(\text{dtbbpy})]\text{PF}_6$, or an organocatalyst, 4CzIPN, illustrated in

Figure 1.6 using iridium as an example. Initially, a photon of blue light absorbed by the Ir(III) catalyst (**1**), promotes it to a stable excited state Ir(III)*, this can relax back to the ground state by emitting a photon. Alternatively, the active state can act as a reducing agent for TBPA, the activated peroxide, via a proton coupled electron transfer (**2**). Coordination to the peroxide carbonyl creates an electron deficient oxygen–oxygen bond that can be readily reduced to generate a *tert*-butoxy radical and an acetic acid by-product while the iridium complex is oxidised to Ir(IV). The butoxy radical can then abstract a hydrogen atom from the donor substrate, *N*-Boc-pyrrolidine (**3**). Pyrrolidines alpha hydrogen is most acidic, and more reactive to abstraction by the butoxy radical, the resulting alpha-radical is then stabilised by electron resonance from the neighbouring amide lone pair⁵². This radical can then react with an electron deficient heteroarene in the Minisci-type reaction (**4**). Finally, Ir(IV) quenches the cross-coupled species via a single electron transfer (**5**), reforming the heteraromatic ring and regenerating the Ir(III) catalyst⁴¹.

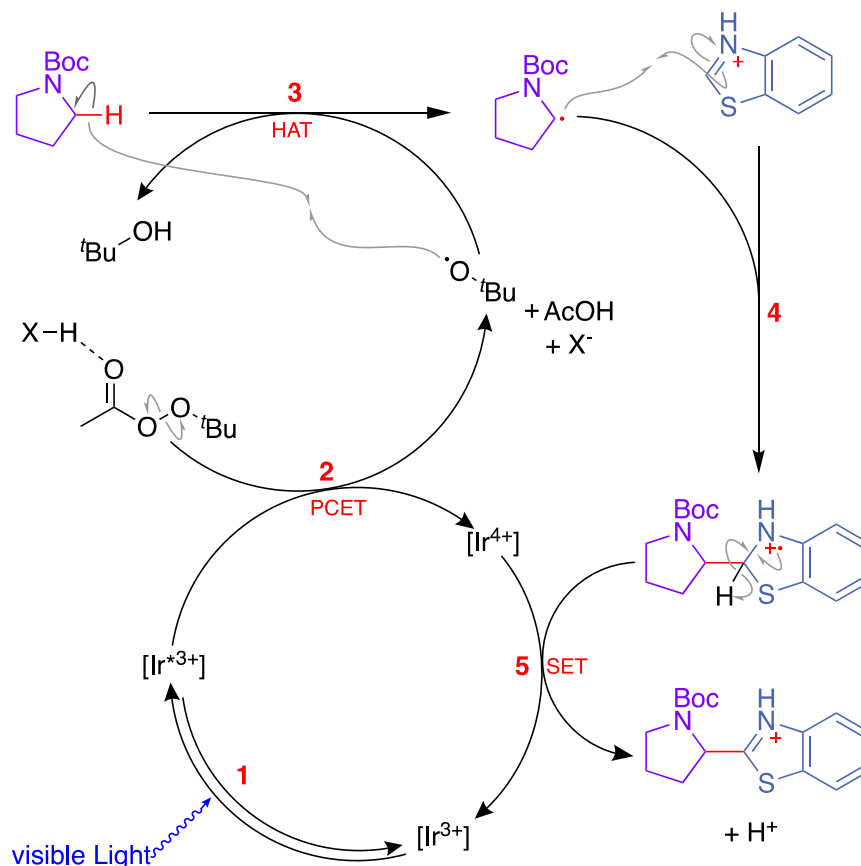
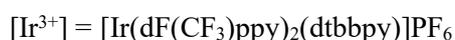


Figure 1.6: Reaction cycle of an iridium catalysed photo-coupling, between *N*-Boc-pyrrolidine and benzothiazole⁴¹. Figure adapted from ⁴¹.



Building on this reaction, previous in currently unpublished worked within the group by Dr Andrew Gomm optimised this reaction to run under ambient conditions for use in a

high-throughput array format. Using the coupling between benzothiazole and *N*-Boc-pyrrolidine (**Figure 1.5**) as a model reaction. A series of reaction were carried out across a 96-well plate on a 500 μ L scale (0.05 mmol scale with respect to the hetarene), following a standard protocol (**5.2.1**). The reagents were prepared as stock solutions in acetone, adding the benzothiazole hetarene (100 μ L, 0.5 M), along with varying concentrations of the hydrogen donor, TFA, the iridium catalyst, and *t*-BPA. The reactions were irradiated under blue UV light (390 nm) for 24 hours and monitored the conversion using LC-MS and analytical HPLC. From this, an optimised set of conditions were identified (**Table 1.3**), improving the reaction conversion from 15% to 70%.

Table 1.3: Optimisation of the dehydrogenative photocoupling reaction for ambient conditions carried out by Dr Andrew Gomm

	Literature Conditions	Optimised Ambient Conditions
Hetarene	1 eq	1 eq
Hydrogen Donor	2 eq	5 eq
Iridium Catalyst	1 mol%	1 mol%
TFA	2 eq	2 eq
<i>t</i>-BPA	2 eq	5 eq
Conversion	15%	70%

These optimised conditions were then used to explore the scope of hetarenes and hydrogen donors that are compatible with this dehydrogenative photocoupling. A series of substrates were selected from commercially available compounds, or compounds that required only a single step to protect free amines. Selecting fragments with less than 15 heavy atoms for decoration with this chemistry, aiming to produce molecules in ‘lead-like’ chemical space⁴³. Compounds were selected to include multiple potential sites of reactivity, to produce multiple products per reaction, to further increase the size and diversity of the library. 23 hetarenes substrates (**Figure 1.7**) were examined by reacting with *N*-Boc-pyrrolidine under the standard procedure as described above and analysed by LC-MS and HPLC to identify an intermolecular mass (HA + HD -H₂), and novel peak formation in the HPLC chromatograph. Additionally, 25 hydrogen donors were investigated by reacting with benzothiazole for analysis. Results from this experiment showed 16 of the 23 hetarenes and 16 out of 25 hydrogen donors (green) were compatible with the dehydrogenative coupling to form intermolecular products with the benzothiazole or *N*-Boc-pyrrolidine (**Figure 1.7**). These substrates can then be used to form the bases of a reaction array for compound generation, while incompatible substrates (red) were removed from consideration for future synthesis.

product formation, assuming 100% conversion of the heterene as the limiting reagent to product. A selection of promising reactions were identified that showed clear product formation by LC-MS and NMR. These reactions were repeated on a larger scale and purified to isolate intermolecular products (**Figure 1.8**) in work carried out by Dr Andrew Gomm and Dr Sam Griggs, highlighting the scope of this chemistry to produce an interesting and diverse compound library for exploration of chemical space.

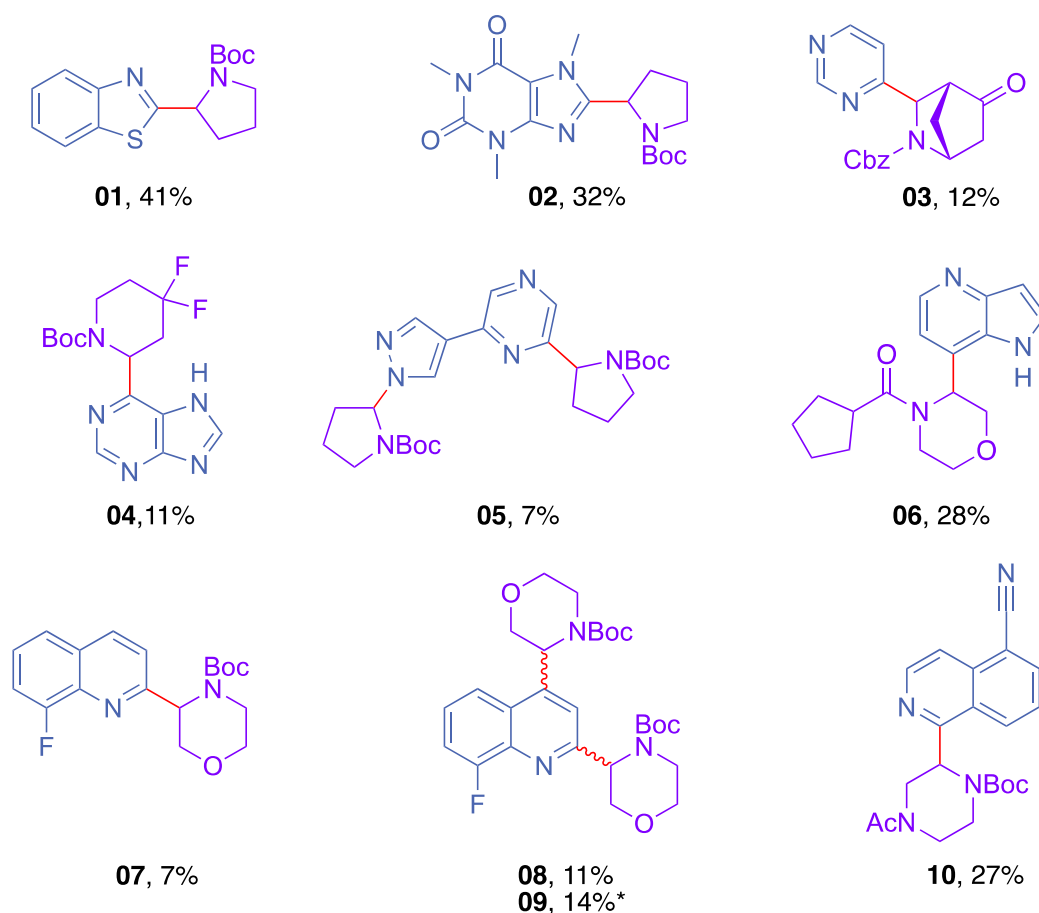


Figure 1.8: Isolated compounds from a dehydrogenative coupling array, between a set of heterenes (blue) and hydrogen donors (purple), showing the sites of reactivity in red, highlighting the scope and diversity of compounds accessible to this chemistry. Work carried out by Dr Andrew Gomm and Dr Sam Griggs of the University of Leeds.

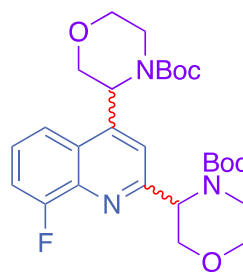
These isolated compounds were taken forward for screening against *T. brucei brucei*, by Dr Will Mosedale at the University of St. Andrews. This led to the discovery of two potent anti-trypanosomal compounds (**Figure 1.9**) to be taken forward for further investigation to explore their selectivity against human cells. Generation of photo-reactive chemical probe analogues of these compounds (**Appendix A**) will reveal these

compounds protein targets and explore their mode of action within cells, currently being investigated in on-going work.

***T.brucei* EC₅₀:**



01 = $14.0 \pm 0.1 \mu\text{M}$



11 = $3.7 \pm 0.3 \mu\text{M}$

12 = $7.3 \pm 0.2 \mu\text{M}$

Figure 1.9: EC₅₀ values of active compounds identified from a phenotypic screen against *T. brucei brucei*, taken for further investigation (**Appendix A**).

1.3. Covalent Inhibitor Discovery

Covalent inhibitors are designed to disrupt protein function by forming a covalent bond to the protein and blocking its reactivity. These interactions can be reversible or irreversible depending on the kinetics and thermodynamic reactivity of the electrophile^{53,54}.

1.3.1. An Introduction to Covalent Inhibitors

Covalent inhibitors contain weakly electrophilic warheads that require a catalytically activated nucleophile to react, found in the active sites of proteins. This means that the warheads are unable to react indiscriminately with nucleophiles in the protein side chains⁵⁴. Selectivity for specific amino acid residues in the active sites can be gained by tuning the type of electrophilic warhead used⁵⁵.

Ideally, covalent inhibitors should contain specificity groups to improve their selectivity (**Figure 1.10**) and reduce off-target effects. These groups allow the inhibitor to come into proximity of the active sites, initially forming non-covalent interactions (**1**). This increases the effective concentration of the inhibitor at the target site, facilitating covalent bond formation (**2**) between the electrophilic warhead and the activated residue. The active site can no longer react with native substrates to hinder a biological response⁵⁶.

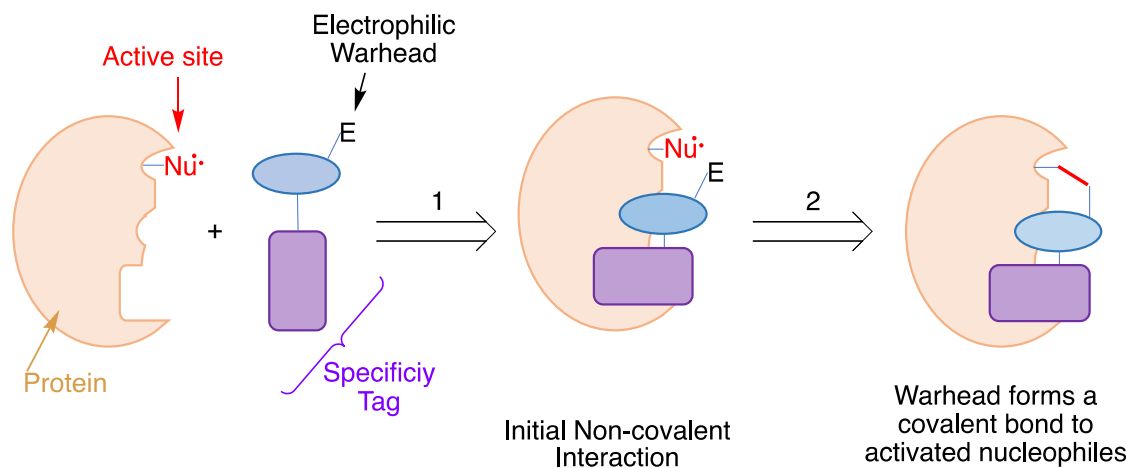


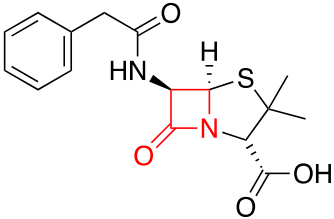
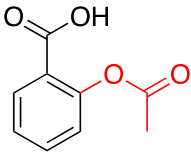
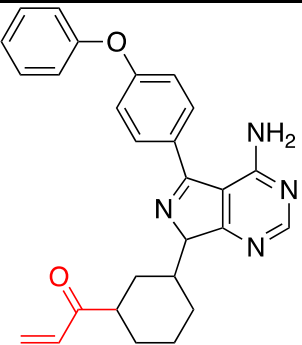
Figure 1.10: A schematic representation of covalent drug inhibition. Initially, non-covalent interactions between the ligand and protein (**1**) bring the electrophilic warhead into proximity with the catalytic nucleophile. Now the electrophilic can react with the activated nucleophile of a specific protein, forming a covalent bond to produce a therapeutic effect⁵⁶.

Non-covalent inhibitors produce a biological effect by out-competing natural substrates for the proteins reactive site. The half-lives of these compounds are dependent on a

variety of factors, including their metabolic stability and rate of elimination from the body⁵⁴. Covalent inhibitors permanently bind to the protein active site, rendering it inactive. The activity window of covalent inhibitors becomes the time taken to re-synthesise the inactivated protein so creating a longer therapeutic effect. Inhibition of the protein target is stoichiometric, thus requiring lower, and less frequent dosing⁵³.

Around two thirds of market drugs that target enzyme active sites either contain a native substrate mimic or undergo covalent interactions with the protein^{53,57}. These covalent inhibitors include penicillin and aspirin, as well as the blockbuster drug ibrutinib (**Table 1.4**)⁵⁸⁻⁶⁰. Many of these inhibitors were not designed with covalent intention, and their mechanisms of action were discovered later on⁵⁷.

Table 1.4: Common commercially available covalent drugs, highlighting their reactive functional groups (red), along with their biological target to cause a therapeutic effect⁵⁸⁻⁶⁰.

	Penicillin	Aspirin	Ibrutinib
Structure			
Treatment	Anti-bacterial	Anti-inflammatory	Lymphocytic Leukaemia
Target	DD-transpeptidase ⁶¹	Cyclooxygenase Enzymes ⁵⁹	Bruton Tyrosine Kinase ⁶⁰

The anti-trypanosomal drug eflornithine (**Table 1.2, p4**), used to treat the late stage form of gHAT¹³ acts as a covalent suicide inhibitor⁶². The drug irreversibly binds in the ornithine decarboxylase active site, blocking the native substrate, ornithine to inhibit polyamine biosynthesis (**Figure 1.11**). The suicide inhibitor is structurally similar to the native substrate (**Figure 1.11a**) to allow binding to the target. The enzyme active site is activated by a molecule of pyridoxal phosphate (PLP) to form a reactive Schiff base via a condensation of the aldehyde group (**Figure 1.11b**). Eflornithine then reacts with PLP via a transamination reaction, substituting lysine. Here, the native substrate ornithine will react via a decarboxylation to form the polyamine product⁶³. Whereas, with eflornithine, the difluorides act as leaving groups to form a highly reactive imine electrophile to react

with an activated thiol in the enzyme active site (**Figure 1.11c**)⁶⁴. The PLP transaminates back to the lysine residue to complete the catalytic cycle. The molecule of eflornithine is irreversible bound to the cysteine residue and can cyclise by loss of ammonia to form a cyclic imine, blocking the active site to produce a therapeutic effect(**Figure 1.11d**)⁶³.

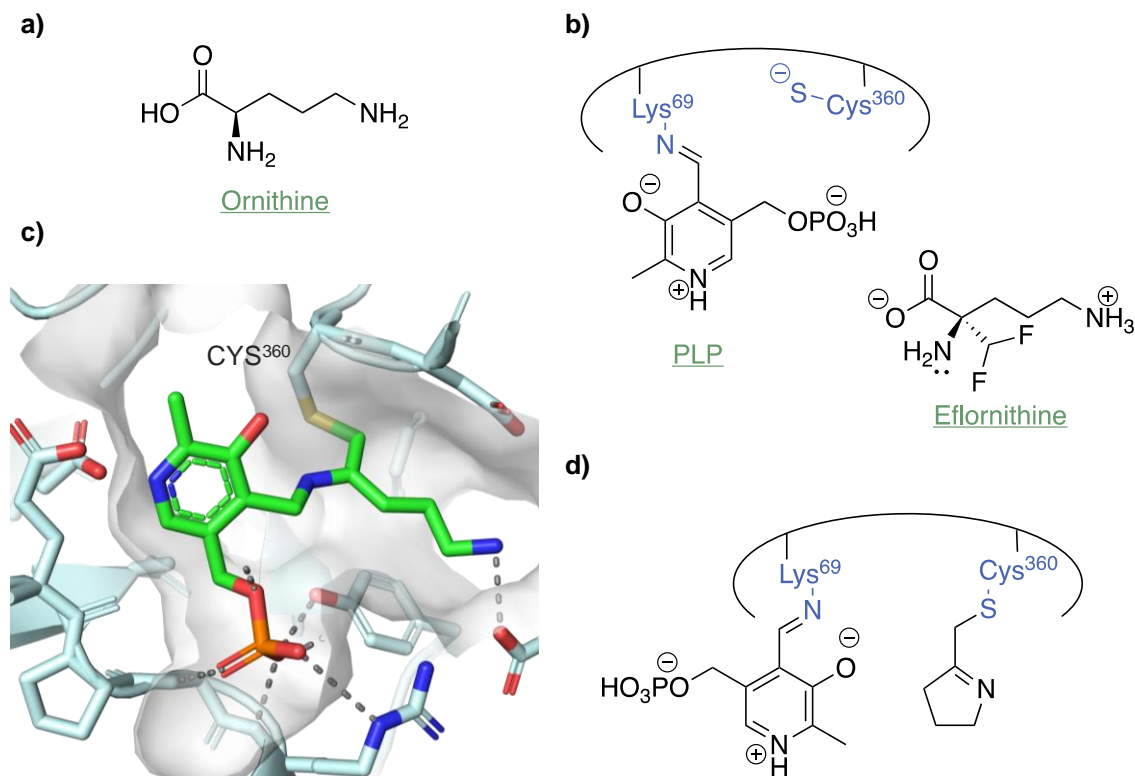


Figure 1.11: Covalent inhibition ornithine decarboxylase for treating gHAT. Outcompeting the native substrate ornithine (a) for the binding site (b), catalysed by a molecule of PLP⁶³. The crystal structure (c) highlights the reaction intermediate (green) on binding to a cysteine residue after substitution of the fluorine groups, stabilised by hydrogen bonding to neighbouring residues (blue)⁶⁴. The complex cyclises (d) to permanently inhibit the protein active site and reforming PLP^{63,64}.

1.3.2. Reactive Electrophilic Warheads

The covalent warhead is a weakly electrophilic group that requires an activated nucleophile in a protein active site to react⁵⁴. The selectivity of these covalent inhibitors to this active site can be tuned by varying the specificity tag groups⁵⁶. In addition, the type of covalent warhead used can be altered to tune the reactivity and selectivity of the inhibitor⁵⁵. There is a diverse range of functional groups that are used in covalent ligand design, each with different affinities for specific nucleophilic amino acid residues in protein active sites such as cysteine, serine, lysine, and tyrosine (**Table 1.5**). These warheads can react reversibly, such as Michael acceptors⁶⁵⁻⁶⁹ and nitriles^{70,71}, or irreversibly, to permanently deactivate the protein site, such as epoxides^{72,73} and S_N(AR) warheads^{74,75}. The reactivity of covalent inhibitors can be tuned using different warhead groups, depending on the properties of the active site. For example, fluorosulfate warheads are less electrophilic than sulfonyl fluorides, due to the additional electron donation from the oxygen. While both warheads favour binding to activated lysine residues, the fluorosulfate can be used as milder warheads, increasing selectivity, and reducing off target reactivity of the inhibitor⁷⁶⁻⁷⁹.

Table 1.5: Examples of electrophilic covalent warheads, divided by their reactivity preferences for specific nucleophilic amino acids, highlighting their mechanism of action as well as additional reactive residue⁷⁹.

Reactive Class	Warhead Structure	Further Residues	General Mechanism of Action
Cysteine			
Acrylamide ^{65,66}		Lys	
Propiolamide ⁶⁹			
Acrylonitrile ^{67,68}		His	
Electron Deficient Alkyne ⁸⁰		—	
Aldehyde ^{72,81} (X = H)		Lys	
Ketone ^{72,82} (X = CRH)			
Aziridine (X = NH) ⁷²		Glu, Asp	
Epoxide ^{72,73} (X = O)		Lys, His	
Disulfide ^{83,84}		—	
S _N (AR) Substrate ^{74,75}		Lys, Tyr	
α-Halo Ketone ^{63,72}		Lys, His, Thr	

Reactive Class	Warhead Structure	Further Residues	General Mechanism of Action
----------------	-------------------	------------------	-----------------------------

Cysteine Cont.

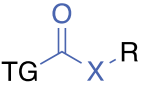
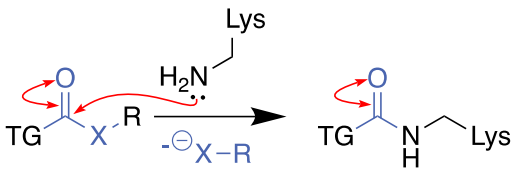
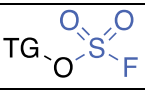
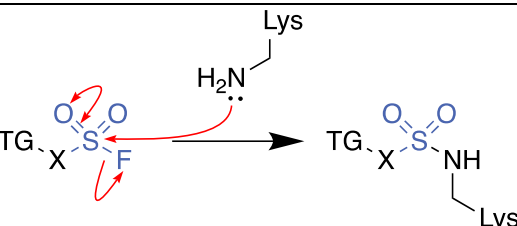
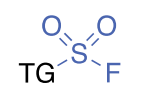
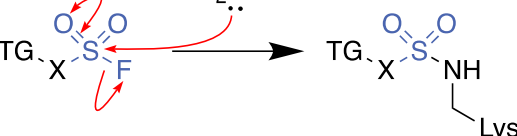
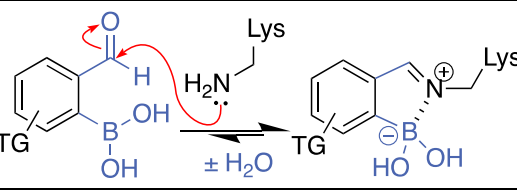
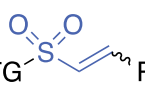
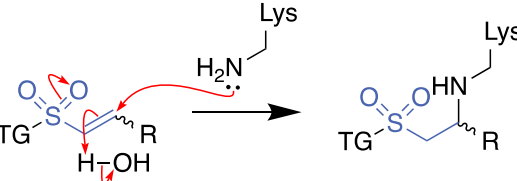
Isothiocyanate ⁷¹ <chem>TG-N=C=S</chem>	<chem>TG-N=C=S</chem>	Lys	
Nitrile ^{70,85,86} <chem>TG-X-C#N</chem> X = EWG	<chem>TG-X-C#N</chem> X = EWG	Ser	
Nitroalkane ⁸⁷ <chem>TG-CH2-NO2</chem>	<chem>TG-CH2-NO2</chem>	—	

Glutamic acid

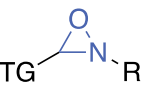
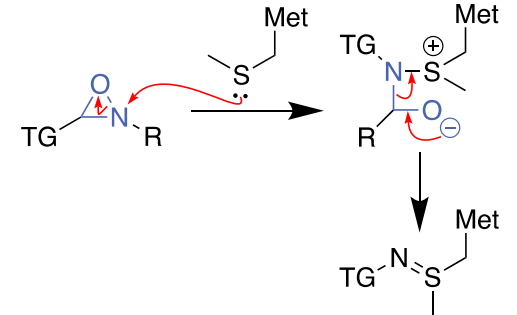
N-methyl Isoxazolium ⁸⁸ <chem>TG-C5H4N+</chem>	<chem>TG-C5H4N+</chem>	Asp, Cys	
--------------------------------------------------------------	------------------------	----------	--

Reactive Class	Warhead Structure	Further Residues	General Mechanism of Action
----------------	-------------------	------------------	-----------------------------

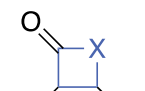
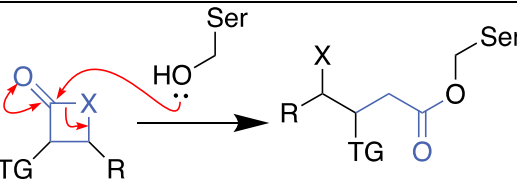
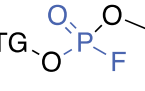
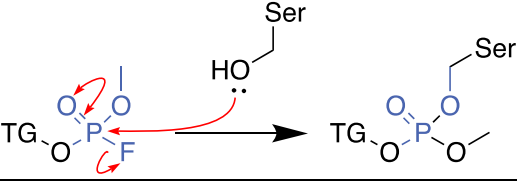
Lysine

Amide (X = NH) ⁸⁹		—	
Ester (X = O) ⁵⁹			
Thioester (X = S) ⁹⁰			
Fluorosulfate _{76,77}		Tyr, Ser	
Sulfonyl Fluoride ⁷⁸		Tyr, Cys, Ser	
Oxoborazole _{91,92}		—	
Vinyl Sulfone ⁹³		Cys	

Methionine

Oxaziridine ⁹⁴		Met	
---------------------------	-------------------------------------------------------------------------------------	-----	--------------------------------------------------------------------------------------

Serine

β -Lactam ⁹⁵ (X = N)		—	
β -Lactone ⁹⁶ (X = O)			
Fluoro-phosphonate ⁹⁷		Ser	

1.3.2.a Sulfonyl Fluorides as Reactive Electrophilic Warheads

Of particular interest to this work, sulfonyl fluorides form interesting interactions with protein and are explored further in this work, forming the bases of an electrophilic library of potential inhibitors. Chosen for their reactive promiscuity, reacting predominately with lysine and tyrosines, sulfonyl fluorides are also known to react with serine, threonine, cysteine, and histidine residues^{98,99}. The reactivity of sulfonyl fluorides with activated amino acids is relatively slow compared to other electrophilic warheads, meaning their reactivity is heavily templated by additional functionality of the probes targeting groups¹⁰⁰, so can allow for selective binding to a protein target, aiming to limit broad-spectrum toxicity, typically associated with electrophilic warheads⁵⁴.

Simple sulfonyl fluoride containing compounds, have been shown to exhibit anti-trypanosomal activity against parasites such as *T. brucei*^{101–103}. Phenylmethylsulfonyl fluoride (PMSF), an alkyl sulfonyl fluoride used in protease inhibitor cocktails (**Figure 1.12**) is known to inhibit the serine protease inositol acyltransferase, necessary for Glycosylphosphatidylinositol (GPI) biosynthesis. GPI is used to anchor proteins such as transporters and receptors to the cell membrane, playing an important role its survival and virulence. Therefore, interruption of GPI synthesis can lead to a range of defects in cell division, motility, and infectivity¹⁰¹. The absence of GPI-anchored proteins can also make the parasite more susceptible to the hosts immune response. GPI anchors are significantly more abundant in trypanosomes than in other eukaryotic cells¹⁰², making its biosynthetic pathway an attractive target for new therapeutics, based around sulfonyl fluoride containing compounds.

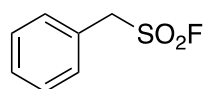


Figure 1.12: PMSF, a simple alkyl sulfonyl fluoride with known anti-trypanosomal activity against *T. brucei*^{101–103}.

Sulfonyl fluorides are known to react predominately with lysine and tyrosine residues, forming stable sulfonamide and aryl sulfonate adducts^{98,99} (**Figure 1.13a**), both with nucleophilic amino acids in protein active sites⁹⁹, and with non-activated amino acid side chains¹⁰⁴. They also show potential to react with activated serine and threonine residues but form unstable sulfonate adducts that are readily hydrolysed, or substituted by reactive nucleophiles such as DTT, used as a reducing agent^{98,105} (**Figure 1.13b**). Using sulfonyl fluorides in the design of an electrophilic compound library can aid in the discovery of

novel protein targets, moving away from traditional, cysteine-reactive warheads. Further work towards stabilising the interactions between sulfonyl fluorides and serines and threonines residues can be used as a method to profile lysine, tyrosine, serine, and threonine amino acids.

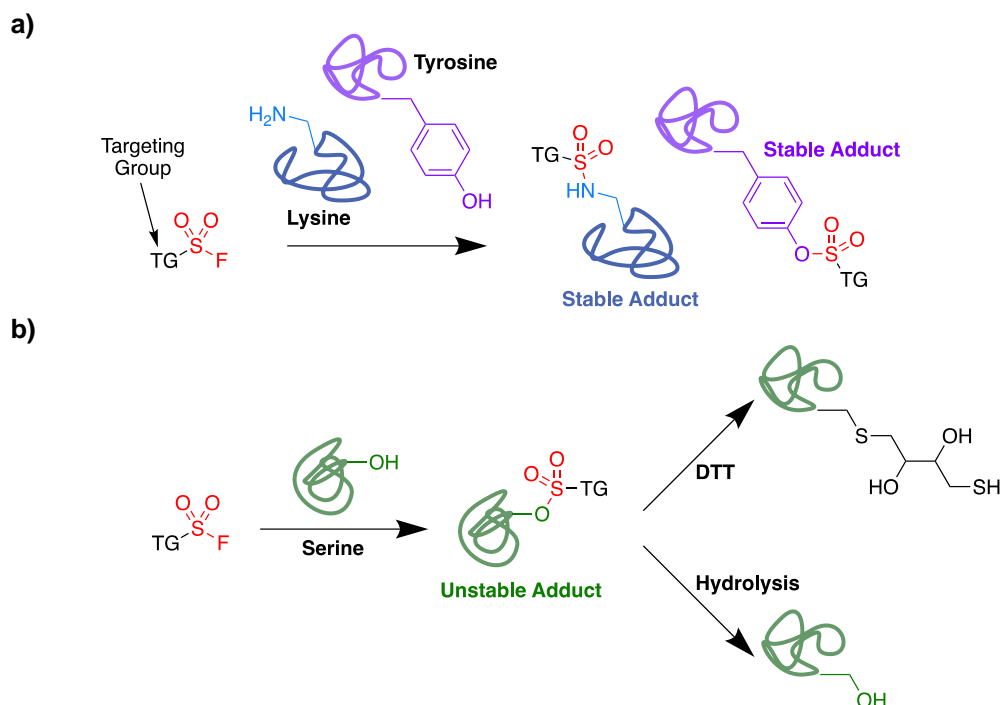


Figure 1.13: The reactivity of sulfonyl fluorides with amino acid side chains, forming stable adducts with lysines and tyrosine residues^{99,104} (**a**), and unstable interactions with serines (**b**) that can be readily hydrolyse or substituted^{98,105}.

1.3.2.b α -Nitriles as Reactive Electrophilic Warheads

α -Nitrile groups are known to react as a reversible electrophilic warhead reacting with serine and cysteine proteases⁸⁶. This is evidenced in α -nitrile containing drugs (**Figure 1.14a**), Nirmatrelvir¹⁰⁶, reacting with a cysteine proteases and Saxagliptin⁸⁵, reacting with a serine protease (**Figure 1.14b**). This can be illustrated by the crystal structure of Saxagliptin bound to the target protein DPP-4, a surface glycoprotein, by reacting with the activity serine residue, Ser592 (**Figure 1.14c**). inhibition of this protein prevents the breakdown of the incretin hormone and promotes insulin formation to treat type 2 diabetes.

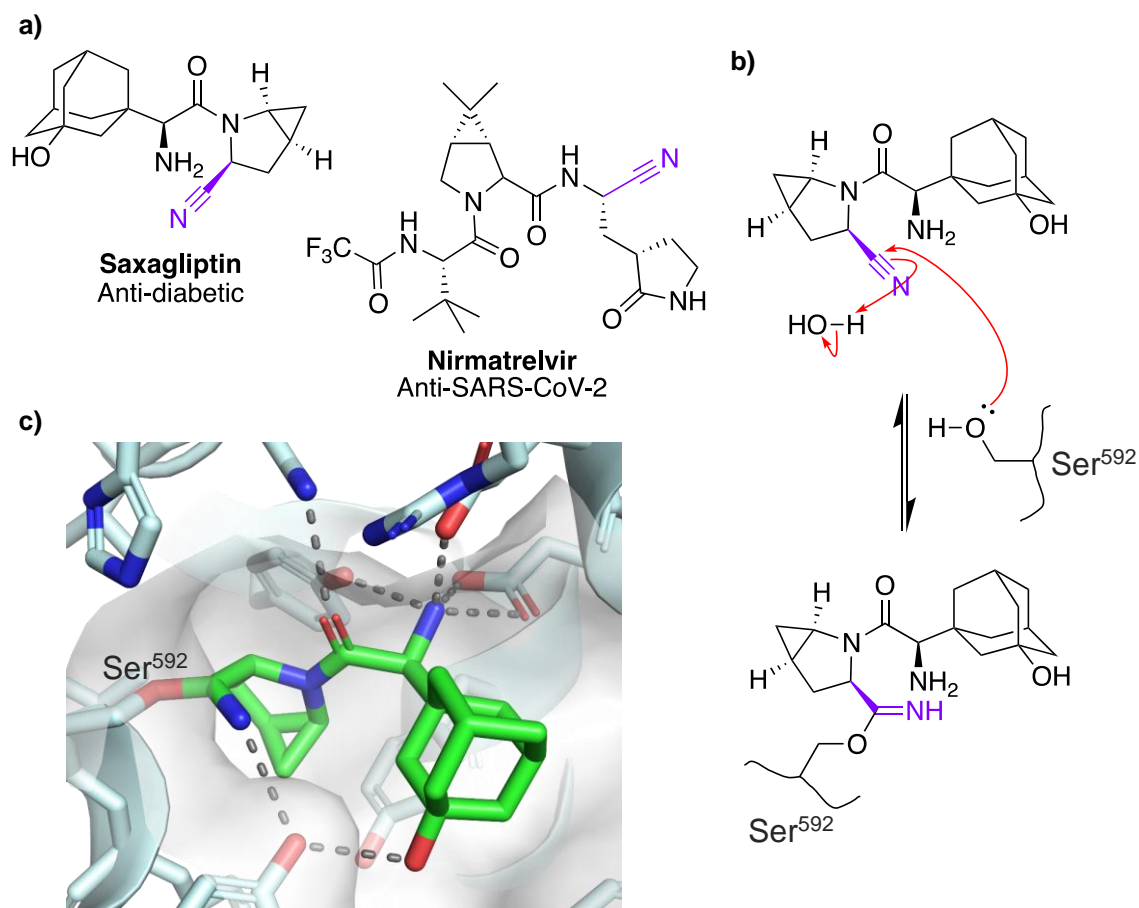


Figure 1.14: α -Nitriles as reversible electrophilic warheads, illustrated by drug compounds containing α -nitriles, Nirmatrelvir¹⁰⁶ and Saxagliptin^{85,107} (a) shown to react with activated cysteine or serine residues (b). Saxagliptin is known to react via attack of the electrophilic carbon by an activated serine residue (Ser⁵⁹²) of the DPP-4 glycoprotein as shown in its crystal structure (c), PDB = 3BJM¹⁰⁸.

The reactivity of these α -nitrile warheads will be explored further in this work, exploring their anti-trypanosomal activity. Aiming to identify their protein targets, amino acid selectivity, and their stability as reversible warheads through chemical proteomics.

1.4. Chemical Proteomics

Proteomics terms the study of proteomes and their function. Chemical proteomics is the use of small molecule tools that can interact with proteins of interest to identify proteins for identification and to understand their function¹⁰⁹.

1.4.1. Chemical Probes

In chemical proteomics, a small molecule chemical tool is used to label specific proteins in a proteome to be visualised or pulled down for analysis. The aim is to give an insight into the protein interactions occurring within the cell¹¹⁰.

There are several definitions of a chemical probe¹¹¹. In this report, a chemical probe is made up of three components (*Figure 1.15*). The main body of the probe (purple) acts as a recognition unit, optimising its structure to allow for strong and selective binding to a target. Once the probe interacts with the target protein, the warhead (red), can react to form a covalent bond, fixing the probe to the binding site. Here the reactive group can be a photo-activatable species that can insert into X–H bonds on the protein of interest after irradiation with light, to form a new covalent bond, crosslinking the probe and protein. The reactive group could also be an electrophile that reacts specifically with an activated nucleophile in a protein's active site. The probe can be used to identify or isolate the probe-protein complex for analysis. To do this, the probe is fitted with a tagging group (blue) which can incorporate a fluorescent group to visualise the pulled-down proteins on SDS-PAGE gels. An affinity or bioorthogonal tag can be used to attach a variety of labels.¹¹².

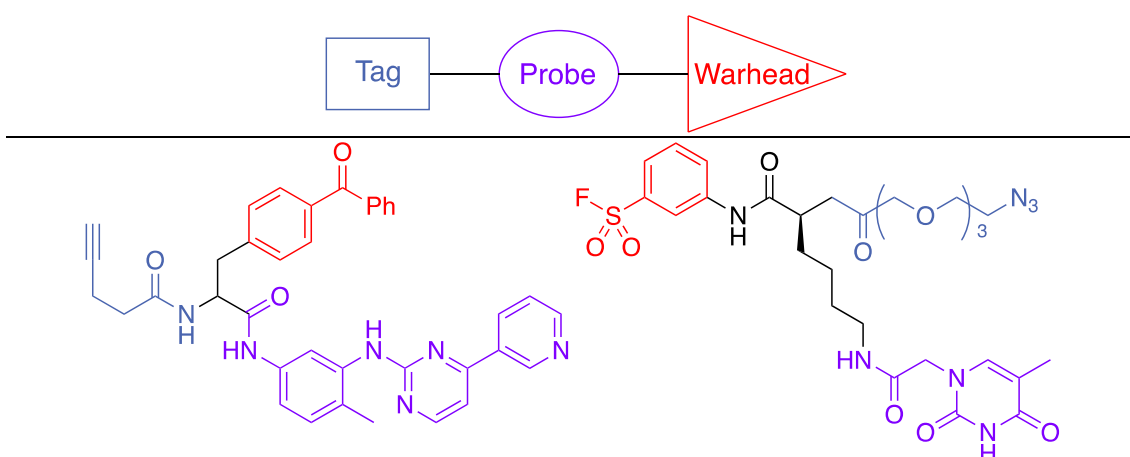


Figure 1.15: The key components of a chemical probe, showing the selective binding groups to the target protein (purple), the reactive warhead (red) and the tagging group (blue). This is highlighting on two probes used for labelling kinases^{113,114}.

During this project, it is intended to use two main classes of chemical probes, reactive electrophilic probes⁷⁹, and affinity based, photoreactive probes¹¹⁵. Electrophilic warheads have been outlined previously (**Section 1.3.2**). In chemical proteomics they are used to identify the active sites of proteins, the electrophiles are too mild to react with nucleophiles along the protein backbone. Electrophilic probes are used to label protein reactive sites, but are not reactive enough to label other types of proteins in a cell⁷⁹.

Photoreactive warheads are used in photoaffinity labelling. A reactive species is formed *in situ* after irradiation with UV light, so can be activated after the probe interacts with the target protein. There are three main types of photoreactive warhead that form reactive groups on irradiation with light (**Figure 1.16**). Diazirines¹¹⁶ (**Figure 1.16a**), predominately react via a diazo species with acidic residues, to create an ester with glutamic acid, aspartic acid or the C-terminus of the protein¹¹⁷. Diazirines can also react via activated carbenes, to react indiscriminately with the proteins X–H bonds¹¹⁸. The reaction pathway of diazirines is heavily dependent on neighbouring group properties. Electron withdrawing groups such as trifluoromethyl drive and stabilise the formation of a triplet state carbene, having a longer lifetime and higher reactivity than singlet state. Inversely, electron donating groups favour the formation of the less reactive, and less stable singlet state carbene, and also promote its rearrangement to the diazo species. Other factors such as the presence of oxidising agents and catalysts, temperature, and wavelength of light used also influence the diazirine reactivity. The small size of these diazirine groups make them ideal for proteomics experiments and target identification of hit compounds, making minimal changes to the original parent compound, and having a higher chance of retaining its activity. Benzophenones¹¹⁹ (**Figure 1.16b**), react with UV light to form a di-radical species, reacting favourably with methionine residues. The lifetime of these radicals is very short, typically nano- to micro-seconds¹¹⁹, requiring a potent and selective recognition unit to ensure proximal binding to react once irradiated. The bulky diphenyl group also limits these probes binding ability, appending them to active compounds for target identification may significantly impact their potency. Arylazides (**Figure 1.16c**), form a high active nitrene species and reacts with any X–H bond in the protein. The nitrene can also rearrange to the less reactive didehydroazepine, reacting as a covalent electrophile¹²⁰. The didehydroazepine is significantly more stable than the nitrene but requires activated nucleophile to react with a protein target.

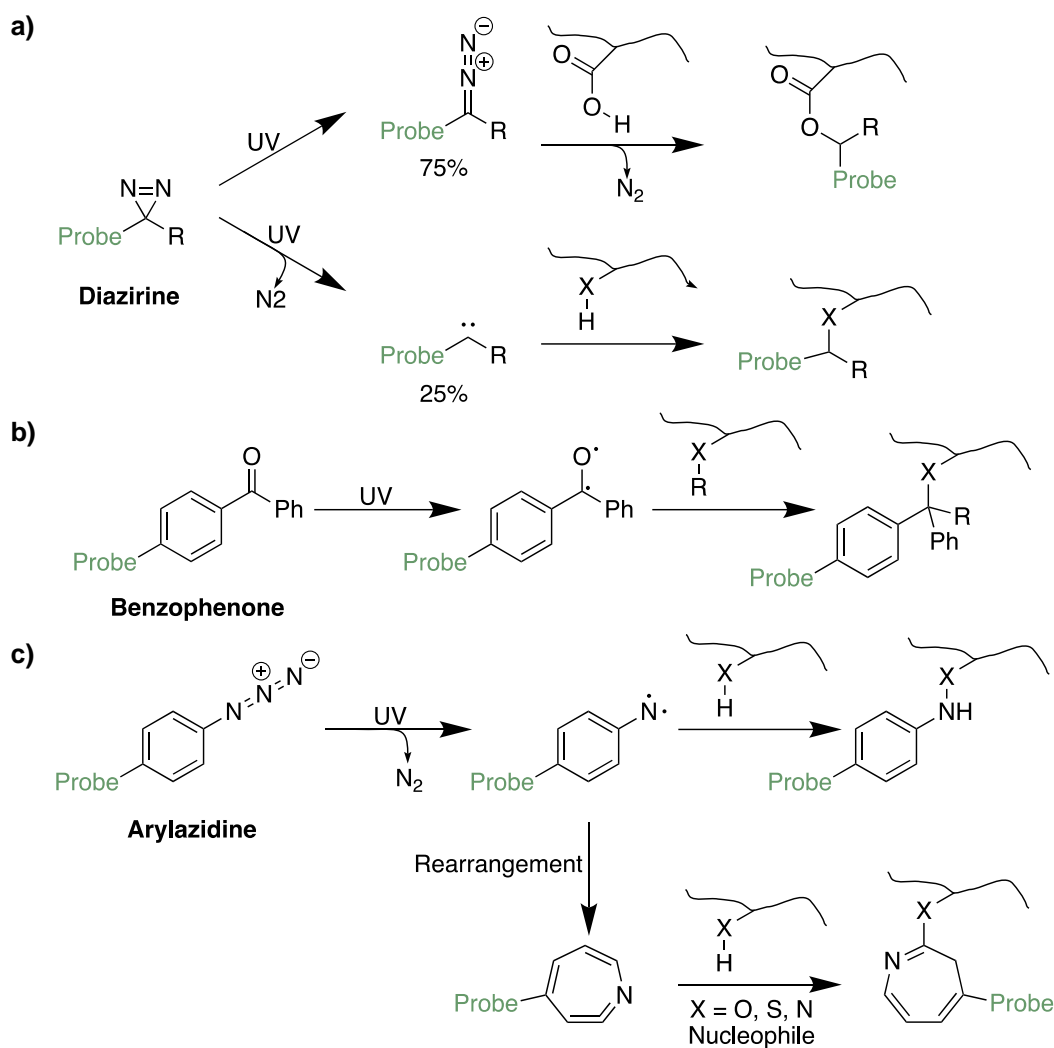


Figure 1.16: Photoreactive groups used to label proteins. UV light between 300–350 nm activates the species, allowing it to react with X–H bonds on the protein. These reactive groups include diazirines¹¹⁷ (a), benzophenones¹¹⁹ (b) and arylazides¹²⁰ (c).

The active species formed from these photoreactive groups can insert into X–H bonds, (X= C, O, N, S etc.)¹¹⁵, so react more broadly with protein chains than electrophilic moieties. The probe has high selectivity for the target if the half-life of the active species is shorter than that of the equilibrium interactions of the probe and protein. For example, depending on the wavelength of UV light use, the diazirines reactive carbene species has a half-life of around 20 seconds, while the diazo has a longer half-life of over 20 minutes¹¹⁵. The probe is able to react with the nearest X–H bond, so can be used more generally than electrophilic groups which require activated nucleophiles. One limitation of photoreactive probes is that the short wavelengths of light required to activate the warhead (300-350 nm) can be damaging to proteins and cells^{121,122}.

These activity-based and photoaffinity probes can be used to isolate proteins of interest (**Figure 1.17**). The small molecule probe is designed to interact with a target site in the cell (1), so that the reactive warhead, containing an electrophile or a photoreactive group, can then form a covalent bond to the protein (2). The cell can then be lysed, and the proteins extracted (3) so that a label can be attached to the probe-protein complex for analysis, for example, via a copper-catalysed click reaction between the alkyne and an azide. Attachment of a fluorophore (4) can be used to visualise the protein of interest following an SDS-PAGE gel. Alternatively, attachment of an affinity tag allows the protein to be isolated. When passed through a resin, the protein complex containing the tag will bind and everything else can be washed away. The protein can be digested from the resin into peptides and analysed by LC-MS/MS mass spectrometry for identification¹²³.

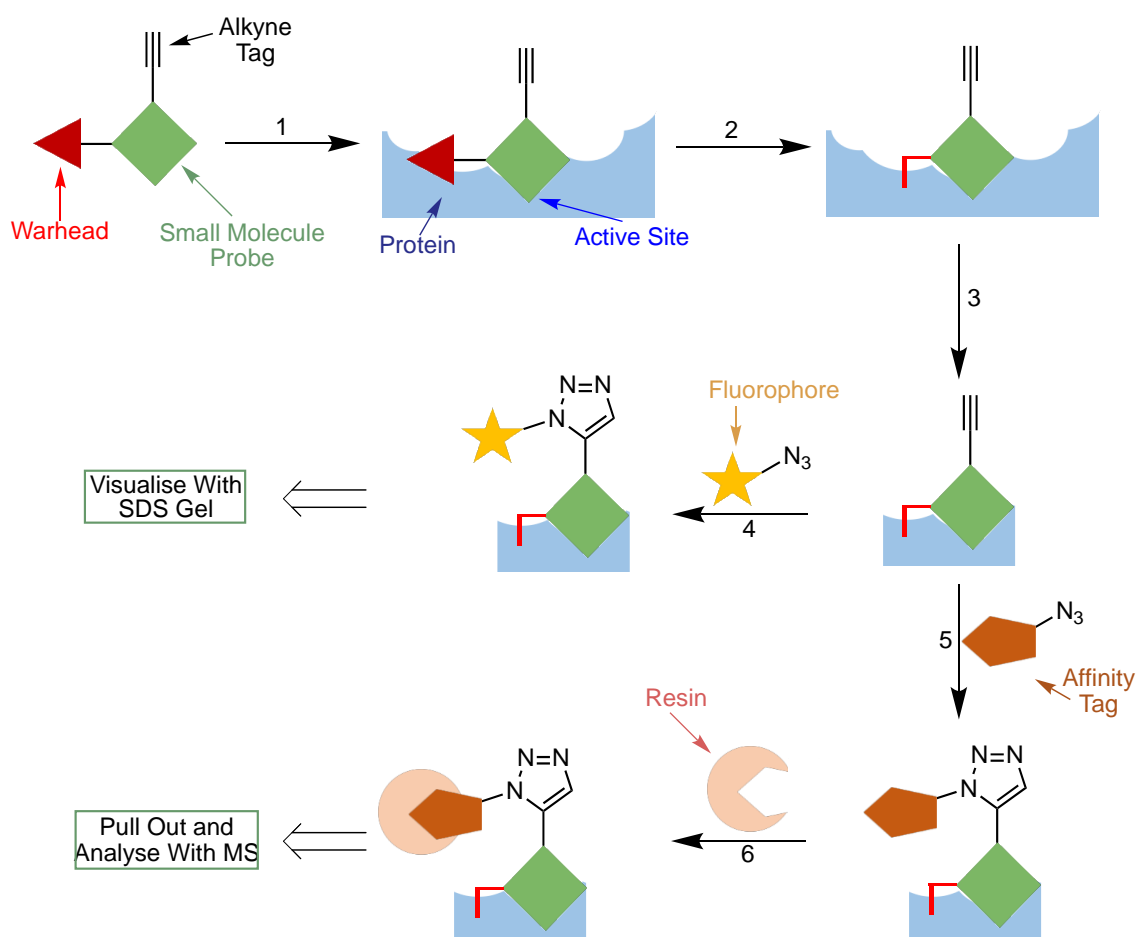


Figure 1.17: Workflow of chemical proteomics, using a two-step labelling strategy with a chemical probe to covalently bind to the active site of the protein (2), before cell lysis (3). The probe can then be linked to a fluorophore (4) or an affinity tag (5) for analysis to characterise the protein of interest. Figure adapted from reference ¹¹⁰.

In order to visualise or isolate the target protein, the probe could be directly fitted with a fluorophore or affinity label (**Figure 1.17**), but this can add a lot of bulk to the probe, interfering with or preventing it from binding to the target site so is not as reliable for identifying the interaction site of an inhibitor. Click reactions use small, bioorthogonal groups that are incorporated into the probe which have minimal or no effect on the probes binding interactions but can be further functionalised with a fluorophore or affinity label. This process requires a bioorthogonal reaction that allows the selective addition of groups to the probe in a manner that is biocompatible with the cell. The reagents used and the products formed in these reactions must be stable and the reaction must proceed in physiological conditions¹¹⁰. Click chemistry encompasses bioorthogonal reaction that allows the coupling of two reagents in a high yielding and selective manner. These reactions are performed under mild conditions and must be water stable with few by-products, making it ideal for tagging probes¹²⁴. **Figure 1.18** outlines some common click reactions used in proteomics to functionalise probes. This includes the copper-catalysed [3+2] cycloaddition (CuAAC) between azide and alkyne groups¹²⁵ (**a**), the tetrazine ligation¹²⁶ (**b**) and the Staudinger ligation¹²⁷ (**c**). The reagents used in these reactions do not interfere with biological molecules and only form nitrogen or methanol by-products. The tagging groups can be fitted into the probes design so that the click reaction can be carried out in situ to add fluorophores or affinity labels to the molecule¹²⁸. In this work, the CuAAC click reaction (**Figure 1.18a**) has been used, primarily due to the small functional groups needed. Alkyne tags can be appended to electrophilic molecules to generate chemical probe, by only making small changes to the molecule, the aim is to conserve the chemical and physical properties of the parent molecule to give accurate probe mimics. The high stability of alkyne groups also makes them idea for synthesising probes using the diverse chemistries explored in this work. Limitations of this copper-catalysed click reaction arise from coppers toxicity to cells when used in phenotypic work, as well as the reactions sensitivity to oxygen, requiring fresh reagent stocks to be used for each reaction¹²⁵.

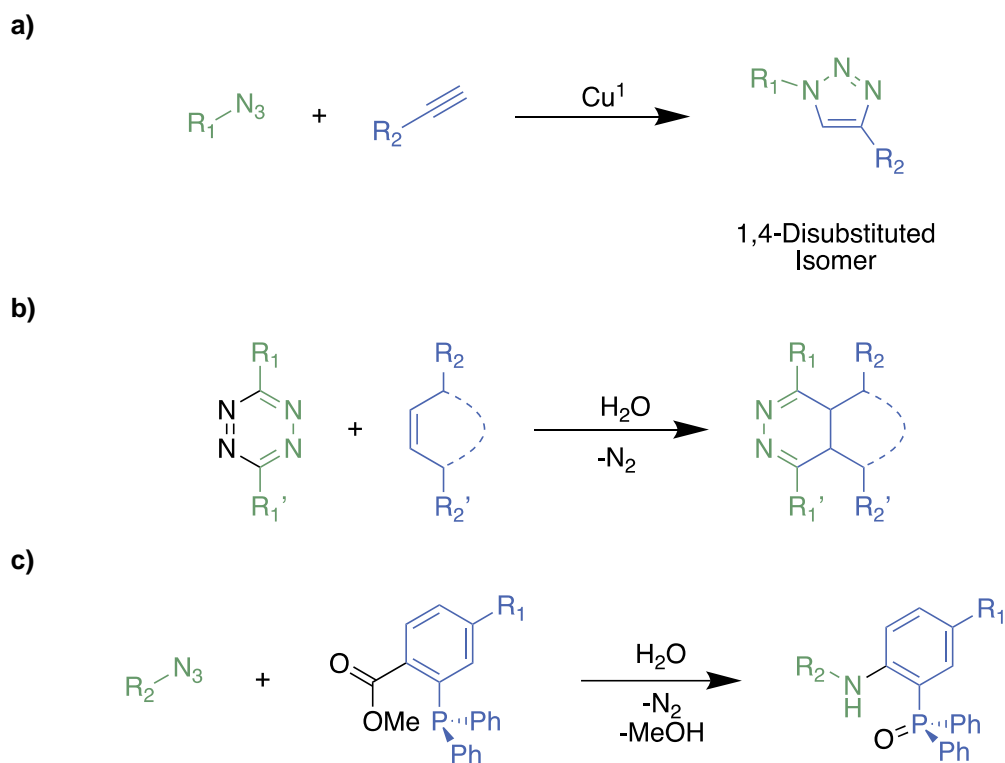


Figure 1.18: Bioorthogonal click reactions used in chemical proteomics for attaching affinity tags and fluorophores to chemical probes, including CuAAC¹¹⁰ (a), the tetrazine ligation¹²⁶ (b) and the Staudinger ligation¹²⁷ (c).

A key reaction is the [3+2] cycloaddition between a terminal alkyne and an azide group (**Figure 1.18a**, **Figure 1.19**). The uncatalyzed reaction, without constrained substrates, proceeds very slowly, and requires heating to 100 °C, so is not suitable when working with proteins. The reaction also forms a mixture of isomers, depending on the orientation the reagents come together¹²⁸. Alternatively, a copper(I) catalyst can be used to selectively form the single 1,4 triazole isomer, in a quick and biocompatible reaction, so is more suitable for tagging probes. **Figure 1.19** outlines the proposed catalytic cycle of Cu(I), formed in situ from CuSO₄, to form the triazole. The reaction is shown to depend on two copper ions in the reaction rate determining step (3)¹²⁹. Initially the catalyst inserts into the terminal alkyne while a second coordinates to the alkyne (1), the electron rich azide can then coordinate to the copper ion (2). The second copper ion withdraws alkyne electron density, promoting the cyclisation reaction (3) as the rate determining step. The catalyst fixes the conformation of the azide with the alkyne, so the 1,4-isomer is formed selectively in the cyclisation steps (3, 4). Finally, a reductive elimination releases the triazole product, reforming the catalyst (5)¹³⁰. This reaction gives a high yield of triazole, so can be used to couple an affinity label or fluorophore to the probe for analysis.

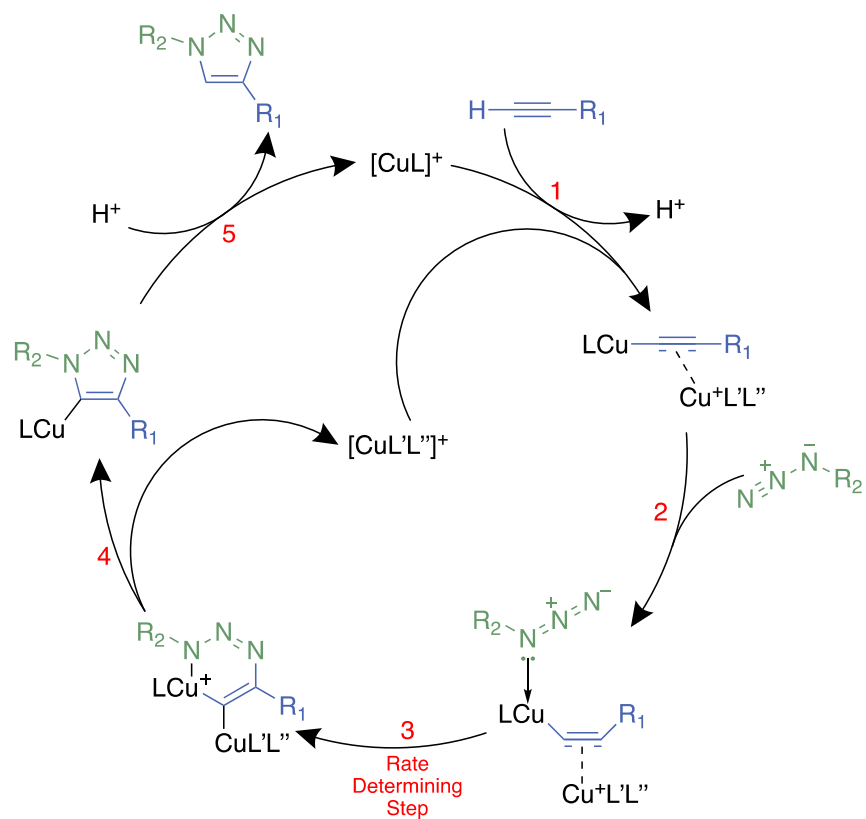


Figure 1.19: Reaction cycle of the copper catalysed click reaction to form a single 1,4-disubstituted isomer preferentially. Showing the dependence of two copper ions in the mechanism^{131,132}.

1.4.2. Mass Spectrometry in Chemical Proteomics

The final stage in the chemical proteomics workflow (*Figure 1.17, p29*) involves analysis of the isolated protein, labelled with the probe group, by liquid chromatography tandem mass spectrometry (LC-MS/MS).

Figure 1.20 shows the typical workflow for analysis of proteins using LC-MS/MS following the bottom-up approach. The protein of interest is first digested into peptides via proteases (1) so that the sample can be ionised (2) and separated based on their mass to charge (m/z) ratio. The isolated peptide chains are then fragmented, typically across the peptide's amide bonds (4) followed by a second m/z separation (5) so that fragments can be detected as daughter ions of the peptides in the spectrometer (6). Sequence data can then be gained from analysis of these ionised peptide fragments^{133,134}. The alternative top-down approach either limits or does not involve an initial digestion of the protein, instead, fragmentation occurs in the mass spectrometer so creates later ionised fragments for detection, to build up the protein sequence^{134,135}.

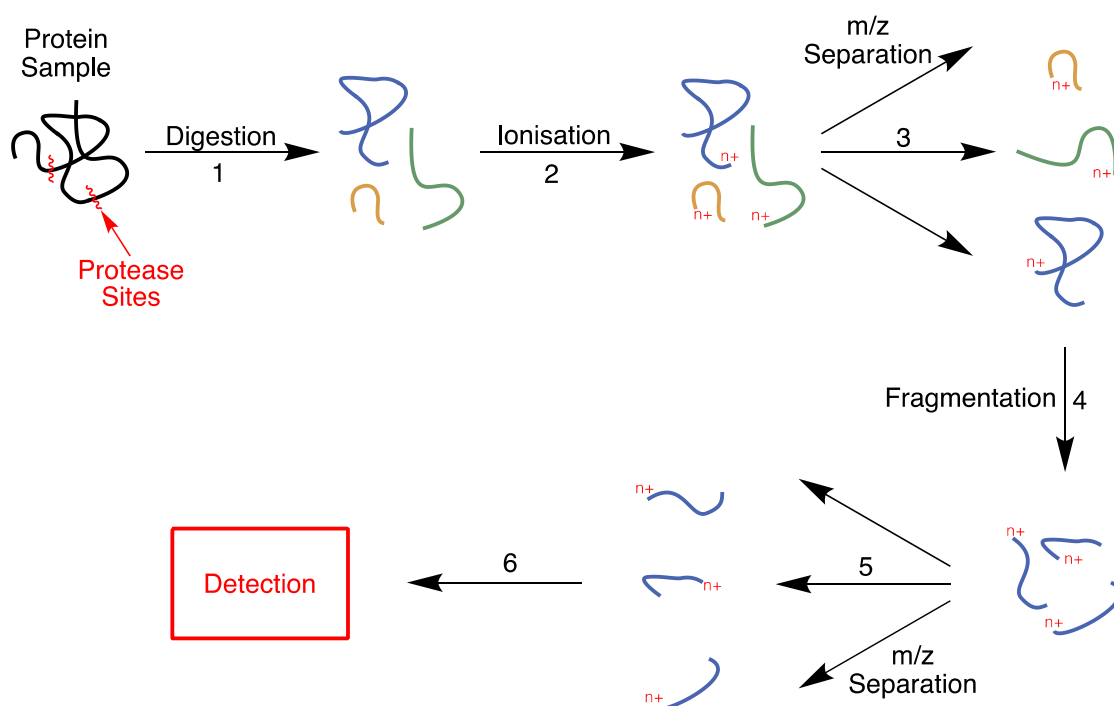


Figure 1.20: A bottom-up workflow of LC-MS/MS used to separate and identify proteins of interest in chemical proteomics experiments. The labelled proteins are digested into peptide chains (1) and ionised in the spectrometer for separation, where n^+ is a charged protein (2,3). The isolated peptides can then be fragmented and separated again (4,5) to analyse the fragments compositions (6).

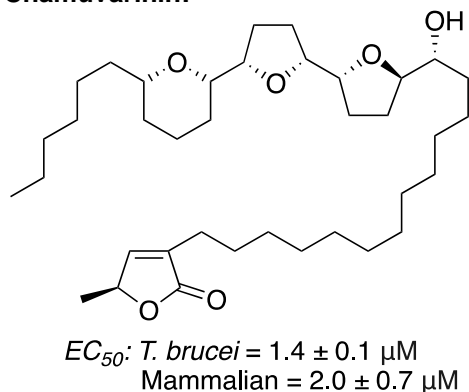
1.4.3. Functionalising Trypanocidal Compounds for Target Identification

Previously, chemical probes have successfully been applied to further develop the understanding of trypanosoma kinetoplasts, for example to explore the folate pathway^{135,136} as potential target for drug design. It is also a valuable technique for exploring the mode of action of trypanosoma inhibitors¹³⁷. Identification of the protein target can be used to aid further drug design and to optimise compound selectivity and potency to the target. Limitations in designing these chemical probes arise from the structural changes made to the initial active compound to incorporate an alkyne tag and warhead. The effects of these changes on the inhibitors binding affinity and reactivity are difficult to predict and may cause a reduction in activity, render the probe inactive, or change the protein target^{138,139}.

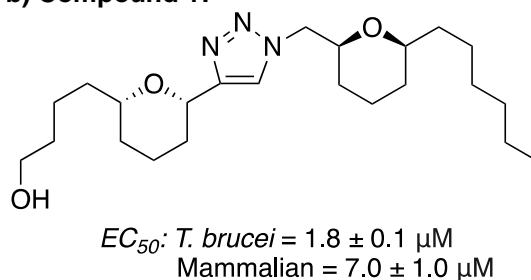
Previously, analysis of a species of medicinal plants, the Custard Apple Family, identified a potent natural-product inhibitor of *T. brucei*, chamuvarinin (**Figure 1.21a**)^{140,141}. Simplified analogues were designed that maintained the compounds trypanocidal activity, based around a core 1,4-triazole structure, made via a copper catalysed click reaction. From this, compound 1 was identified which maintained its potency as an inhibitor of *T. brucei* and showed slightly reduced toxicity to mammalian cells (**Figure 1.21b**)¹⁴⁰. In order to explore the mode of action of compound 1, a bifunctional photoaffinity chemical probe was designed, 3 (**Figure 1.21d**). The probe incorporated a diazirine reaction group, to bind to the protein of interest, and an alkyne tag, to retrofit a fluorophore, cyanine5.5, or a biotin affinity tag, via the copper catalysed click reaction for analysis. Incorporation of these probe groups only had a small effect on the molecule's potency, suggesting the groups do not change the inhibitors mode of action. Compound 2 (**Figure 1.21c**) was used as a control, to confirm labelling by in-gel fluorescence resulting from the bound protein-probe-fluorophore complex and not non-selective sticking of the fluorophore to the target protein¹⁴⁰.

Compound 3 was used in a chemical proteomics experiment using *in vivo* pulse-chase photo affinity labelling. The compound was incubated with live cells that were immobilised on a surface before irradiation with a UV pulse to activate the carbene to react with the bound proteins. A subsequent copper click reaction was used to functionalise Compound 3 with a fluorophore. Imaging of the cells via fluorescence microscopy showed that the inhibitors were reacting with proteins localised in the mitochondria of cells.

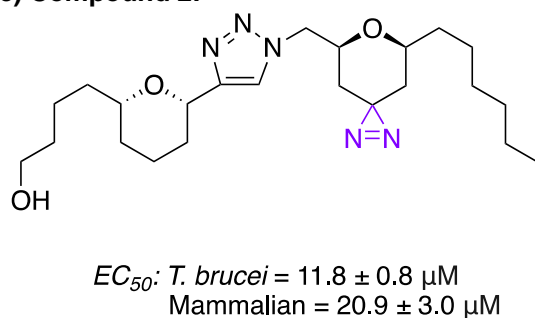
a) Chamuvarinin:



b) Compound 1:



c) Compound 2:



d) Compound 3:

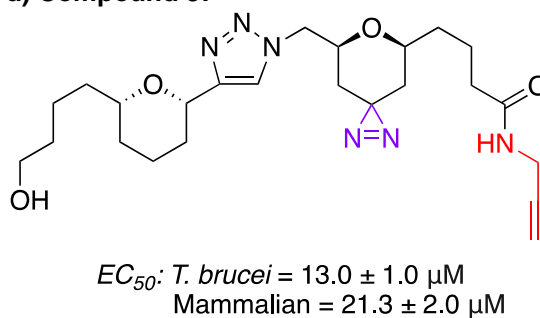


Figure 1.21: Exploring the mode of action of potent *T. brucei* inhibitors (**a**, **b**), designing analogous chemical probes (**d**) to identify the proteins of interest. Showing the effect these changes had on the EC_{50} of the molecules against both parasite and human cell lines¹⁴⁰.

In another experiment, after incubation of Compound 3, the cells were lysed to extract proteins before a click reaction was carried out to incorporate either a fluorophore, for visualisation of the labelled proteins with SDS-PAGE, or an affinity tag via the alkyne group to extract the proteins of interest. A biotin-azide tag was reacted with the probe-protein complex to bind to streptavidin beads, to identify the bound proteins by mass spectrometry. A control reaction without the probe present enabled the non-specific binding proteins to streptavidin to be identified, so they can be ignored from the probe screen. Analysis of the probe-bound species identified 18 proteins, two of which are found in the parasite's mitochondria, binding to both the α and β subunits of the F_0F_1

ATP synthase. Inhibition of these protein functions caused an interruption in oxidation phosphorylation, decreasing the formation of ATP in the parasite. The ATP reaction is essential in both replicating amastigotes in infected cells and trypomastigotes in the blood stream during secondary infection (*Figure 1.2, p2*), so can provide a promising drug target. Characterising these proteins target sites can be used to optimise the selectivity and potency of the inhibitors to develop potential trypanocidal drug molecules.

1.5. Project Outline

This project aims to develop an approach to combine a diversity generating synthesis of electrophilic compounds with chemical proteomics to identify novel, anti-protozoan unnatural products, to be functionalised into chemical probes for target evaluation. The specific aims were to:

1. Develop a high-throughput method for synthesis of a target-agnostic compound library containing electrophilic warheads.
2. Screen the electrophilic library to identify anti-trypanosomal compounds in a phenotypic screen and profile their activity.
3. Design, synthesise and exploit fully functionalised electrophilic chemical probes for target identification.

1.5.1. Design and Synthesis of a Library of Covalent Inhibitors

Covalent inhibition is a highly useful, but underexplored area of drug design (*Section 1.3.2*). Here, a library of covalent compounds has been designed based around photo-redox chemistry⁴¹, configured for a high-throughput methodology, aiming to test the compatibility of this chemistry with electrophilic warheads (*Figure 1.22*). These reactions were screened to identify intermolecular product formation, and successful reactions taken forward for purification. The library is designed to be target agnostic, meaning that the compounds created can be screened against several cell lines and phenotypes.

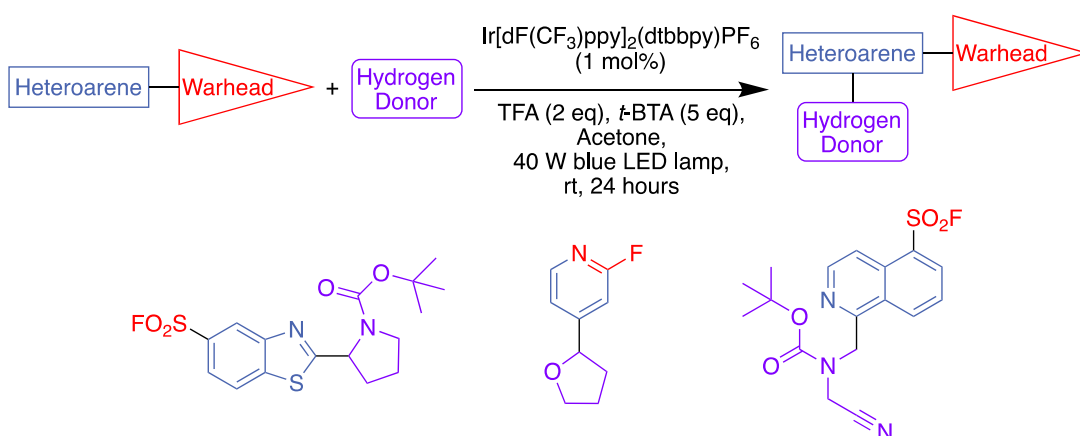


Figure 1.22: Schematic representation of the photo-redox reaction between a heteroarene (blue), functionalised with a reactive warhead (red) and a hydrogen donor (purple), to form a covalent inhibitor. Three potential covalent inhibitors are given as examples⁴¹.

1.5.2. Phenotypic Discovery of Anti-trypanosomal Activity

In collaboration with the Smith group at the University of St. Andrews, a phenotypic assay was designed to screen the compound library against trypanosoma organelles based on a resazurin viability assay. AlamarBlue (resazurin) is reduced in cells by NADH (**Figure 1.23**). Live cells have a reducing environment, so the observed fluorescence is proportional to the number of living cells in the system. An active anti-parasitic compound will cause a reduced fluorescent readout, quantifying their activity against the known inhibitor, pentamidine, as the positive control¹⁴². The compound library was screened for activity against *T. brucei brucei*, along with a counter screen against human HeLa cells, following the same assay protocol, to gage the compounds selectivity as an anti-trypanosomal compound.

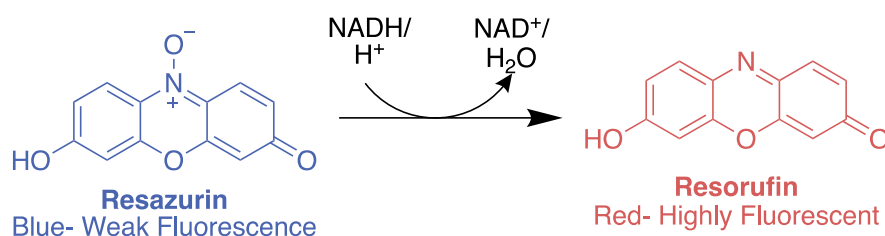


Figure 1.23: Schematic representation of the phenotypic resazurin based viability assay¹⁴².

Working in parallel to this, the reactivity of these electrophilic compounds across the *T. brucei* and HeLa cell proteome was profiled in cell lysate, by competition with a series of broad-spectrum reactive probes. Visualised by in-gel fluorescence to highlight reactive trends in the compound series and to identify selectivity for nucleophilic amino acid side chains in proteins.

1.5.3. Synthesis of Functionalised Electrophilic Probes

Analogous chemical probes were then designed and synthesised based around the anti-trypanosomal compounds identified in these phenotypic screens. These probes were designed to identify the mode of action and protein targets of the active compounds (**Figure 1.24**). This illustrative example outlines how chemical probes were designed, based around the structures of active compounds. Initially, sites suitable for alkyne addition were identified (**1**), aiming to modify functional groups that are non-essential for the compounds activity. The generated probes were then screened in the phenotypic assay to explore the effect of these structural changes on the inhibitor's anti-trypanosomal activity (**2**). An investigation into their protein targets and mode of action was then

initiated, by attachment of a fluorophore (3) via a click reaction to visualise protein labelling in cell lysate using SDS-PAGE. An affinity tag can also be incorporated (4), to pull-down and characterise the bound proteins via LC-MS/MS.

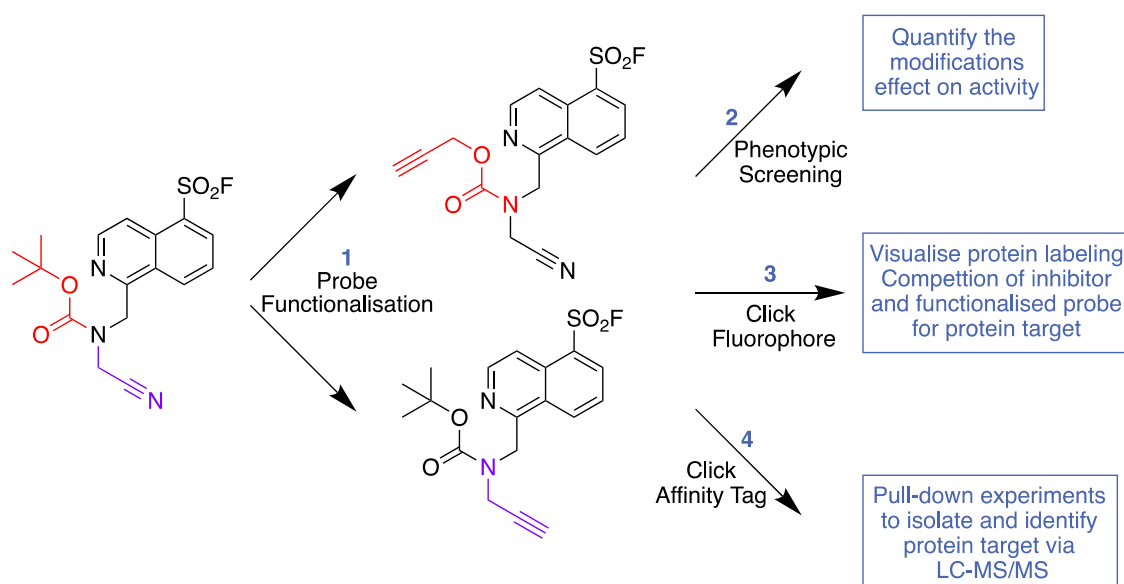


Figure 1.24: An illustrative example of chemical probe design and applications, functionalised from covalent inhibitors (1). These new compounds will be screened for activity in the phenotypic assay (3) to see if activity is conserved, then using chemical proteomics to identify the protein target (4, 5).

2. Design and Synthesis of a Diverse Library of Electrophilic Ligands

2.1. Generating a Library of Electrophilic Ligands

Photoredox mediated dehydrogenative couplings can be used to react a large range of hetarenes with hydrogen donor substrates in a high-throughput format. Here, the potential for this chemistry to synthesis a diverse library of reactive ligands containing electrophilic warheads has been explored.

2.1.1. Selection and Synthesis of Functionalised Hetarenes

A set of eight hetarenes was identified, six containing sulfonyl fluoride warheads (**HA1-6**), and two $S_N(\text{Ar})$ warheads (**HA7-8**). The sulfonyl fluorides were inspired by commercially available precursors, synthesised from the sulfonyl chloride, or in the case of hetarene 4 (**HA4**), from the sulfonic acid (**Figure 2.1a**). The sulfonic acid was dissolved in thionyl chloride (18 eq) with DMF (0.3 eq) and reaction sealed in a crimped vial, heating to reflux for 4 hours. The sulfonyl chloride (**11**) precipitated from solution as a white solid, so was collected *via* filtration and washed¹⁴³. Analysis by ^1H (500 MHz) and ^{13}C (125 MHz) NMR showed sufficient purify to be used in the next reaction without further purification. The sulfonyl chloride, and other commercially available sulfonyl chlorides were treated with KHF_2 in a biphasic reaction with water and acetonitrile overnight to yield the sulfonyl fluoride as a colourless solid, after a series of basic workups to extract residual sulfonyl chloride and salts¹⁴⁴ (**Figure 2.1b**). Hetarene 2, 7 and 8 (**HA2**, **HA7** and **HA8**) were commercially available (**Figure 2.1c**).

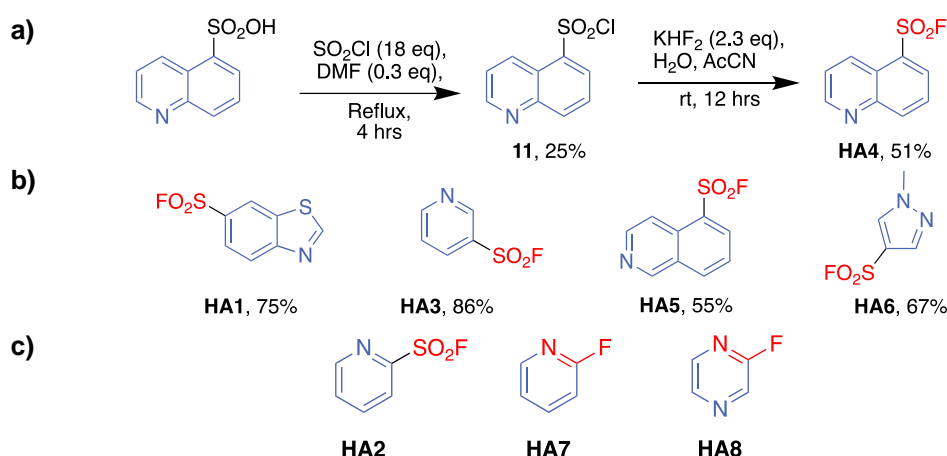


Figure 2.1: Reaction conditions to synthesise sulfonyl fluorides from sulfonic acids. Using quinoline-3-sulfonic acid as an example (a), along with the sulfonyl fluorides generated from sulfonyl chloride precursors (b)^{143,144}, along with the commercially available hetarenes (c).

2.1.2. Identification of Viable Hetarene Substrates

The functionalised hetarenes previously synthesised (Section 2.1.1) were screened for viability in the dehydrogenative coupling reaction. Screening 6 sulfonyl fluoride containing hetarenes, along with two $S_N(\text{Ar})$ warheads, chosen for their commercial availability and ease to explore potential scope of compatible warheads. An efficient dehydrogenative coupling reaction involves benzothiazole and *N*-Boc-pyrrolidine, combining the most reactive hetarene and substrate to produce a good yield of the coupled product (Section 1.2.2, Figure 1.5, p9)⁴¹. Because of this, *N*-Boc-pyrrolidine was used as a test hydrogen donor for the set of hetarenes (Figure 2.2), along with a control reaction with benzothiazole. These reactions were carried out on both a 1 mL (100 mmol) and a 100 μL (10 mmol) to compare their productivity across larger volumes, ensuring enough product could be generated for the library. The reaction mixtures were analysed by LC-MS and NMR, before purification of the those where product formation was observed by mass-directed HPLC.

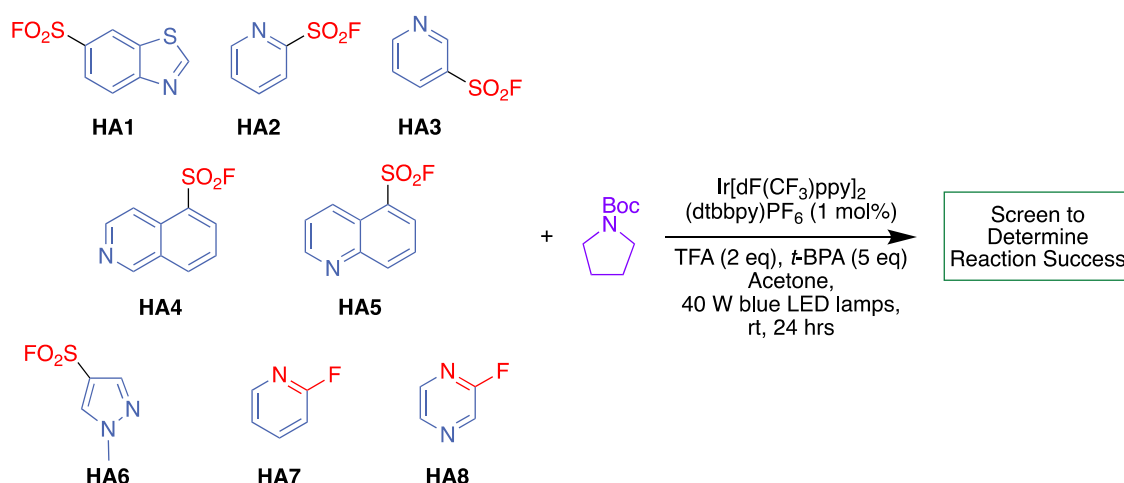


Figure 2.2: Screening to identify hetarenes compatible with photoredox chemistry, against *N*-Boc-pyrrolidine as the model coupling agent to determine reaction success by LC-MS and NMR⁴¹.

Initially stock solutions of the substrate, reagents and catalyst were prepared in acetone. The functionalised hetarenes and a benzothiazole control (20 μL , 0.5 M) were added to separate 1.5 mL glass vials, along with *N*-Boc-pyrrolidine (33.3 μL , 1.5 M), TFA (10 μL , 2 M), the iridium catalyst (10 μL , 10 mM) were added with TBPA (15.9 μL , 50% w/v) and acetone (10.8 μL). This gave final concentrations of hetarene (100 mM), hydrogen donor (500 mM), TFA (200 mM), catalyst (1 mM) and *t*-butyl peracetate (500 mM). This process was also carried out on a 10-fold higher scale, at a total volume of 1 mL. The

reaction vials were sealed with stirrer bars in and irradiated with a 390 nm Kessil Lamp whilst stirring in a fan cooled HepatoChem lightbox for 24 hours. The reaction mixtures were then concentrated for analysis.

An effective method to screen these reaction mixtures for success was required, to help streamline the synthetic protocol and efficiently build a library of electrophilic inhibitors. A combination of analytical techniques can be used to gain confidence in the success of these reactions. Initially, a LC-MS was carried out on the reaction mixtures, aiming to identify an intermolecular product between the hetarene and hydrogen donor $-H_2$, for mono- and di-substituted products (**Appendix B**). After the reaction mixtures have been evaporated to dryness, 1H NMRs (500 MHz) are carried out to determine success based on characteristic peaks, from the loss of an aromatic proton, as well as a novel characteristic peak forming 5.0–6.0 ppm, for the proton, alpha to the aromatic ring, often appearing as a broad doublet when rotameric (**Appendix B**).

The most useful method for analysing sulfonyl fluoride containing reactions is through ^{19}F NMR (565 MHz), due to their unusual chemical shift, between +65 – 70 ppm¹⁴⁵. The shifts of fluorine atoms are highly varied, depending on several conditions such as temperature and pH. TFA present in the reaction can protonate the hetarene, reducing the electron density around fluorine, to lower its chemical shift. TFA also reduces the solvents polarity, thus reducing fluorines electron density, lowering its shift¹⁴⁶. **Figure 2.3** shows how the chemical shift of sulfonyl fluorides can vary with the amount of acid present in the reaction. On a 1 mL scale, the photoredox reactions contain TFA (15.2 μ L, 200 mM), but an unknown amount of TFA is present in the crude mixtures once evaporated to dryness. To control for this, a sample of 6-benzothiazolesulfonyl fluoride, was dissolved in 600 μ L of deuterated chloroform and treated with varying concentrations of TFA from 330 mM, (pink), if no TFA evaporates (15.2 μ L) to no TFA (red). A clear trend can be observed (**Figure 2.3**) where the chemical shift reduces with increasing amounts of TFA. This creates an expected range for the sulfonyl fluoride starting material in the reaction mixture, between 67.45–67.75 ppm. When comparing this to a reaction mixture, it can be assumed that the starting material peak appears within this range, while any external peaks are predicted to be reaction products. The NMR's contained an ampoule of pure TFA to reference the spectra (-76.55 ppm) to allow for this comparison. Fluorine NMR also allows for an estimate conversation to assess the success of these reactions, based on the ratio between the starting material and product integrations.

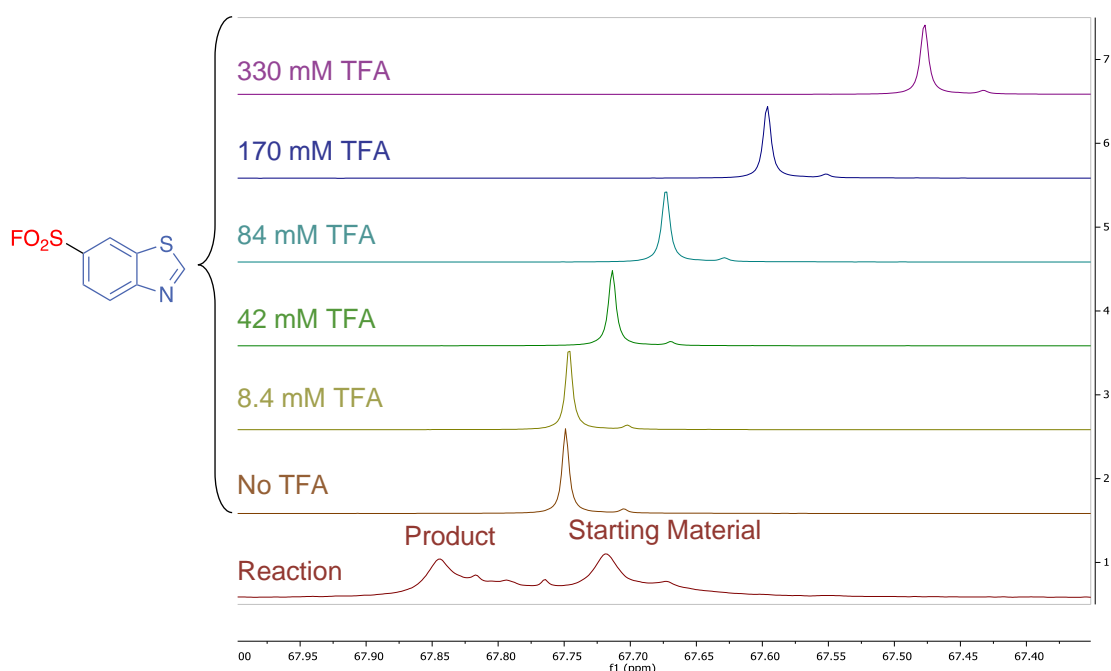


Figure 2.3: Variability in fluorine shift in the ^{19}F NMR of 6-benzothiazolesulfonyl fluoride (21.7 mg, 0.166 M) depending on TFA concentration. Compared to a crude reaction mixture of benzothiazole and *N*-Boc-pyrrolidine. Referenced against an ampoule of TFA at -76.55 ppm.

On analysis of these reactions (**Table 2.1**), three heteroarenes were found to react with *N*-Boc-pyrrolidine, **HA1**, **HA3** and **HA5**, showing clear product formation by LC-MS and NMR, illustrated by the reaction of **HA1** and *N*-Boc-pyrrolidine in **Appendix B**. Whereas the other heteraryl sulfonyl fluorides **HA2**, **4** and **6**, showed no product formation. The $\text{S}_{\text{N}}(\text{Ar})$ warheads, **HA7** and **8** showed new peaks weakly in both LC-MS and NMR compared to starting material. Purification was attempted but did not yield significant product for analysis. Cross-coupled products were isolated from the sulfonyl fluoride containing **HA1**, **HA3** and **HA5** reactions as well as the model test reaction between benzothiazole and *N*-Boc-pyrrolidine (**Figure 2.4**). The regioselectivity of these reactions were assigned by the loss of the distinctive aromatic protons in 500 MHz ^1H NMR, and confirmed by analysis of 2-D, COSY, HSQC and HMBC spectra. The reaction with **HA1** was isolated in a comparable yield to the model, showing the compatibility of these sulfonyl fluoride containing compounds with the photoredox chemistry. The isolated yield decreases significantly when moving away from the model in **HA3** and **HA5**, although this was to be expected, pyridine substrates are known to be less reactive for this chemistry⁴⁹, due to the ring system being less electron deficient, making them less reactive towards the hydrogen donor radical in the mechanism⁴¹.

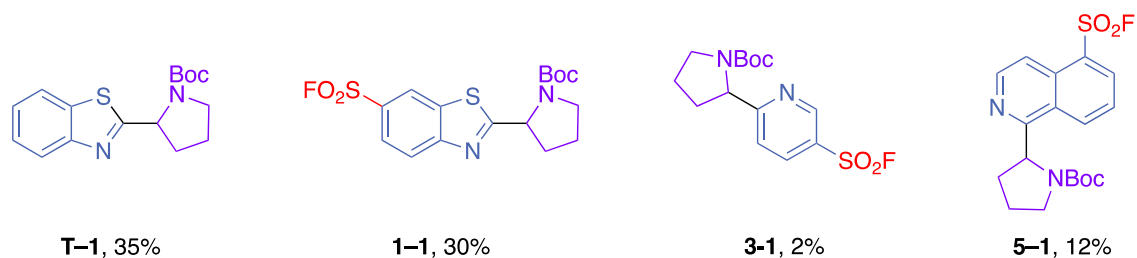
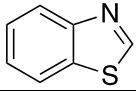
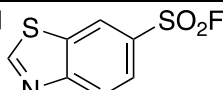
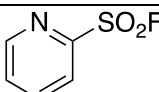
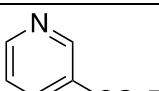
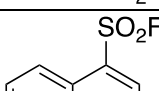
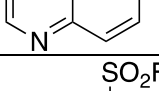
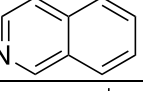
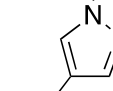
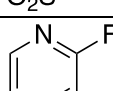


Figure 2.4: Isolated compounds from the test screen of hetaryl sulfonyl fluorides with a known substrate, *N*-Boc-pyrrolidine, showing the three hetarenes to be used in the array compared to the known reaction.

Isolating these compounds highlights the success and reliability of the reaction screening (**Table 2.1**) to identify reactions suitable for purification. A reaction mixture characterised as successful gave a clear product mass was identified by LC-MS $[HA + nHD - nH_2]^+$, where n was either one or two. Successful reactions also showed characteristic peaks in 1H NMR, through a new peak between 4 – 5 ppm, and removal of an aromatic proton as illustrated in **Appendix B**, as well as seeing novel peaks forming in ^{19}F NMR spectrums. From the fluorine NMR spectrum, an estimated conversion was gained by integration of the new peaks relative to starting material. This tended to overestimate conversion compared to the isolated yields, likely due to loss of material during analysis and purifications, as well as impurities in the crude mixtures. Three electrophilic hetarenes, **HA1**, **HA3** and **HA5** performed successful couplings, and represent viable substrates for the library. With both reaction scales being successful (**Table 2.1**), the 1 mL scale will be used to generate sufficient product material, although a smaller scale is also productive, for example, if starting materials are precious.

Table 2.1: Screening of compatible hetarenes, functionalised with electrophilic warheads, against *N*-Boc-pyrrolidine as a model substrate on a 100 μ L and 1 mL scale, using LC-MS, ^1H and ^{19}F NMR.

*Conversion determined from starting material to product peaks ratio in ^{19}F NMR (565 MHz).

		100 μ L			1 mL				
		LC-MS	^1H NMR	^{19}F NMR	LC-MS	^1H NMR	^{19}F NMR	Conversion*	Isolated Yield
HAT		✓	✓	–	✓	✓	–	–	–
HA1		✓	✓	✓	✓	✓	✓	40%	30%
HA2		X	X	X	X	X	X	X	
HA3		✓	✓	✓	✓	✓	✓	30%	2%
HA4		?	X	X	X	X	X	X	
HA5		✓	✓	X	✓	✓	✓	20%	12%
HA6		X	X	?	X	X	?	X	
HA7		?	✓	✓	?	✓	✓	–	
HA8		?	X	?	?	X	?	–	

LC-MS ✓: Clear peak of cross-coupled product mass identified
 ? : No or weak cross-coupled mass seen, no starting material found
 X: No cross-coupled mass, predominantly starting material

^1H NMR ✓: found the characteristic peak around 5 ppm and loss of an aromatic proton
 ? : New peaks identified but minor to starting material
 X: No new peaks seen

^{19}F NMR ✓: New distinct peak from that observed for the substrate in the presence of TFA
 ? : New peaks identified but minor to starting material
 X: No new peaks seen

pyrrolidine in DCM (0.4 M in respect to **HD1**) with Boc-anhydride (0.9 eq), catalysed by DMAP (0.1 eq) and triethylamine (1.1 eq) in an overnight reaction (**Figure 2.6a**). Pyrrolidine was also used to form a urea-based substrate (**HD20**), using CDI (1.1 eq) in water, to form a reactive carbonylimidazolide intermediate, before coupling with a secondary amine, 2-methoxy-*N*-methylethanamine (1.2 eq)¹⁴⁷. Additional reactions were carried out to form a series of carbamates using the corresponding acid chlorides¹⁴⁸, illustrated by the formation of **HD18**, (**Figure 2.6b**). The amine was dissolved in DCM (0.4 M), with triethylamine (1.2 eq), and cooled to 0 °C, before the acid chloride was added dropwise. The reaction was warmed to room temperature and stirred overnight. These amines were often HCl salts, so an additional equivalent of triethylamine was used. This procedure was followed to generate substrates **HD5**, **HD16**, **HD18** and **HD19** (**Figure 2.6c**). A final reaction used to protect a carboxylic acid precursor as a methyl ester (**HA17**)¹⁴⁹. The acid (1 M) was dissolved in methanol, cooled to 0 °C and reacted with thionyl chloride (1.3 eq) to form the acid chloride *in situ*. The activated acid reacts with methanol to form the methyl ester. Each of these substrates was purified via an aqueous workup, followed by column chromatography, before use in the reaction array.

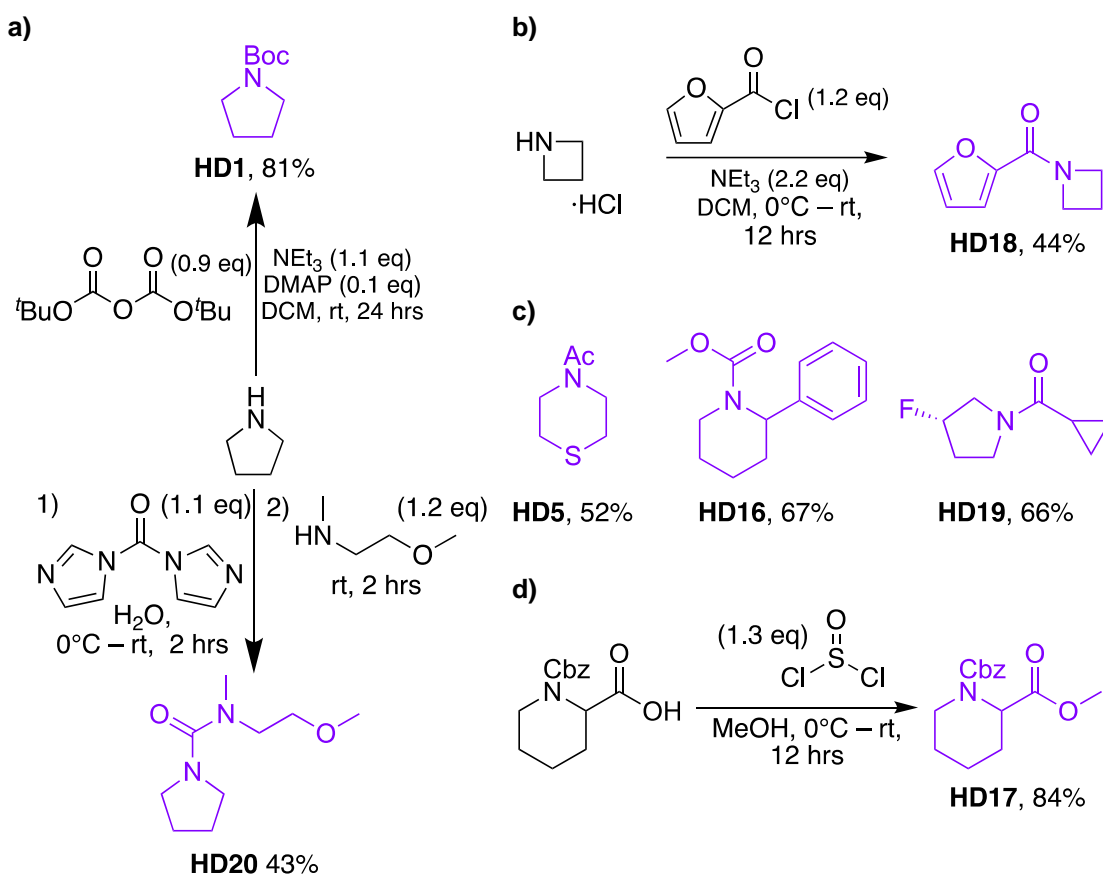


Figure 2.6: Preparation of the hydrogen donor substrates from secondary amine cores. Functionalised to form carbamates (**a** and **b**), ureas (**a**) and protect carboxylic acids (**d**)^{147–149}.

The hydrogen donor substrates were reacted with the electrophilic hetarenes in the photoredox reaction. Initially, reacting with **HA1** and screening for reaction success by MS and NMR allowed for viable hydrogen donors to be identified, and then reacted with subsequent hetarenes, whereas those that were not compatible with **HA1** were removed from future synthesis. The reactions were carried out on a 1 mL scale, following the procedure previously outlined (**Section 2.1.2**), and in accord to the standard protocol (**Section 5.2.2**). After the reaction was complete LC-MSs were run of the reaction, before concentrating the mixtures to run ^1H (500 MHz) and ^{19}F NMR (565 MHz) for analysis (**Table 2.2**). In cases where potential cross-coupled products were observed, the reaction mixtures were purified by mass directed HPLC.

Table 2.2: Summary of analysis and purifications of the compound library. Reactions showing intermolecular product formation (green) by MS and NMR were taken forward to purify by HPLC-MS, while unsuccessful reactions are highlighted in red. Several reactions showed potential product formation (yellow), so a purification was also attempted. Structures of these isolated compounds can be found in *Figure 2.7*.

*Conversion determined from starting material to product peaks ratio in ^{19}F NMR (565 MHz).

Combination		Reaction Success			Purification		
Hetero-arene	Hydrogen Donor	MS	^1H NMR	^{19}F NMR	Conversion*	Product	Isolated Yield
HAT	HD1	✓	✓	–	–	T-1	32%
HA1	HD1	✓	✓	✓	40%	1-1	30%
	HD2	✓	✓	✓	15% 25%	1-2a 1-2b	5% 13%
	HD3	✓	✓	✓	25% 25%	1-3a 1-3b	6% 7%
	HD4	✓	✓	✓	25%	1-4	6%
	HD5	X	X	X	–	–	–
	HD6	?	✓	✓	20%	1-6	10%
	HD7	X	X	X	–	–	–
	HD8	?	✓	✓	30%	1-8	16%
	HD9	X	X	?	–	–	–
	HD10	?	✓	✓	15%	1-10	15%
	HD11	X	X	X	–	–	–
	HD12	✓	✓	✓	20%	1-12	25%
	HD13	✓	✓	✓	20%	1-13	15%
	HD14	✓	✓	✓	30%	1-14	24%
	HD15	X	X	X	–	–	–
	HD16	✓	✓	✓	20%	1-16	6%
	HD17	✓	?	✓	30%	1-17	3%
	HD18	?	✓	?	20%	X	–
	HD19	?	✓	?	20%	X	–
	HD20	✓	✓	?	40%	1-20	18%

✓: Clear peak of cross-coupled product mass identified

LC-MS ? : No or weak cross-coupled mass seen, no starting material found

X: No cross-coupled mass, predominantly starting material

✓: found the characteristic peak around 5 ppm and loss of an aromatic proton

^1H NMR ? : New peaks identified but minor to starting material

X: No new peaks seen

✓: New distinct peak from that observed for the substrate in the presence of TFA

^{19}F NMR ? : New peaks identified but minor to starting material

X: No new peaks seen

Combination		Reaction success			Purification		
Hetero-arene	Hydrogen Donor	MS	¹ H NMR	¹⁹ F NMR	Conversion*	Product	Isolated Yield
HA3	HD1	✓	✓	✓	30%	3-1	2%
	HD2	✓	✓	✓	30%	3-2	23%
	HD3	✓	✓	✓	20% 25%	3-3	11%
	HD4	✓	?	✓	15%	3-4	9%
	HD6	✓	✓	✓	10%	3-6	4%
	HD8	✓	✓	?	10% 20% 5%	3-8a 3-8b 3-8c	8% 17% 1%
	HD10	✓	✓	✓	30% 40%	3-10a 3-10b	11% 10%
	HD12	X	?	?	–	–	–
	HD13	X	?	X	–	–	–
	HD14	?	X	X	–	–	–
	HD16	X	?	?	–	–	–
	HD17	X	X	X	–	–	–
	HD18	?	X	?	–	–	–
	HD19	?	X	X	–	–	–
HD20	?	?	?	–	–	–	
HA5	HD1	✓	✓	✓	20%	5-1	12%
	HD2	✓	✓	✓	15%	5-2	2%
	HD3	✓	✓	✓	20% 15%	5-3a 5-3b	13% 12%
	HD4	✓	✓	✓	20%	5-4	11%
	HD6	✓	?	X	–	–	–
	HD8	✓	✓	✓	20%	5-8	22%
	HD10	✓	✓	✓	20% 10%	5-10a 5-10b	9% 3%
	HD12	X	X	X	–	–	–
	HD13	✓	?	X	15%		8%
	HD14	X	X	?	–	–	–
	HD16	✓	✓	?	5%	5-16	1%
	HD17	✓	✓	✓	20%	5-17	7%
	HD18	✓	?	✓	25%	5-18	16%
	HD19	✓	?	?	5% 5%	5-19a 5-19b	3% 5%
HD20	X	?	X	–	–	–	

From these reactions with **HA1**, 15 hydrogen donors showed potential product formation with LC-MS, ^1H (500 MHz) and ^{19}F NMR (565 MHz) NMR. These hydrogen donors were then used in reactions with **HA3** and **HA5**. Reaction purification was attempted on all mixtures that showed clear (green) and strong potential (yellow) for an intermolecular product formation (*Table 2.2*).

A Summary of the reaction and purification success can be seen in *Table 2.3* to compare the three hetarenes. **HA1** was shown to be the most reactive hetarene, with clear product formation with 13 substrates, observing the cross-coupled mass in LC-MS and new peaks forming clearly in NMR, two additional reactions showed potential product formation, with weak peaks seen in LC-MS and NMR compared to the starting materials. **HA3** was shown to be less reactive with this chemistry, with seven mixtures successfully purified after clear product formation is seen in NMR and LC-MS. This was expected due to the lower reactivity seen from **HA3** with *N*-Boc-pyrrolidine (**HD1**). Finally, **HA5** was seen to be relatively compatible with the chemistry, with 12 reactions purified to yield cross-coupled products. Several of these reactions produced multiple products, either as regioisomers (e.g., **1-2a**, **1-2b**), diastereomers (e.g., **1-3a**, **1-3b**) or combinations of mono- and di- substitution (e.g., **3-8a**, **3-8b**, **3-8c**). outlining their structures in *Figure 2.7*.

In total, the array contained 61 potential reaction combinations, 51 reactions were carried out after screening with **HA1** removed 5 incompatible hydrogen donors. Analytical screening (*Table 2.2*, *Table 2.3*) found 30 reactions with clear product formation and an 9 that showed potential. On purification of these reaction mixtures by HPLC-MS, 33 of the 39 reactions successfully yielded products to isolate 39 electrophilic compounds plus the control compound (*Figure 2.7*), after several reactions formed multiple products.

Table 2.3: Summary of hydrogen donor reactivity against the three hetarenes used to build up the compound library.

	Reaction success by NMR and MS	Reaction success by NMR or MS	Reactions successfully Purified	Total products isolated
HA1	13 / 20	2 / 20	13 / 15	15
HA3	7 / 15	3 / 15	7 / 10	10
HA5	9 / 15	4 / 15	12 / 13	14
Total	29 / 50	9 / 50	32 / 38	39

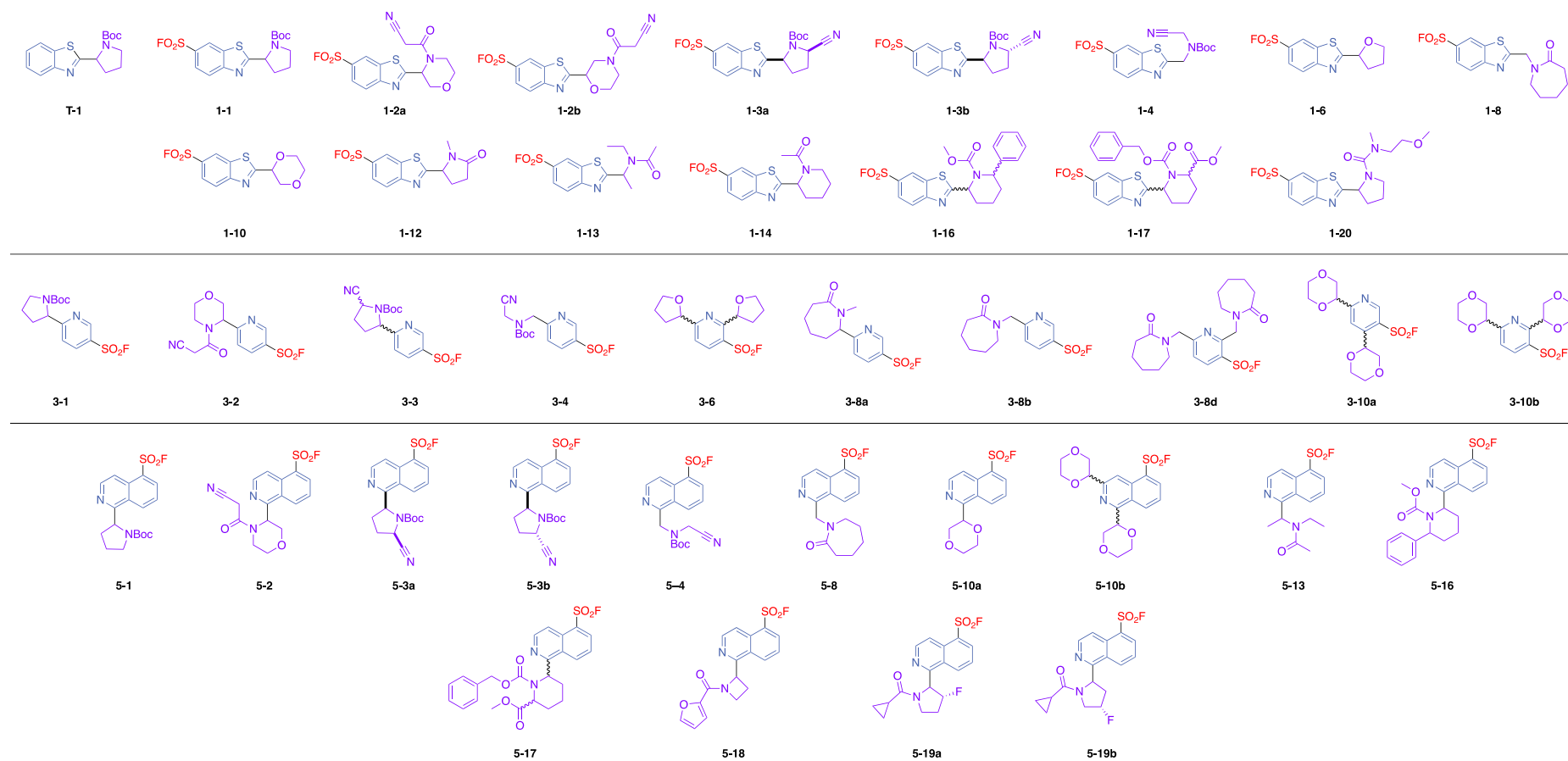


Figure 2.7: Covalent library of 40 compounds, formed in the dehydrogenative coupling reaction between sulfonyl fluoride (red) containing hetarenes (blue) and a diverse set of hydrogen donor compounds (purple)⁴¹, and purified by Mass directed HPLC.

Reaction screening and isolated yields are shown in **Table 2.2**.

2.2. Compound Screening Against Trypanosome Kinetoplasts

The library of covalent compounds containing reactive sulfonyl fluoride warheads was screened in a phenotypic assay against *T. brucei brucei*⁹. These phenotypic screens were carried out by Will Mosedale of the Smith group in St. Andrews.

2.2.1. Initial Identification of Active Compounds

An initial activity test was carried out on the three hetarene cores used in the library, along with a control compound, phenylmethylsulphonyl fluoride, PMSF, a sulfonyl fluoride protease inhibitor with known activity against *T. brucei*^{101,150}. This was included to gain an activity baseline and demonstrate how functionalising these cores via dehydrogenative coupling can influence their activity. These compounds were screened against *T. brucei brucei* in quadruplicate in a 10-point screen at final concentrations between 200 – 0.4 μM via a two-fold dilution in a resazurin based, viability assay (**Figure 1.23, p37**). The compounds were incubated for 66 hours before resazurin was added and the fluorescence recorded after a total of 72 hours. The hetarenes were shown to have limited activity against the parasites, with EC_{50} values greater than 100 μM (**Figure 2.8**). From this, library screening at 100 μM can identify compounds where activity is improved by functionalisation of the inactive core.

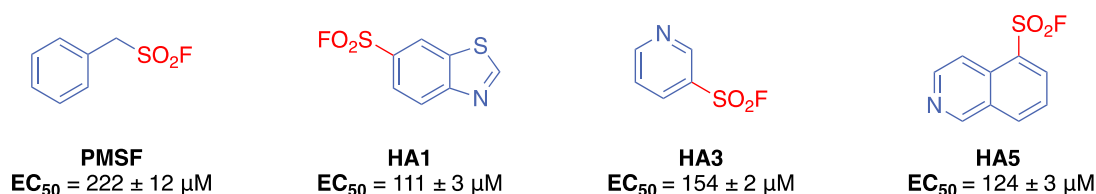


Figure 2.8: EC_{50} values of the hetarene cores screened against *T. brucei brucei* to identify an appropriate screening concentration for the compound library. The dose response curves are shown in **Appendix C**.

Based on this, the complete compound library was screened for activity against *T. brucei brucei* to identify compounds with significant activity over the hetarene cores for further investigation. Stock solutions were prepared in DMSO (20 mM) to be screened in the phenotypic assay. A 10-point, 2-fold serial dilution was carried out for screening at final concentrations between concentrations of 100 – 0.1 μM with 0.5% DMSO. These experiments were carried out as a single replicate to gain a provisional insight into the library's activity.

The fluorescence response of resorufin was normalised between the positive control, containing pentamidine (100 nM), and the negative control of DMSO (0.5%) to give cell viability as a percentage. The data is presented as a heat map (**Appendix D**). pEC₅₀ values were calculated to determine interesting hits (**Figure 2.9**) showing a range of activity from 100 μM (pEC₅₀ = 4.0) to sub-micromolar (pEC₅₀ > 6.0). An initial activity threshold was set for pEC₅₀'s greater 5.0, (10 μM), to allow interesting hits to be pursued in detail, to gain accurate EC₅₀ values and selectivity against mammalian cells. This threshold gave 12 interesting hits to investigate. These compounds contain varied structures across the hetarene cores and several hydrogen donor substrates, suggesting several of these compounds have unique protein targets causing their anti-trypanosomal activity.

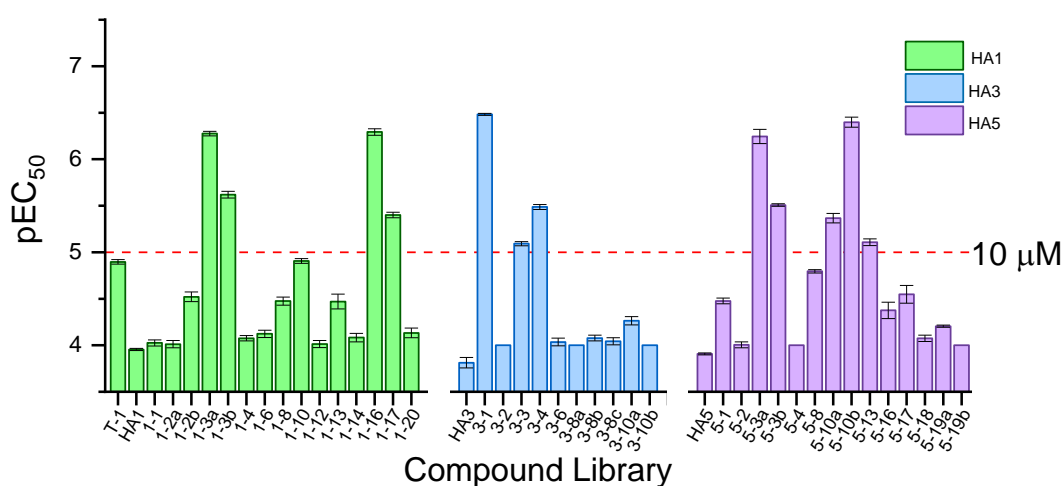


Figure 2.9: Initial screening data of the compound library against *T. brucei brucei* in a resazurin based viability assay. pEC₅₀ values have been plotted from the summarised normalised data (**Appendix D**) to determine interesting hits to investigate further. An activity threshold (red) was implemented, characterising a hit with a sub-10 μM activity, identifying hits across the three hetarene cores, HA1 (green), HA3 (blue) and HA5 (purple). Screening as a single replicate, the error is indicating a fitting error in the EC₅₀ calculation.

2.2.2. Validation of Potential Hit Compounds

The 12 most active compounds found in the initial screening (**Figure 2.9**) were taken for further investigation, validating their activity against *T. brucei brucei*. The compounds were screened in a 10-point serial dilution, screening over a narrower concentration range. The assay was carried out in quadruplicate to gain technical replicates, illustrated by compound **3-1** (**Figure 2.10**). The full screening data can be found in **Appendix E**.

The selectivity of these compounds was determined via a counter screen against a human cell line, HeLa, to examine whether these active compounds act specifically as trypanocidal compounds or show broad toxicity. This was carried out using a resazurin based viability assay. HeLa cells at around 15% confluency were incubated with an active compound at 37 °C for 66 hours, before adding resazurin for a final 6 hours and reading the resorufins fluorescence response, correlating to cell viability. Quadruplicate screening was carried out and the data was normalised between a positive (no cell) control, and a negative control (DMSO, 0.5%), to gain a dose response (**Figure 2.10**) for comparison to *T. brucei brucei* screening (**Appendix E**).

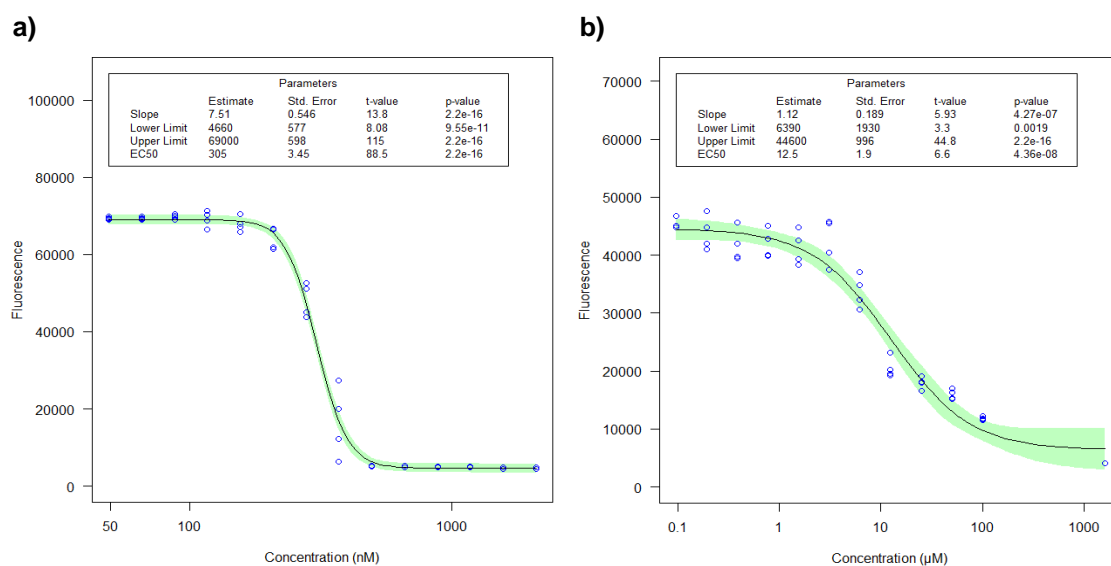


Figure 2.10: Comparison of toxicity for compound **3-1** against *T. brucei* (**a**) and HeLa (**b**) cells. Collected from a resazurin based, comparing their EC₅₀'s to identify selectivity for the parasites. The full screening data is shown in **Appendix E**.

This focused screen, and human counter screen was carried out on all 12 provisional hits with an activity lower than 10 μM (**Figure 2.11**), aiming to identify the most potent and selective compounds to pursue into further study while eliminating any compounds that showed broad toxicity to cells. Following this screen (**Figure 2.11a**), the activity threshold was reduced, and a hit characterised as having an EC₅₀ lower than 1 μM and at

least a 10-fold selectivity for *T. brucei* over human cells. From this, 5 active compounds were identified (**Figure 2.11b**) with sub-micromolar activities, showing between a 35 and 66-fold selectivity over human cells.

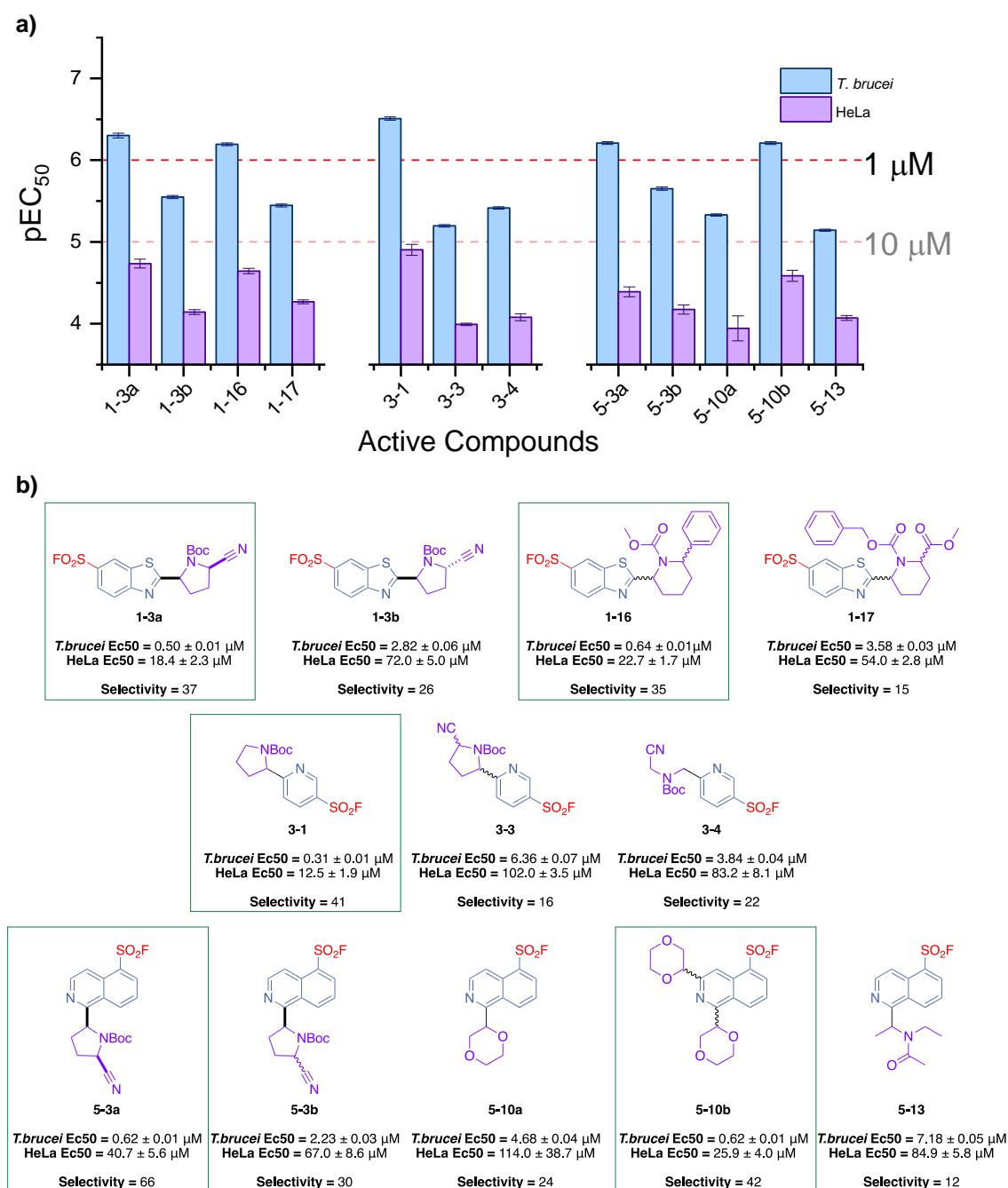


Figure 2.11: Full screening data of the 12 active compounds comparing *T. brucei brucei* and HeLa cells (**a**), identifying 5 compounds with sub-micromolar activity (**b**) with at least a 10-fold selectivity over human cells. The data of these assays are shown in **Appendix E**.

From this screen, the 5 active compounds with sub-micromolar activity, all show a significant selectivity for *T. brucei brucei* compared to the human, HeLa cell line. Decoration of hetarene cores using the photoredox coupling created compounds with a broad range of potencies against the parasites, identifying compounds with a greater than 100-fold improvement in activity compared to the parent compounds. Active compounds arise from each of the three hetarene cores and exhibit a broad range of chemical properties such as CLogP and heavy atom count (**Figure 2.12**), highlighting the potential for exploring multiple targets. A comparison of these properties shows the library explores a broad range of chemical space across all three hetarene cores, **HA1** (green), **HA3** (blue) and **HA5** (purple). Highlighting the trend of increasing activity with decoration, from initially inactive cores, to identify active compounds from each hetarene core, covering a range of lipophilicities.

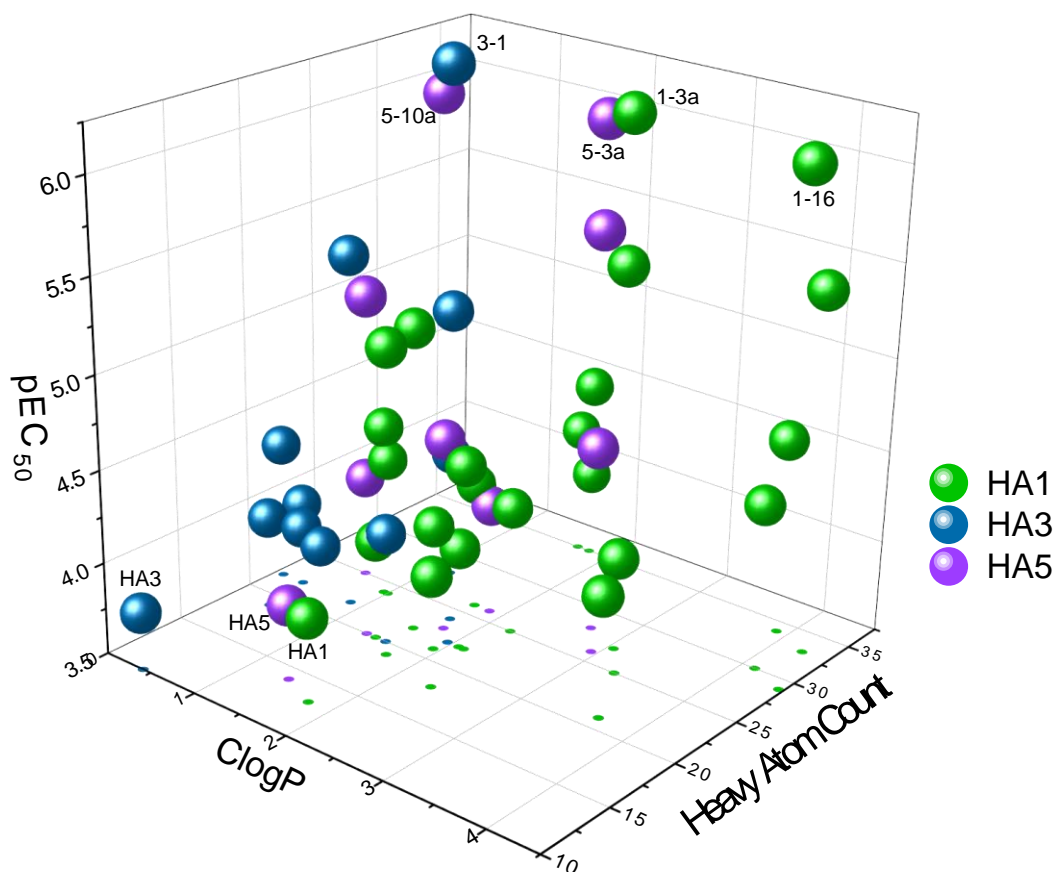


Figure 2.12: Plotting molecular properties of the compound library vs activity (pEC_{50}), relative to heavy atom count and CLogP, calculated with ChemAxon, at $pH = 7.4^{151}$.

The compound library was designed to be structurally diverse and so contain limited SAR between these active compounds. A key trend observed was a potency change between diastereomers of the hit compounds, illustrated by compounds **1-3a/b** and **5-3a/b**, suggesting there is a stereoselective binding interaction with their target proteins.

Whereas some of the library's most active compounds were screened as a mixture of diastereomers (**1-16**, **5-10b**), or enantiomers (**3-1**), so an improvement in binding affinity could be observed on purification and screening of these isolated compounds, separating diastereomer pairs using longer gradients on HPLC-MS or separating the enantiomers using chiral chromatography. Interestingly, the increase in activity shown between the di-substituted **5-10b**, compared to the mono substituted **5-10a**, this could be used to further functionalise other active compounds containing the **HA5** core along the 3- position of isoquinoline and could further improve their activity. For example, taking compounds **5-3a/b** and reacting with dioxane to functionalise into the 3-position of the isoquinoline core to explore this modifications effect on activity.

The SAR of these active compounds could be explored further with the design and synthesis of hit analogues, aiming to improve activity by identifying key areas to decorate into or avoid. These can also indicate sites for potential alkyne addition, without disrupting the compounds activity, to create fully functionalised covalent probes for use in target identification.

2.2.3. Potential α -Nitrile Electrophiles, a Second Covalent Warhead

A common feature of these hit compounds was the presence of an α -nitrile group, occurring in 6 of the 12 actives. This group could be forming important interactions within the protein binding site that help promote sulfonyl fluoride reactivity, but there is also precedent for these groups to react covalently themselves (**Section 1.3.2**), thus potentially functionalising these compounds with two warheads.

The α -nitrile group could act as a stable leaving group, reacting via [1,2]-elimination to form a reactive iminium that reacts with a nucleophilic residue. This route is unlikely due to the carbamate protecting group delocalising the lone pair and would require an initial deprotection to occur. Alternatively, α -nitriles have been shown to react as reversible electrophiles^{85,106}. This was investigated by further analysis of the pyrrolidine-based benzothiazole structures from the compound library (**Figure 2.13**), highlighting the nitrile groups (purple). An additional compound was synthesised, **T-3**, by reacting benzothiazole, **HAT**, with *N*-Boc-2-cyanopyrrolidine, **HD3** using the photoredox chemistry, to explore the effect of both the sulfonyl fluoride and α -nitrile functionality has on the compound's activity.

Compounds in this family without an α -nitrile (**T-1**, **1-1**) show limited/ no activity for the parasites but including the nitrile group (**1-3a/b**) creates some of the library's most potent hits. This activity is retained in the control compound, **T-3**, when screened as a mixture of diastereomers, and has a significantly improved selectivity for the parasites compared to the sulfonyl fluoride containing analogues. This shows that the α -nitrile is not just acting as an important directing group for the compound's reactivity via the sulfonyl fluoride and could be reacting covalently with the protein target. This will be investigated further in **Chapter 3**, with chemical proteomics.

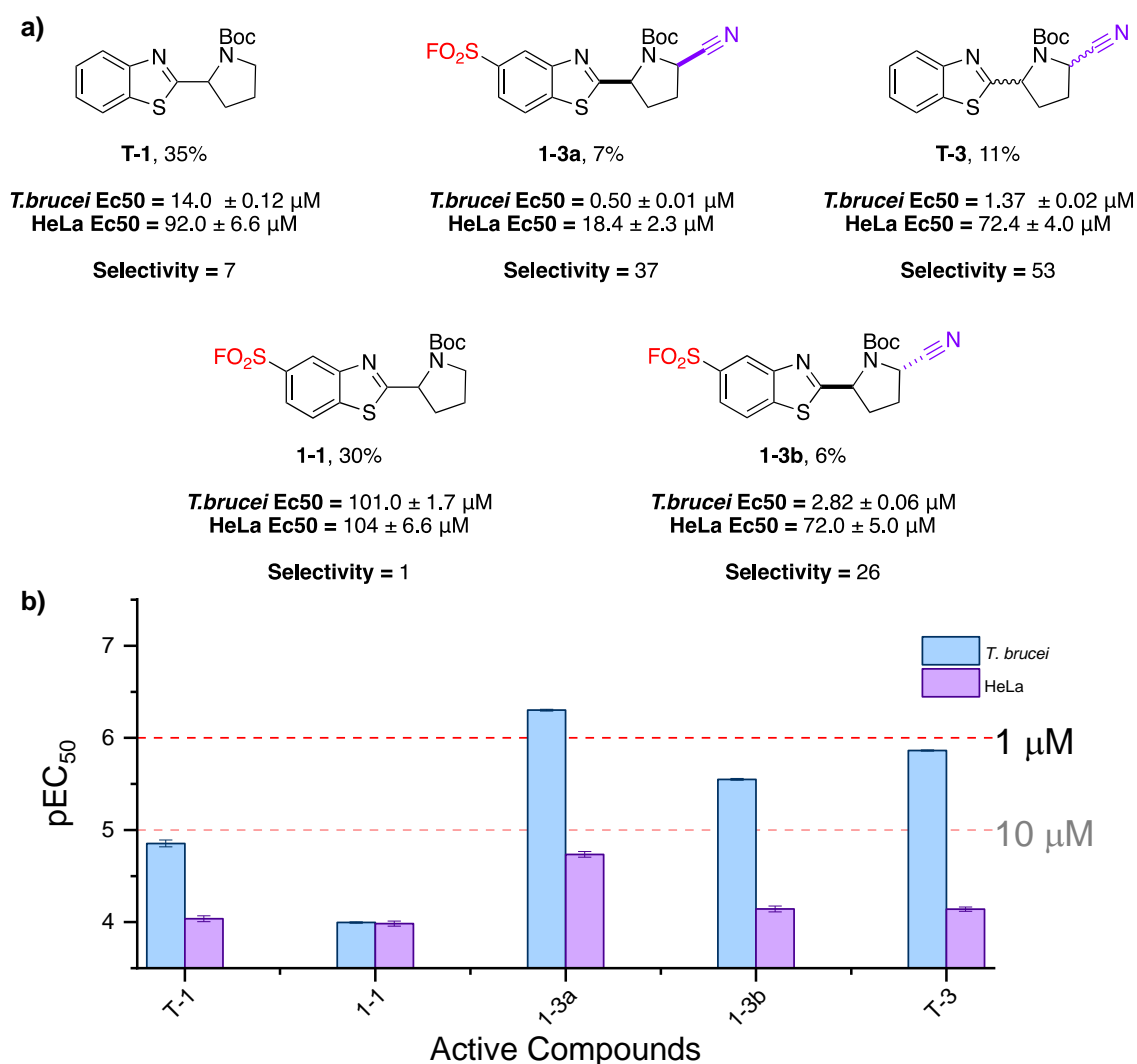


Figure 2.13: Comparison of the benzothiazole-pyrrolidine compound family, highlighting the effects of α -nitrile groups (purple) and sulfonyl fluorides (red) on the compounds E_{c50} 's (**a**) and pEC_{50} 's (**b**).

2.3. Conclusion of Covalent Library Generation

A diverse library of covalently functionalised compounds was designed and synthesised, aiming to better explore chemical space compared to traditional covalent libraries^{46,48}.

This library was generated using a dehydrogenative photocoupling to functionalise heteroarene cores, containing reactive warheads with a series of diverse hydrogen donating substrates.

Using a workflow designed to screen the crude reaction mixtures by LC-MS, ^1H NMR and ^{19}F NMR, successful reactions were identified for purification by HPLC-MS (**Table 2.2, p48**). This created a high-throughput method to generate this compound library. This method was used to yield a library of 40 electrophilic ligands, including pairs of regioisomers, diastereomers and mono- and di-substituted products. The generated library contains a diverse range of functionalities to form interesting interactions with protein targets, creating potentially lead-like compounds, ranging in molecular weight from 300 – 450 da, allowing space for further decoration, and hit optimisation through additional rounds of screening. Each reaction that showed significant product formation by LC-MS and NMR was successfully purified to yield an intermolecular product. Of the 9 reaction mixtures where potential product formation was seen, as weak signals in both NMR and LC-LS, only 3 were purified successfully. In future, the screening procedure could be made stricter, only purifying reactions where a clear product formation is shown in LC-MS and NMR, could improve the efficiency of library generation.

The compound library was screened against *T. brucei brucei* parasites at St. Andrews initially by a 10-point serial dilution as a single replicate. An initial activity threshold of 10 μM was identified, identifying compounds with similar activities to existing anti-trypansomal activity^{15,16}, leading to 12 compounds been taken forward for further investigation. A full screen in quadruplicate against the parasites was carried out against these 12 compounds, as well as a counter screen against human, HeLa cells to assess broad toxicity. Five potent and selective compounds were identified with a sub-micromolar activity, and at least a 30-fold selectivity over human cells (**Figure 2.14**). These compounds can be taken forward, for mode of action studies using chemical proteomics. Screening of these compounds resulted in the identification of α -nitrile functional groups as a potential second covalent warhead, appearing in six of the 12 active compounds, which can be investigated further using chemical proteomics.

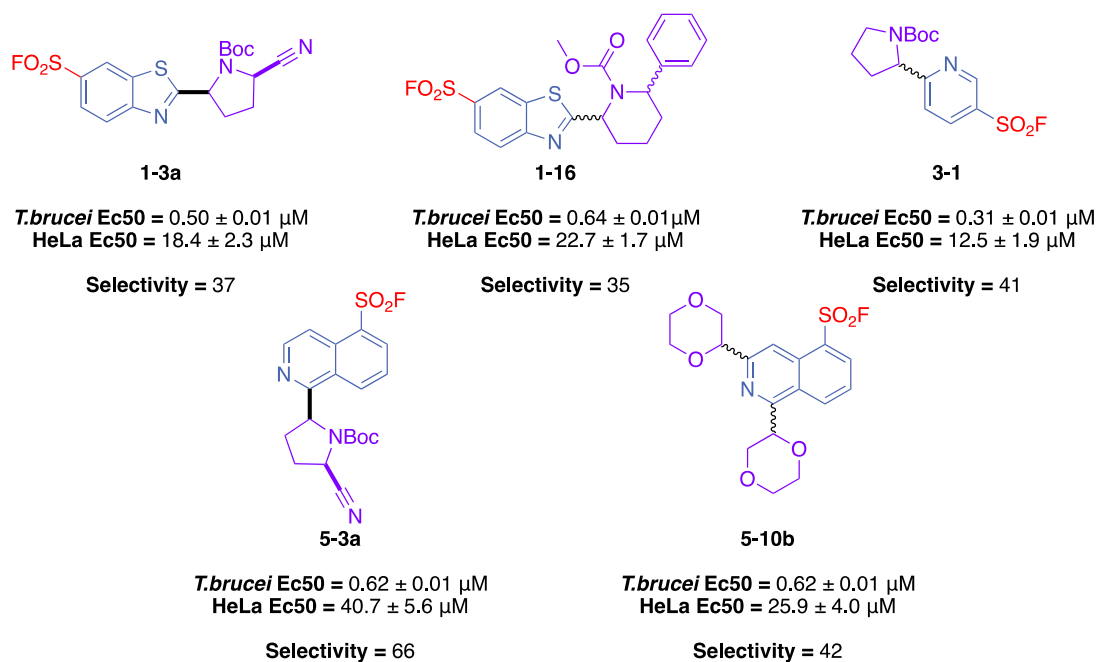


Figure 2.14: The five active compounds identified in the library screening, each with sub-micromolar activity, and at least a 30-fold selectivity over human, HeLa cells.

The library was generated around sulfonyl fluoride warheads due to a known activity against trypanosomal parasites^{101–103} (Section 1.3.2a), but the resulting library was designed to be target agnostic by focusing on substrate diversity. This means the library could be screened against a variety of phenotypes. When performed alongside a counter screen to ensure selectivity for the chosen target.

3. Chemical Proteomics for Target Identification of Anti-Trypanosomal Compounds

3.1. Profiling the Reactivity of the Electrophilic Ligand Library

In **Chapter 2**, a library of sulfonyl fluoride-based compounds was synthesised and screened against *T. brucei brucei* in a phenotypic, cell viability assay to identify five compounds with sub-micromolar anti-trypanosomal activity. Here, we theorise that their bioactivity is caused by the covalent mechanism of the compound's electrophilic warheads when interacting with proteins. We aimed to identify the proteins these compounds engage, to deduce a potential mode of action that causes anti-trypanosomal activity.

Broad-spectrum electrophilic probes containing a reactive warhead and a tagging group (**Section 1.4.1**) can be used to label cell proteomes by reacting with activated amino acid sides chains^{54,56}, tuning their reactivity and amino acid specificity depending on the reactive warhead used⁵⁵ (**Table 1.5, p19**). These probe interactions can be visualised by in-gel fluorescence of fluorophore containing probes, or by quantification by mass spectrometry. When used in competition with the sulfonyl fluoride-based library, we can indirectly visualise protein labelling, building a unique competitive profile of the library compound, identifying key protein interactions that could be responsible for the compound's activity.

3.1.1. Synthesis of Broad-Spectrum Sulfonyl Fluoride probes

A series of sulfonyl fluoride-based probes were synthesised to broadly label cell proteomes. Sulfonyl fluorides are known to react with lysines, tyrosines⁹⁹, and potentially also serines and threonines^{98,105}. These broad-spectrum probes were used in competition with the electrophilic compounds prepared in (**Section 2.1.3**). Incubating these compounds with cell lysate, followed by the addition of a broad-spectrum probe to visualise labelling *via* in-gel fluorescence. Providing these probes label similar protein targets, the library compound can outcompete select bands, due to their more specific reactive nature to identify potential protein targets.

Initially, a sulfonyl fluoride-rhodamine probe was synthesised, based around commercially available 4-(2-aminoethyl)benzenesulfonyl fluoride, AEBSF, an aryl

sulfonyl fluoride, to mimic the reactivity of the ligand library. A functional fluorescent probe was formed via an amide coupling with 5(6)-carboxy-tetramethyl-rhodamine using Oxyma Pure and DIC (**Figure 3.1**). Carboxy tetramethyl rhodamine (2.2 eq) was dissolved in DCM with the coupling reagents to a concentration of 20 mM relative to the sulfonyl fluoride. AEBSF·HCl (1 eq) was added in one portion as the limiting reagent, to avoid over substitution to the rhodamine. The reaction was stirred at room temperature overnight in the dark and the product was observed by LC-MS, concentrated *in vacuo* and purified via mass-directed HPLC in a gradient of water – acetonitrile to yield the sulfonyl fluoride-rhodamine (**SF-RH**) probe, as a 50:50 mixture of the 5- and 6-regioisomers¹⁰⁵ (41%, 80% purity).

The reactivity of sulfonyl fluorides are known to be heavily templated¹⁵², relative to other electrophilic warheads; the reaction is slow so requires proximal binding to an reactive nucleophilic site to facilitate a reaction. This means that the structure of the probe can direct its reactivity and prevent an exploration of the full proteome. To mitigate this, two control probes (**SF-PEG-RH** and **SF-Alkyne**) were synthesised to limit the templating effect of the bulky rhodamine group on the sulfonyl fluoride's reactivity (**Figure 3.1**). The second probe, **SF-PEG-RH**, includes a PEG chain linker to separate the sulfonyl fluoride and rhodamine groups. Initially, AEBSF was coupled to Boc-NH-(PEG)-CO₂H (1 eq), via an amide coupling using oxyma pure (1.2 eq), DIC (1.2 eq), DIPEA (2.0 eq), dissolved in DCM (40 mM) in respect to AEBSF. The reaction was stirred overnight at room temperature until product formation was shown by LC-MS. The reaction was concentrated, and the crude mixture dissolved in a solution of 20% TFA in DCM (40 mM) and stirred for 1 hour, until deprotection of the Boc group was shown by LC-MS. The rhodamine group (2.2 eq) was attached by a final amide coupling following the procedure previously discussed, reacted in excess to avoid over substitution, and purified *via* mass-directed HPLC to afford the PEG containing probe, **SF-PEG-RH**, as a 50:50 mixture of regioisomers (41%, 80% purity). A final sulfonyl fluoride probe, was made to containing an alkyne tag, **SF-Alkyne**, for visualising proteins by attaching a fluorophore azide in the CuAAC reaction, removing functionality from the probe that could cause templating^{105,152}. This probe was also synthesised via an amide bond formation, between AEBSF and 6-hexynoic acid using the coupling agents Oxyma pure and DIC (**Figure 3.1**), to yield **SF-Alkyne** in a 30% yield. The three broad-spectrum probes were dissolved in DMSO to give master stock solutions (10 mM) for use in future experiments.

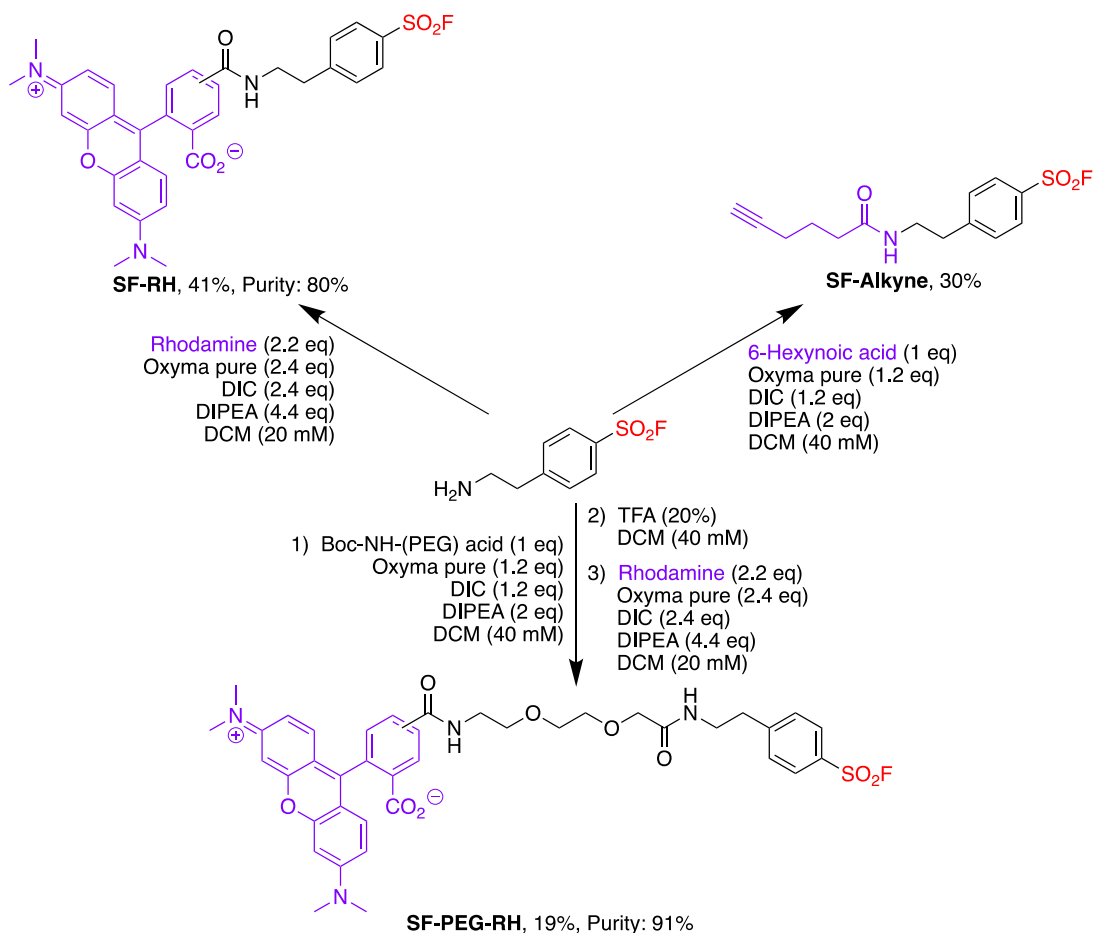


Figure 3.1: Synthesis of broad-spectrum sulfonyl fluoride reactive probes, using 5(6)-carboxy-tetramethyl-rhodamine dye or an alkyne linker, for broad proteome labelling¹⁰⁵.

The labelling profiles of these sulfonyl fluoride probes were compared on HeLa cell lysate (**Figure 3.2**). Cell lysate was prepared from a confluent plate of HeLa cells, washed with PBS (pH = 7.4), and scraped to detach from the surface and lysed by sonication. The suspension was centrifuged to pellet whole cells, and the supernatant retained for proteome-labelling experiments. The protein concentration of the lysate was determined by DC assay¹⁵³, and aliquots of lysate (100 μ g) were snap-frozen and stored at -80 °C for future use to avoid freeze-thaw cycles. Protease inhibitors were omitted from lysate preparation due to the broad reactivity of sulfonyl fluorides to several activity amino acids. Additional experimentation should be carried out to test each protease inhibitor used in standard cocktails to identify those that do not compete with the reactivity probes and could be included to increase lysate stability .

The labelling profile of these three broad-spectrum sulfonyl fluoride probes was visualised with gel electrophoresis. Due to the known instability of sulfonyl fluorides reacting with serine adducts^{98,105}, a series of optimised conditions were explored to visualise sulfonyl fluoride labelling of serine proteases in research projects carried out by Sanya Hussain and Alfie Doherty. This work, not shown here, illustrated the susceptibility of these adducts to thiol-based reducing agents such as DTT, as well as sample boiling. In order to mitigate this for future experiments, TCEP was used as a reducing agent and samples were not boiled prior to gel loading. But this preliminary data requires further validation and optimisation to improve sulfonyl fluoride-serine stability.

Each of the sulfonyl fluoride-based probes were incubated individually with HeLa cell lysate (25 μ g) at a final probe concentration of 10 μ M, adjusted to 1 mg/mL with PBS (pH = 7.4) at a final DMSO concentration of 1%. The reactions were incubated with shaking at room temperature for 30 minutes. A CuAAC reaction was carried out on the alkyne containing probe (**SF-Alkyne**) through incubation with a mixture of click reagents, containing a final concentration of rhodamine azide (100 μ M), CuSO₄ (1 mM), TCEP (1 mM) and TBTA (100 μ M) for one hour, following the procedure outlined in **Section 5.4.4**. After these incubations, the click reaction was quenched with EDTA (10 mM), and the reactions precipitated in acetone overnight to remove excess probe and reagents before being resuspended for gel electrophoresis with 2% SDS and 2 \times sample loading buffer (**SLB**) using TCEP (200 mM final concentration) as the reducing agent. 10 μ g of each sample was loaded onto a 12% SDS-PAGE gel to compare labelling profile of the three broad spectrum probes using in-gel fluorescence scanning (**Figure 3.2a**).

Comparing the three broad-spectrum probes (**Figure 3.2a**) shows a strong difference in their labelling intensity. The short linker rhodamine probe (**SF-RH**) shows significantly stronger labelling, likely due to the templating effect of the rhodamine group. Rhodamine is able to form strong protein interactions from electrostatic interactions, hydrogen bonding and π - π stacking, bringing the sulfonyl fluoride into the proximity of active nucleophiles to react. This is evidenced by the weaker labelling of the longer rhodamine probe (**SF-PEG-RH**), where rhodamine presumably has less of an influence on binding, and with the alkyne containing probe, **SF-Alkyne**. Without these stabilising interactions from rhodamine to enhance binding, these probes are less reactive with a weaker fluorescent response. Manually adjusting the image contrast of each probe (**Figure 3.2b**)

allows for a better comparison of the three probes, having high similarity in their labelling profiles, suggesting they hit similar protein targets, particularly the two rhodamine containing probes, highlighting the influence of bulky templating groups on the probe's selectivity.

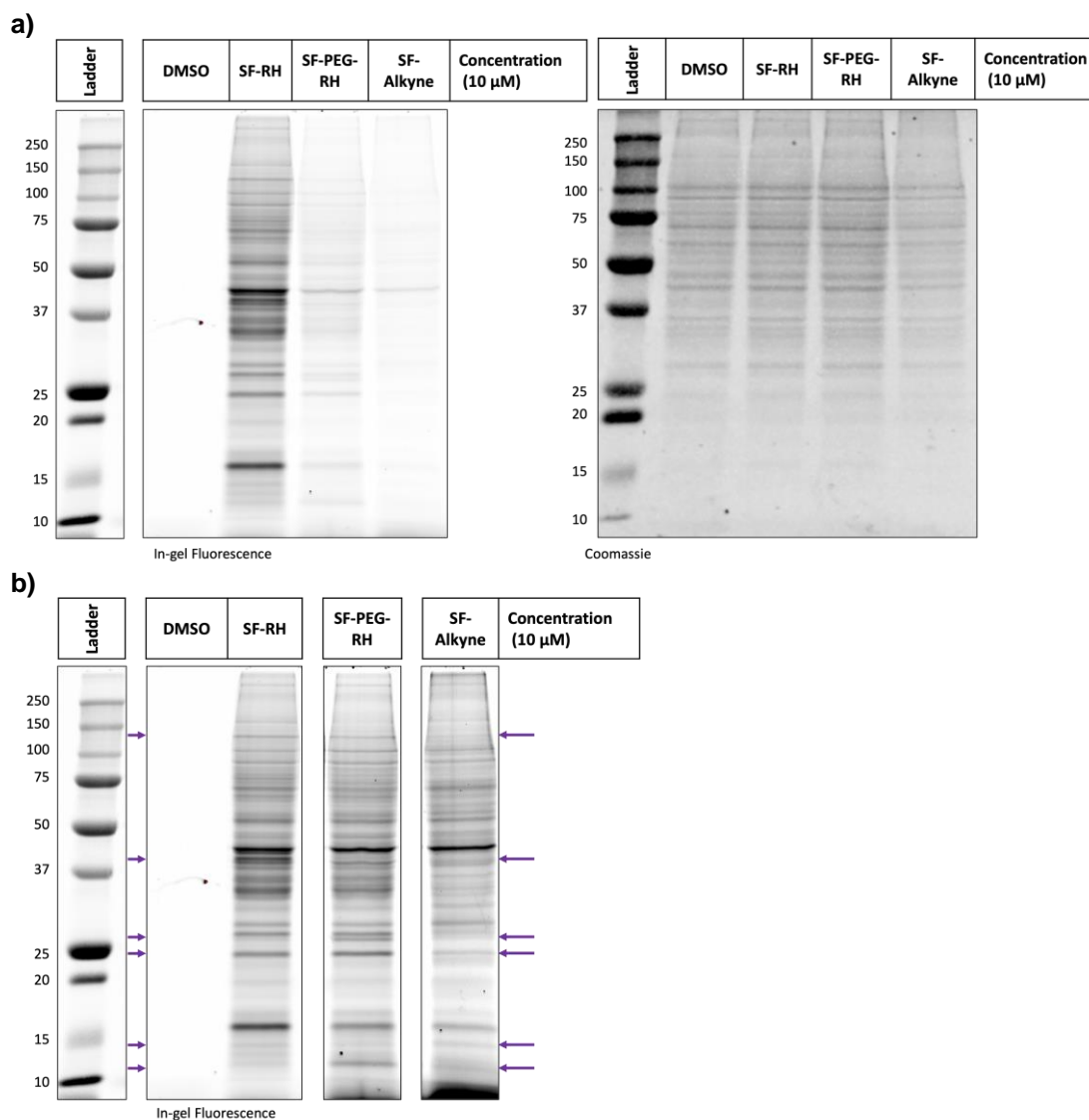


Figure 3.2: Comparative gel of broad-spectrum sulfonyl fluoride probes (**a**) along with an enhanced image to better compare the labelling profiles of each probe (**b**) highlighting key differences (purple). Incubating each probe (10 μ M, 1% DMSO) with HeLa cell lysate, loading 10 μ g protein to each lane, running against a pre-stained molecular weight ladder, and reaction DMSO control containing lysate and DMSO (1%). Showing in-gel fluorescence using a DyLight 550 602/50 epifluorescence filter overlaid with Coomassie image of the pre-stained protein ladder using 715/30 far red epifluorescence filter (left), compared to the total protein Coomassie stain (right).

Although these three probes show broadly similar labelling profiles, **Figure 3.2b** highlights key differences (purple), particularly between the rhodamine containing

probes, and **SF-Alkyne**. Proteins labelled that are unique to the rhodamine-based probes, e.g. ~125 kDa and 25 kDa, could be caused by the templating effect, with rhodamine directing probe labelling to specific binding sites. This can also be seen in the labelling of **SF-PEG-RH** with a specific protect around 12 kDa, this could be caused by rhodamine templating, as well as the longer linker, allowing the sulfonyl fluoride to access a buried binding pocket.

From these experiments, broad labelling was shown across the proteome after 30 minute incubations at 25 °C with each sulfonyl fluoride probe. These conditions were then used for all gel-based experiments with sulfonyl fluoride probes. For future work, the effect of reaction time and temperature can be explored to optimise these labelling reactions, coupled with exploring reaction conditions to stabilise serine and threonine labelling¹⁰⁵. These three probes were then taken forward, to indirectly visualise the labelling of the compound library previously generated through competitive labelling experiments.

3.1.2. Competitive Profiling Against Sulfonyl Fluoride Probes

Using these broad-spectrum sulfonyl fluoride probes, a series of competition experiments were carried out. Following a standard workflow (**Figure 3.3**), the probes can be used to label reactive proteins (**A**) and can be used as a control. If the lysate is pre-incubated with an electrophilic compound (**B**), the compound can interact with these proteins and prevent probe labelling (**C**), resulting in a loss of specific protein bands in fluorescent scanning SDS-PAGE (**D**) when compared to the control.

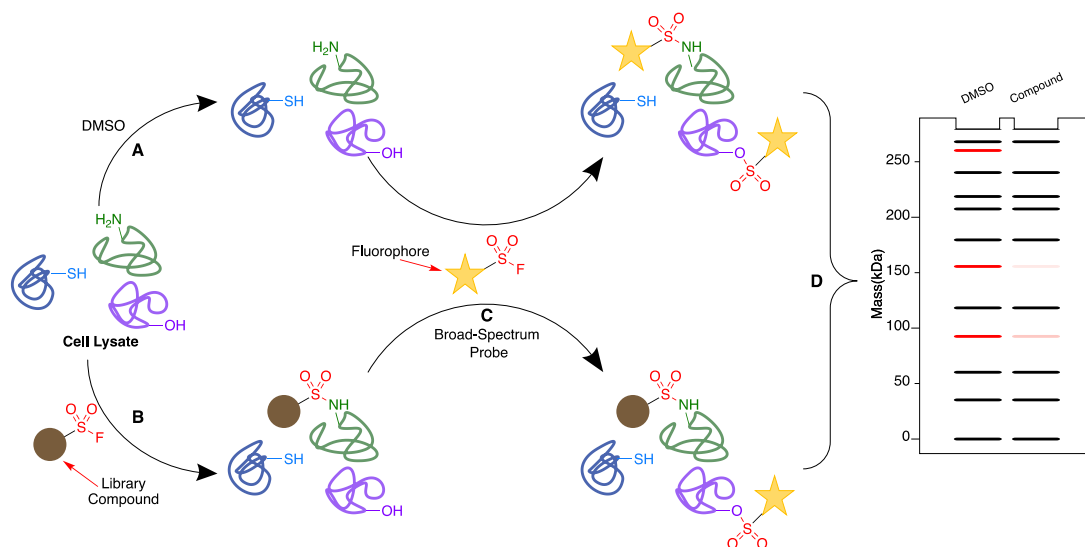


Figure 3.3: Illustrative example of competitive reactivity profiling. Comparing preincubated cell lysate with DMSO (**A**) or competitor (**B**), Showing the reactivity of broad-spectrum probes and a loss of labelling (**C**), visualised by SDS-PAGE (**D**). Figure adapted from ¹⁵⁴.

This profiling was initially attempted using the **SF-RH** and **SF-PEG-RH** probes following the procedure outlined in 5.4.3. For each of the 40 library compounds, HeLa cell lysate (25 μg) was adjusted to 1 mg/mL with PBS (pH = 7.4), to which the competitor (2.5 μL , 1 mM) or a DMSO control (2.5 μL , 10%) was added from a fresh 10-fold stock prepared by diluting the competitor in PBS. The reactions were incubated at room temperature with shaking for 30 minutes. The probes, **SF-RH** or **SF-PEG-RH** were then added to each reaction (2.5 μL , 100 μM) from a 10-fold stock containing 10% DMSO and incubated for a further 30 minutes. The reaction mixtures contained final concentrations of competitor (library compound, 100 μM) and probe (10 μM) in 2% DMSO. After this incubation, the reactions were precipitated with acetone (4 volumes) overnight to remove excess probe, washed, and resuspended, separated by SDS-PAGE gel and imaged using in-gel fluorescence scanning as before (**Figure 3.4**).

a)

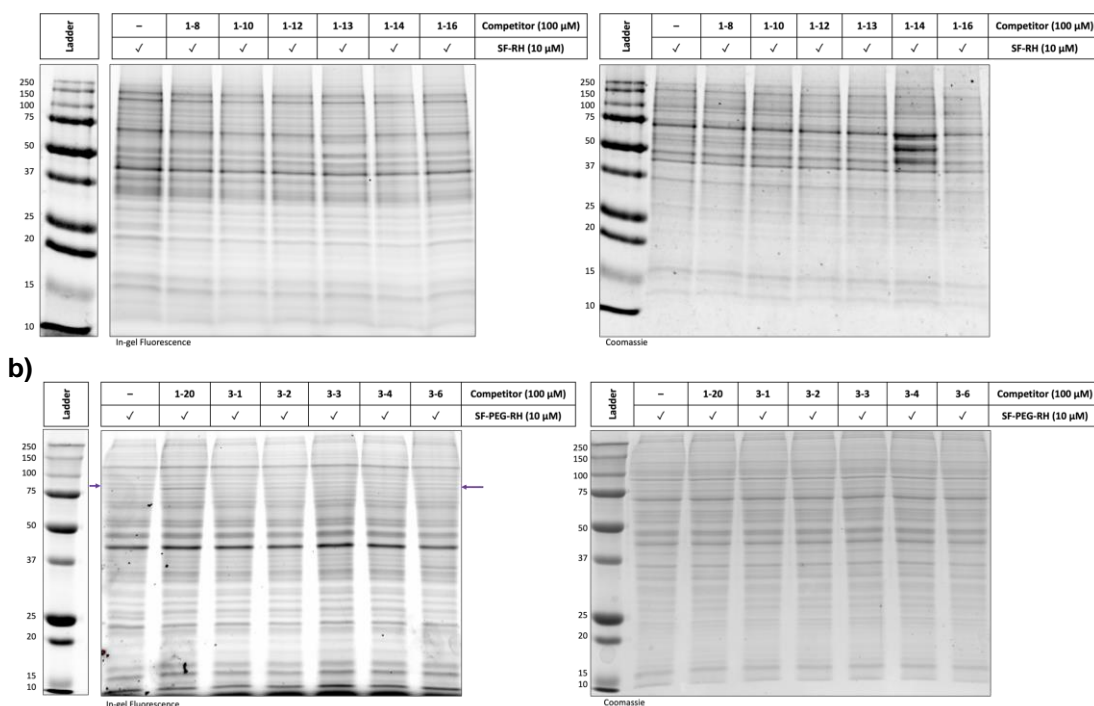


Figure 3.4: Competitive labelling of the broad-spectrum sulfonyl fluoride probes, **SF-RH** (a) and **SF-PEG-RH** (b) against a set of electrophilic compounds. Incubated on HeLa lysate with a final concentration of competitor (100 μ M) and probe (10 μ M), at 2% DMSO, loading 10 μ g protein to each lane, running against a pre-stained molecular weight ladder, and reaction no-competitor control containing lysate and probe. Imaging fluorescence using a DyLight 550 602/50 epifluorescence overlaid with Coomassie image of the pre-stained ladder using 715/30 far red epifluorescence (left), compared to the total protein Coomassie stain (right).

Figure 3.4a shows an example gel of the compound library between **1-8** and **1-16** in competition with **SF-RH**. Unfortunately showing no clear or significant competition across the compounds against any specific proteins. This trend is also seen for the other library compounds, with no clear competition observed, so for that reason the full data set has not been included in this report. The lack of competition could be due to the **SF-RH** probe and the competitor compounds not hitting the same protein targets, or the competitors don't label strongly enough of each protein to see a change in fluorescence.

A templating effect could also cause the lack of competition in this experiment, the bulky rhodamine group could prevent the probe from binding in smaller pockets that the competitors may sit more favourable in. This was explored by competition with the **SF-PEG-RH** probe (**Figure 3.4b**), designed to contain a longer linker to reduce any templating effects. A test experiment was carried out between six compounds from the library competing against **SF-PEG-RH**. Again, there was no significant competition observed against this probe except for a protein (~75 kDa), highlighted in purple, where

a slight increase in labelling is seen when competed with compound **3-1**. An increase in labelling of this protein can also be seen when competing against **1-20**, which could be caused by weak competition across the proteome resulting in additional probe available to label.

Screening of the full compound library against **SF-RH**, and the test experiment against **SF-PEG-RH**, all showed competitive labelling against broad-spectrum sulfonyl fluoride probes is not a viable option to visualise the reactive profiles of these compounds. This is likely due to the unselective labelling of these probes meaning there is enough free protein for both competitor and probes to react with. These reactions could be attempted at a higher ratio between competitor and probe in order to drive competition but lowering probe concentration would cause a weaker fluorescence and increase noise. A cleaner labelling profile, with sharper bands was seen with the **SF-PEG-RH** probe. This probe should be used preferentially for any future experiments, to minimise any templating and also allow labelling in smaller nucleophilic pockets accessible to the compound library.

3.1.3. Competitive Profiling Against a Fluorophosphonate Probe

Sulfonyl fluorides are known to form unstable interactions with serine residues⁹⁸ (**Section 1.3.2.a**). We can use competitive profiling to indirectly visualise these adducts when competing against a serine selective probe such as a fluorophosphonate¹⁵⁵. For these experiments a commercially available fluorophosphonate-rhodamine probe (**FP-RH**), ActivX™ TAMRA-FP Thermo: 88318), was used, a fluorescent probe highly selective for serine hydrolases¹⁵⁵ (**Figure 3.5**).

Competitive labelling experiments with the fluorophosphonate probe, **FP-RH**, were carried out following the same procedure previously outlined, (**Section 3.1.2**, **Section 5.4.3**) on HeLa cell lysate. The competitor compounds were added at a final concentration of 100 μM and incubated for 30 minutes. **FP-RH** (2 μM final concentration; final overall DMSO concentration 2%) was added, and the reactions shaken at room temperature for an additional 30 minutes. Following this, the reactions were precipitated and analysed by SDS-PAGE and fluorescent scanning as described above.

An initial experiment was carried out to visualise the effect of decorating the hetaryl cores in the photoredox chemistry, by comparing the initial, inactive cores, **HA1**, **HA3**, and **HA5**, against those decorated with **HD1**, *N*-Boc pyrrolidine (**Figure 3.5**). These compounds were tested in competition with **FP-RH** to detect any changes in labelling using in-gel fluorescence. When compared to a no-competitor control, we see some interesting competitions across the proteome, highlighted with purple arrows. In particular, **HA3** and **3-1** both show specific competition of protein labelling, with the hetarene core competing bands at ~75 and 35 kDa and the functionalised compound competing with a band at 250 kDa. This highlights how a compound's selectivity depends on its structure. Presumably decoration enhances binding to a certain protein, promoting binding and hence reactivity via non-covalent interactions in some cases, but in others prevents binding, due to the decorated compound not being able to access certain pockets.

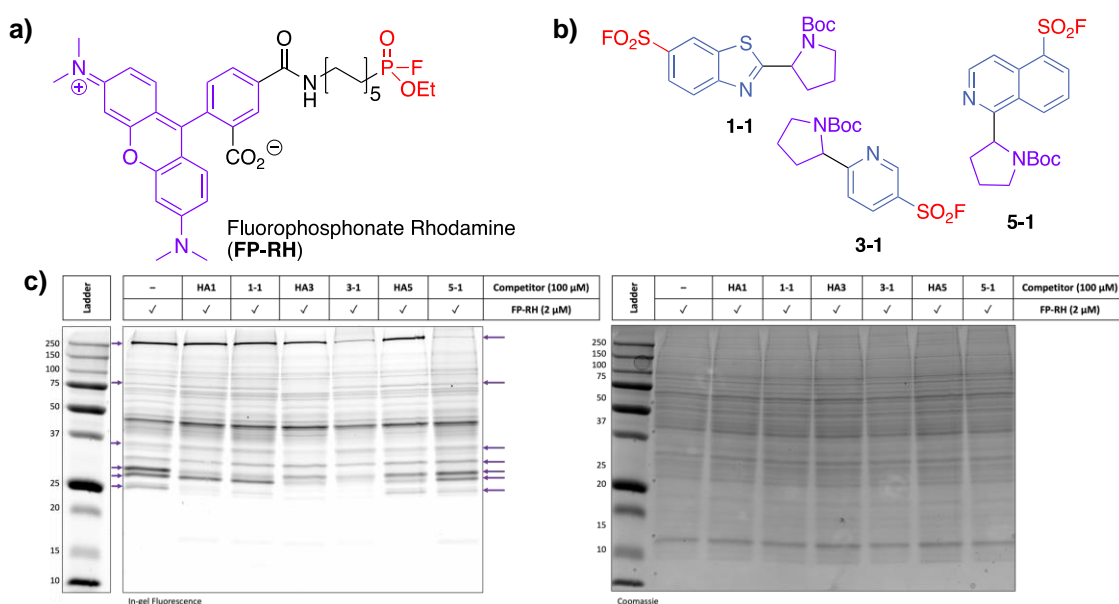


Figure 3.5: Competitive profiling against a serine selective fluorophosphonate, **FP-RH** on HeLa cell lysate (a), screening the library compounds (**X-1**), (b), based around *N*-Boc-pyrrolidine (**HD1**), in comparison with their hetaryl cores (**HAX**) at a final concentration of 100 μM against the **FP-RH** (2 μM) at 2% DMSO, loading 10 μg protein to each lane against a pre-stained molecular weight ladder, and reaction no-competitor control containing lysate and probe (c). Imaging fluorescence using a DyLight 550 602/50 epifluorescence overlaid with Coomassie image of the pre-stained ladder using 715/30 far red epifluorescence (left), compared to the total protein Coomassie stain (right).

Following this, the entire compound library was competed against the fluorophosphonate, to build up a unique reactive profile for each compound, following the procedure previously outlined (library compound at 100 μM and reactive probe, **FP-RH** at 2 μM).

The reactions were analysed by in-gel fluorescence (**Appendix F**). From this, clear competition can be seen across multiple bands in a compound-dependent manner. The degree of competition was quantified by densitometry. Initially, key bands were identified by eye that showed clear competition compared to the control lane. The degree of competition was calculated from the fluorescence intensity of these bands, taken using the software 'Image Lab' and normalised against the control lane, as 0% competition.

This data is represented as a heat map (**Figure 3.6**) for 10 key protein bands shown to compete with a significant portion of the compound library. Other proteins in the control lane that are not highlighted did not show any significant competition with any compounds. From this, each compound is shown to have a unique competitive profile, competing with several protein targets. For example, compounds **1-6** and **5-4** show degrees of competition for all 10 proteins. There are also some interesting trends, for example protein 10 (~25 kDa), where competition is seen by every compound in the library. This suggests that protein 10 may possess a highly reactive, solvent exposed serine for the sulfonyl fluorides to react with. Protein 1 (~250 kDa) also shows an interesting selectivity for the compounds based around **HA3** and **HA5**, the pyridine and isoquinoline cores, while being unreactive to benzothiazole containing, **HA1**, compounds.

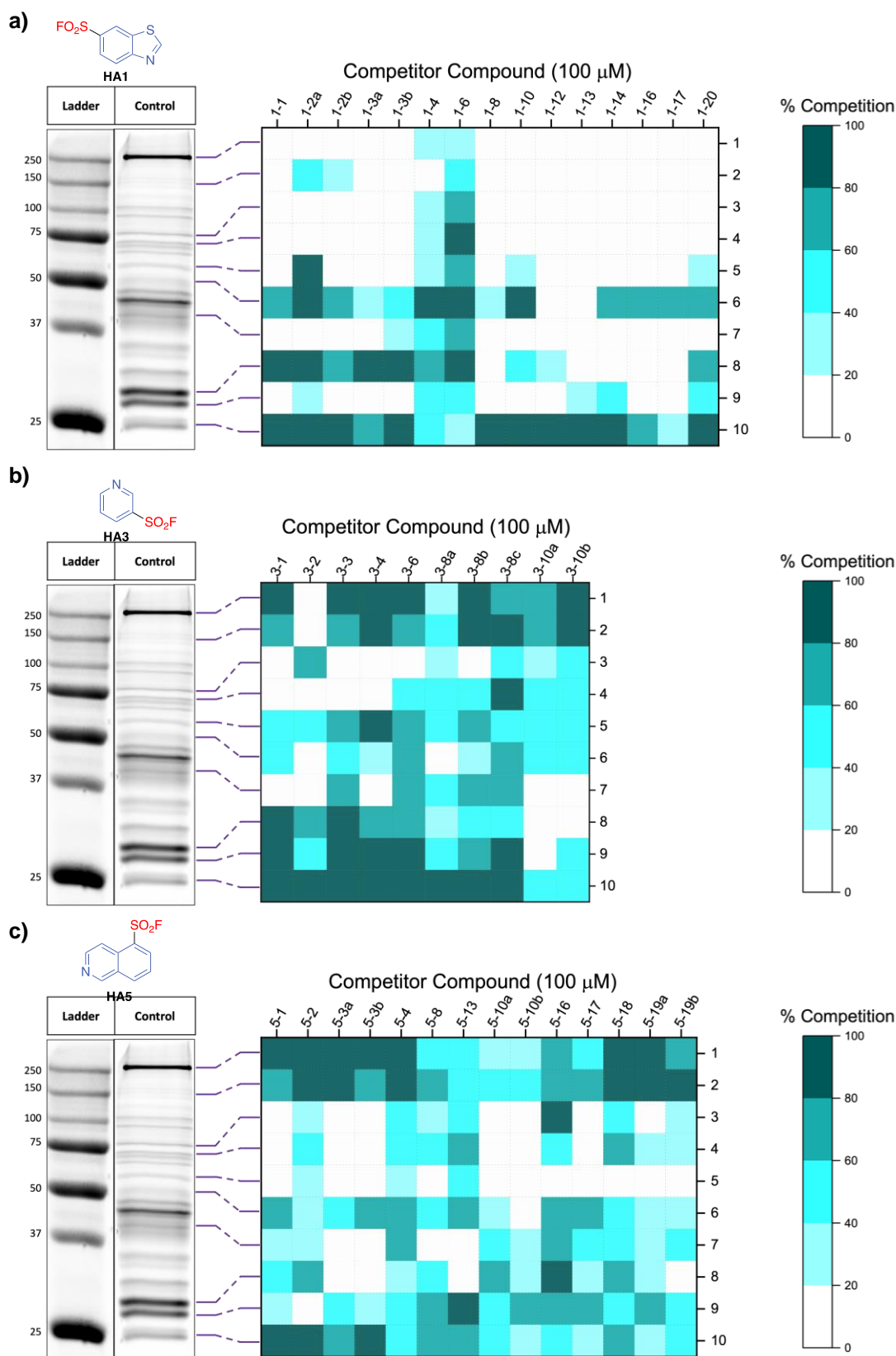


Figure 3.6: Competitive profiling of the reactive library against FP-RH, visualised with in-gel fluorescence in SDS-PAGE. Separated into the family of Hetarenes, HA1 (a), HA3 (b) and HA5 (c). Quantifying competition with densitometry of specific protein bands by their % fluorescence, relative to the control lane. Fluorescent gels can be found in **Appendix F**.

When profiled against a more residue-selective probe such as **FP-RH**, competitive profiling is an effective method to indirectly visualise the labelling profiles of electrophilic compounds. Competition of the serine-selective fluorophosphonate probe shows that these sulfonyl fluoride compounds are likely reactive to serine hydrolases and can be used to indirectly visualise serine–sulfonyl fluoride adducts, although it is possible that these sulfonyl fluorides could be acting as allosteric competitors, reacting with neighbouring groups to indirectly inhibit serine–fluorophosphonate binding, without being serine-reactive themselves. Competition with a **FP-Biotin** reagent in conjunction with a proteomics (mass spectrometry-based) workflow could be used to identify these putative reactive serine hydrolases in future. A similar experiment could be carried out using a sulfonyl fluoride probe such as **SF-Alkyne** to identify reactive lysine and tyrosine groups⁹⁹, in order to quantify the full reactive proteome of sulfonyl fluorides.

3.2. Competitive Identification of Protein Targets

The library compounds outcompete **FP-RH** binding for selective proteins in select proteins of HeLa cell lysate in a compound-dependent manner. Following the established protocol, the labelling of *T. brucei brucei* lysate was evaluated, aiming to identify selective competition in active compounds that could represent the biologically relevant protein targets responsible for their anti-trypanosomal activity.

3.2.1. Serine Hydrolases as Potential Anti-Trypanosomal Targets

Previously, we have demonstrated the ability of the sulfonyl fluoride compound library to react with serine hydrolases, visualised using in-gel fluorescence when in competition with the serine hydrolase selective probe, **FP-RH**. This can be applied to the reactive serine proteases of *T. brucei brucei* lysate, exploring the key interactions that could be responsible for the active compound's toxicity.

T. b. brucei cells lysate was prepared by osmotic pressure lysis by Will Mosedale. Confluent cells were pelleted by centrifugation and washed with trypanosome dilution buffer. The cells were resuspended in pure water, and freeze-thawed twice over cardice. Unlysed cells were pelleted by centrifugation for 5 minutes and the supernatant retained for proteomic labelling experiments. The lysate was buffered in PBS (pH = 7.4) without protease inhibitors to give a final protein concentration of 2.0 mg/mL. Aliquots of lysate were snap-frozen and stored at $-80\text{ }^{\circ}\text{C}$ for future use to avoid freeze-thaw cycles.

The 12 active compounds identified from phenotypic screening against *T. Brucei brucei* (**Figure 2.11, p55**) were profiled in competition against the fluorophosphonate probe, **FP-RH**. The compounds were incubated with *T. brucei brucei* lysate for 30 minutes at a final concentration of 100 μM , before addition of **FP-RH** to a final concentration of 2 μM . The reactions were then precipitated overnight in acetone (4 volumes) and prepared to run on a 12% acrylamide gels to visualise competition via in-gel fluorescence (**Figure 3.7**). Comparing these competitions to the probe-only control, several protein bands show competition by the sulfonyl fluoride active compounds. Labelling of protein **Band 6** (~27 kDa) by **FP-RH** is shown to be outcompeted by each of the active compounds, demonstrating a potential target of anti-trypanosomal activity. In addition, there a several FP-RH labelled bands at ~75 kDa (band 1) and ~37 kDa (bands 2 and 3)

that are more selectively inhibited by compounds in the **HA3** and **HA5** hetarene sets, suggesting the active compounds could have several modes of action.

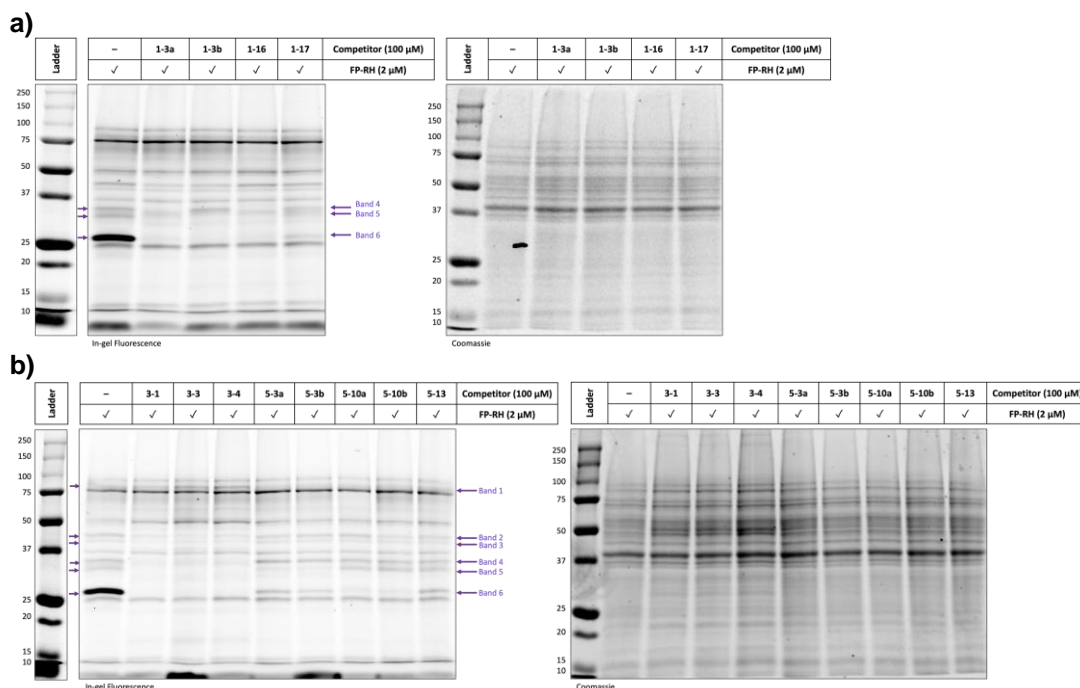


Figure 3.7: Competitive profiling of the 12 active compounds against **FP-RH** in *T. brucei brucei* lysate, based around hetaryl cores **HA1** (a) and **HA3/ HA5** (b) at a final concentration of 100 μ M against the **FP-RH** (2 μ M), at 2% DMSO, loading 10 μ g protein to each lane against a pre-stained molecular weight ladder, and reaction no-competitor control containing lysate and probe. Imaging fluorescence using a DyLight 550 602/50 epifluorescence overlaid with Coomassie image of the pre-stained ladder using 715/30 far red epifluorescence (left), compared to the total protein Coomassie stain (right).

The most potent active compound, **3-1**, was selected for further investigation. A serial dilution against **FP-RH** was performed to gauge the compound's binding affinity, densitometry was used to quantify the change in fluorescence relative to concentration, giving a labelling IC_{50} (the concentration required to inhibit 50% of **FP-RH** labelling), (**Figure 3.8**). Initially, compound **3-1** was incubated with *T. brucei* lysate at concentrations of between 1 – 200 μ M (**Figure 3.8a**), or with a DMSO control, before adding **FP-RH** (final concentration: 2 μ M). The samples were analysed by in-gel fluorescence. From this, five key proteins between 50 – 25 kDa were competed by **3-1**, causing a loss in **FP-RH** fluorescence. One protein around 25 kDa was competed at all tested concentrations, so the experiment was repeated at lower screening concentrations from 1 nM – 5 μ M (**Figure 3.8b**). Competition by **3-1** of these five protein bands was quantified using densitometry. Fluorescence intensity of each concentration was normalised against the

FP-RH probe only control (lane 2) and plotted to calculate a labelling affinity IC_{50} for each protein (**Figure 3.8c**). **3-1** has a labelling affinity IC_{50} of 10 – 50 μM for the four protein bands between 50 – 30 kDa. In comparison to this, **band 6** (red) gave an IC_{50} of 60 nM, showing highly potent labelling of this protein by **3-1**.

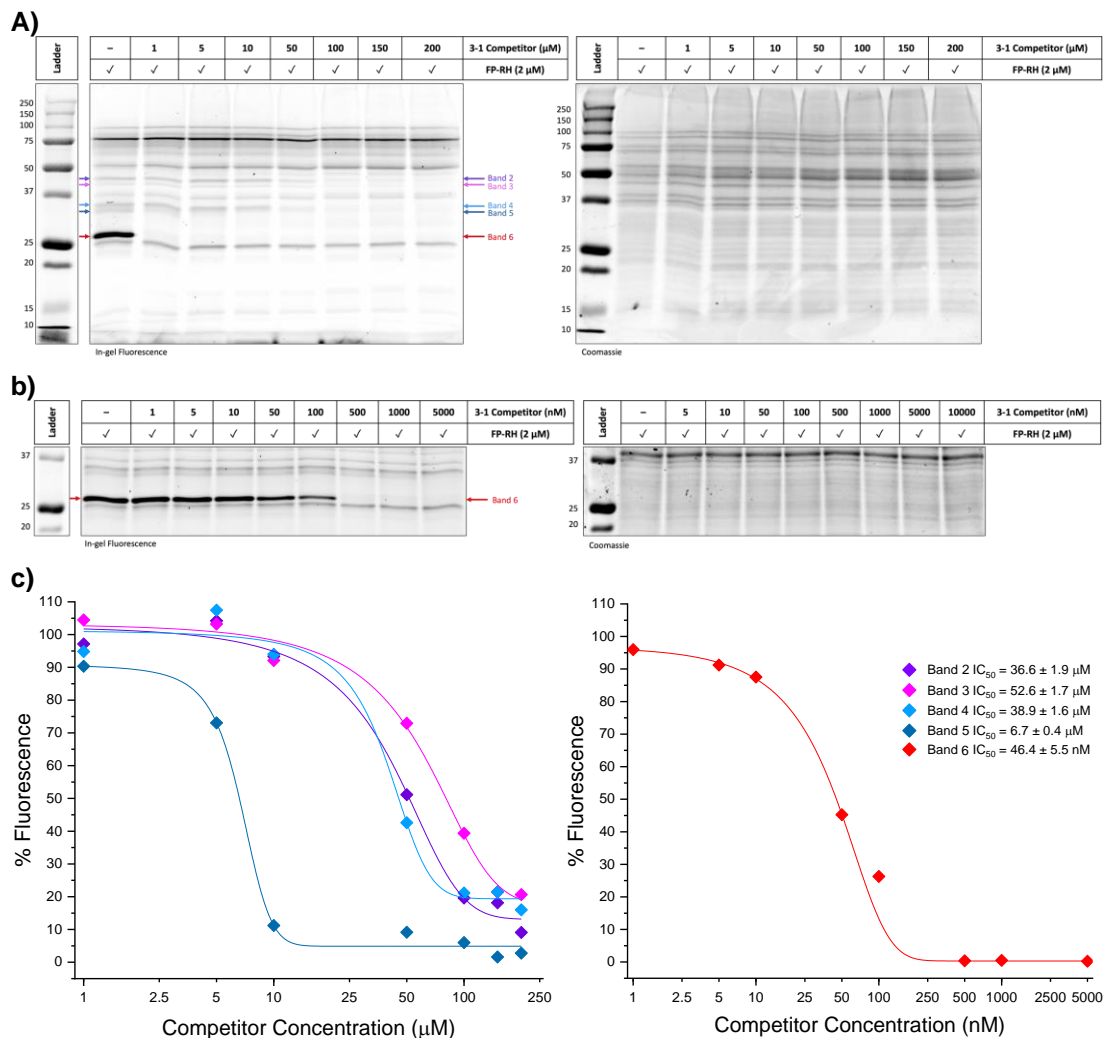


Figure 3.8: Competitive profiling of the compound **3-1** in dilution against **FP-RH**. Screening at micromolar (**a**) and nanomolar (**b**) concentrations of **3-1** with *T. brucei* lysate to calculate a labelling affinity IC_{50} for five protein bands shown to compete (**c**). Quantifying competition with densitometry of specific protein bands by their % fluorescence, relative to the control lane, calculated from a single replicate, representing the fitting error in IC_{50} calculation.

Labelling of these protein bands was shown to be inhibited by several of the active compounds tested, and at low concentrations of **3-1**. In order to validate these as potential protein targets responsible for their anti-trypanosomal activity, we'd expect competition of these to be unique to active compounds. This was explored by comparing the competitive profile **3-1** against **FP-RH** (2 μM) with the inactive hetaryl core, **HA3**, and an inactive analogue, **3-2**, each at a final concentration of 1 μM (**Figure 3.9**). At this

concentration, a similar profile can be seen between **3-1** and **3-2**, both partially inhibiting fluorescence of protein bands between 50 – 30 kDa. The strong protein **band 6** (~ 25 kDa) is partially inhibited by the hetaryl core, **HA3**, and mostly competed with **3-2**, compared to completely inhibited by **3-1**. The inhibition of **band 6** at low concentrations could be a biologically relevant interaction for the activity **3-1**, which can be validated through mass spec-based experiments to identify this protein.

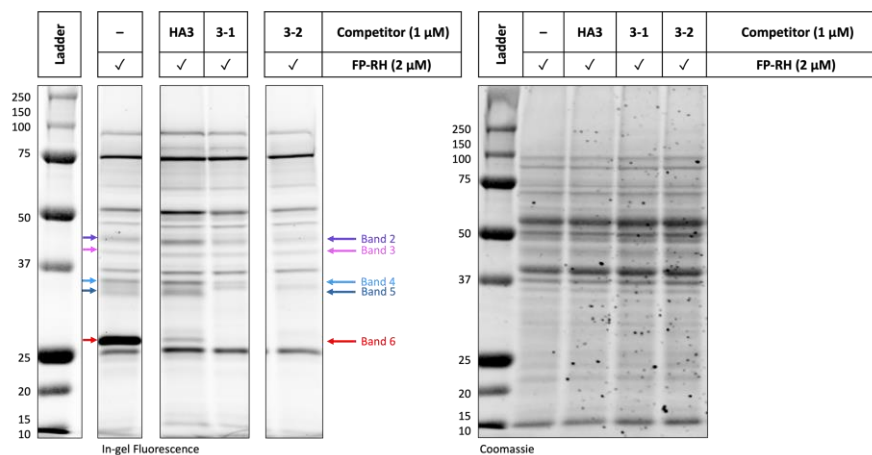


Figure 3.9: Comparison of competitive profiling of the active compound **3-1** against inactive hetaryl core **HA3** and inactive analogue **3-2** at a final concentration of 1 μM. Competing against **FP-RH** (2 μM), at 2% DMSO, loading 10 μg protein to each lane against a pre-stained molecular weight ladder, and reaction no-competitor control containing lysate and probe. Imaging fluorescence using a DyLight 550 602/50 epifluorescence overlaid with Coomassie image of the pre-stained ladder using 715/30 far red epifluorescence (left), compared to the total protein Coomassie stain (right).

This methodology highlights proteins interactions that could contribute to the compound biological activity. This can be explored further in future work, carrying out a serial dilution of **HA3** and **3-2** to gauge selectivity for these specific protein interactions. Applying these competitive experiments on live cells, initially reacting with the competitor followed by lysis and incubation with the fluorescent probe could give a deeper understanding into a compound's activity, accounting for additional variables such as compound uptake and transport throughout the cell. This protocol can be applied to mass spectrometry-based proteomics, competing a fluorophosphonate-biotin probe against the active compounds for enrichment and identification of these proteins. This can be used to build up a picture of the compounds mode of action.

3.2.2. Competitive Profiling of α -Nitrile Protein Targets

Previous literature reported examples of α -nitrile containing inhibitors (Section 1.3.2.b) have a preference for reacting with active site serine and cysteine residues^{85,106}, as well as potential interactions with lysines and tyrosines⁸⁶. We explored the reactivity of the electrophilic library compounds that contain α -nitriles (Figure 2.13, p58) through competition against several broad-spectrum reactive probes: **FP-RH**, which is active site serine-reactive, a maleimide, **Mal-Flu**¹⁵⁶, which is cysteine-reactive, and iodoacetamide **IA-Flu**¹⁵⁴, also cysteine reactive (Figure 3.10a).

The residue selectivity of α -nitriles was explored using the compounds **T-3a** and **b**, synthesised to include a nitrile warhead but no sulfonyl fluoride group to determine the α -nitriles influence on bioactivity. The reactivity of these compounds to serine hydrolases was explored through competition with **FP-RH**, carried out using *T. brucei brucei* lysate, by incubating the control compounds at a final concentration of 100 μ M for 30 minutes, before addition of the broad-spectrum probe following the procedure previously outlined to visualise their reactivity using in-gel fluorescence of the rhodamine fluorophore (Figure 3.10b). From this experiment, no competition was observed, including of the strong fluorescent band \sim 25 kDa, previously competed by all sulfonyl fluoride containing active compounds. A second experiment was carried out to test for competition against the probes **Mal-Flu** and **IA-Flu**, using HeLa cell lysate due to limited supply of parasite lysate. These two broad-spectrum probes have high specificity for cysteine residues, but show largely different reactive profiles, targeting unique cysteine-containing proteins^{157,158}, by competing against both we aimed to explore a larger portion of the cysteine-proteome. A short serial dilution was carried out screening the competitor **T-3a** between 0 – 100 μ M before addition of the cysteine reactive probes to a final concentration of 10 μ M, using in-gel fluorescence of the fluorescein fluorophore to assess competition (Figure 3.10c). No competition was seen against these probes either. It is unclear whether this result is caused by these α -nitrile compounds being unreactive towards labelled cysteine residues, or these nitriles are not reactive towards the same cysteines as the broad-spectrum probes. The short linkers of **Mal-Flu** and **IA-Flu** could bias labelling away from smaller binding pockets, accessible to **T-3a** and **b**.

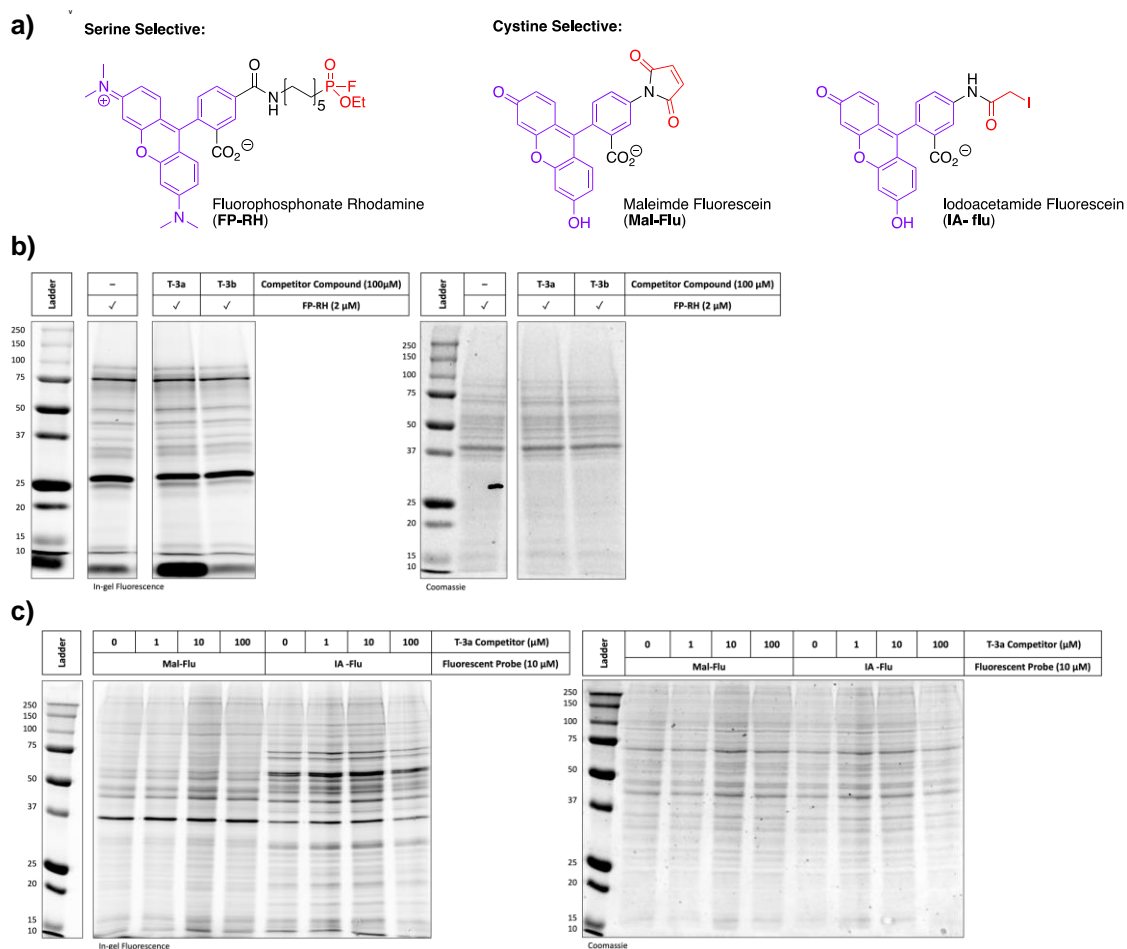


Figure 3.10: Competitive profiling of α -nitriles to identify amino acid selectivity against broad-spectrum serine and cysteine reactive probes (a). Screening the compounds **T-3** (100 μ M) in competition against a serine selective broad-spectrum probe, **FP-RH** (2 μ M) in *T. brucei* lysate (b) and cysteine reactive probes, **Mal-Flu**, and **IA-Flu** (10 μ M) (c) at 2% DMSO, loading 10 μ g protein to each lane against a pre-stained molecular weight ladder, and reaction no-competitor control containing lysate and probe. Imaging fluorescence using a DyLight 550 602/50 epifluorescence overlaid with Coomassie image of the pre-stained ladder using 715/30 far red epifluorescence (left), compared to the total protein Coomassie stain (right).

An alternative method to investigate the reactivity of these α -nitrile towards activity amino acid residues would be to evaluate labelling of serine and cysteine proteases by intact protein MS. This could also be explored using short peptides or protected amino acids, assessing labelling by LC-MS or by changes in ^1H NMR. The reactivity and amino acid selectivity of these compounds can also be explored with the development of chemical probes, functionalising the molecules with an alkyne tag to visualise protein labelling by attachment of a fluorophore for in-gel analysis, or by target identification using an affinity tag, and identify residue specific interactions using mass spectrometry.

3.3. Identification of Reactive Protein Targets with Chemical Probes

Competitive profiling was used to indirectly visualise a series of protein targets reactive with the sulfonyl fluoride compound library, identifying potential protein targets that could contribute to their activity. Next, we explored a more direct method of target identification through the synthesis of functional electrophilic probes. Previously, five anti-trypanosomal compounds have been identified, exhibiting sub-micromolar activity against *T. brucei brucei* (**Figure 2.14, p60**). Functionalised chemical probe analogues were then designed and synthesised to incorporate alkyne tags, to explore the mode of action and identify potential protein targets of both the sulfonyl fluoride and α -nitrile containing compounds.

3.3.1. Generation of Anti-Trypanosomal Electrophilic Probes

Two active and selective sulfonyl fluoride containing compounds with sub-micromolar activity, and at least a 40-fold selectivity over human cells, **1-16** and **3-1**, were selected for further investigation (**Figure 3.11a**). Alongside these, analogues of **1-3** and **T-3** were designed to explore the reactivity of the α -nitrile warheads (**Figure 3.11b**). These compounds were evaluated for sites for potential inclusion of a terminal alkyne for downstream click chemistry. Each compound contains a secondary amine, representing an accessible site for addition of an alkyne via an amide bond formation, using an analogous propargyl alkyne group to mimic the small Boc and ester protecting groups in the active compounds. Structural variations between the two active compounds **1-16** and **1-17**, based around a benzothiazole heteroarene, and a piperidine hydrogen donor, suggest the 1- and 6-piperidine positions could be suitable sites for alkyne addition. Both compounds contain an ester group or an aromatic system in these positions and retain their activity, so additional variation in these groups could be tolerated. A comparison of the compounds **3-1** and **3-3** show the nitrile substituent in the pyrrolidine 5-position is not essential for the compound activity, having a slightly negative effect, so could be a suitable position for alkyne insertion. Analysis of the **T-3** family shows the sulfonyl fluoride has no effect on the compound's activity, so can be used as a point of alkyne decoration.

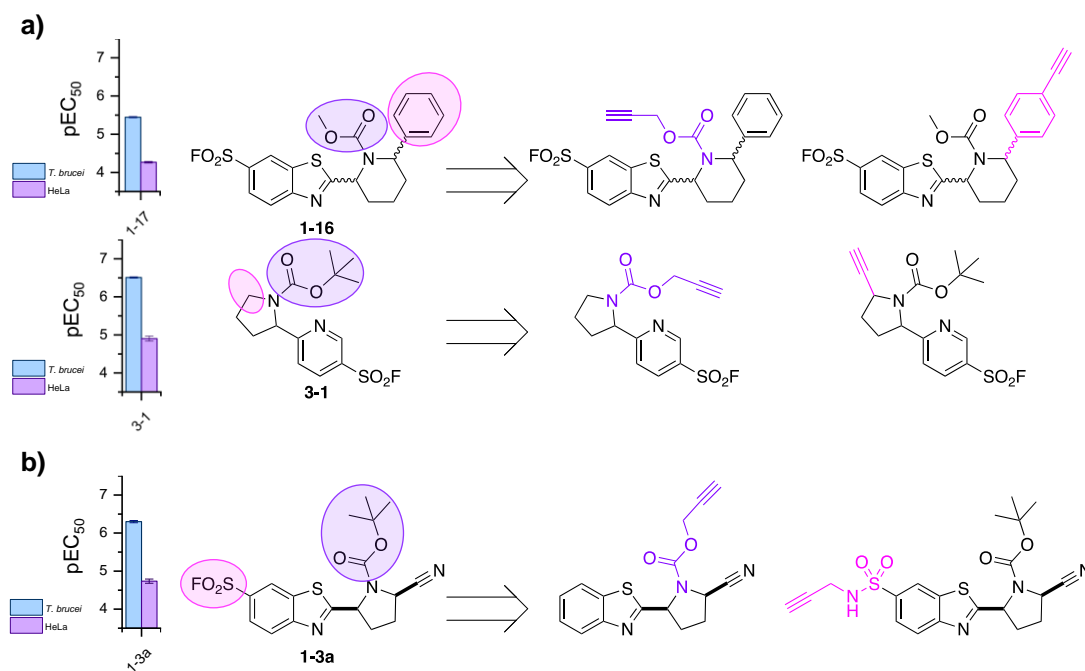


Figure 3.11: Potential alkyne containing analogues of the most active hits compounds for chemical probe design. Areas for alkyne addition are highlighted for the sulfonyl fluoride-based (a) or α -nitrile (b) compounds by reaction with the amine group (purple) or additional functionality of the molecule (pink).

Initially, synthesis of these probes of these hit compounds was attempted by making alkyne-containing analogues of the hydrogen donor substrates. These could then be coupled to heteroarenes via the photoredox reaction previously utilised (Section 2.1.3). These hydrogen donor analogues were synthesised or purchased. The free amines were protected with a *N*-Poc-protecting group, using propargyl chloroformate (Figure 3.12a)¹⁴⁸ as previously outlined for similar amine protections (2.1.3). For synthesis of hydrogen donor analogues of **1-16**, the aryl alkyne, compound **15**, was synthesised via a Sonogashira coupling to attach an alkyne group (Figure 3.12b)¹⁵⁹. After an initial protection of the piperidine amine using methyl chloroformate, **13**, the Sonogashira reaction was used to couple the aryl bromide, **13**, with (triisopropylsilyl)acetylene using $\text{Pd}(\text{Cl})_2(\text{PPh}_3)_2$, CuI, and heating to reflux in triethylamine for four hours, until shown to be complete by TLC and MS. The protected alkyne was purified by an aqueous workup and column chromatography to yield compound **14**. A portion of this was deprotected to remove the silane group using TBAF and stirring overnight to isolate the free alkyne after aqueous workup. For synthesis of the α -nitrile based probe analogues of **T-3**, an attempted synthesis of the alkyne analogue of **HD3** (Figure 3.12c) was made by first deprotecting the commercially available substrate, *N*-Boc-2-cyanopyrrolidine, followed by reaction of the product amine with

propargyl chloroformate. From this reaction, only *N*-Poc-pyrrolidine was isolated and confirmed by NMR and MS. It is likely that the nitrile group was lost via an iminium ion formation after the Boc group was removed, catalysed by triethylamine. This method was therefore deemed not suitable for this **T-3** analogue synthesis.

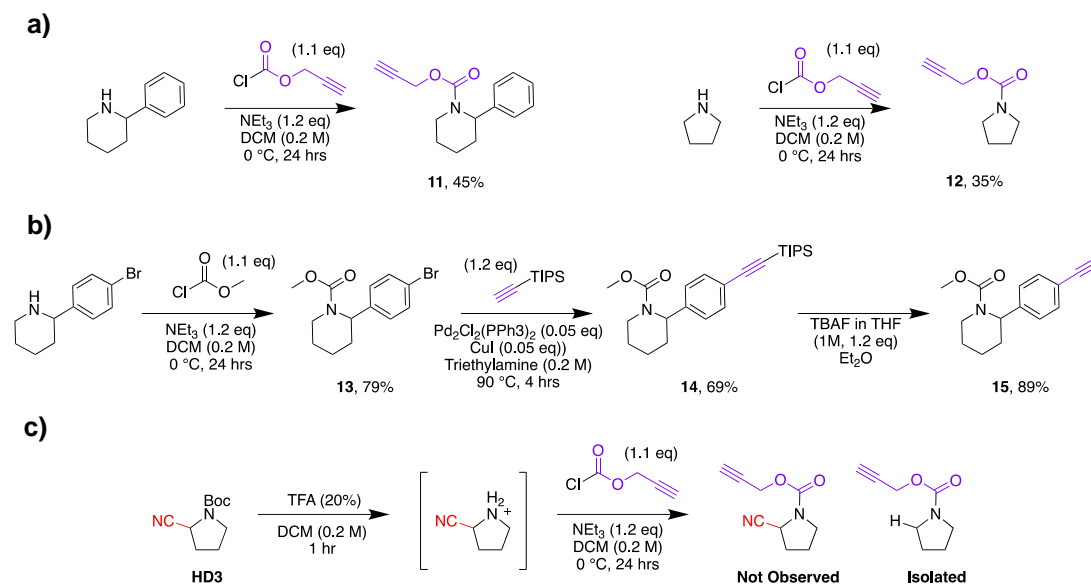


Figure 3.12: Preparation of hydrogen donor analogues containing alkynes. Synthesised by amine protection with propargyl chloroformate¹⁴⁸ (a), or through a Sonogashira coupling to make the aryl alkyne¹⁵⁹ (b). Attempted synthesis of a **HD3** analogue (c) was unsuccessful.

The synthesised alkyne-containing hydrogen donor substrates, **11**, **12**, **13** and **14**, along with the commercially available compound, *N*-Boc-2-ethynylpyrrolidine, were then reacted with their corresponding hetaryl cores *via* the dehydrogenative photocoupling reaction. Unfortunately, analysis of the crude reaction mixtures by NMR and LC-MS showed very little product formation, showing predominately hetarene starting material in ¹H NMR, and multiple species present in ¹⁹F NMR. An attempt at purification was made using HPLC-MS but no product was isolated. The lack of reactivity could be due to these hydrogen donor substrates being incompatible with the chemistry, or potential side reactions between the alkynes and the iridium catalyst^{160,161} could be interfering with the reaction. Synthesis was attempted using both the protected and deprotected alkyne analogues of **HD16**, compounds **14** and **15** under the photoredox reaction, but no product formation was observed.

An alternative route for synthesising chemical probes was used, by directly modifying the original parent compounds **1-16** and **3-1** after their synthesis in the dehydrogenative photoredox reaction. Alkyne groups were installed by removal of the amine protecting group using TFA (20%) and then reacting the free amine with propargyl chloroformate (**Figure 3.13**). This removed the issue of alkyne compatibility with the photoredox reaction. Due to the ease of removing a *N*-Boc group, compared to an acetyl protecting group, the synthesis of a Boc-protected analogue of **1-16** was attempted. Initially synthesising *N*-Boc-2-phenylpiperidine from the free amine, using Boc-anhydride, following the procedure previously outlined (**Figure 2.6, p46**). A coupling between the Boc-protected analogue of **HD16** and the hetaryl core **HA1** was then attempted via the dehydrogenative photocoupling reaction (**Figure 3.13a**). Unfortunately, this coupling was not successful, and no product formation was observed, so instead we chose to focus on synthesising a **3-1** based alkyne probe, 6-(*N*-Poc-pyrrolidin-2-yl)pyridine-3-sulfonyl fluoride, referred to as **3-1 Alkyne**. Initially synthesised **3-1** by the photocoupling of **HA3** and **HD1**, carried out on a 1 mL scale (**Section 5.2.2**) in triplicate to generate enough material for the subsequent reactions. The hit compound, **3-1**, was then deprotected by stirring in TFA (20%) and DCM (0.2 M) for one hour (**Figure 3.13b**). The free amine, **16**, was then isolated as a TFA salt by concentrating *in vacuo*. The intermediate was reacted with propargyl chloroformate (1.1 eq) and NEt₃ (2.2 eq) at 0 °C for one hour, before warming to room temperature overnight with product formation shown by LC-MS. The crude reaction was concentrated *in vacuo* and purified by HPLC-MS to afford the functionalised probe, **3-1 Alkyne** (**Figure 3.13b**).

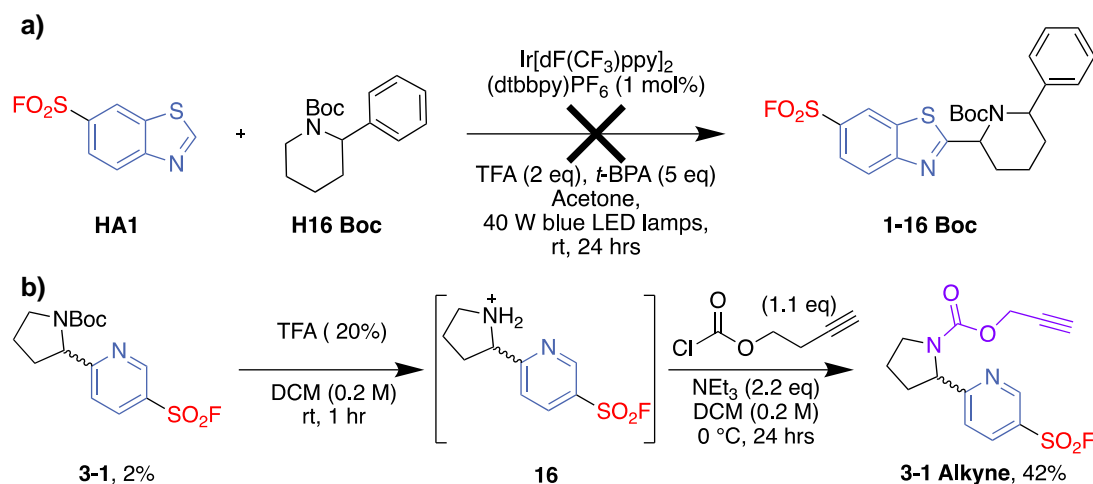


Figure 3.13: Alternative route to synthesising sulfonyl fluoride probe analogues, by additional functionalisation of the parent compound¹⁵⁹. Synthesis of a **1-16**-based probe (**a**) *via* forming a Boc-protected adduct was unsuccessful, so focus was shifted to synthesis of **3-1 Alkyne** (**b**).

This method was also utilised to synthesise an α -nitrile probe analogue, **T-3a Alkyne**. The synthesis and purification of the parent compounds **T-3a** and **T-3b** (**Figure 3.14**) was repeated, they were deprotected with TFA (20% in DCM) and reacted with propargyl chloroformate (1.1 eq) and NEt_3 (2.2 eq) before purification of the crude reaction mixtures by mass-directed HPLC. Initial deprotection with TFA did not result in the loss of the nitrile group as previously seen with **HD3**, (**Figure 3.12c**). The aromatic ring may be providing additional electronic stabilisation to make the nitrile less susceptible to hydrolysis. This reaction was successful for the syn-diastereomer, **T-3a**, forming α -nitrile probe, **T-3a Alkyne** (**Figure 3.14a**), but the reaction of the anti-diastereomer, **T-3b**, was unsuccessful, with only the deprotected intermediate, **09**, observed by LC-MS and isolated on attempted purification by mass-directed HPLC (**Figure 3.14b**), it is unclear why this reaction did not proceed like the syn diastereomer.

Finally, because the sulfonyl fluoride group was shown to be unimportant for this compound family's anti-trypanosomal activity, we considered this as a potential site for alkyne decoration. The isolated diastereomers of parent compound **1-3** (**Figure 3.14c**), were reacted with propargyl amine as a 50% solution in acetone (0.2 M) to assist solubility. The reactions were stirred overnight at room temperature, until complete consumption of the starting material was observed by LC-MS. The crude reactions were then concentrated *in vacuo* before purification by mass-directed HPLC to afford the sulfonamide probes, **1-3a** and **1-3b Alkyne**.

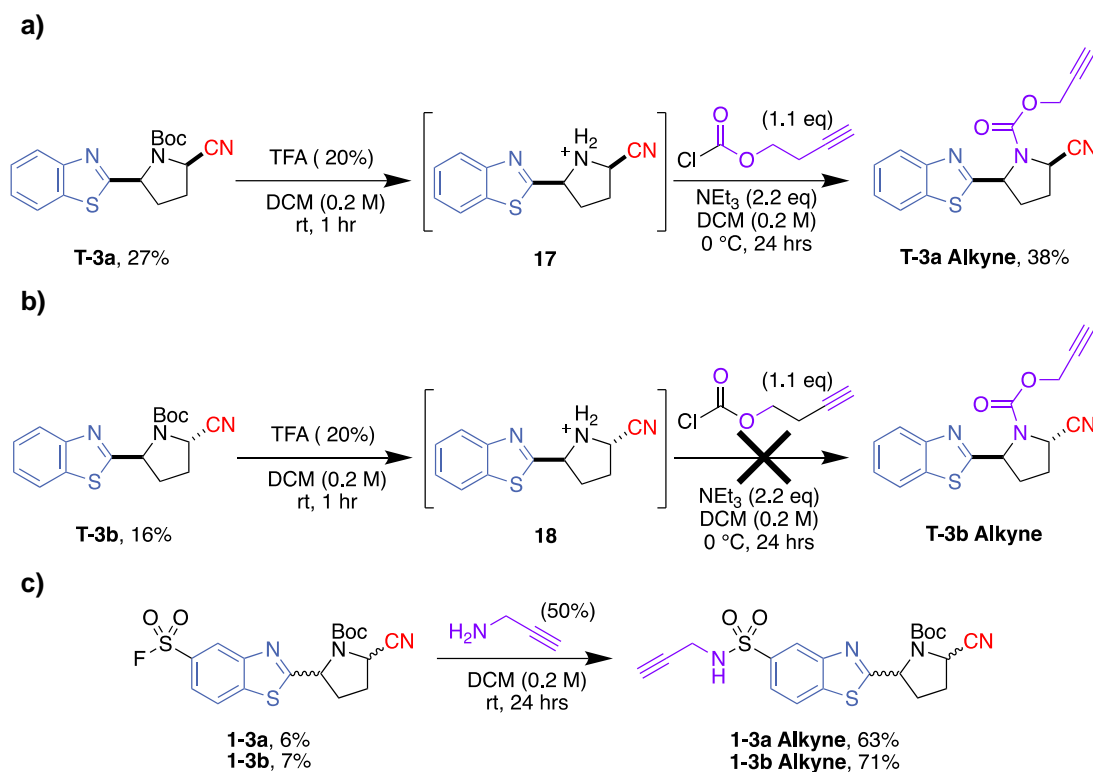


Figure 3.14: Synthesis of α -nitrile probes, highlighting the successful (**a**) and attempted (**b**) synthesis of **T-3 Alkyne** analogues¹⁵⁹, and synthesis of sulfonamide-based probe (**c**).

In conclusion, a series of alkyne functionalised chemical probes were successfully prepared to be used for target identification of these anti-trypanosomal compounds. Due to the poor apparent compatibility of the photoredox chemistry with alkyne-containing substrates, generating probes is limited to using the existing functionality of the parent compounds, so alternative synthetic routes may be required to install alkynes in other positions.

3.3.2. Validation of Chemical Probe's Anti-Trypanosomal Activity

To explore the protein targets of the active compounds, the alkyne containing probes must retain the anti-trypanosomal activity of the parents. Comparable activity suggests similar reactive profile and thus suggests that the modifications do not perturb important probe-protein interactions. The alkyne analogues were screened at varying concentrations, against *T. brucei brucei* in the resazurin-based cell viability assay, producing a dose response to calculate an EC₅₀ value for comparison to the parent compound.

The alkyne analogues were prepared as 10 mM DMSO stock solutions for screening. A 2-fold serial dilution of stock concentrations was carried out from 10 mM – 0.5 μ M. In a

96 well plate, blood stream form *T. brucei brucei* (200 μ L) was seeded at 5×10^3 cells/mL. The cells were incubated in quadruplicate with the alkyne probes, added from $100 \times$ stocks at final concentrations between 100 μ M – 50 nM for 66 hours at 37 $^{\circ}$ C, before adding Resazurin sodium salt (10 μ L, 1.1 mg/ mL) to incubate for a further 6 hours. The fluorescence response of resorufin was normalised between the positive control, containing pentamidine (100 nM), and the negative control of DMSO (0.5%) to give cell viability as a percentage, and plotted as a dose response (**Appendix G**) to calculate and pEC₅₀ value (**Figure 3.15**) for comparison to the active parent compounds.

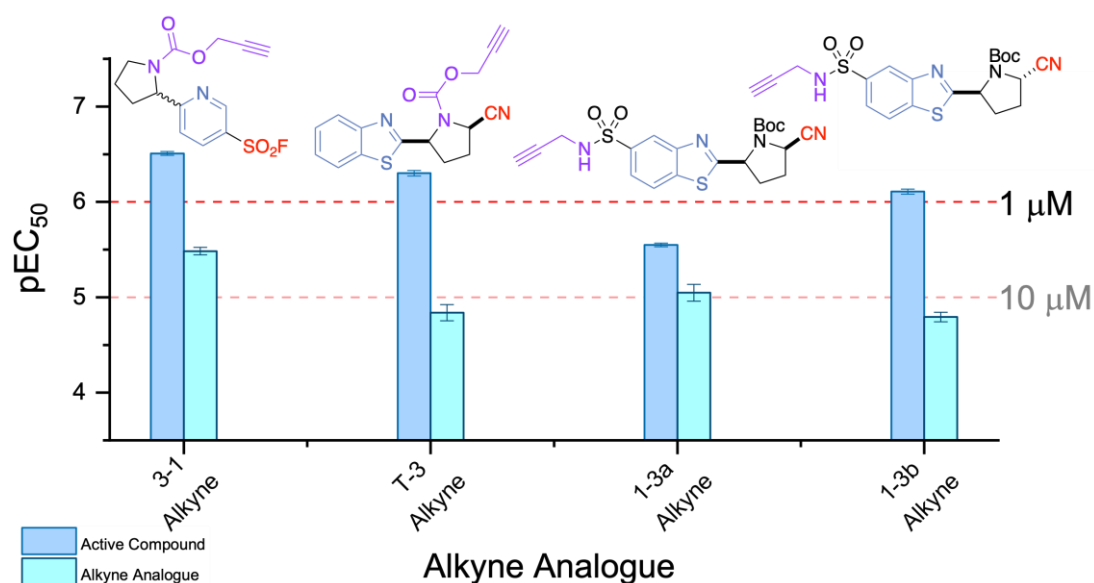


Figure 3.15: Comparison of activities between the parent compounds (blue) and their alkyne analogues (cyan). Screening the alkyne probes in quadruplicate against *T. brucei brucei* by Will Mosedale, in a resazurin-based cell viability assay, presenting the data as PEC₅₀ values. Full assay data is shown in **Appendix G**. Alkyne probe screening data was compared to the original library screening of active parent compounds (**Figure 2.11, p55**).

Compared to the parent compounds, a large decrease in activity is seen in the synthesised alkyne analogues, suggesting that the modified positions provide key interactions that contribute to the parent compound activities. It should be noted that the screening data of probe analogues is being compared to the previous library screening, so variability in the assay and cells used should be considered. Two of the probes, **3-1 Alkyne** and **1-3a Alkyne**, both gave a better retention of activity compared to the parent compound, also maintaining an activity of lower than 10 μ M, previously identified as an activity threshold during the initial screening. By retaining their activity, these probes are more likely to react with the same protein targets as the parent compounds, giving higher validity to future proteomics experiments when working towards target identification. The probe's

alkyne tags can be functionalised with a fluorophore group *via* a click reaction and used to visualise protein labelling with in-gel fluorescence. An enrichment group such as biotin could also be attached to assist protein identification by mass spectrometry. Using the active parent compounds in competition with these probe analogues can be achieved by pre-incubation of the parent compound with the cell lysate prior to probe addition. These competition experiments could be useful in identifying key proteins responsible for their anti-trypanosomal activity. Further investigation into the structure-activity relationship of these hit compounds could identify alternative sites for alkyne addition that results in probes that better retain the compound's activity.

3.3.3. Visualisation of Anti-Trypanosomal Protein Targets

The alkyne containing analogues of anti-trypanosomal hits can be used to identify these compounds protein targets by functionalisation with a click reaction to attach an azide-tag. Incorporating fluorophore or biotin group can be used to visualise protein labelling by in-gel fluorescence, or for enrichment and quantification by MS.

To explore the labelling profile of the sulfonyl fluoride probe **3-1 Alkyne** against *T. brucei brucei*, a serial dilution was carried out, incubating the probe with cell lysate at final concentrations between 50 and 0.1 μM for 30 minutes at 25 °C. A click reaction was then used to attach a rhodamine fluorophore, following the standard protocol previously described for alkyne containing probes (**Section 3.1.1, Figure 3.2, p65**). The click reagents were added from a master stock mixture to a final concentration of 100 μM rhodamine-azide as the limiting reagent, incubating for one hour at 25 °C. The click reaction was then quenched with EDTA (10 mM final concentration), and the proteins precipitated in acetone overnight at -20 °C, pelleted by centrifugation and washed to remove excess probe and click reagent. The samples were dried and prepared to run on a 12% SDS-PAGE gel, to visualise fluorescent labelling (**Figure 3.16a**). **3-1 Alkyne** shows a very broad labelling profile across the proteome. By scaling the fluorescent intensity of each probe concentration, we can compare the labelling profiles (**Figure 3.16b**) to see the broad labelling profile is maintained even at low concentrations around the probes EC_{50} (3.28 μM). The labelling profile of this probe is comparable to the total Coomassie stain, suggesting the probe is non-selectively labelling the abundant proteins in the proteome. In parallel with this, competition with the parent compound, **3-1**, was attempted. Cell

lysate was preincubated with 3-1 at concentrations of between 100 – 1 μ M for 30 minutes at 25 °C before addition of the alkyne probe and click reagents as previously described (**Figure 3.16c**). As previously seen with broad-spectrum sulfonyl fluoride-based probes (**Section 3.1.2**), no detectable levels of competition were observed. This result could be due to the broad reactivity of the competitor and probe meaning low levels of competition are not detectable by in-gel fluorescence, or the **3-1** and **3-1 Alkyne** are not reacting the same proteins, and **3-1 Alkyne** may not be a good probe for understanding the anti-trypansomal activity of **3-1** proteins.

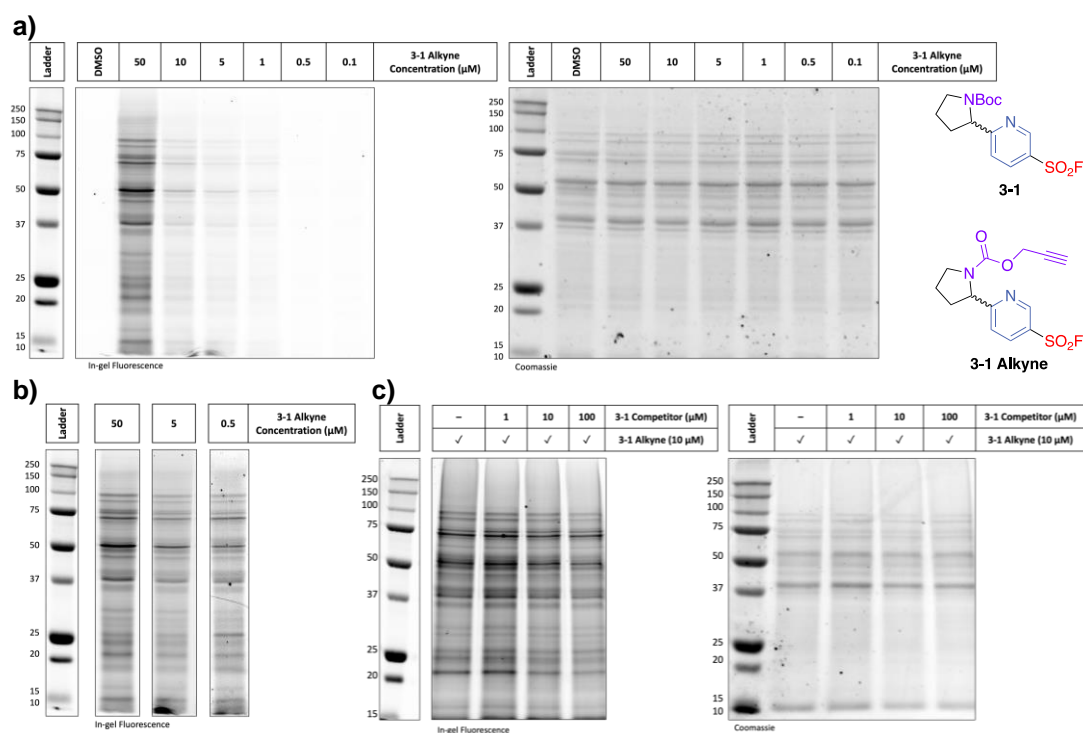


Figure 3.16: Labelling profile of the sulfonyl fluoride probe, **3-1 Alkyne**, on *T. brucei brucei* lysate screening from 50 – 0.1 μ M (**a**), comparing the labelling profile scaling fluorescence response at different concentrations (**b**), and attempted competition against the parent compound, **3-1** (100 – 1 μ M) (**c**), loading 10 μ g protein to each lane against a pre-stained molecular weight ladder, and reaction no-competitor control containing lysate and probe. Imaging fluorescence using a DyLight 550 602/50 epifluorescence overlaid with Coomassie image of the pre-stained ladder using 715/30 far red epifluorescence (left), compared to the total protein Coomassie stain (right).

α -Nitriles are known to act as reversible electrophiles^{70,85,86}, because of this it was unknown whether these α -nitrile based probes would form stable adducts with proteins to be identified by chemical proteomics methods. To investigate this, the α -nitrile probe **1-3a Alkyne** was incubated with human, HeLa cell lysate at a final concentration of 10

μM (1% DMSO). Following the standard procedure previously described for these experiments, the probe was incubated for 30 minutes at 25 °C before addition of the click reagents to a final concentration of 100 μM with respect to the rhodamine-azide. The lysate was then precipitated in acetone (4 \times volume) overnight and the samples prepared for SDS-PAGE. The samples were resuspended in sample loading buffer containing either no reducing agent, or TCEP or DTT (100 mM) and half of the samples were then boiled at 95 °C for 2 minutes before running onto a gel to visualised probe labelling *via* in-gel fluorescence (**Figure 3.17**). Comparison of the gel conditions shows a high stability of these probe protein adducts to the gel-based workflow, the modification is stable to different reducing agents with comparable labelling to the no-reduction controls, though there are small differences between the labelling profiles, suggesting the reducing agent could cleave less stable α -nitrile-protein adducts. The probe adducts are also stable to heat, showing no difference in labelling when comparing the boiled/ no-boiled controls, and probe labelling also survives precipitation in acetone.

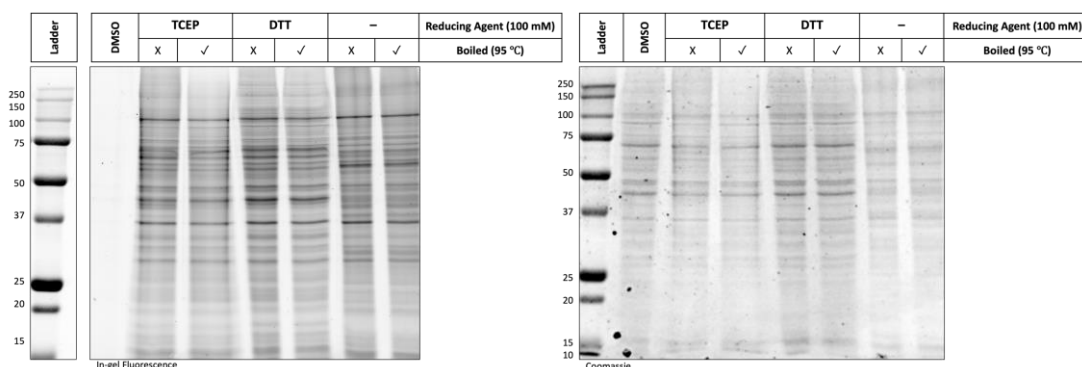


Figure 3.17: Assessing the stability of α -nitrile-protein adducts *via* in-gel fluorescence. Incubation of the probe **1-3a Alkyne** (10 μM) with HeLa cell lysate to compare the effect of reducing agents, TCEP or DTT (100 mM) and sample boiling (2 min, 95 °C) by loading 10 μg protein to each lane against a pre-stained molecular weight ladder, and reaction no-competitor control containing lysate and probe. Imaging fluorescence using a DyLight 550 602/50 epifluorescence overlaid with Coomassie image of the pre-stained ladder using 715/30 far red epifluorescence (left), compared to the total protein Coomassie stain (right).

To further validate the stability of α -nitrile based probes, additional controls should be run, to compare precipitation to non-precipitation, to see if significant labelling loss is seen. It is also worth noting the presence of TCEP during the click reaction, at a final concentration of 1 mM that could affect labelling efficiency and alternative click conditions could be explored.

p88) we see similarities in the labelling pattern, suggesting the α -nitrile probes could be reacting with lysine or tyrosine residues too.

3.4. Conclusion of A Chemical Proteomics Investigation into Protein Targets

A series of broad-spectrum reactive alkyne and fluorophore probes were synthesised to explore the reactive profiles of sulfonyl fluorides in lysate conditions, investigating the impact of templating, and stability to amino acid residues. Sulfonyl fluorides have been shown to be reactive with serine proteases^{98,105} so a broad-spectrum fluorophosphate probe, **FP-RH**, used in competition experiments with the electrophilic compound library was successfully used to visualise potential interactions of sulfonyl fluorides with serine hydrolases. However, the same level of competition was not seen when using broad-spectrum reactive probes including sulfonyl fluoride-based probes, **SF-RH** and **SF-PEG-RH**, as well as cysteine reactive iodoacetamides and maleimides probes. This lack of competition could be caused by the competitors and probes hitting different protein targets, or the unspecific labelling meaning low levels of competition are not detectable by in-gel fluorescence. The lack of competition seen in these experiments could be due to the reaction conditions being sub-optimal for each probe, these could be optimised by exploring the effects of increasing competitor equivalents, as well as increasing incubation times to be in line with similar literature experiments¹⁰⁴, especially considering the slower reactivity of sulfonyl fluorides, and their dependence on templating effects for binding, as well as the relatively unknown reactivity of α -nitrile containing compounds under these conditions. For future experiments working with these lysates, the effects of incubating with specific protease inhibitors should be explored to identify those that do not interfere with competition and can be used to prevent lysate degradation.

To investigate the activity of the electrophilic, anti-trypanosomal compounds identified from phenotypic screening against *T. brucei brucei*, a series of probes were generated, functionalising the parent compounds with alkyne handles for exploration in-gel and by mass spectrometry. Initial attempts at synthesis proved unsuccessful due to an incompatibility of alkyne groups in the photoredox reaction. This could be caused by competition reactions occurring with the alkyne functional group, such as carboxylations¹⁶⁰ and insertions¹⁶¹ which proceed under similar photoredox conditions. The probes were eventually formed utilising the existing functionality of the parent compounds, either by a deprotection of the amine followed by a coupling, or a reaction with the sulfonyl fluoride group to install an alkyne tag, where SAR indicated that this was appropriate. When screened for activity against *T. brucei brucei*, each of the alkyne analogues showed a loss in trypanosomal activity compared to their parent compounds. Two probes, **3-1 Alkyne** and **1-3a Alkyne** retained an activity of less than 10 μ M,

showing the smallest reduction in activity. This suggests they could be hitting the same protein targets as the parent compounds so should be prioritised for future experimental work. Further investigation into the SAR of active compounds can be carried out, by designing and synthesising a second compound library using similar heterene and hydrogen donor substrates to the active compounds. This can be used to home in on active functionality, aiming to identify compounds with a higher potency and selectivity than the initial library. Analogous compounds can also be used to identify groups non-essential to the compounds activity to provide potential sites for alkyne addition that are less detrimental to the compounds activity, making probes that are better mimics of the parent compounds.

Next, these probes can be used in MS-based proteomics, by attachment of a biotin tag for enrichment to identify their protein targets. When used in competition with the parent compound, key proteins that bind both probe and parent can be identified using the workflow described. While both the sulfonyl fluoride and α -nitrile based probes exhibited broad labelling across the *T. brucei* proteome when analysed by in-gel fluorescence, the increased sensitivity of MS may identify key competing proteins. The α -nitrile probes also showed strong labelling of proteins under a range of gel-based conditions considering the reversible nature of these warheads. This suggests that at least some nitrile-protein adducts are stable enough for the proteomic workflow, meaning that identification of protein targets and amino acid selectivity should be possible by mass spectrometry.

4. Conclusions and Future Work

This project aimed to develop a workflow from design of a target-agnostic electrophilic compound library through to phenotypic screening and target identification by integrating a high-throughput synthetic strategy with chemical proteomics methods. Here, this work will be summarised along with some scope of future potential for this work.

4.1. Generation of an Electrophile Library

Summary

This work tested the ability to generate a library of electrophilic compounds using diversity generating chemistry that moves away from traditional methods of design to better explore chemical space⁴⁰. Utilising a photoredox-based dehydrogenative coupling⁴¹ a heteroarene core functionalised with sulfonyl fluoride warheads was reacted with a range of compatible substrates, combined with a high-throughput approach to synthesis and reaction screening to identify successful product formation by LC-MS, ¹H and ¹⁹F NMR, for purification. Sulfonyl fluoride warheads were well tolerated with this chemistry, leading to the synthesis of 40 isolated compounds making up the reactive library. These compounds highlight the diversity in chemical structure accessible to this chemistry for coverage of biologically interesting chemical space¹⁶², broadly covering a range of chemical properties such as lipophilicity and heavy atom count to access lead-like space⁴³.

Future Work

A significant reduction in reaction yield was observed in this library generation compared to the model substrates such as benzothiazole and *N*-Boc-pyrrolidine, initially reported by *Dong et al*⁴¹. Further optimisation of these reaction, as well as running them under inert conditions could be used to improve the success rate of these reactions. Alternatively, exploring other dehydrogenative coupling conditions, such as those reported by *Grainger et al*⁴⁹, could further increase the scope of substrates for this chemistry. This could also be used to explore alternative reactive warheads, such as the S_N(Ar) warheads previously attempted, along with other non-cysteine reactive electrophiles, to increase the diversity of protein targets accessible to this library. Building on the success of sulfonyl fluorides, screening other S(VI)-based warheads, such as sulfuramidimidoyl fluorides¹⁶³, fluorosulfonates^{76,77}, or sulfurtriazoles¹⁶⁴ could be initial

starting point for exploring compatible warheads with non-cysteine based amino acid selectivity.

4.2. Phenotypic Screening for Anti-Trypanosomal Activity

Summary

Working in collaboration with the Smith group at the University of St. Andrews led to the discovery of several compounds with sub-micromolar anti-trypanosomal activity and at least a 30-fold selectivity over human, HeLa cells. These compounds had diverse structures, with active compounds arising from each of the three hetaryl cores giving the potential for these compounds to have different modes of action as anti-trypanosomals.

Future Work

Synthesis of a second covalent library based around similar structures to these active compounds could be used to build up a structure-activity relationship (SAR), aiming to identify key functional groups, and areas for further elaboration to increase the potency and selectivity of these anti-trypanosomal compounds. The compound library was also designed to be target agnostic, so could also be screened in other phenotypic assays, against other trypanosomal parasites such as *trypanosoma cruzi* or *leishmania*, or other organisms including bacteria cells. A full library screen could also be carried out against HeLa cells, and other human cancer cell lines to identify potential anti-cancer agents. This work would aim to identify inhibitors that are potent and selective for specific organisms and rule out compounds that show broad toxicity.

4.3. Synthesis of Electrophilic Probes

Summary

The most potent anti-trypanosomal compounds identified from phenotypic screening, **31** and **1-3**, were taken forward for further investigation. Alkyne containing analogues of these compounds were synthesised to generate functional chemical probes to explore their protein targets and mode of action. The initial synthesis attempted utilising the dehydrogenative coupling of alkyne-containing hydrogen donors was unsuccessful due to an incompatibility with alkynes and the dehydrogenative coupling reaction. This is

potentially due to competing reactions with the alkyne functionality under the iridium catalysed photoredox conditions^{160,161}. Therefore, an alternative method was used, by modifying the active, parent compound after its initial synthesis in the photoredox reaction, to install an alkyne containing group. This was accomplished by utilising the existing functionality of these molecules, *via* addition of alkyne containing protecting groups to hydrogen donor amines. Alternatively, for the compounds **1-3a/b Alkyne**, a sulfonamide was formed using the sulfonyl fluoride group, shown to be non-essential for the compound's activity by analysis of its SAR. These alkyne probes were screened in the cell viability assays and showed a significant loss of activity compared to the parent compounds. This suggests the areas used for alkyne addition are important for the compound to bind to its target protein. For example, replacing a Boc protecting group with a more polar Poc group could disrupt a favourable interaction in a hydrophobic pocket. Two of the alkyne probes, **3-1 Alkyne** and **1-3a Alkyne**, still showed a significant activity, of less than 10 μM and the smallest reduction in activity so should be prioritised for future experiments.

Future Work

Further investigation using chemical proteomics methods is required to determine if these probes are reactive to the same protein targets as the active compounds. In addition to this, exploring the active compounds SAR by generating a second library based around the active structures could be useful to identify areas of the compounds more productive for alkyne addition. Ideally these areas would not be important for compound activity, such that the activity of the parent compound would be retained in the alkyne probe. Exploring alternative reaction conditions to improve the scope of the photoredox reaction could be applied to the compatibility with alkyne substrates. Alternative reactions could also be identified to synthesise these probes¹⁶⁵.

4.4. Identifying α -Nitriles as A Second Reactive Warhead

Summary

α -Nitriles were shown to be a common functional group in active anti-trypanosomal compounds, leading to an investigation to their potential electrophilic reactivity. There are many examples of nitrile-based warheads, acting as reversible electrophiles⁸⁶, including α -nitrile containing- drug compounds known to react covalently with serine⁸⁵ and cysteine¹⁰⁶ proteases. Exploring the reactivity of an α -nitrile containing- family of active anti-trypanosomal compounds showed that the α -nitrile was essential for their activity. This work highlighted α -nitriles as a second covalent warhead compatible with the photoredox chemistry. Furthermore, α -nitriles are known in the literature to react reversibly with proteins, but the synthesised alkyne probes showed highly stable labelling of proteins under a range of gel-based conditions including precipitation, the click reaction, reduction, and heating.

Future Work

The α -nitrile containing probes generated, **1-3a/b Alkyne** and **T-3a Alkyne**, can be used to explore the reactivity of α -nitriles. Using them to investigate the anti-trypanosomal activity of the parent compounds, as well as using them to broadly assess the reactivity of these warheads in terms of their amino acid selectivity and stability.

4.4.1. Identifying Protein Targets Using Chemical Proteomics

Summary

In preliminary work the profile of proteins by these alkyne-containing analogues of the active compounds were visualised in *T. brucei brucei* cell lysate, visualised by in-gel fluorescence after attachment of a fluorescent tag *via* a click reaction. Under these conditions, reacting in cell lysate, the sulfonyl fluoride-based probe, **3-1 Alkyne** was shown to have a broad reactivity across the proteome.

Competitive profiling against a broad-spectrum serine hydrolase probe, **FP-RH**⁹⁷, highlighted the reactivity of the sulfonyl fluorides with active site serines in enzymes. These labelled proteins could be responsible for the compound's biological activity. The broad-spectrum labelling of these compounds under these lysate-based conditions, could

be irrelevant to the bioactivity seen in cells. α -Nitriles are shown to react reversibly with proteins⁸⁶ but the synthesised alkyne probes showed high stability and broad labelling across the proteome, under a range of gel-based conditions.

Future work

Next, the protein targets of these active compounds can be explored using the alkyne probes, functionalising with a biotin tag can be used to enrich the samples for identifying of target proteins by MS/MS. When used in competition, by pre-incubating cell lysate with the active parent compound, we could highlight key proteins potentially responsible for the anti-trypanosomal activity. Labelling can also be carried out on live cells after incubation with the probe compound, this may increase the selectivity of labelling by restricting probe concentration able to permeate the cell, and track how the compounds move throughout the cell, a feature which is lost when cells are lysed^{166,167}.

5. Experimental Procedures

5.1. General Information

All commercially available starting materials used were acquired from Sigma-Aldrich, Flurochem and Alfa Aesar. All larger scale reactions were carried out under nitrogen atmosphere unless stated otherwise, the reaction arrays were carried out under normal conditions, with care taken to minimise exposure to water, using dry solvent, when carrying out the reaction array. Anhydrous solvents for reactions obtained from a PureSolv MDS Purification System. Anhydrous 1,4-dioxane and ethyl acetate were obtained from SureSeal bottles. All other solvents and reagents were of analytical grade and used as supplied. Solvents were removed using a reduced pressure, Büchi rotary evaporator and a Vacuubrand PC2001 Vario Diaphragm pump.

Thin layer chromatography was carried out with commercial, aluminium backed silica plates (Merck silica 2880 gel, 60 F254) and visualised using an ultraviolet lamp ($\lambda_{\text{max}} = 254 \text{ nm}$). Flash column chromatography was carried out with silica gel 60 (35-75 μm particles).

Analytical LC-MS was performed using Ultimate3000 HPLC, with a UV diode array detector and a MS detector Bruker Amazon Speeds with electrospray ionisation run positive and negative switching mode. This uses Phenomenex Kinetex C₁₈ 2.1 \times 50 mm 2.6 micron column and two solvent systems: MeCN/H₂O + 0.1% formic acid or MeCN/H₂O. Accurate masses were obtained with a Bruker MaXis Impact with electrospray ionisation in positive mode. Purifications by HPLC-MS was carried out using a Agilent 1290 Infinity with Diode Array Detection and an Ascentis Express C₁₈ Column, 50 \times 2.1 mm, 2.7 μm particle size.

Infrared analysis was performed using a Perkin-Elmer One FT-IR spectrometer. ¹H and ¹³C NMR spectra were gained at 300 K on a Bruker 300, 400 or 500 MHz NMR spectrometer. Chemical shifts (δ) are stated in parts per million (ppm) and referenced to the residual solvent peak trimethylsilane (0 ppm) and coupling constants (J) are reported in Hertz (Hz). The splitting patterns of ¹H NMR data is reported: s (singlet), d (doublet), dd (doublet of doublets), t (triplet), m (multiplet). Assignment of structures were aided by COSY, DEPT and HMQC spectrums.

All buffers were prepared in 18.2 M Ω H₂O to the final volume stated. The pH of the solutions was adjusted using 1 M NaOH or 5 M HCl. Thermo Electron Corporation Holten LaminAir laminar flow cabinet was used to maintain a sterile environment when necessary. Centrifugation was performed using either a Heraeus multifuge 3 S-R centrifuge or a Heraeus Fresco-17 centrifuge. SDS-PAGE was carried out using a BioRad Mini-PROTEAN Tetra Cell system and a BioRad Power PAC 1000. A BioRad ChemiDoc MP Imaging System was used to image polyacrylamide gels using a combination of UV and white light (Rhodamine- DyLight 550 602/50 green epifluorescence, Fluorescein- DyLight 488 532/28, Coomassie Blue- 715/30 far red epifluorescence).

5.2. General Procedures for Chemical Synthesis

5.2.1. Synthesis of Sulfonyl Fluoride Hetarenes

The relevant hetarene sulfonic acid was dissolved in thionyl chloride to a final concentration of 1 M with a catalytic amount of DMF (0.1 eq). The solution was sealed in a crimped vial and heated to reflux at 75 °C for 2 hours. Solvent was removed *in vacuo* and the crude product resuspended in DCM and washed with saturated NaHCO₃. The organic layer was dried with Na₂SO₄ and concentrated *in vacuo* to afford the sulfonyl chloride. Without further purification, the hetarene sulfonyl chloride was dissolved in acetonitrile (1 mM, 1 eq) and added to a suspension of potassium hydrogenfluoride in water (4.5 mM, 2.3 eq), stirring for 12 hours at RT. The reaction mixture was diluted in water (5 × volumes) and the product extracted with DCM three times. The combined extracts were washed once with a 10% solution of NaHCO₃, and saturated NaCl before drying (Na₂SO₄) and concentrated *in vacuo* to give the pure sulfonyl fluoride¹⁶⁸.

5.2.2. Synthesis of Photoredox Mediated Dehydrogenative Coupling Array

100 µL Test Scale: To a LC-MS vial as acetone stock solutions, a functionalised hetarene (20.0 µL of a 1.5 M stock) were added, followed by a hydrogen donor (33.3 µL of a 1.5 M stock), TFA (10.0 µL of a 2 M stock), the iridium catalyst*, (Ir[dF(CF₃)ppy]₂(dtbpy))PF₆ (10.0 µL of a 0.01 M stock, CAS: 870987-63-6) and *t*-butyl peracetate (15.9 µL of a 50% w/v solution) were added along with acetone (10.7 µL) to a total volume of 100 µL, giving final concentrations of hetarene (100 mM), hydrogen donor (500 mM), TFA (200 mM), catalyst (1 mM) and *t*-butyl peracetate (500 mM). The reaction vials were sealed and stirred on a fan cooled HepatoChem lightbox with irradiation under a 390 nm Kessil Lamp for 24 hrs⁴¹. The mixtures were concentrated under air to give the crude product. The crude reaction mixture was dissolved in acetonitrile and purified via Mass-Directed HPLC with acetonitrile to water with a gradient between 5-95%, the eluted samples were lyophilised to give the pure product.

*In some cases, an alternative, organocatalyst was used, 4CzIPN (10.0 µL, 0.05 M, CAS: 1416881-52-1) and the reaction irradiated with a Kessil A160WE LED Tuna Blue lamp.

1 mL Array Scale: To a LC-MS vial as stock solutions, a functionalised hetarene (200 µL, 1.5 M), a hydrogen donor (333 µL of a 1.5 M stock), TFA (100 µL of a 2 M

stock), the iridium catalyst*, (Ir[dF(CF₃)ppy]₂(dtbpy))PF₆ (100 μL of a 0.01 M stock CAS: 870987-63-6) and *t*-butyl peracetate (159 μL of a 50% w/v solution) were added along with acetone (107 μL) to a total volume of 1 mL, to give final concentrations of hexarene (100 mM), hydrogen donor (500 mM), TFA (200 mM), catalyst (1 mM) and *t*-butyl peracetate (500 mM). The reaction vials were sealed and stirred on a fan cooled HepatoChem lightbox with irradiation under a 390 nm Kessil Lamp for 24 hrs⁴¹. The mixtures were concentrated under air to give the crude product. The crude reaction mixture was dissolved in acetonitrile and purified via Mass-Directed HPLC with acetonitrile to water with a gradient between 5-95%, the eluted samples were lyophilised to give the pure product.

*In some cases, an alternative, organocatalyst was used, 4CzIPN (100 μL, 0.05 M, CAS: 1416881-52-1) and the reaction irradiated with a Kessil A160WE LED Tuna Blue lamp.

5.3. General Procedures for Cell Culture

All Cell culture of trypanosomes and cell viability assays of both HeLa and *T. brucei* were carried out by Will Mosedale at the University of St. Andrews.

5.3.1. General Procedure for HeLa Cell Culture

HeLa Cell Culture

HeLa cells were grown at 37 °C, in DMEM media, containing FBS (10%), L-glutamine (1%) and penicillin/ streptomycin (1%). The cells were grown in EZ Nunclon vented flasks in an atmosphere containing 5% CO₂. The cells were passaged by transferring into fresh media as to not exceed a cell density of around 4×10^6 cells/mL.

Cryogenic Storage of HeLa Cells

HeLa cells at confluent density (4×10^6 cells/mL) in a T75, were washed with PBS (2×5 mL), trypsinised, and diluted in media. The suspension was centrifuged at $800 \times g$ for 5 minutes. The supernatant was removed, and cells resuspended in 9 mL of fresh media containing DMSO (5%) to a density of around 0.5×10^6 cells/mL. The cell suspension was aliquoted into cryovials (1 mL), and frozen in a Mr Frosty (ThermoFisher Scientific Cat No. 5100-0001) containing isopropan-1-ol, which was then surrounded with dry ice and left for 24 hours. Cryovials were then stored at -170°C in the liquid nitrogen vapour phase for long-term storage.

Cells were revived from cryogenic storage by first removing them from liquid nitrogen onto ice for 15 minutes. The cells are then allowed to warm to room temperature in a culture hood. Once defrosted, the cells were transferred into a non-vented 25 mL cell culture flask with fresh medium (9 mL) and incubated at 37°C. After 4 hours, the DMSO-containing media was removed, and fresh media was added.

Standard HeLa Resazurin Cell Viability Assay

Performed by Will Mosedale at the University of St. Andrews.

Cell viability assays carried out in 96 well plates with 200 µL of media per well. Cells were seeded at 2.5×10^4 cells/mL and incubated with the library compound in quadruplicate as technical replicates for 66 hours (in the same conditions as culturing). The plate included wells containing a no-cell positive control, and the negative control of 0.5% DMSO. After 66 hours, 10 µL of 1.1 mg/mL Resazurin sodium salt (in PBS) was

added and plates incubated for a further 6 hours (for a total assay duration of 72 hours). Plates were then read on a plate reader using excitation/emission 560/590 nm. Ec50 values were calculated using a sigmoidal dose response fitting algorithm programmed in R using the LL.4() logarithmic fitting function and plotting the replicate data to output an Ec50 and error values.

Preparation of HeLa Cell Lysate

HeLa cells at confluent density (4×10^6 cells/mL) in a T75, were washed with PBS (2×5 mL). PBS (1 mL) was added, and cells scraped to detach from the surface, transferred to an Eppendorf with additional PBS (1mL) and centrifuged for 5 minutes ($500 \times g$, 4 °C). The cell pellet was resuspending in PBS (1 mL) and sonicated at 60% intensity, (3×10 seconds) over ice, cooling for 30 seconds between sonications. Unlysed cells were pelleted by centrifugation for 5 minutes ($1000 \times g$, 4 °C) and the supernatant transferred to a new Eppendorf. The protein concentration was determined by DC assay, and aliquots of lysate were snap-frozen in liquid nitrogen and stored at -80 °C.

5.3.2. General Procedure for *Trypanosoma brucei* Cell Culture

Performed by Will Mosedale at the University of St. Andrews

***Trypanosoma brucei brucei* culture**

Trypanosoma brucei brucei (*T. b. brucei*) bloodstream form strain 427 were grown at 37 °C, in HMI-11 media in vented flasks in an atmosphere containing 5% CO₂. The cells were passaged by transferring into fresh media as to not exceed a cell density of 2×10^6 cells/mL.

Cryogenic Storage of *Trypanosoma brucei brucei*

T. b. brucei (5 mL) at confluent density (2×10^6 cells/mL) was centrifuged at $800 \times g$ for 5 minutes. The supernatant was removed, and cells resuspended in fresh media to a density of around 2×10^7 cells/mL. A sterile solution of 60% glycerol in water was added to the cell suspension to give a final concentration of 10% glycerol. The cell suspension was transferred to a cryovial, into a Mr Frosty (ThermoFisher Scientific Cat No. 5100-0001) containing isopropan-1-ol, which was then surrounded with dry ice and left

for 24 hours. Cryovials were then stored at -170 °C in the liquid nitrogen vapour phase for long term storage.

Cells are revived from cryogenic storage by first removing them from liquid nitrogen onto ice for 15 minutes. The cells are then allowed to warm to room temperature in a culture hood. Once defrosted, the cells can be transferred into a non-vented 25 mL cell culture flask with fresh medium (9.4 mL) and left to grow in a 37 °C shaking incubator.

Standard *Trypanosoma brucei brucei* Resazurin Cell Viability Assay

Cell viability assays carried out in 96 well plates with 200 µL of culture per well. Cells were seeded at 5×10^3 cells/mL and incubated in quadruplicate as technical replicates with the library compound for 66 hours (in the same conditions as culturing). The plate included wells containing the positive control pentamidine (100 nM) and the negative control of 0.5% DMSO. After 66 hours, 10 µL of 1.1 mg/mL Resazurin sodium salt (in PBS) was added and incubated for a further 6 hours (for a total assay duration of 72 hours). Plates were then read on a plate reader using excitation/emission 560/590 nm. Ec50 values were calculated using a sigmoidal dose response fitting algorithm programmed in R using the LL.4() logarithmic fitting function and plotting the replicate data to output an Ec50 and error values for replicate data.

Preparation of *Trypanosoma brucei brucei* Cell Lysate

T. b. brucei cells at confluent density (2×10^6 cells/mL) were transferred to a falcon tube and pelleted by centrifugation for 10 minutes ($500 \times g$, 4 °C). the cells were washed by resuspending in trypanosome dilution buffer (5 mM KCl, 80 mM NaCl, 1 mM MgSO₄, 20 mM NaH₂PO₄ and 2 mM glucose in water) and centrifuged. The cells were then resuspended in pure water, and freeze-thawed twice over cardice. The suspension was then sonicated at 60% intensity, (1 × 10 seconds) over ice, Unlysed cells were pelleted by centrifugation for 5 minutes ($1000 \times g$, 4 °C) and the supernatant transferred to a new Eppendorf, the lysate was then diluted in 1 volume of 2 × PBS solution to give a final protein concentration of 2 mg/mL. The lysate was snap-frozen in liquid nitrogen and stored at -80 °C.

5.4. General Procedures for Gel-Based Imaging

5.4.1. Buffer Preparation

Phosphate-Buffered Saline (PBS): pH 7.4 (purchased as tablets from Sigma-Aldrich, 79382) containing phosphate (10 mM), potassium chloride (2.7 mM) and Sodium chloride (137 mM).

SDS-PAGE Resolving Gel Buffer: pH 8.8, Tris (1.5 M)

SDS-PAGE Stacking Gel Buffer: pH 6.8, Tris (0.5 M)

SDS-PAGE Running Buffer: Tris (25 mM), Glycine (192 mM), SDS (0.1% w/v).

2 × Sample loading buffer (SLB): Tris (100 mM), SDS (4% w/v), Glycerol (20%), bromophenol blue (0.002% w/v) and a reducing agent* (0.4 M).

*When required DTT was added to the buffer mixture for use, or TCEP was added separately to reactions from a fresh 1M stock made in water.

Coomassie Stain: Coomassie G250 (0.2% w/v), Methanol (50%), Acetic Acid (10%).

Coomassie De-stain: Methanol (50%), Acetic Acid (10%).

5.4.2. Protein Labelling with Alkyne Containing Probes

On a 25 µL scale, cell lysate was diluted to 1 mg/ml with PBS (pH 7.4) in an Eppendorf. A 100-fold stock solution of the probe compound was prepared in DMSO and stored at -20 or -80 °C depending on probe stability. A fresh 10-fold stock was prepared for each reaction by dilution into PBS to give a final DMSO concentration of 10%. The probe stocks (2.5 µL, 10-fold stock) were prepared to give the final probe concentration as specified in each reaction, typically between 0.1 – 100 µM, with a final DMSO concentration of 1%. A DMSO-lysate control was also used containing 1% DMSO to explore the effect of probe addition on the proteins. The Eppendorfs were then incubated with gentle agitation for 30 minutes* at 25 °C.

*Incubation for 30 minutes was found to be sufficient to produce strong labelling with sulfonyl fluorides across the proteome. Using a shorter incubation time to prevent protein degradation caused by lack of protease inhibitors. When using other warheads, initial experiments should be carried out to find optimal reaction times, and to test for protease inhibitor interference.

5.4.3. Competitive Profiling of Electrophilic Compounds

On a 25 μL scale, cell lysate was diluted to 1 mg/ml with PBS (pH 7.4). A 10 mM stock solution of the electrophilic competitor compound was prepared in DMSO. A fresh 10-fold stock of competitor was prepared for each experiment by dilution into PBS to a concentration of 1 mM, 10% DMSO. The competitor (2.5 μL , 1mM) along with a DMSO control (2.5 μL , 10% DMSO) was then added to the lysate to a final concentration of 100 μM in 1% DMSO. the samples were incubated with agitation for 30 minutes at 25 $^{\circ}\text{C}$.

From a 100-fold stock solution in DMSO of the relevant probe, a 10-fold stock was prepared by dilution into PBS. The probe (2.5 μL , 10-fold stock) was then added to every reaction to give the final probe concentration as specified in each reaction, typically between 1 – 10 μM *, now with a final DMSO concentration of 2%. The reactions were incubated for a further 30 minutes at 25 $^{\circ}\text{C}$.

*Additional experiments required to increase competitor: probe ratio for stronger competition. Experiments limited by stock concentrations of competitor library.

5.4.4. Visualisation of Probe Labelling

Labelling of alkyne or fluorophore containing probes used in the above experiments were visualised through SDS-PAGE following a standard procedure outlined below.

Click Reaction:

As required (for alkyne-containing probes). A master mixture of click reagents was prepared as a fresh stock for each reaction. The reagents as stocks in DMSO or water were added together in the order given below and vortexed briefly. For experiments with a probe concentration of $<100 \mu\text{M}$, including the DMSO control, the click reagents (1.5 μL) were added to each reaction Eppendorf and incubated at 25 $^{\circ}\text{C}$ for one hour with gentle agitation. For experiments with a probe concentration $\geq 100 \mu\text{M}$, the master stock was added to give a final concentration of azide of 2 equivalents over the probe.

Reagent	Final concentration	Reagent stock	Per Reaction
Fluorophore-azide	100 μM	10 mM in DMSO	0.6 μL
CuSO_4	1 mM	50 mM in H_2O	1.2 μL
TCEP	1 mM	50 mM in H_2O	1.2 μL
TBTA	100 μM	10 mM in DMSO	0.6 μL

After one hour incubation, the reaction was quenched with EDTA (0.5 μL , 0.5 M) to give a final concentration of 10 mM in solution.

Protein Precipitation:

To remove excess probes and/or excess click reagents, the reactions were precipitated by addition of cold acetone (4 volumes), vortexed, and left to precipitate overnight at -20 °C. The suspension was then centrifuged, (20 mins, 13000 × g) and the protein pellet washed with cold methanol (2 × 2 volumes) with brief sonication. The pellet was then vortexed and centrifuged (10 mins, 13000 × g) to remove additional reagents. The methanol was then removed, and the pellet left to air dry for 5 minutes.

Preparation of SDS-PAGE gels:

Each gel-based experiment used a 1 mm gel with 10 lanes, containing a 12% acrylamide resolving gel, and a 5% acrylamide stacking gel. SDS-PAGE gels were made following a standard recipe, by mixing the listed reagents in this order:

Reagent	Stacking Gel (5%)	Resolving Gel (12%)
Water	3.00 mL	4.20 mL
Acrylamide (40% w/v)	0.625 mL	3.00 mL
Stacking Gel Buffer	0.945 mL	–
Resolving Gel Buffer	–	2.60 mL
SDS (10% w/v)	50 µL	100 µL
APS (10% w/v)	50 µL	100 µL
TEMED	5 µL	10 µL

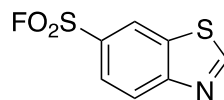
Running SDS-PAGE Gels and Imaging:

Unless described otherwise, precipitated protein samples (25 µg) were resuspended in SDS solution (2% in PBS, 12.5 µL) and 2 × SLB (12.5 µL) with mixing. The samples were then boiled for 2 minutes at 95 °C and centrifuged briefly. Samples were loaded onto a SDS-PAGE gel (10 µL, 10 µg) along with an all-blue pre-stained protein standard (7.5 µL, Bio-Rad: 1610373). Gels were run with a Bio-Rad power supply unit at 180 V, 400 mAmps, for between 40 – 60 minutes.

Gels were imaged using a BioRad ChemiDoc MP Imaging System. Imaging fluorescence using filters DyLight 550 602/50 green epifluorescence for rhodamine, and DyLight 488 532/28 filters for fluorescein. The pre-stained ladder was imaged with Coomassie filter 715/30 far red epifluorescence. Total protein visualisation was achieved by staining with Coomassie blue G250 solution overnight, before removing background with de-staining solution for gel imaging using the Coomassie filter.

5.5. Experimental Details of Isolated Compounds

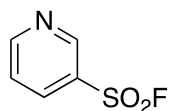
1,3-benzothiazole-6-sulfonyl fluoride



HA1

Following the general procedure (Section 5.2.1), 1,3-benzothiazole-5-sulfonyl chloride (500 mg, 2.1 mmol) was reacted to form the sulfonyl fluoride **HA1** as a yellow amorphous solid (347 mg, 75%). δ_{H} (500 MHz, CDCl_3) 9.33 (1H, s, 2-H), 8.71 (1H, d, J 1.9, 7-H), 8.36 (1H, d, J 8.7, 4-H), 8.14 (1H, dd, J 8.7, 1.9, 5-H). δ_{C} (125 MHz, CDCl_3) 159.9 (2-C), 157.4 (7a-C), 134.8 (3a-C), 130.0 (1C, d, J 25.2, 6-C), 125.7 (5-C), 125.1 (4-C), 124.1 (7-C). δ_{F} (565 MHz, CDCl_3) 68.2. ν_{max} (neat)/ cm^{-1} 3091, 3069, 1405, 1200, 1017. HRMS (ESI) $\text{C}_7\text{H}_4\text{NO}_2\text{S}_2$ requires $[\text{M}+\text{H}]^+$, calculated 217.9746, found 217.9740.

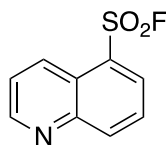
Pyridine-3-sulfonyl fluoride



HA3

Following the general procedure (**Section 5.2.1**), pyridine-3-sulfonyl chloride (500 mg, 2.82 mmol) was reacted to form the sulfonyl fluoride **HA3**¹⁶⁹ as a clear oil (392 mg, 86%). δ_{H} (500 MHz, CDCl_3) 9.24 (1H, appt t, J 1.6, 2-H), 9.01 (1H, dd, J 4.9, 1.6, 6-H), 8.31 (1H, ddd, J 8.2, 2.5, 1.6, 4-H), 7.61 (1H, dd, J 8.2, 4.9, 5-H). δ_{C} (125 MHz, CDCl_3) 156.1 (6-C), 149.2 (2-C), 136.2 (4-H), 130.4 (1C, d, J 25.5, 3-C), 124.3 (5-H). δ_{F} (565 MHz, CDCl_3) 69.2. ν_{max} (neat)/ cm^{-1} 3071, 1572, 1406, 1209, 1111. HRMS (ESI) Unable to acquire.

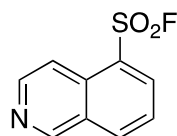
Quinoline-5-sulfonyl fluoride



HA4

Following the general procedure (**Section 5.2.1**), quinoline-6-sulfonic acid (1.00 g, 4.74 mmol) was reacted to form the sulfonyl fluoride **HA4**¹⁷⁰ as a cream amorphous solid (236 mg, 26%). δ_{H} (500 MHz, CDCl_3) 9.19 (1H, dd, J 4.3, 1.8, 2-H), 8.53 (1H, dd, J 7.4, 1.4, 6-H), 8.32 (1H, dd, J 8.3, 1.8, 4-H), 8.24 (1H, dd, J 8.2, 1.4, 8-H), 7.72 (1H, ddd, J 8.5, 7.5, 1.3, 7-H), 7.64 (1H, dd, J 8.3, 4.3, 3-H). δ_{C} (125 MHz, CDCl_3) 152.7 (2-C), 143.8 (4a-C), 136.6 (4-C), 136.1 (8-C), 133.1 (6-C), 131.4 (1C, d, J 21.0, 5-C), 129.1 (8a-C), 125.3 (7-C), 123.0 (3-C). δ_{F} (565 MHz, CDCl_3) 65.3. ν_{max} (neat)/ cm^{-1} 3050, 1491, 1399, 1197, 1156. HRMS (ESI) $\text{C}_9\text{H}_6\text{FNO}_2\text{S}$ requires $[\text{M}+\text{H}]^+$, calculated 212.0182, found 212.0173.

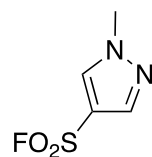
Isoquinoline-5-sulfonyl fluoride



HA5

Following the general procedure (**Section 5.2.1**), isoquinoline-5-sulfonyl chloride (500 mg, 2.37 mmol) was reacted to form the sulfonyl fluoride **HA5** as a colourless amorphous solid (254 mg, 55%). δ_{H} (500 MHz, CDCl_3) 9.40 (1H, d, J 1.2, 1-H), 8.78 (1H, d, J 6.1, 3-H), 8.54 (dt, J 8.3, 1.2, 8-H), 8.39 (1H, dd, J 8.3, 1.2, 6-H), 8.28 (1H, ddd, J 6.1, 2.6, 1.2, 4-H), 7.77 (1H, td, J 7.8, 1.2, 7-H). δ_{C} (125 MHz, CDCl_3) 153.4 (1-C), 146.5 (3-C), 136.5 (8-C), 135.0 (7-C), 131.5 (4a-C), 128.7 (8a-C), 128.6 (1C, d, J 24.8, 5-C), 126.0 (6-C), 116.7 (4-C). δ_{F} (565 MHz, CDCl_3) 64.9. ν_{max} (neat)/ cm^{-1} 3061, 2982, 1491, 1400, 1319, 1078. HRMS (ESI) $\text{C}_9\text{H}_6\text{FNO}_2\text{S}$ requires $[\text{M}+\text{H}]^+$, calculated 212.0182, found 212.0176.

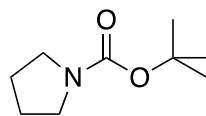
1-Methylpyrazole-4-sulfonyl fluoride



HA6

Following the general procedure (**Section 5.2.1**), 1-methylpyrazole-4-sulfonyl fluoride (500 mg, 3.05 mmol) was reacted to form the sulfonyl fluoride **HA6** as a colourless amorphous solid (300 mg, 67%). δ_{H} (500 MHz, CDCl_3) 8.02 (1H, s, 5-H), 7.94 (1H, s, 3-H), 4.01 (3H, s, Me). δ_{C} (125 MHz, CDCl_3) 140.0 (3-C), 133.9 (5-C), 144.6 (1C, d, *J* 31.4, 4-C), 40.1 (Me). δ_{F} (565 MHz, CDCl_3) 71.4. ν_{max} (neat)/ cm^{-1} 2136, 2958, 1525, 1410, 1389, 1068. HRMS (ESI) Unable to acquire.

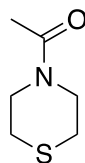
N-Boc-pyrrolidine



HD1

Di-tert-butyl dicarbonate (6.98 g, 54 mmol) was dissolved in DCM (250 mL, 0.2 M) with DMAP (659 mg, 5.4 mmol) and cooled to 0 °C. Pyrrolidine (5 mL, 60 mmol) was added dropwise via an addition funnel before warming to room temperature and stirring overnight for 24 hours, with consumption of starting material shown by TLC. The solution was then washed with brine (2 × 50 mL) and water (2 × 50 mL) before drying with Na₂SO₄ and concentrated *in vacuo*. The crude product was purified through a silica plug, eluting with DCM to give *N*-Boc-pyrrolidine, **HD1**¹⁷¹ as a colourless oil (8.23 g, 81%). δ_{H} (500 MHz, CDCl₃) 3.30 (2H, t, *J* 6.2, 2- and 5-H_a), 3.24 (2H, t, *J* 6.2, 2- and 5-H_b), 1.83-1.80 (4H, m, 3- and 4-H₂), 1.44 (9H, s, ^tBu 2-H₃). δ_{C} (125 MHz, CDCl₃) 154.8 (^tBu C=O), 79.0 (^tBu C₁), 46.1 (2- or 5-C), 45.7 (2- or 5-C), 28.7 (^tBu C₃), 25.9 (3- or 4-C), 25.1 (3- or 4-C). *R*_F 0.42 (DCM). ν_{max} (neat)/cm⁻¹ 2974, 2876, 1692. HRMS (ESI) C₉H₁₇NO₂ requires [2M+Na]⁺, calculated 365.2416 found 365.2413.

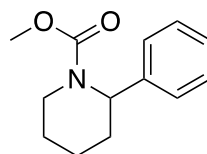
4-Acetyl-thiomorpholine



HD5

Thiomorpholine (500 mg, 4.85 mmol), was dissolved in dry DCM (20 mL) and cooled to 0 °C on ice, to which triethylamine (850 μ L, 5.50 mmol) was added and the solution stirred. Acetyl chloride (3.15 mL, 4.4 mmol) was added dropwise to the solution, and stirred for 1 hour before warming to room temperature overnight, until consumption of acetyl chloride was shown by TLC. The reaction mixture was then washed with brine (2 \times 10 mL) and water (2 \times 10 mL), dried with Na₂SO₄ and concentrated *in vacuo*. The crude product was purified through a silica plug, eluting with DCM to give 4-acetylthiomorpholine, **HD5**¹⁷² as a yellow oil (332 mg, 52%). δ_{H} (500 MHz, CDCl₃) 3.84 (2H, t, *J* 5.2, 3- and 5-H_a), 3.70 (2H, t, *J* 5.2, 3- and 5-H_b), 2.61-2.57 (4H, m, 2- and 6-H₂), 2.07 (3H, s, Ac 2-H₃). δ_{C} (125 MHz, CDCl₃) 169.0 (Ac C=O), 49.1 (3- or 5-C), 44.1 (3- or 5-C), 27.9 (2- or 6-C), 27.4 (2- or 6-C), 21.7 (Ac 2-C). ν_{max} (neat)/cm⁻¹ 2910, 1628. *R*_F 0.51 (DCM). HRMS (ESI) C₆H₁₁NOS requires [M+Na]⁺, calculated 168.0459, found 168.0446.

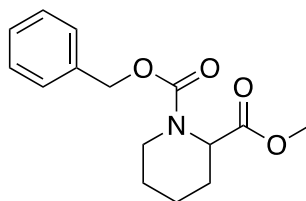
Methyl 2-phenylpiperidine-1-carboxylate



HD16

2-Phenyl piperidine (500 mg, 3.20 mmol) was dissolved in dry DCM with triethylamine (500 μ L, 3.55 mmol) and cooled to 0 °C on ice. Methyl chloroformate (225 μ L, 2.91 mmol) was added dropwise, and the solution stirred for 1 hour before warming to room temperature overnight, until consumption of the chloroformate shown by TLC. The reaction mixture was then washed with brine (2 \times 10 mL) and water (2 \times 10 mL), dried with Na₂SO₄ and concentrated *in vacuo*. The crude product was purified through a silica plug to elute methyl 2-phenylpiperidine-1-carboxylate, **HD16**¹⁷² as a colourless oil (427, 67%), δ_{H} (500 MHz, CDCl₃) 7.35 (2H, m, Ph 2- and 6-H), 7.24 (3H, m, Ph 3-, 4- and 5-H), 5.48 (1H, appt br. s, 2-H), 4.13-4.07 (1H, br. m, 6-H_a), 3.74 (3H, s, Me) 2.82 (1H, ddd, *J* 13.8, 10.4, 3.9, 3-H_a), 2.32 (1H, dd, *J* 10.4, 3.9, 6-H_b), 1.93-1.87 (1H, m, 3-H_b), 1.63-1.42 (4H, m, 3- and 4-H₂). δ_{C} (125 MHz, CDCl₃) 156.8 (C=O), 139.8 (Ph 1-C), 128.6 (Ph 3- and 5-C), 126.5 (Ph 2-, 4- and 6-C), 53.4 (2-C), 52.7 (Me), 40.4 (6-C), 28.1 (3-C), 25.5 (5-C), 19.3 (4-C). ν_{max} (neat)/cm⁻¹ 3048, 3021, 2931, 2895, 1675, 1525, 1486. *R*_F 0.80 (DCM). HRMS (ESI) C₁₃H₁₇NO₂ requires [M+Na]⁺, calculated 242.1157, found 242.1160.

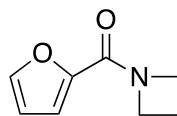
1-Benzyl-2-methyl piperidine-1,2-dicarboxylate



HD17

1-Benzyloxy-2-piperidine carboxylic acid (500 mg, 1.9 mmol) was dissolved in methanol (1.9 mL) and sealed in a vial under nitrogen. The vial was cooled to 0 °C on ice, before thionyl chloride (179 μ L, 2.5 mmol) was added dropwise, and the solution stirred for 1 hour. The reaction was then warmed to room temperature and stirred overnight. The reaction diluted in DCM (10 mL) and quenched with water (2 \times 10 mL), dried with Na₂SO₄ and concentrated *in vacuo* to afford the pure methyl ester, **HD17**¹⁴⁹ as a colourless solid (444 mg, 84%, 50:50 Rot_a:Rot_b). δ_{H} (500 MHz, CDCl₃) 7.38-7.35 (2H, m, Ph 2- and 6-H), 7.32-7.29 (3H, m, Ph 3-, 4- and 5-H), 5.16 (2H, s, Cbz CH₂), 4.97-4.94 (1H, br. m, 2-H_{rotA}), 4.86-4.84 (1H, br. m, 2-H_{rotB}), 4.11 (1H, appt d, *J* 11.0, 6-H_{rotA}), 4.06 (1H, appt d, *J* 11.0, 6-H_{rotB}), 3.74 (3H, s, Me_{rotA}), 3.68 (3H, s, Me_{rotB}), 3.06 (1H, appt t, *J* 13.0, 6-H_{rotA}), 2.96 (1H, appt t, *J* 13.0, 6-H_{rotB}), 2.25-2.19 (1H, m, 3-H_a), 1.70-1.61 (4H, m, 3-H_b 4-H_a and 5-H_{a/b}), 1.46-1.40 (1H, m, 4-H_b), 1.30-1.24 (1H, m 4-H_b). δ_{C} (125 MHz, CDCl₃) 172.3 (Ester C=O), 156.6 (Cbz C=O_a), 156.1 (Cbz C=O_b), 136.8 (Ph 1-C), 128.6 (Ph 3- and 5-C), 128.0 (Ph 2-, 4- and 6-C), 67.5 (Cbz 1-C_a), 67.3 (Cbz 1-C_b), 54.8 (2-C_a), 54.5 (2-C_b), 52.3 (Me), 42.0 (6-C_a), 41.9 (6-C_b), 26.9 (3-C_a), 26.8 (3-C_b), 24.9 (5-C_a) 24.7 (5-C_b), 20.9 (4-C_a), 20.8 (4-C_b). ν_{max} (neat)/cm⁻¹ 3032, 2946, 2860, 1739, 1697, 1586, 1498. *R_F* 0.80 (10:90 EtOAc–DCM). HRMS (ESI) C₁₅H₁₉NO₄ requires [M+Na]⁺, calculated 300.1212, found 300.1205.

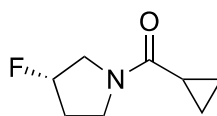
1-(Furan-2-carbonyl)azetidine



HD18

Azetidine hydrochloride (500 mg, 5.34 mmol) was dissolved in DCM with triethylamine (1.60 mL, 11.40 mmol) and cooled to 0 °C on ice. 2-Furoyl chloride (480 μ L, 4.86 mmol) was added dropwise, and the solution stirred for 1 hour before warming to room temperature overnight, until consumption of the chloroformate shown by TLC. The reaction mixture was then washed with brine (2 \times 10 mL) and water (2 \times 10 mL), dried with Na₂SO₄ and concentrated *in vacuo*. The crude product was purified via column chromatography, eluting with a gradient of 0 – 50% EtOAc in DCM to give the amide, **HD18**¹⁷² as a colourless amorphous solid (351 mg, 44%). δ_{H} (500 MHz, CDCl₃) 7.46 (1H, dd, *J* 1.8, 0.9, 3-H), 7.00 (1H, dd, *J* 3.5, 0.9, 5-H), 6.45 (1H, dd, *J* 1.8, 3.5, 4-H), 4.51 (2H, t, *J* 7.8, 2-H₂), 4.17 (2H, t, *J* 7.8, 4-H₂), 2.36 (2H, p, *J* 7.8, 3-H₂). δ_{C} (125 MHz, CDCl₃) 158.9 (C=O), 148.2 (2-C), 144.4 (3-C), 115.2 (4-C), 111.5 (5-C), 52.6 (2-C), 48.6 (4-C), 16.5 (3-C). ν_{max} (neat)/cm⁻¹ 3121, 3094, 3013, 2951, 2875, 1621, 1564, 1484, 1474, 1450. *R*_F 0.2 (50:50 DCM–EtOAc). HRMS (ESI) C₈H₉NO₂ requires [2M+Na]⁺, calculated 325.1164, found 325.1161.

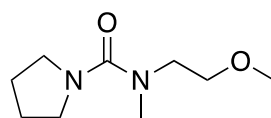
(3S)-1-Cyclopropanecarbonyl-3-fluoropyrrolidine



HD19

(3S)-Fluoropyrrolidine hydrochloride (500 mg, 3.98 mmol) was dissolved in dry DCM with triethylamine (1.14 mL, 8.15 mmol) and cooled to 0 °C on ice. Cyclopropane carbonyl chloride (328 μ L, 3.62 mmol) was added dropwise, and the solution stirred for 1 hour before warming to room temperature overnight, until consumption of the chloroformate shown by TLC. The reaction mixture was then washed with brine (2 \times 10 mL) and water (2 \times 10 mL), dried with Na₂SO₄ and concentrated *in vacuo*. The crude product was purified through a silica plug to elute (3S)-1-cyclopropanecarbonyl-3-fluoropyrrolidine, **HD19**¹⁷² as a yellow oil (412 mg, 66%, 50:50 mixture of rotamers). δ_{H} (500 MHz, CDCl₃) 5.29 (1H, ddt, *J* 13.5, 8.2, 3.0, 3-H), 3.90-3.50 (4H, m, 2- and 5-H₂), 2.40-1.90 (2H, m, 4-H₂), 1.63 (1H, m, prop 1-H_{Rot}a), 1.53 (1H, m, 1-H_{Rot}b), 1.00 (2H, m, prop 2- and 3-H_a), 0.77 (2H, m, prop 2- and 3-H_b). δ_{C} (125 MHz, CDCl₃) 172.6 (C=O_a) 172.4 (C=O_b), 93.5 (1C, d, *J* 175.0, 3-C_a), 91.63 (1C, d, *J* 175.0, 3-C_b), 53.2 (1C, d, *J* 22.4, 2-C_a), 52.7 (1C, d, *J* 22.4, 2-C_b), 44.3 (5-C_a), 43.8 (5-C_b), 32.8 (1C, d, *J* 22.4, 4-C_a), 31.2 (1C, d, *J* 22.4, 4-C_b), 12.7 (prop 1-C_{Rot}a), 12.6 (prop 1-C_{Rot}b), 7.9 (prop 2- or 3-C_a), 7.8 (prop 2- or 3-C_a), 7.6 (prop 2- or 3-C_b), 7.5 (prop 2- or 3-C_b). δ_{F} (565 MHz, CDCl₃) -177.0 (Rot_a), -177.8 (Rot_b). ν_{max} (neat)/cm⁻¹ 2979, 2889, 1689, 1435. *R*_F 0.43 (50:50 DCM–EtOAc). HRMS (ESI) C₈H₁₂FNO requires [2M+Na]⁺, calculated 337.1704, found 337.1704.

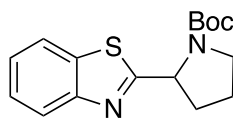
***N*-(2-methoxyethyl)-*N*-methylpyrrolidine-1-carboxamide**



HD20

Pyrrolidine (355 mg, 5.00 mmol) was dissolved in water (10 mL) and cooled to 0 °C over ice. CDI (890 mg, 5.50 mmol) was added, and the solution stirred for 1 hour before warming to room temperature. Formation of the carbonylimidazolide was monitored by TLC. Once completed, (2-methoxyethyl)methylamine (650 μ L, 6.00 mmol) and stirred for 2 hours. The coupled product was then extracted with ethyl acetate (3 \times 5 mL) and concentrated *in vacuo* without further purification to afford the carboxamide, **HD20**¹⁴⁷ as a yellow oil (398 mg, 43%). δ_{H} (500 MHz, CDCl₃) 3.52 (2H, t, *J* 5.9, Et 2-H₂), 3.36 (2H, t, *J* 5.9, Et 1-H₂), 3.33-3.30 (7H, m, NMe and pyrrolidiny 2- and 5-H₂), 2.87 (3H, s, OMe), 1.79 (4H, m, 3- and 4-H₂). δ_{C} (125 MHz, CDCl₃) 163.3 (C=O), 71.3 (Et 2-C), 58.9 (OMe), 49.7 (Et 1-C), 48.5 (pyrrolidiny 2- and 5-C), 37.4 (NMe), 25.7 (pyrrolidiny 3- and 4-C). ν_{max} (neat)/cm⁻¹ 2979, 2889, 1689, 1435. *R*_F 0.27 (DCM). HRMS (ESI) C₉H₁₈N₂O₂ requires [M+H]⁺, calculated 187.1447, found 187.1437.

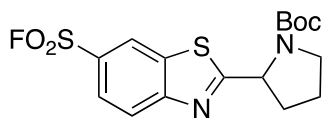
2-(*N*-Boc-pyrrolidin-2-yl)-1,3-benzothiazole



T-1

Following the general procedure (**Section 5.2.2**), 1,3-benzothiazole (13.5 mg, 0.10 mmol) was reacted with *N*-boc-pyrrolidine (85.6 mg, 0.5 mmol) following purification by Mass-Directed HPLC from a 10 minute gradient of 35 – 95% acetonitrile in water, collecting at 8.5 mins to isolate the cross coupled product, **T-1**⁴¹, as a pale brown amorphous solid (8.7 mg, 28%, 60:40 mixture of rotamers). δ_{H} (500 MHz, CDCl_3) 7.9 (1H, d, J 8.1, 7-H), 7.87-7.84 (1H, m, 4-H), 7.48-7.44 (1-H, m, 6-H), 7.38-7.34 (1H, m, 5-H), 5.24 (1H, br. s, pyrrolidinyl 2- H_{min}), 5.22 (1H, br. d, pyrrolidinyl 2- H_{maj}), 3.60-3.55 (2H, m, pyrrolidinyl 5-H), 2.43-2.33 (2H, m, pyrrolidinyl 3-H), 2.02-1.92 (2H, m, pyrrolidinyl 4-H), 1.49 (9H, s, ^tBu 2- H_{min}) 1.30 (9H, s, ^tBu 2- H_{maj}). δ_{C} (125 MHz, CDCl_3) 177.1 (^tBu $\text{C}=\text{O}_{\text{maj}}$), 176.3 (^tBu $\text{C}=\text{O}_{\text{min}}$) 162.0 (2-C), 154.9 (7a-C), 153.6 (3a-C), 126.1 (6-C), 124.9 (5-C), 122.8 (7-C), 121.9 (4-C), 80.5 (^tBu $\text{C}_{2\text{maj}}$), 80.3 (^tBu $\text{C}_{2\text{min}}$) 60.2 (pyrrolidinyl 2- C_{maj}), 59.7 (pyrrolidinyl 2- C_{min}), 47.2 (pyrrolidinyl 5- C_{min}), 46.9 (pyrrolidinyl 5- C_{maj}), 34.3 (pyrrolidinyl 3- C_{maj}), 33.1 (pyrrolidinyl 3- C_{min}), 28.6 (^tBu $\text{C}_{3\text{min}}$), 28.4 (^tBu $\text{C}_{3\text{maj}}$) 24.2 (pyrrolidinyl 4- C_{min}), 23.5 (pyrrolidinyl 4- C_{maj}). ν_{max} (neat)/ cm^{-1} 3064, 2975, 2930, 2879, 1697, 1477, 1455, 1437. HRMS (ESI) $\text{C}_{16}\text{H}_{20}\text{N}_2\text{O}_2\text{S}$ requires $[\text{M}+\text{H}]^+$, calculated 212.0182, found 212.0176.

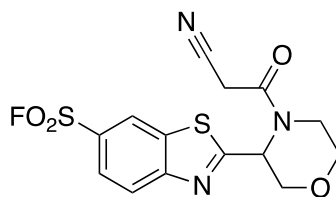
2-(*N*-Boc-pyrrolidin-2-yl)-1,3-benzothiazole-6-sulfonyl fluoride



1-1

Following the general procedure (**Section 5.2.2**), 1,3-benzothiazole-6-sulfonyl fluoride (16.2 mg, 0.10 mmol) was reacted with *N*-Boc-pyrrolidine (85.6 mg, 0.5 mmol), following purification by Mass-Directed HPLC from a 15 minute gradient of 5 – 95% acetonitrile in water, collecting at 12.5 mins to isolate the cross coupled product, **1-1**⁴¹, as a colourless amorphous solid (9.9 mg, 25%, 50:50 mixture of rotamers). δ_{H} (500 MHz, CDCl_3) 8.58 (1H, appt br. d, J 17.5, 7-H), 8.14 (1H, appt br. d, J 9.0, 4-H), 8.06 (1H, m, 5-H), 5.28 (1H, appt br. s, pyrrolidinyl 2- H_{RotA}), 5.26 (1H, appt br. s, pyrrolidinyl 2- H_{RotB}), 3.60-3.54 (2H, m, pyrrolidinyl 5- H_2), 2.45-2.25 (2H, m, pyrrolidinyl 3- H_2), 2.05-1.95 (2H, m, pyrrolidinyl 4- H_2), 1.49 (9H, s, ^tBu 2- H_3_{RotA}), 1.31 (9H, s, ^tBu 2- H_{RotB}). δ_{C} (125 MHz, CDCl_3) 184.1 (^tBu $\text{C}=\text{O}_{\text{maj}}$), 183.4 (^tBu $\text{C}=\text{O}_{\text{min}}$) 158.1 (2-C), 155.0 (7a-C), 135.6 (3a-C), 128.9 (6-C), 125.6 (5-C), 124.1 (7-C), 123.7 (4-C), 84.6 (^tBu 1- C_{RotA}), 81.0 (^tBu 1- C_{RotB}) 60.4 (pyrrolidinyl 2- C_{RotA}), 60.0 (pyrrolidinyl 2- C_{RotB}), 47.4 (pyrrolidinyl 5- C_{RotA}), 47.0 (pyrrolidinyl 5- C_{RotB}), 34.3 (pyrrolidinyl 3- C_{RotA}), 33.0 (pyrrolidinyl 3- C_{RotB}), 28.5 (^tBu 3- C_{RotA}), 28.4 (^tBu 3- C_{RotB}) 24.4 (pyrrolidinyl 4- C_{RotA}), 23.6 (pyrrolidinyl 4- C_{RotB}). δ_{F} (565 MHz, CDCl_3) 67.1. ν_{max} (neat)/ cm^{-1} 3066, 2976, 2931, 1693, 1507, 1477, 1409, 1208, 1116. HRMS (ESI) $\text{C}_{16}\text{H}_{19}\text{F N}_2\text{O}_4\text{S}_2$ requires $[\text{M}+\text{Na}]^+$, calculated 409.0668, found 409.0675.

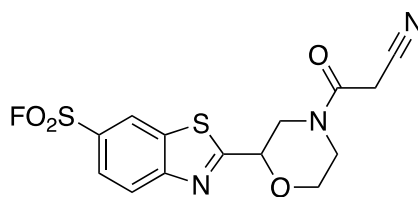
2-[N-(2-Cyanoacetyl)morpholin-3-yl]-1,3-benzothiazole-6-sulfonyl fluoride



1-2a

Following the general procedure (**Section 5.2.2**), 1,3-benzothiazole-6-sulfonyl fluoride (21.7 mg, 0.10 mmol) was reacted with 4-cyanoacetylmorpholine (77.1 mg, 0.5 mmol), following purification by Mass-Directed HPLC from a 20 minute gradient of 25 – 40% acetonitrile in water, isolating two cross coupled products, initially collecting at 13.0 mins, **1-2a** as a colourless amorphous solid (2.0 mg, 5%, 65:35 mixture of rotamers). δ_{H} (500 MHz, CDCl_3) 8.64 (1H, appt br. s, 7- H_{min}), 8.60 (1H, d, J 1.9, 7- H_{maj}), 8.24 (1H, appt d J 8.4, 4- H_{min}), 8.23 (1H, appt d J 8.4, 4- H_{maj}), 8.14 (1H, br. d J 8.7, 5- H_{min}), 8.10 (1H, dd J 1.9, 8.4, 5- H_{maj}), 5.93 (1H, s, morph 3- H_{maj}), 5.19 (1H, s, morph 3- H_{min}), 4.75 (1H, appt d, J 12.2, morph 5- H_{maj}), 4.52 (1H, appt d, J 12.2, morph 5- H_{amin}), 4.31 (1H, appt d, J 12.1, morph 5- H_{bmin}), 4.09 (1H, appt d, J 12.1, 5- H_{bmaj}), 4.01-3.60 (4H, m, morph 2- and 6- H_2). δ_{C} (125 MHz, CDCl_3) 174.5 ($\text{C}=\text{O}_{\text{maj}}$), 173.0 ($\text{C}=\text{O}_{\text{min}}$), 162.5 (2- C_{min}), 161.9 (2- C_{maj}), 157.2 (7a- C_{maj}), 156.6 (7a- C_{min}), 136.3 (3a- C_{maj}), 136.2 (3a- C_{min}), 129.8 (1C, d, J 25.5, 6-C), 126.2 (5- C_{min}), 125.9 (5- C_{maj}), 125.0 (4- C_{min}), 124.8 (4- C_{maj}), 123.9 (7- C_{min}), 123.8 (7- C_{maj}), 113.7 (CN_{min}), 113.1 (CN_{maj}), 69.0 (morph 2- C_{maj}), 68.5 (morph 2- C_{min}), 66.5 (morph 6- C_{min}), 66.9 (morph 6- C_{maj}), 56.2 (morph 3- or 5- C_{min}), 52.9 (morph 3- or 5- C_{maj}), 43.9 (morph 3- or 5- C_{maj}), 39.3 (morph 3- or 5- C_{min}), 25.3 (acetyl 2- C_{min}), 25.1 (acetyl 2- C_{maj}). δ_{F} (565 MHz, CDCl_3) 67.8. ν_{max} (neat)/ cm^{-1} 3047, 2950, 1725, 1669, 1409, 1198, 1043. HRMS (ESI) $\text{C}_{14}\text{H}_{12}\text{FN}_3\text{O}_4\text{S}_2$ requires $[\text{M}+\text{Na}]^+$, calculated 392.0151, found 392.0141.

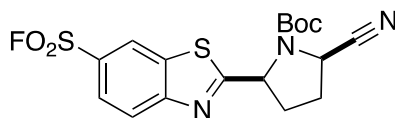
2-[*N*-(2-cyanoacetyl)morpholin-2-yl]-1,3-benzothiazole-6-sulfonyl fluoride



1-2b

Also obtained from the above reaction, isolated at 16.0 mins was **1-2b** as a colourless amorphous solid (4.9 mg, 13%, 70:30 mixture of rotamers). δ_{H} (500 MHz, CDCl_3) 8.68-8.68-8.62 (1H, br. m, 7-H), 8.24-8.20 (1H, br. m, 4-H), 8.14-8.10 (1H, br. m, 5-H), 5.04 (1H, dd, J 7.9, 3.3, morph 2- H_{maj}), 4.95 (1H, dd, J 7.9, 3.3, morph 2- H_{min}), 4.18-4.12 (2H, m, morph 3- H_2), 3.92-3.86 (2H, m, morph 5- and 6- H_a), 3.76 (2H, s, acetyl 2- H_2), 3.58-3.45 (2H, m, morph 5- and 6- H_b). δ_{C} (125 MHz, CDCl_3) 175.8 ($\text{C}=\text{O}_{\text{maj}}$), 175.1 ($\text{C}=\text{O}_{\text{min}}$), 160.8 (2- C_{maj}), 160.5 (2- C_{min}), 157.3 (7a- C_{min}), 157.0 (7a- C_{maj}), 135.9 (3a- C_{maj}), 135.6 (3a- C_{min}), 129.9 (1C, d, J 25.3, 6-C), 126.0 (5- C_{maj}), 125.8 (5- C_{min}), 124.8 (4- C_{min}), 124.6 (4- C_{maj}), 124.0 (7- C_{maj}), 123.9 (7- C_{min}), 113.6 (CN_{maj}), 113.5 (CN_{min}), 75.5 (morph 2- C_{maj}), 74.6 (morph 2- C_{min}), 66.6 (morph 3- C_{min}), 66.0 (morph 3- C_{min}), 49.3 (morph 5- C_{maj}), 46.4 (morph 5- C_{min}), 46.3 (morph 6- C_{min}), 42.3 (morph 6- C_{maj}), 25.1 (acetyl 2- C_{min}), 25.0 (acetyl 2- C_{maj}). δ_{F} (565 MHz, CDCl_3) 67.9. ν_{max} (neat)/ cm^{-1} 3087, 2995, 2877, 1684, 1439, 1412, 1210, 1094. HRMS (ESI) $\text{C}_{14}\text{H}_{12}\text{FN}_3\text{O}_4\text{S}_2$ requires $[\text{M}+\text{Na}]^+$, calculated 392.0151, found 392.0147.

2-[*N*-Boc-(2*R*)-5-cyano-pyrrolidin-2-yl]-1,3-benzothiazole-6-sulfonyl fluoride

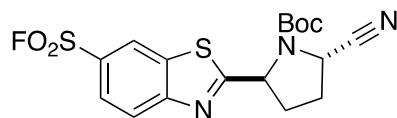


1-3a

Following the general procedure (**Section 5.2.2**), 1,3-benzothiazole-6-sulfonyl fluoride (21.7 mg, 0.10 mmol) was reacted with *N*-Boc-2-cyano-pyrrolidine (98.1 mg, 0.5 mmol), following purification by Mass-Directed HPLC from a 20 minute gradient of 25 – 60% acetonitrile in water, isolating two cross coupled products, initially collecting at 16.5 mins, **1-3a**, as a yellow oil (2.4 mg, 6%, 55:45 mixture of rotamers). δ_{H} (500 MHz, CDCl_3) 8.60 (1H, br. s, 7-H), 8.17 (1H, d, J 8.7, 4-H), 8.10 (1H, br. s, 5-H), 5.42 (1H, br. s, pyrrolidinyl 2- H_{maj}), 5.31 (1H, br. s, pyrrolidinyl 2- H_{min}), 4.81 (1H, br. s, pyrrolidinyl 5- H_{maj}), 4.65 (1H, br. s, pyrrolidinyl 5- H_{min})*, 2.56-2.44 (4H, m, pyrrolidinyl 3- and 4- H_2), 1.56 (9H, s, ^tBu 2- $\text{H}_{3\text{min}}$), 1.35 (9H, s, ^tBu 2- $\text{H}_{3\text{maj}}$). δ_{C} (125 MHz, CDCl_3) 180.2 (^tBu $\text{C}=\text{O}_{\text{min}}$), 178.1 (^tBu $\text{C}=\text{O}_{\text{maj}}$), 170.3 (2-C), 157.9 (7a-C) 153.0 (3a-C), 129.5 (1C, d, J 25.0, 6-C), 125.8 (7-C), 124.4 (4-C), 123.9 (5-C), 118.5 (CN_{maj}), 118.4 (CN_{min}), 83.7 (^tBu 1- C_{maj}), 83.3 (^tBu 1- C_{min}), 61.1 (pyrrolidinyl 5- C_{min}), 60.5 (pyrrolidinyl 5- C_{maj}), 48.3 (pyrrolidinyl 2- C_{maj}), 48.0 (pyrrolidinyl 2- C_{min}), 33.4 (pyrrolidinyl 4- C_{min}), 32.6 (pyrrolidinyl 4- C_{maj}), 31.9 (pyrrolidinyl 3- C_{maj}), 30.6 (pyrrolidinyl 3- C_{min}), 28.4 (^tBu 2- C_{min}), 28.3 (^tBu 2- C_{maj}). δ_{F} (565 MHz, CDCl_3) 67.9. ν_{max} (neat)/ cm^{-1} 3026, 2980, 2959, 2930, 1722, 1405, 1212, 1129. HRMS (ESI) $\text{C}_{17}\text{H}_{18}\text{FN}_3\text{O}_4\text{S}_2$ requires $[\text{M}+\text{Na}]^+$, calculated 434.062, found 434.0611.

*Stereochemistry assigned relative to literature similar compounds as illustrated in **Appendix H**^{173,174}.

2-[*N*-Boc-(2*S*)-5-cyano-pyrrolidin-2-yl]-1,3-benzothiazole-6-sulfonyl fluoride

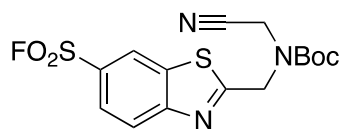


1-3b

Also obtained from the above reaction, isolated at 17.0 mins was **1-3**, as a pale yellow oil (3.1 mg, 7%, 55:45 mixture of rotamers). δ_{H} (500 MHz, CDCl_3) 8.57 (1H, d, J 7.6, 7-H), 8.16 (1H, d, J 7.6, 4-H), 8.08 (1H, dd, J 5.6, 7.6, 5-H), 5.45 (1H, d, J 8.5, pyrrolidinyl 2- H_{maj}), 5.37 (1H, d, J 8.5, pyrrolidinyl 2- H_{min}), 4.85 (1H, d, J 7.5, pyrrolidinyl 2- H_{maj})*, 4.75 (1H, d, J 7.5, pyrrolidinyl 2- H_{min})*, 2.84-2.38 (4H, m, pyrrolidinyl 3- and 4- H_2), 1.55 (9H, s, ^tBu 2- $\text{H}_{3\text{min}}$), 1.33 (9H, s, ^tBu 2- $\text{H}_{3\text{maj}}$). δ_{C} (125 MHz, CDCl_3) 180.3 (^tBu $\text{C}=\text{O}_{\text{min}}$), 179.5 (^tBu $\text{C}=\text{O}_{\text{maj}}$), 157.6 (2- C_{maj}), 157.5 (2- C_{min}), 152.9 (7a- C_{min}), 152.6 (7a- C_{maj}), 135.9 (3a- C_{maj}), 135.4 (3a- C_{min}), 129.4 (1C, d, J 24.9, 6-C), 126.1 (5- C_{min}), 125.8 (5- C_{maj}), 124.5 (7-C), 123.8 (4- C_{min}), 123.7 (4- C_{maj}), 118.5 (CN_{maj}), 118.4 (CN_{min}), 83.5 (^tBu 1- C_{maj}), 83.1 (^tBu 1- C_{min}), 59.7 (pyrrolidinyl 5- C_{min}), 59.4 (pyrrolidinyl 5- C_{maj}), 48.5 (pyrrolidinyl 2- C_{maj}), 48.3 (pyrrolidinyl 2- C_{min}), 32.7 (pyrrolidinyl 4- C_{min}), 31.2 (pyrrolidinyl 4- C_{maj}), 30.0 (pyrrolidinyl 3- C_{maj}), 28.8 (pyrrolidinyl 3- C_{min}), 28.4 (^tBu 2- C_{maj}), 28.2 (^tBu 2- C_{min}). δ_{F} (565 MHz, CDCl_3) 67.8. ν_{max} (neat)/ cm^{-1} 3082, 3054, 2987, 2955, 1702, 1409, 1210, 1149. HRMS (ESI) $\text{C}_{17}\text{H}_{18}\text{FN}_3\text{O}_4\text{S}_2$ requires $[\text{M}+\text{Na}]^+$, calculated 434.0620, found 434.0618.

*Stereochemistry assigned relative to literature similar compounds as illustrated in **Appendix H**^{173,174}.

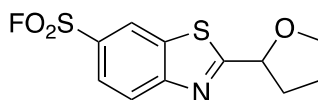
2-(*N*-Boc-*N*-cyanomethyl-methyl)-1,3-benzothiazole-6-sulfonyl fluoride



1-4

Following the general procedure (Section 5.2.2), 1,3-benzothiazole-6-sulfonyl fluoride (21.7 mg, 0.10 mmol) was reacted with 2-(*N*-Boc-*N*-methylamino)-acetonitrile (85.1 mg, 0.5 mmol), following purification by Mass-Directed HPLC from a 15 minute gradient of 30 – 80% acetonitrile in water, collecting at 6.0 mins to isolate the cross coupled product, **1-4**, as a brown amorphous solid (2.4 mg, 6%, 50:50 mixture of rotamers). δ_{H} (500 MHz, CDCl_3) 8.61 (1H, appt br. s, 7-H), 8.22 (1H, appt br. d, J 8.7, 4-H), 8.10 (1H, appt br. d, J 8.7, 5-H), 4.96 (2H, br. s, *N*-cyanomethyl), 4.43 (2H, br. s, 2- $\text{H}_{2\text{RotA}}$), 4.30 (2H, br. s, 2- $\text{H}_{2\text{RotB}}$), 1.55 (9H, br. s, ^tBu 2- $\text{H}_{3\text{RotA}}$), 1.50 (9H, br. s, ^tBu 2- $\text{H}_{3\text{RotB}}$). δ_{C} (125 MHz, CDCl_3) 173.4 (^tBu C=O $_{\text{RotA}}$), 173.3 (^tBu C=O $_{\text{RotB}}$), 157.2 (2-C), 153.5 (7a-C), 136.0 (3a-C), 129.9 (1C, d, J 24.1, 6-C), 126.1 (5-C), 124.6 (7-C), 123.9 (4-C), 115.4 (CN $_{\text{RotA}}$). 115.2 (CN $_{\text{RotB}}$), 83.9 (^tBu 1-C $_{\text{RotA}}$), 83.7 (^tBu 1-C $_{\text{RotB}}$), 49.6 (*N*-cyano 1-C $_{\text{RotA}}$), 49.4 (*N*-cyano 1-C $_{\text{RotB}}$), 36.6 (Me $_{\text{RotA}}$), 35.9 (Me $_{\text{RotB}}$), 28.6 (^tBu 2-C $_{\text{RotA}}$), 28.2 (^tBu 2-C $_{\text{RotB}}$). δ_{F} (565 MHz, CDCl_3) 66.9. ν_{max} (neat)/ cm^{-1} 3068, 2977, 2932, 1706, 1592, 1508, 1410, 1210, 1051. HRMS (ESI) $\text{C}_{15}\text{H}_{16}\text{FN}_3\text{O}_4\text{S}_2$ requires $[\text{M}+\text{Na}]^+$, calculated 408.0464, found 408.0456.

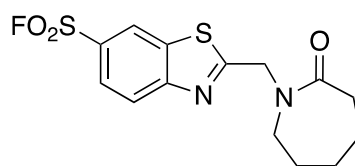
2-(Oxolan-2-yl)-1,3-benzothiazole-6-sulfonyl fluoride



1-6

Following the general procedure (Section 5.2.2), 1,3-benzothiazole-6-sulfonyl fluoride (21.7 mg, 0.10 mmol) was reacted with tetrahydrofuran (216.3 mg, 3 mmol), following purification by Mass-Directed HPLC from a 15 minute gradient of 5 – 95% acetonitrile in water, collecting at 11.5 mins to isolate the cross coupled product, **1-6**, as a yellow amorphous solid (2.9 mg, 10%). δ_{H} (500 MHz, CDCl_3) 8.60 (1H, d, J 1.9, 7-H), 8.15 (1H, d, J 8.7, 4-H), 8.07 (1H, dd, J 8.7, 1.9, 5-H), 5.38 (1H, dd, J 8.0, 5.4, oxo 2-H), 4.19 (1H, ddd, J 8.4, 7.3, 5.7, oxo 5-Ha), 4.05 (1H, ddd, J 8.4, 7.3, 5.7, oxo 5-Hb), 2.56 (1H, appt ddd, J 8.4, 7.3, 5.8, oxo 3-Ha), 2.28 (1H, appt ddd, J 8.4, 7.3, 5.8, oxo 3-Hb), 2.04 (2H, m, oxo 4-H₂). δ_{C} (125 MHz, CDCl_3) 182.7 (2-C), 157.1 (7a-C), 134.6 (3a-C), 127.8 (1C, d, J 24.8, 6-C), 124.4 (5-C), 122.9 (4-C), 122.7 (7-C), 77.2 (oxo 2-C), 68.5 (oxo 5-C), 32.4 (oxo 3-C), 24.7 (oxo 4-C). δ_{F} (565 MHz, CDCl_3) 67.0. ν_{max} (neat)/ cm^{-1} 3065, 2955, 2875, 1697, 1591, 1509, 1409, 1210, 1066. HRMS (ESI) $\text{C}_{11}\text{H}_{10}\text{FNO}_3\text{S}_2$ requires $[\text{M}+\text{H}]^+$, calculated 266.0164, found 288.0153.

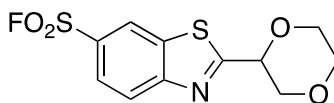
2-((2-Oxoazepan-1-yl)-methyl)-1,3-benzothiazole-6-sulfonyl fluoride



1-8

Following the general procedure (**Section 5.2.2**), 1,3-benzothiazole-6-sulfonyl fluoride (21.7 mg, 0.10 mmol) was reacted with *N*-methylcaprolactam (381.6 mg, 3 mmol), following purification by Mass-Directed HPLC from a 10 minute gradient of 5 – 95% acetonitrile in water, collecting at 3.5 mins to isolate the cross coupled product, **1-8**, as a brown oil (5.6 mg, 16%). δ_{H} (500 MHz, CDCl_3) 8.57 (1H, d, J 1.9, 7-H), 8.17 (1H, d, J 8.7, 4-H), 8.06 1H, dd, J 8.7, 1.9), 5.02 (2H, s, Me H₂), 3.54 (2H, t, J 5.1, 7-H₂), 2.64 (2H, t, J 5.1, 3-H₂), 1.76-1.73 (4H, m, 4- and 6-H₂), 1.65-1.60 (2H, m, 5-H₂). δ_{C} (125 MHz, CDCl_3) 176.5 (C=O), 175.6 (2-C), 157.1 (7a-C), 136.7 (3a-C), 129.4 (1C, d, J 25.0, 6-C), 125.7 (5-C), 124.2 (4-C), 123.7 (7-C), 50.9 (aze 7-C), 50.7 (aze 3-C), 36.9 (Me), 30.0 (aze 6-C), 28.5 (aze 5-C), 23.3 (aze 4-C). δ_{F} (565 MHz, CDCl_3) 69.0. ν_{max} (neat)/ cm^{-1} 3063, 2933, 2857, 1643, 1508, 1481, 1408, 1209, 1161. HRMS (ESI) $\text{C}_{14}\text{H}_{15}\text{FN}_2\text{O}_3\text{S}_2$ requires $[\text{M}+\text{H}]^+$, calculated 343.0586, found 343.0586.

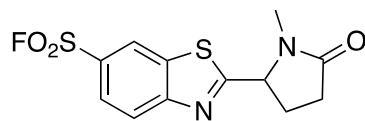
2-(1,4-Dioxan-2-yl)-1,3-benzothiazole-6-sulfonyl fluoride



1-10

Following the general procedure (Section 5.2.2), 1,3-benzothiazole-6-sulfonyl fluoride (21.7 mg, 0.10 mmol) was reacted with 1,4-dioxane (264.3 mg, 3 mmol), following purification by Mass-Directed HPLC from a 15 minute gradient of 5 – 50% acetonitrile in water, collecting at 7.0 mins to isolate the cross coupled product, **1-10**, as a cream amorphous solid (4.5 mg, 15%). δ_{H} (500 MHz, CDCl_3) 8.64 (1H, d, J 2.0, 7-H), 8.18 (1H, d, J 8.7, 4-H), 8.09 (1H, dd, J 8.7, 2.0), 5.10 (1H, dd, J 9.6, 3.2, dio 2-H), 4.05-3.98 (2H, m, dio 3-H₂), 3.88-3.68 (4H, m, dio 5- and 6-H₂). δ_{C} (125 MHz, CDCl_3) 176.3 (2-C), 157.4 (7a-C), 135.6 (3a-C), 129.4 (1C, d, J 25.1, 6-C), 125.7 (5-C), 124.4 (4-C), 123.9 (7-C), 75.4 (dio 2-C), 70.3 (dio 3-C), 67.2 (dio 6-C), 66.5 (dio 5-C). δ_{F} (565 MHz, CDCl_3) 69.1. ν_{max} (neat)/ cm^{-1} 3067, 2968, 2920, 2859, 1696, 1515, 1444, 1409, 1211, 1064. HRMS (ESI) $\text{C}_{11}\text{H}_{10}\text{FNO}_4\text{S}_2$ requires $[\text{M}+\text{H}]^+$, calculated 304.0114, found 304.0103.

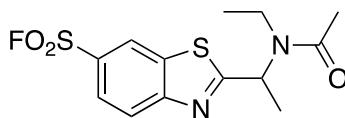
2-(1-Methyl-5-oxopyrrolidin-2-yl)-1,3-benzothiazole-6-sulfonyl fluoride



1-12

Following the general procedure (Section 5.2.2), 1,3-benzothiazole-6-sulfonyl fluoride (21.7 mg, 0.10 mmol) was reacted with 1-methyl-pyrrolidin-2-one (49.6 mg, 0.5 mmol), following purification by Mass-Directed HPLC from a 10 minute gradient of 5 – 95% acetonitrile in water, collecting at 6.5 mins to isolate the cross coupled product, **1-12**, as a yellow oil (7.78 mg, 25%). δ_{H} (500 MHz, CDCl_3) 8.63 (1H, d, J 1.9, 7-H), 8.22 (1H, d, J 8.7, 4-H), 8.11 (1H, dd, J 8.7, 1.9), 5.09 (1H, dd, J 7.6 4.0, pyrrolidinyl 2-H), 2.91 (3H, s, Me), 2.74-2.70 (2H, m, pyrrolidinyl 4- H_2), 2.55-2.49 (1H, m, pyrrolidinyl 3- H_a), 2.24-2.19 (1H, m, pyrrolidinyl 3- H_b). δ_{C} (125 MHz, CDCl_3) 179.3 (C=O), 175.3 (2-C), 157.5 (7a-C), 136.7 (3a-C), 129.9 (1C, d, J 25.3, 6-C), 126.1 (5-C), 124.7 (4-C), 123.9 (7-C), 62.9 (pyrrolidinyl 2-C), 29.2 (pyrrolidinyl 4-C), 26.8 (pyrrolidinyl 3-C). δ_{F} (565 MHz, CDCl_3) 69.0. ν_{max} (neat)/ cm^{-1} 3068, 2929, 2162, 1693, 1591, 1508, 1409, 1209, 1050. HRMS (ESI) $\text{C}_{12}\text{H}_{11}\text{FN}_2\text{O}_3\text{S}_2$ requires $[\text{M}+\text{Na}]^+$, calculated 337.0093, found 337.0089.

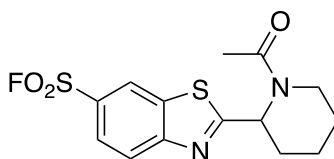
2-[1-(*N*-Ethylacetamido)ethyl]-1,3-benzothiazole-6-sulfonyl fluoride



1-13

Following the general procedure (**Section 5.2.2**), 1,3-benzothiazole-6-sulfonyl fluoride (21.7 mg, 0.10 mmol) was reacted with *N,N*-diethylacetamide (57.6 mg, 0.5 mmol), following purification by Mass-Directed HPLC from a 15 minute gradient of 20 – 80% acetonitrile in water, collecting at 9.5 mins to isolate the cross coupled product, **1-13**, as a yellow oil (5.1 mg, 15%). δ_{H} (500 MHz, CDCl_3) 8.55 (1H, d, J 2.0, 7-H), 8.18 (1H, d, J 8.7, 4-H), 8.05 (1H, dd, J 8.7, 2.0), 6.02 (1H, q, J 7.1, Et 1-H), 3.52-3.44 (1H, m, *N*-Et 1-Ha), 3.38-3.30 (1H, m, *N*-Et 1-Hb), 2.22 (3H, s, Ac 2-H₃), 1.83 (3H, d, J 7.1, Et 2-H₃), 1.21 (3H, t, J 7.1 *N*-Et 2-H₃). δ_{C} (125 MHz, CDCl_3) 179.5 (Ac C=O), 171.1 (2-C), 157.2 (7a-C), 136.5 (3a-C), 129.2 (1C, d, J 24.9, 6-C), 125.5 (5-C), 124.3 (4-C), 123.6 (7-C), 52.4 (Et 1-C), 40.9 (*N*-Et 1-C), 21.9 (Ac 2-C), 17.2 (Et 2-C), 16.1 (*N*-Et 2-C). δ_{F} (565 MHz, CDCl_3) 66.7. ν_{max} (neat)/ cm^{-1} 3052, 3020, 2990, 2891, 2779, 1679, 1415, 1193. HRMS (ESI) $\text{C}_{13}\text{H}_{15}\text{FN}_2\text{O}_3\text{S}_2$ requires $[\text{M}+\text{Na}]^+$, calculated 337.0089, found 353.0400.

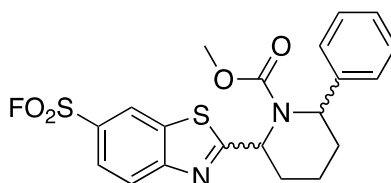
2-(*N*-Acetylpiperidin-2-yl)-1,3-benzothiazole-6-sulfonyl fluoride



1-14

Following the general procedure (**Section 5.2.2**), 1,3-benzothiazole-6-sulfonyl fluoride (21.7 mg, 0.10 mmol) was reacted with *N*-Acetylpiperidine (63.6 mg, 0.5 mmol), following purification by Mass-Directed HPLC from a 10 minute gradient of 5 – 95% acetonitrile in water, collecting at 8.0 mins to isolate the cross coupled product, **1-14**, as a yellow oil (8.4 mg, 24%). δ_{H} (500 MHz, CDCl_3) 8.55 (1H, d, J 1.9, 7-H), 8.17 (1H, d, J 8.7, 4-H), 8.07 (1H, dd, J 8.7, 1.9, 5-H), 6.30 (1H, appt d, J 5.7, pip 2-H), 3.84-3.82 (1H, m, pip 6-Ha), 3.29-3.24 (1H, m, pip 6-Hb), 2.70-2.67 (1H, m, 3-Ha), 2.26 (3H, s, Ac 2-H₃), 1.97-1.90 (1H, m, pip 3-Hb), 1.83-1.81 (1H, m, pip 5-Ha), 1.74-1.56 (3H, m, pip 4-H₂ and 5-Hb). δ_{C} (125 MHz, CDCl_3) 179.2 (Ac C=O), 170.4 (2-C), 157.7 (7a-C), 136.6 (3a-C), 129.2 (1C, d, J 25.0, 6-C), 125.6 (5-C), 124.3 (4-C), 123.5 (7-C), 51.7 (pip 2-C), 44.1 (pip 6-C), 27.9 (pip 3-C), 25.6 (pip 5-C), 21.8 (pip 4-C), 20.1 (Ac 2-C). δ_{F} (565 MHz, CDCl_3) 69.0. ν_{max} (neat)/ cm^{-1} 2935, 2861, 1720, 1648, 1591, 1503, 1410, 1209, 1048. HRMS (ESI) $\text{C}_{14}\text{H}_{15}\text{FN}_2\text{O}_3\text{S}_2$ requires $[\text{M}+\text{Na}]^+$, calculated 365.0406, found 365.0402.

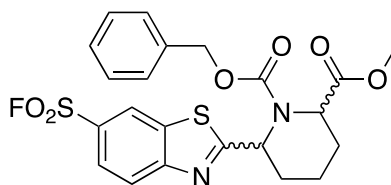
2-(*N*-Methylcarbonyl-6-phenylpiperidin-2-yl)-1,3-benzothiazole-6-sulfonyl fluoride



1-16

Following the general procedure (Section 5.2.2), 1,3-benzothiazole-6-sulfonyl fluoride (21.7 mg, 0.10 mmol) was reacted with methyl 2-phenylpiperidine-1-carboxylate (109.6 mg, 0.5 mmol), following purification by Mass-Directed HPLC from a 15 minute gradient of 5 – 95% acetonitrile in water, collecting at 9.5 mins to isolate the cross coupled product, **1-16** as a mixture of diastereomers, as a yellow oil (2.7 mg, 6%, 60:40 mixture of rotamers). δ_{H} (500 MHz, CDCl_3) 8.59 (1H, d, J 2.0, 7- H_{min}), 8.58 (1H, d, J 2.0, 7- H_{maj}), 8.21-8.17 (1H, m, 4-H), 8.06-8.01 (1H, m, 5-H), 7.42-7.37 (2H, m, Ph 2- and 6-H), 7.32-7.28 (3H, m, Ph 3-, 4- and 5-H), 5.65 (1H, broad s, pip 2- H_{maj}), 5.63 (1H, broad s, pip 2- H_{min}), 4.24-4.22 (1H, m, pip 6-H), 3.78 (3H, s, Me H_3), 2.34-1.92 (6H, m, pip 3-H, 4-H, 5- H_2). δ_{C} (125 MHz, CDCl_3) 181.9 (Ac C=O $_{\text{maj}}$), 180.2 (Ac C=O $_{\text{min}}$), 172.1 (2-C), 157.8 (7a-C), 157.5 (Ph 1-C), 136.6 (3a-C), 129.3 (Ph 3- and 5-C), 129.0 (1C, d, J 25.9, 6-C), 127.3 (Ph 4-C), 126.4 (Ph 2- and 6-C), 125.6 (5-C), 124.3 (4-C), 123.6 (7-C), 57.0 (pip 2-C), 53.2 (pip 6-C), 42.7 (Me), 30.7 (pip 3-C), 24.7 (pip 5-C), 20.6 (pip 4-C). δ_{F} (565 MHz, CDCl_3) 69.1. ν_{max} (neat)/ cm^{-1} 3089, 3078, 3056, 2922, 2833, 1697, 1495, 1410, 1209, 1108. HRMS (ESI) $\text{C}_{20}\text{H}_{19}\text{FN}_2\text{O}_4\text{S}_2$ requires $[\text{M}+\text{H}]^+$, calculated 435.0849, found 435.0847.

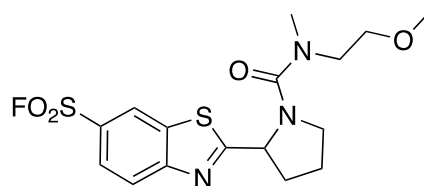
2-(*N*-Phenyl-6-methylcarbonylpiperidin-2-yl)-1,3-benzothiazole-6-sulfonyl fluoride



1-17

Following the general procedure (Section 5.2.2), 1,3-benzothiazole-6-sulfonyl fluoride (21.7 mg, 0.10 mmol) was reacted with 2-methyl 1-phenyl piperidine-1,2-dicarboxylate (132.0 mg, 0.5 mmol), following purification by Mass-Directed HPLC from a 10 minute gradient of 40 – 95% acetonitrile in water, collecting at 5.0 mins to isolate the cross coupled product, **1-17** as a mixture of diastereomers, as a clear oil (1.4 mg, 3%, 80:20 mixture of rotamers). δ_{H} (500 MHz, CDCl_3) 8.58 (1H, d, J 2.0, 7- H_{min}), 8.55 (1H, broad s, 7- H_{maj}), 8.17 (1H, d, J 8.7, 4- H_{min}), 8.13 (1H, d, J 8.7, 4- H_{maj}), 8.08 (1H, dd, J 8.7, 2.0, 5- H_{min}), 8.03 (1H, dd, J 8.7, 2.0, 5- H_{maj}), 7.34 (5H, m, Cbz), 5.73 (1H, m, pip 2-H), 5.27 (2H, s, Cbz CH_2), 5.17-5.10 (1H, m, pip 6-H), 3.21 (3H, s, Me), 2.32-1.96 (6H, m, pip 3-, 4- and 5-H). δ_{C} (125 MHz, CDCl_3) 181.1 (Me C=O), 171.6 (2-C), 164.0 (Cbz C=O), 158.7 (7a-C), 156.8 (Ph 1-C), 135.8 (3a-C), 128.6 (Cbz 3- and 5-C), 128.5 (1C, d, J 25.0, 6-C), 128.0 (Cbz 4-C), 127.9 (Cbz 2- and 6-C), 125.2 (5-C), 124.2 (4-C), 123.5 (7-C), 68.5 (Cbz CH_2), 66.9 (Me), 52.1 (pip 2-C), 40.2 (pip 6-C), 29.8 (pip 3-C), 25.6 (pip 5-C), 16.8 (pip 4-C). δ_{F} (565 MHz, CDCl_3) 68.9. ν_{max} (neat)/ cm^{-1} 3067, 2953, 2926, 2855, 1698, 1499, 1409, 1210, 1086. HRMS (ESI) $\text{C}_{22}\text{H}_{21}\text{FN}_2\text{O}_6\text{S}_2$ requires $[\text{M}+\text{H}]^+$, calculated 493.0903, found 493.0894.

2-[*N*-(2-Methoxyethyl)(methyl)carbamoyl]pyrrolidin-2-yl]-1,3-benzothiazole-6-sulfonyl fluoride



1-20

Following the general procedure (Section 5.2.2), 1,3-benzothiazole-6-sulfonyl fluoride (21.7 mg, 0.10 mmol) was reacted *N*-(2-methoxyethyl)-*N*-methylpyrrolidine-1-carboxamide (93.1 mg, 0.5 mmol), following purification by Mass-Directed HPLC from a 10 minute gradient of 20 – 95% acetonitrile in water, collecting at 6.5 mins to isolate the cross coupled product, **1-20**, as a brown oil (7.1 mg, 18%). δ_{H} (500 MHz, CDCl_3) 8.52 (1H, d, J 1.9, 7-H), 8.12 (1H, d, J 8.7, 4-H), 8.03 (1H, dd, J 8.7, 1.9, 5-H), 5.64 (1H, t, J 7.4, pyrrolidinyl 2-H), 3.71-3.69 (2H, m, OCHa and NCHa), 3.59-3.55 (2H, m, OCHb and NCHb), 3.46-3.44 (1H, m, pyrrolidinyl 5-Ha), 3.35 (OMe), 3.33-3.29 (1H, m, pyrrolidinyl 5-Hb), 3.07 (NMe), 2.61-2.59 (1H, m, pyrrolidinyl 3-Ha), 2.10-2.02 (2H, m, pyrrolidinyl 3-Hb and 4-Ha), 1.90-1.88 (1H, m, 4-Hb). δ_{C} (125 MHz, CDCl_3) 184.2 (C=O), 163.0 (2-C), 158.4 (7a-C), 135.6 (3a-C), 128.7 (1C, d, J 24.7, 6-C), 125.5 (5-C), 124.0 (4-C), 123.6 (7-C), 71.1 (OCH_2), 61.3 (pyrrolidinyl 2-C), 59.0 (OMe), 51.5 (NCH_2), 49.6 (pyrrolidinyl 5-C), 37.4 (NMe), 33.3 (pyrrolidinyl 3-C), 26.3 (pyrrolidinyl 4-C). δ_{F} (565 MHz, CDCl_3) 69.0. ν_{max} (neat)/ cm^{-1} 2931, 2889, 1727, 1635 1496, 1445, 1408, 1209, 1068. HRMS (ESI) $\text{C}_{17}\text{H}_{20}\text{FN}_3\text{O}_4\text{S}_2$ requires $[\text{M}+\text{Na}]^+$, calculated 412.1706, found 412.1699.

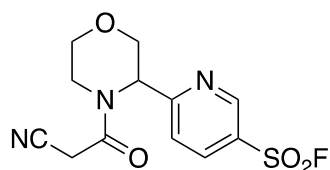
6-(*N*-Boc-pyrrolidin-2-yl)pyridine-3-sulfonyl fluoride



3-1

Following the general procedure (**Section 5.2.2**), pyridine-3-sulfonyl fluoride (16.1 mg, 0.10 mmol) was reacted *N*-Boc pyrrolidine (85.6 mg, 0.5 mmol), following purification by Mass-Directed HPLC from a 15 minute gradient of 40 – 80% acetonitrile in water, collecting at 8.5 mins to isolate the cross coupled product, **3-1**, as a colourless oil (0.8 mg, 2%, 55:45 mixture of rotamers). δ_{H} (500 MHz, CDCl_3) 9.11 (1H, s, 2-H), 8.21 (1H, appt t, J 9.8, 4-H), 7.47 (1H, m, 5-H), 5.06-5.04 (1H, m, pyrrolidinyl 2- H_{min}), 4.99-4.95 (1H, m, pyrrolidinyl 2- H_{maj}), 3.66-3.57 (2H, m, 5- H_2), 2.44-2.38 (1H, m, 3- H_a), 2.02-1.94 (3H, m, 4- H_2 and 3- H_b), 1.45 (9H, s, ^tBu 3- $\text{H}_{3\text{min}}$), 1.21 (9H, s, ^tBu 2- $\text{H}_{3\text{maj}}$). δ_{C} (125 MHz, CDCl_3) 172.1 (^tBu C=O $_{\text{maj}}$), 171.0 (^tBu C=O $_{\text{min}}$), 154.9 (6- C_{min}), 154.2 (6- C_{maj}), 149.0 (2- C_{min}), 148.8 (2- C_{maj}), 136.7 (4- C_{min}), 136.4 (4- C_{maj}), 128.1 (1C, d, J 25.3, 3-C), 121.0 (5- C_{min}), 120.4 (5- C_{maj}), 80.3 (^tBu 1-C), 63.0 (pyrrolidinyl 2- C_{maj}), 62.5 (pyrrolidinyl 2- C_{min}), 47.7 (5- C_{min}), 47.3 (5- C_{maj}), 34.4 (3- C_{maj}), 33.2 (3- C_{min}), 28.6 (^tBu 2- C_{min}), 28.3 (^tBu 2- C_{maj}), 24.2 (4- C_{min}), 23.5 (4- C_{maj}). δ_{F} (565 MHz, CDCl_3) 69.5 ($\text{SO}_2\text{F}_{\text{maj}}$), 69.3 ($\text{SO}_2\text{F}_{\text{min}}$). ν_{max} (neat)/ cm^{-1} 2977, 2928, 1697, 1477, 1391, 1214, 1117. HRMS (ESI) $\text{C}_{14}\text{H}_{19}\text{FN}_2\text{O}_4\text{S}$ requires $[\text{M}+\text{Na}]^+$, calculated 353.0947, found 353.0931.

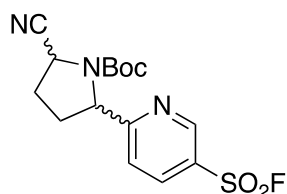
6-[4-(*N*-cyanoacetyl)morpholin-3-yl]-3-sulfonyl fluoride



3-2

Following the general procedure (**Section 5.2.2**), pyridine-3-sulfonyl fluoride (16.1 mg, 0.10 mmol) was reacted 4-cyanoacetylmorpholine (77.1 mg, 0.5 mmol), following purification by Mass-Directed HPLC from a 15 minute gradient of 5 – 95% acetonitrile in water, collecting at 14.5 mins to isolate the cross coupled product, **3-2**, as a brown oil (7.2 mg, 23%, 70:30 mixture of rotamers). δ_{H} (500 MHz, CDCl_3) 9.16 (1H, s, 2- H_{min}), 9.15 (1H, s, 2- H_{maj}), 8.36 (1H, dd, J 8.4, 2.4, 4- H_{maj}), 8.32 (1H, dd, J 8.4, 2.4, 4- H_{min}), 7.88 (1H, d, J 8.4, 5- H_{maj}), 7.81 (1H, d, J 8.4, 5- H_{min}), 5.00 (1H, t, J 2.4, morph 3- H_{min}), .4.98 (1H, t, J 2.4, morph 3- H_{maj}), 4.76 (2-H, dd, J 9.7, 3.0, morph 2- H_{amaj}), 4.70 (2-H, dd, J 9.7, 3.0, morph 2- H_{amin}), 4.37-4.34 (2-H, m, morph 2- H_{bmaj}), 4.22-4.12 (2-H, m, morph 2- H_{bmin}), 3.88-3.72 (2-H, m, morph 5- and 6- H_a), 3.60-3.50 (2-H, m, morph 5- and 6- H_b). δ_{C} (125 MHz, CDCl_3) δ_{C} (125 MHz, CDCl_3) 165.1 (Ac C=O $_{\text{maj}}$), 164.9 (Ac C=O $_{\text{min}}$), 160.8 (6-C $_{\text{maj}}$), 160.6 (6-C $_{\text{min}}$), 148.5 (2-C $_{\text{min}}$), 148.4 (2-C $_{\text{maj}}$), 137.4 (4-C $_{\text{maj}}$), 137.2 (4-C $_{\text{min}}$), 128.7 (1C, d, J 25.8, 3-C), 121.6 (5-C $_{\text{maj}}$), 121.3 (5-C $_{\text{min}}$), 113.7 (CN $_{\text{maj}}$), 113.6 (CN $_{\text{min}}$), 77.3 (morph 2-C $_{\text{maj}}$), 76.6 (morph 2-C $_{\text{min}}$), 66.4 (morph 6-C $_{\text{min}}$), 66.3 (morph 6-C $_{\text{min}}$), 50.0 (morph 3-C), 46.7 (morph 5-C $_{\text{min}}$), 46.3 (morph 5-C $_{\text{maj}}$), 25.1 (acetyl 2-C $_{\text{min}}$), 25.0 (acetyl 2-C $_{\text{maj}}$). δ_{F} (565 MHz, CDCl_3) 67.5 (SO $_2$ F $_{\text{maj}}$), 67.4 (SO $_2$ F $_{\text{min}}$). ν_{max} (neat)/ cm^{-1} 3064, 2927, 2870, 1657, 1413, 1210, 1116. HRMS (ESI) $\text{C}_{12}\text{H}_{12}\text{FN}_3\text{O}_4\text{S}$ requires $[\text{M}+\text{Na}]^+$, calculated 336.043, found 336.0428.

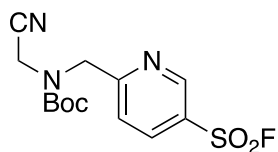
6-(*N*-Boc-5-cyanopyrrolidin-2-yl)pyridine-3-sulfonyl fluoride



3-3

Following the general procedure (Section 5.2.2), pyridine-3-sulfonyl fluoride (16.1 mg, 0.10 mmol) was reacted *N*-Boc-2-cyano-pyrrolidine (98.1 mg, 0.5 mmol), following purification by Mass-Directed HPLC from a 20 minute gradient of 30 – 40% acetonitrile in water, collecting at 11.0 mins to isolate the cross coupled product, **3-3** as a yellow oil (3.9 mg, 11%, 50:50 mixture of diastereomers, 60:40 mixture of rotamers,). δ_{H} (500 MHz, CDCl_3) 9.15 (1H, s, 2- H_{min}), 9.09 (1H, s, 2- H_{maj}), 8.29 (1H, dd, J 8.3, 2.4, 4- H_{maj}), 8.24 (1H, dd, J 8.3, 2.4, 4- H_{min}), 7.60 (1H, d, J 8.3, 5- H_{maj}), 7.52 (1H, d, J 8.3, 5- H_{min}), 5.17 (1H, appt d, J 8.0, pyrrolidinyl 2S- H_{maj}), 5.13-5.11 (1H, m, pyrrolidinyl 2R- H_{maj}), 5.07 (1H, appt d, J 8.0, pyrrolidinyl 2S- H_{min}), 5.02-5.00 (1H, m, pyrrolidinyl 2R- H_{min}), 4.89 (1H, appt d, J 8.0, pyrrolidinyl 5S- H_{min}), 4.89-4.87 (1H, m, pyrrolidinyl 2R- H_{min}), 4.77 (1H, appt d, J 8.0, pyrrolidinyl 5S- H_{maj}), 4.72-4.70 (1H, m, pyrrolidinyl 2R- H_{maj}), 2.62-2.22 (4H, m, pyrrolidinyl 3- and 4- H_2), 1.50 (9H, s, ^tBu 2- $\text{H}_{3\text{maj}}$), 1.22 ((9H, s, ^tBu 2- $\text{H}_{3\text{min}}$). δ_{C} (125 MHz, CDCl_3) 168.6 (^tBu C=O $_{\text{min}}$), 168.5 (^tBu C=O $_{\text{maj}}$), 153.0 (6- C_{min}), 152.9 (6- C_{maj}), 149.0 (2- C_{min}), 148.8 (2- C_{maj}), 137.0 (4- C_{maj}), 136.7 (4- C_{min}), 129.0 (1C, d, J 25.7, 3- C_{min}), 128.8 (1C, d, J 25.7, 3- C_{maj}), 122.1 (5- C_{maj}), 121.1 (5- C_{min}), 120.4 (CN $_{\text{min}}$), 119.0 (CN $_{\text{maj}}$), 83.0 (^tBu 1- C_{maj}), 82.8 (^tBu 1- C_{min}), 63.2 (pyrrolidinyl 5- C_{min}), 61.7 (pyrrolidinyl 5- C_{maj}), 48.7 (pyrrolidinyl 2- C_{maj}), 48.6 (pyrrolidinyl 2- C_{min}), 32.5 (pyrrolidinyl 4- C_{min}), 31.3 (pyrrolidinyl 4- C_{maj}), 30.4 (pyrrolidinyl 3- C_{min}), 29.7 (pyrrolidinyl 3- C_{maj}), 28.4 (^tBu 2- C_{maj}), 28.2 (^tBu 2- C_{min}). δ_{F} (565 MHz, CDCl_3) 67.7 and 67.6 (S $_{\text{min}}$ and R $_{\text{min}}$), 67.5 and 67.4 (S $_{\text{maj}}$ and R $_{\text{maj}}$). ν_{max} (neat)/ cm^{-1} 2975, 2930, 1702, 1582, 1475, 1367, 1214, 1120. HRMS (ESI) $\text{C}_{15}\text{H}_{18}\text{FN}_3\text{O}_4\text{S}$ requires $[2\text{M}+\text{Na}]^+$, calculated 733.1902, found 733.1906.

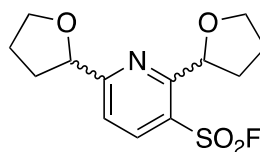
6-(*N*-Boc-*N*-cyanomethyl-methyl) pyridine-3-sulfonyl fluoride



3-4

Following the general procedure (**Section 5.2.2**), pyridine-3-sulfonyl fluoride (16.1 mg, 0.10 mmol) was reacted 2-(*N*-Boc-*N*-methylamino)-acetonitrile (85.1 mg, 0.5 mmol), following purification by Mass-Directed HPLC from a 15 minute gradient of 30 – 60% acetonitrile in water, collecting at 11.0 mins to isolate the cross coupled product, **3-4**, as a yellow oil (3.0 mg, 9%, 90:10 mixture of rotamers). δ_{H} (500 MHz, CDCl_3) 9.14 (1H, s, 2- H_{maj}), 8.89 (1H, s, 2- H_{min}), 8.38 (1H, appt s, 4- H_{min}), 8.29 (1H, appt s, 4- H_{maj}), 7.59-7.51 (1H, m, 5-H), 4.73 (2H, s, *N*-cyanomethyl), 4.43 (2H, br. s, 2- $\text{H}_{2\text{min}}$), 4.31 (2H, br. s, 2- $\text{H}_{2\text{min}}$), 1.52 (9H, br. s, ^tBu 2- $\text{H}_{3\text{maj}}$), 1.40 (9H, br. s, ^tBu 2- $\text{H}_{3\text{min}}$). δ_{C} (125 MHz, CDCl_3) 164.1 (^tBu C=O $_{\text{min}}$), 164.3 (^tBu C=O $_{\text{maj}}$), 154.8 (6- C_{min}), 154.4 (6- C_{maj}), 149.0 (2- C_{min}), 148.9 (2- C_{maj}), 137.2 (4-C), 129.3 (1C, d, J 26.3, 3-C), 121.0 (5- C_{min}), 120.4 (5- C_{maj}), 115.7 (CN), 83.2 (^tBu 1- C_{maj}), 82.9 (^tBu 1- C_{min}), 52.6 (*N*-cyano 1- C_{min}), 52.4 (*N*-cyano 1- C_{maj}), 37.1 (Me_{maj}), 36.3 (Me_{min}), 28.3 (^tBu 2- C_{maj}), 28.1 (^tBu 2- C_{min}). δ_{F} (565 MHz, CDCl_3) 67.5 ($\text{SO}_2\text{F}_{\text{maj}}$), 63.5 ($\text{SO}_2\text{F}_{\text{min}}$). ν_{max} (neat)/ cm^{-1} 3068, 2979, 2934, 1703, 1564, 1452, 1313, 1213, 1160. HRMS (ESI) $\text{C}_{13}\text{H}_{16}\text{FN}_3\text{O}_4\text{S}$ requires $[\text{M}+\text{H}]^+$, calculated 330.0924, found 330.0910.

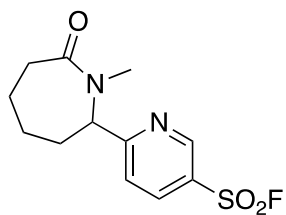
2,6-bis(oxolan-2-yl)pyridine-3-sulfonyl fluoride



3-6

Following the general procedure (Section 5.2.2), pyridine-3-sulfonyl fluoride (16.1 mg, 0.10 mmol) was reacted tetrahydrofuran (216.3 mg, 3 mmol), following purification by Mass-Directed HPLC from a 15 minute gradient of 30 – 50% acetonitrile in water, collecting at 12.0 mins to isolate the cross coupled product, **3-6**, as a pale yellow oil (1.2 mg, 4%). δ_{H} (500 MHz, CDCl_3) 8.28 (1H, appt dd, J 8.4, 2.1, 4-H), 7.61 (1H, appt t, J 8.4, 5-H), 5.67 and 5.13 (2H, dd, J 7.7, 5.8, oxo 2-H), 4.23-4.18 and 4.08-4.02 (4H, m, oxo 5-H₂), 2.51-2.48 and 2.40-2.36 (2H, m, oxo 3-H_a), 2.24-2.17 (2H, m, oxo 3-H_b), 2.07-2.01 (4H, m, oxo 4-H₂). δ_{C} (125 MHz, CDCl_3) 170.4 (6-C), 161.9 (2-C), 138.9 (4-C), 126.8 (1C, d, J 25.3, 3-C), 118.7 (5-C), 81.1 and 80.8 (oxo 2-C), 70.13 and 69.5 (oxo 5-C), 33.1 and 32.2 (oxo 3-C), 26.4 and 25.8 (4-C). δ_{F} (565 MHz, CDCl_3) 66.2. ν_{max} (neat)/ cm^{-1} 3107, 3061, 2981, 1406, 1211, 1132. HRMS (ESI) $\text{C}_{13}\text{H}_{16}\text{FNO}_4\text{S}$ requires $[\text{M}+\text{Na}]^+$, calculated 324.0682, found 374.0847.

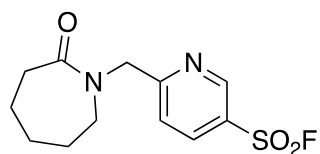
6-(*N*-methyl-7-oxoazepan-2-yl)pyridine-3-sulfonyl fluoride



3-8a

Following the general procedure (**Section 5.2.2**), pyridine-3-sulfonyl fluoride (16.1 mg, 0.10 mmol) was reacted *N*-methylcaprolactam (381.6 mg, 3 mmol), forming three cross coupled compounds as a mixture of mono- and di-substituted products, following purification by Mass-Directed HPLC from a 20 minute gradient of 20 – 30% acetonitrile in water, initially collected at 10.0 mins, **3-8a**, as a yellow oil (2.3 mg, 8%). δ_{H} (500 MHz, CDCl_3) 9.12 (1H, s, 2-H), 8.22 (1H, td, J 10.3, 3.1, 4-H), 7.43 (1H, appt t, J 10.3, 5-H), 3.76-3.70 (1H, m, aze 2-H), 3.44-3.30 (2H, m, aze 6-H₂), 3.05 (3H, s, Me), 2.83-2.77 (2H, m, aze 3-H₂), 1.75-1.65 (4H, m aze 4- and 5-H₂). δ_{C} (125 MHz, CDCl_3) 175.6 (C=O), 171.9 (6-C), 148.9 (2-C), 136.9 (4-C), 128.0 (1C, d, J 25.3, 3-C), 122.5 (5-C), 51.2 (aze 7-C), 42.6 (aze 3-C), 36.4 (aze 3-C), 36.3 (NMe), 35.3 (aze 5-C), 28.8 (aze 4-C). δ_{F} (565 MHz, CDCl_3) 67.7. ν_{max} (neat)/ cm^{-1} 2939, 1708, 1637, 1413, 1212, 1120. HRMS (ESI) $\text{C}_{12}\text{H}_{15}\text{FN}_2\text{O}_3\text{S}$ requires $[\text{M}+\text{H}]^+$, calculated 287.0866, found 287.0854.

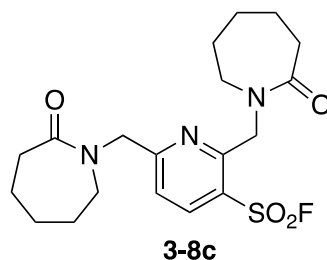
6-[(2-oxoazepan-1-yl)methyl]pyridine-3-sulfonyl fluoride



3-8b

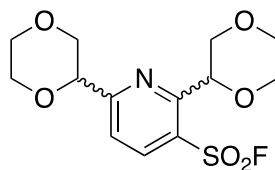
Also obtained from the above reaction, isolated at 11.0 mins was **3-8b**, as a colourless oil (4.7 mg, 17%). δ_{H} (500 MHz, CDCl_3) 9.10 (1H, s, 2-H), 8.21 (1H, dd, J 8.4, 2.4, 4-H), 7.59 (1H, d, J 8.4, 5-H), 4.80 (2H, s, NCH_2), 3.49-3.47 (2H, m, aze 7- H_2), 2.63-2.60 (2H, m, aze 3- H_2), 1.77-1.73 (4H, m, aze 6- and 4- H_2), 1.64-1.61 (2H, m, aze 5- H_2). δ_{C} (125 MHz, CDCl_3) 176.6 (C=O), 166.0 (6-C), 148.7 (2-C), 136.8 (4-C), 128.7 (1C, d, J 25.5, 3-C), 123.1 (5-C), 54.1 (NMe), 50.8 (aze 7-C), 37.0 (aze 3-C), 30.0 (aze 6-C), 28.3 (aze 5-C), 23.4 (aze 4-C). δ_{F} (565 MHz, CDCl_3) 67.6. ν_{max} (neat)/ cm^{-1} 3061, 2930, 2859, 1643, 1562, 1444, 1413, 1211, 1110. HRMS (ESI) $\text{C}_{12}\text{H}_{15}\text{FN}_2\text{O}_3\text{S}$ requires $[\text{M}+\text{H}]^+$, calculated 287.0866, found 287.0856.

2,6-bis(*N*-methyl-7-oxoazepan-2-yl)pyridine-3-sulfonyl fluoride



Also obtained from the above reaction, isolated at 14.0 mins was **3-8c**, as a pale yellow oil (0.29 mg, 1%, 55:45 mixture of rotamers). δ_{H} (500 MHz, CDCl_3) 8.25 (1H, appt d, J 10.0, 4-H), 7.38 (1H, appt d, J 10.0, 5-H), 5.08 and 4.75 (2H, s, aze NCH₂), 3.44-3.39 (4H, m, aze 6-H₂), 2.65-2.60 (4H, m, aze 3-H₂), 1.77-1.74 (8H, m, aze 4- and 5-H₂). δ_{C} (125 MHz, CDCl_3) 175.6 and 174.3 (C=O_{maj}), 172.3 and 171.9 (C=O_{min}) 149.0 (2-C_{min}), 148.9 (6-C_{min}), 136.9 (2-C_{maj}), 136.8 (6-C_{maj}), 137.0 (4-C_{min}), 136.9 (4-C_{maj}), 128.3 (1C, d, J 25.2, 3-C_{min}), 128.1 (1C, d, J 25.2, 3-C_{maj}) 122.5 (5-C_{min}), 121.9 (5-C_{maj}), 51.2 and 50.2 (NMe), 42.6 and 41.2 (aze 7-C), 36.4 and 36.3 (aze 3-C), 36.2 and 36.1 (aze 6-C), 35.3 and 33.1 (aze 5-C), 28.8 and 27.1 (aze 4-C). δ_{F} (565 MHz, CDCl_3) 63.7. ν_{max} (neat)/ cm^{-1} 3100, 3072, 2943, 1643, 1401, 1197. HRMS (ESI) $\text{C}_{19}\text{H}_{26}\text{FN}_3\text{O}_4\text{S}$ requires $[\text{M}+\text{H}]^+$, calculated 412.1706, found 412.1701.

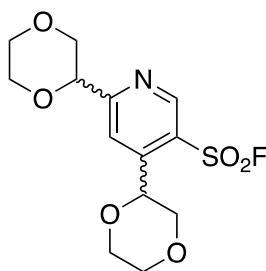
2,6-bis(1,4-dioxan-2-yl)pyridine-3-sulfonyl fluoride



3-10a

Following the general procedure (Section 5.2.2), pyridine-3-sulfonyl fluoride (16.1 mg, 0.10 mmol) was reacted with 1,4-dioxane (264.3 mg, 3 mmol), following purification by Mass-Directed HPLC from a 10 minute gradient of 25 – 60% acetonitrile in water, isolating two cross coupled products as disubstituted regioisomers, initially collecting at 6.0 mins, **3-10a**, as a pale yellow oil (3.7 mg, 11%, 50:50 mixture of diastereomers). δ_{H} (500 MHz, CDCl_3) 8.38 (1H, d, J 8.4, 4-H), 7.74 (1H, appt t, J 8.4, 5-H), 5.28 (1H, dd, J 9.1, 3.3, 2- or 6-dio 2- H_{DiaA}), 5.25 (1H, dd, J 9.1, 3.3, 2- or 6-dio 2- H_{DiaB}), 4.88 (1H, dd, J 9.9, 3.1, 2- or 6-dio 2- H_{DiaA}), 4.80 (1H, dd, J 9.9, 3.1, 2- or 6-dio 2- H_{DiaB}), 4.26 and 4.12 (1H, appt td, J 11.0, 3.1, 2- and 6-dio 3-Ha), 4.04-3.92 (2H, m, dio 3- H_2), 3.83-3.39 (8H, m, 5- and 6- H_2). δ_{C} (125 MHz, CDCl_3) 164.5 (6- C_{DiaA}), 164.2 (6- C_{DiaB}), 155.8 (2- C_{DiaA}), 155.7 (2- C_{DiaB}), 139.8 (4- C_{DiaA}), 139.7 (4- C_{DiaB}), 129.0 (1C, d, J 25.5, 3- C_{DiaA}), 128.1 (1C, d, J 25.5, 3- C_{DiaB}), 120.4 (5- C_{DiaA}), 120.3 (5- C_{DiaB}), 74.5 and 74.4 (dio 2-C), 70.9 and 70.7 (dio 3-C), 69.1 and 69.0 (dio 6-C), 66.5 and 66.4 (dio 5-C). δ_{F} (565 MHz, CDCl_3) 65.3 ($\text{SO}_2\text{F}_{\text{DiaA}}$), 65.2 ($\text{SO}_2\text{F}_{\text{DiaB}}$). ν_{max} (neat)/ cm^{-1} 2965, 2918, 2858, 1730, 1656, 1577, 1449, 1415, 1209, 965. HRMS (ESI) $\text{C}_{13}\text{H}_{16}\text{FNO}_6\text{S}$ requires $[\text{M}+\text{Na}]^+$, calculated 356.0580, found 356.0572.

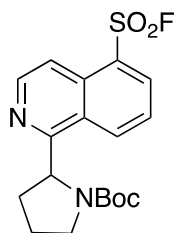
4,6-bis(1,4-dioxan-2-yl)pyridine-3-sulfonyl fluoride



3-10b

Also obtained from the above reaction, isolated at 6.5 mins was **3-10b**, as a pale yellow oil (3.2 mg, 10%, 50:50 mixture of diastereomers). δ_{H} (500 MHz, CDCl_3) 9.09 (1H, s, 2-H), 8.04 (1H, appt d, J 5.0, 5-H), 5.30 (1H, appt t, J 2.7, 4- or 6-dio 2- H_{DiaA}), 5.25 (1H, appt t, J 2.7, 4- or 6-dio 2- H_{DiaB}), 4.84 (1H, appt t, J 2.7, 4- or 6-dio 2- H_{DiaA}), 4.26 (1H, appt t, J 2.7, 4- or 6-dio 2- H_{DiaB}), 4.11-3.96 (4H, m, dio 3- H_2), 3.87-3.70 (8H, m, 5- and 6- H_2). δ_{C} (125 MHz, CDCl_3) 166.5 (6- C_{DiaA}), 166.3 (6- C_{DiaB}), 149.6 (2- C_{DiaA}), 148.5 (2- C_{DiaB}), 149.0 (4-C), 126.4 (1C, d, J 23.5, 3- C_{DiaA}), 126.3 (1C, d, J 23.5, 3- C_{DiaB}), 120.3 (5- C_{DiaA}) 120.1 (5- C_{DiaB}), 73.9 and 73.8 (dio 2-C), 70.7 and 70.6 (dio 3-C), 67.1 and 66.9 (dio 6-C), 66.4 and 66.3 (dio 5-C). δ_{F} (565 MHz, CDCl_3) 69.2 ($\text{SO}_2\text{F}_{\text{DiaA}}$), 69.1 ($\text{SO}_2\text{F}_{\text{DiaB}}$). ν_{max} (neat)/ cm^{-1} 2963, 2920, 2857, 1730, 1590, 1545, 1449, 1416, 1211, 1056. HRMS (ESI) $\text{C}_{13}\text{H}_{16}\text{FNO}_6\text{S}$ requires $[\text{M}+\text{Na}]^+$, calculated 356.0580, found 356.0583.

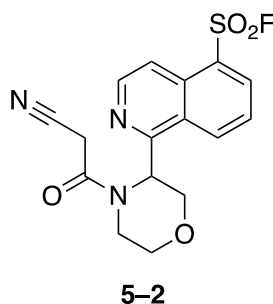
1-(*N*-Boc-pyrrolidin-2-yl)isoquinoline-5-sulfonyl fluoride



5-1

Following the general procedure (Section 5.2.2), isoquinoline-8-sulfonyl fluoride (21.1 mg, 0.10 mmol) was reacted *N*-Boc-pyrrolidine (85.7 mg, 0.5 mmol), following purification by Mass-Directed HPLC from a 15 minute gradient of 5 – 95% acetonitrile in water, collecting at 11.5 mins to isolate the cross coupled product, **5-1**, as a yellow oil (4.7 mg, 12%, 55:45 mixture of rotamers). δ_{H} (500 MHz, CDCl_3) 8.75-8.72 (1H, m, 3-H), 8.68 (1-H, d, J 7.8, 8-H), 8.56 (1H, appt t, J 7.8, 6-H), 8.25 (1H, br. t, J 7.8, 4-H), 7.78 (1H, t, J 7.8, 7-H), 5.87 (1H, dd, J 7.8, 3.8, pyrrolidinyl 2- H_{maj}), 5.68 (1H, dd, J 7.8, 3.8, pyrrolidinyl 2- H_{min}), 3.88-3.61 (2H, m, pyrrolidinyl 5- H_2), 2.14-1.94 (4H, m, pyrrolidinyl 3- and 4- H_2), 1.43 (9H, s, ^tBu 2- $\text{H}_{3\text{maj}}$), 0.95 (9H, s, ^tBu 2- $\text{H}_{3\text{min}}$). δ_{C} (125 MHz, CDCl_3) 163.8 (^tBu C=O $_{\text{min}}$), 162.9 (^tBu C=O $_{\text{maj}}$), 154.9 (1- C_{min}), 144.9 (3- C_{maj}), 144.1 (3- C_{min}), 134.9 (8- C_{min}), 134.9 (8- C_{maj}), 133.1 (7- C_{maj}), 132.7 (7- C_{min}), 132.2 (4a-C), 129.6 (1C, d, J 24.6, 5-C), 126.2 (8a-C), 125.9 (6- C_{min}), 125.7 (6- C_{maj}), 116.3 (4- C_{min}), 115.6 (4- C_{maj}), 80.1 (^tBu 1- C_{min}), 79.5 (^tBu 1- C_{maj}), 59.7 (pyrrolidinyl 2- C_{maj}), 58.7 (pyrrolidinyl 2- C_{min}), 47.5 (pyrrolidinyl 5- C_{maj}), 47.2 (pyrrolidinyl 5- C_{min}), 34.4 (pyrrolidinyl 3- C_{min}), 33.4 (pyrrolidinyl 3- C_{maj}), 28.6 (^tBu 3- C_{maj}), 28.1 (^tBu 3- C_{min}), 24.4 (pyrrolidinyl 4- C_{maj}), 23.8 (pyrrolidinyl 4- C_{min}). δ_{F} (565 MHz, CDCl_3) 63.6 ($\text{SO}_2\text{F}_{\text{min}}$), 63.3 ($\text{SO}_2\text{F}_{\text{maj}}$). ν_{max} (neat)/ cm^{-1} 3002, 2987, 2954, 1675, 1574, 1524, 1409, 1198, 1143. HRMS (ESI) $\text{C}_{18}\text{H}_{21}\text{FN}_2\text{O}_4\text{S}$ requires $[\text{M}+\text{H}]^+$, calculated 381.1284, found 381.1281.

1-[1-Cyano-2-(morpholin-4-yl)-2-oxoethyl]isoquinoline-5-sulfonyl fluoride



Following the general procedure (Section 5.2.2), isoquinoline-8-sulfonyl fluoride (21.1 mg, 0.10 mmol) was reacted 4-cyanoacetylmorpholine (77.1 mg, 0.5 mmol), following purification by Mass-Directed HPLC from a 15 minute gradient of 30 – 95% acetonitrile in water, collecting at 7.0 mins to isolate the cross coupled product, **5-2**, as a brown oil (8.1 mg, 2%, 60:40 mixture of rotamers). δ_{H} (500 MHz, CDCl_3) 8.86 (1H, dt, J 8.7, 1.1, 3- H_{maj}), 8.78 (1H, d, J 8.7, 3- H_{min}), 8.73-8.69 (1H, m, 8-H), 8.60-8.56 (1H, m, 6- H_{maj}), 8.54-8.52 (1H, m, 6- H_{min}), 8.37-8.35 (1H, m, 4- H_{maj}), 8.29-8.27 (1H, m, 4- H_{min}), 7.84-7.79 (1H, m, 7-H), 6.28 (1H, appt d, J 4.3, morph 3- H_{maj}), 5.39 (1H, dd, J 7.3, 3.2, morph 3- H_{min}), 5.28 (1H, dd, J 7.3, 3.2, morph 3a- or 5a- H_{min}), 4.89 (1H, dt, J 12.8, 2.3, 3b- or 5b- H_{min}), 4.55 (1H, td, J 12.8, 4.2, 3b- or 5b- H_{maj}), 4.37 (1H, appt d, J 12.0, morph 3a- or 5a- H_{maj}), 4.30-4.22 (2H, m, 3- or 5- H_{a} and b), 4.13-4.08 (2H, m, 2- and 4- H_{a}) 3.80 (2H, s, acetyl 2- $\text{H}_{2\text{maj}}$), 3.78 (2H, s, acetyl 2- $\text{H}_{2\text{min}}$), 3.58-3.53 (2H, m, 2- and 4- H_{a}). δ_{C} (125 MHz, CDCl_3) 162.8 (Ac C=O $_{\text{maj}}$), 161.1 (Ac C=O $_{\text{min}}$), 158.6 (1- C_{min}), 157.1 (1- C_{maj}), 144.3 (3- C_{maj}), 144.0 (3- C_{min}), 135.2 (8- C_{min}), 134.8 (8- C_{maj}), 134.4 (4a-C), 132.6 (7- C_{maj}), 132.4 (7- C_{min}), 129.5 (1C, d, J 24.7, 5-C), 127.4 (8a-C), 126.3 (6- C_{min}), 126.2 (6- C_{maj}), 117.7 (4- C_{min}), 116.7 (4- C_{maj}), 114.2 (CN $_{\text{maj}}$), 113.6 (CN $_{\text{min}}$), 75.4 (morph 2- C_{min}), 74.5 (morph 2- C_{maj}), 66.4 (morph 6- C_{min}), 65.5 (morph 6- C_{maj}), 51.8 (morph 3- C_{min}), 48.5 (morph 3- C_{maj}), 44.6 (morph 5- C_{min}), 42.4 (morph 5- C_{maj}), 25.3 (acetyl 2- C_{min}), 25.0 (acetyl 2- C_{maj}). δ_{F} (565 MHz, CDCl_3) 63.0 (SO₂F $_{\text{maj}}$), 62.8 (SO₂F $_{\text{min}}$). ν_{max} (neat)/cm⁻¹ 2965, 2938, 1711, 1660, 1615, 1581, 1493, 1411, 1203, 1100. HRMS (ESI) C₁₆H₁₄FN₃O₄S requires [M+H]⁺, calculated 364.0767, found 364.0755.

1-[*N*-Boc-(5*S*)-5-cyanopyrrolidin-2-yl]isoquinoline-5-sulfonyl fluoride

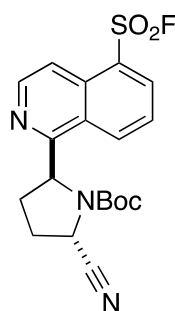


5-3a

Following the general procedure (Section 5.2.2), isoquinoline-8-sulfonyl fluoride (21.1 mg, 0.10 mmol) was reacted *N*-Boc-2-cyano-pyrrolidine (98.1 mg, 0.5 mmol), following purification by Mass-Directed HPLC from a 20 minute gradient of 40 – 60% acetonitrile in water, isolating two cross coupled products, initially collecting at 11.0 mins, **5-3**, as a yellow amorphous solid (5.3 mg, 13%, 60:30 mixture of rotamers). δ_{H} (500 MHz, CDCl_3) 8.63 (1H, m, 3-H), 8.66 (1-H, m, 8-H), 8.58 (1H, m, 6-H), 8.25 (1H, m, 4-H), 7.79 (1H, m, 7-H), 5.95 (1H, br. s, pyrrolidinyl 2- H_{maj})*, 5.75 (1H, br. s, pyrrolidinyl 2- H_{min})*, 4.87 (1H, br. s, pyrrolidinyl 5- H_{min}), 4.75 (1H, br. s, pyrrolidinyl 5- H_{maj}), 2.63-2.49 (4H, m, pyrrolidinyl 3- and 4- H_2), 1.49 (9H, s, ^tBu 2- $\text{H}_{3\text{min}}$), 1.00 (9H, s, ^tBu 2- $\text{H}_{3\text{maj}}$). δ_{C} (125 MHz, CDCl_3) 161.7 (^tBu C=O $_{\text{min}}$), 160.1 (^tBu C=O $_{\text{maj}}$), 153.3 (1- C_{min}), 153.1 (1- C_{maj}), 145.6 (3- C_{min}), 145.4 (3- C_{maj}), 134.9 (8- C_{min}), 134.8 (8- C_{maj}), 134.4 (4a-C), 132.6 (7- C_{maj}), 132.4 (7- C_{min}), 132.0 (8a-C), 129.5 (1C, d, J 24.2, 5-C), 126.2 (6- C_{min}), 126.1 (6- C_{maj}), 119.6 (4- C_{min}), 119.1 (4- C_{maj}), 116.2 (CN $_{\text{maj}}$), 116.1 (CN $_{\text{min}}$), 82.3 (^tBu 1- C_{maj}), 81.1 (^tBu 1- C_{min}), 59.1 (pyrrolidinyl 5- C_{min}), 58.5 (pyrrolidinyl 5- C_{maj}), 48.3 (pyrrolidinyl 2- C_{maj}), 48.2 (pyrrolidinyl 2- C_{min}), 32.3 (pyrrolidinyl 4- C_{min}), 31.9 (pyrrolidinyl 4- C_{maj}), 30.3 (pyrrolidinyl 3- C_{maj}), 29.5 (pyrrolidinyl 3- C_{min}), 28.4 (^tBu 2- C_{min}), 28.3 (^tBu 2- C_{maj}). δ_{F} (565 MHz, CDCl_3) 64.6 (SO $_2$ F $_{\text{min}}$), 64.5 (SO $_2$ F $_{\text{maj}}$). ν_{max} (neat)/ cm^{-1} 3101, 2978, 2940, 1701, 1614, 1580, 1561, 1387, 1197, 1131. HRMS (ESI) $\text{C}_{19}\text{H}_{19}\text{FN}_3\text{O}_4\text{S}$ requires $[\text{M}+\text{Na}]^+$, calculated 428.1056, found 428.1061.

*Stereochemistry assigned relatively to literature similar compounds as illustrated in Appendix H^{173,174}.

1-[*N*-Boc-(5*R*)-5-cyanopyrrolidin-2-yl]isoquinoline-5-sulfonyl fluoride

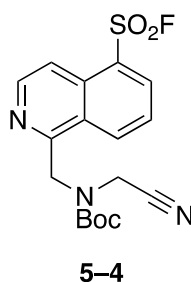


5-3b

Also obtained from the above reaction, isolated at 11.5 mins was **5-3b**, as a yellow amorphous solid (4.8 mg, 12%, 60:40 mixture of rotamers). δ_{H} (500 MHz, CDCl_3) 8.65 (1H, m, 3-H), 8.57 (1-H, m, 8-H), 8.57 (1H, m, 6-H), 8.24 (1H, m, 4-H), 7.81 (1H, m, 7-H), 5.99 (1H, d, J 8.3, pyrrolidinyl 2- H_{maj})*, 5.87 (1H, d, J 8.3, pyrrolidinyl 2- H_{min})*, 5.06 (1H, d, J 8.3, pyrrolidinyl 5- H_{maj}), 4.97 (1H, d, J 8.3, pyrrolidinyl 5- H_{min}), 2.75 (1H, m, pyrrolidinyl 3-Ha), 2.62 (1H, m, pyrrolidinyl 3-Hb), 2.32 (1H, m, pyrrolidinyl 4-Ha), 2.06 (1H, m, pyrrolidinyl 4-Ha), 1.49 (9H, s, ^tBu 2- $\text{H}_{3\text{min}}$), 0.99 (9H, s, ^tBu 2- $\text{H}_{3\text{maj}}$). δ_{C} (125 MHz, CDCl_3) 161.7 (^tBu C=O $_{\text{min}}$), 160.9 (^tBu C=O $_{\text{maj}}$), 153.3 (1- C_{min}), 153.2 (1- C_{maj}), 144.9 (3- C_{min}), 144.5 (3- C_{maj}), 134.9 (8- C_{min}), 134.7 (8- C_{maj}), 134.6 (4a-C), 132.5 (7- C_{maj}), 132.5 (8a-C), 132.0 (7- C_{min}), 129.5 (1C, d, J 24.7, 5-C), 126.2 (6- C_{min}), 126.1 (6- C_{maj}), 119.6 (4- C_{min}), 119.5 (4- C_{maj}), 116.2 (CN $_{\text{maj}}$), 116.1 (CN $_{\text{min}}$), 82.3 (^tBu 1- C_{maj}), 81.1 (^tBu 1- C_{min}), 58.7 (pyrrolidinyl 5- C_{min}), 58.5 (pyrrolidinyl 5- C_{maj}), 48.4 (pyrrolidinyl 2- C_{maj}), 48.3 (pyrrolidinyl 2- C_{min}), 32.3 (pyrrolidinyl 4- C_{min}), 31.3 (pyrrolidinyl 4- C_{maj}), 29.5 (pyrrolidinyl 3- C_{min}), 28.4 (^tBu 2- C_{min}), 28.3 (^tBu 2- C_{maj}), 28.0 (pyrrolidinyl 3- C_{maj}). δ_{F} (565 MHz, CDCl_3) 64.7 (SO $_2\text{F}_{\text{maj}}$), 64.5 (SO $_2\text{F}_{\text{min}}$). ν_{max} (neat)/ cm^{-1} 2977, 2933, 1701, 1614, 1581, 1560, 1381, 1209, 1154. HRMS (ESI) $\text{C}_{19}\text{H}_{19}\text{FN}_3\text{O}_4\text{S}$ requires $[\text{M}+\text{Na}]^+$, calculated 428.1056, found 428.1055.

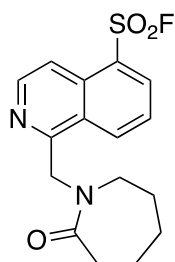
*Stereochemistry assigned relative to literature similar compounds as illustrated in **Appendix H**^{173,174}.

1-(*N*-Boc-*N*-cyanomethyl-methyl)isoquinoline-5-sulfonyl fluoride



Following the general procedure (**Section 5.2.2**), isoquinoline-8-sulfonyl fluoride (21.1 mg, 0.10 mmol) was reacted 2-(*N*-Boc-*N*-methylamino)-acetonitrile (85.1 mg, 0.5 mmol), following purification by Mass-Directed HPLC from a 10 minute gradient of 30 – 95% acetonitrile in water, collecting at 9.0 mins to isolate the cross coupled product, **5-4**, as a brown oil (4.1 mg, 11%, 60:40 mixture of rotamers). δ_{H} (500 MHz, CDCl_3) 8.89 (1H, br. d, J 8.4, 3- H_{maj}), 8.80 (1H, br. d, J 8.4, 3- H_{min}), 8.72 (1-H, d J 6.2, 8-H), 8.61 (1H, d J 6.2, 6-H), 8.39 (1H, br. s, 4- H_{maj}), 8.32 (1H, br. s, 4- H_{min}), 7.89-7.83 (1H, m, 7-H), 5.26 (2H, br. s, $\text{CH}_{2\text{maj}}$), 5.21 (2H, br. s, $\text{CH}_{2\text{min}}$), 4.48 (2H, br. s, *N*-cyanomethyl $_{\text{min}}$), 4.33 (2H, br. s, *N*-cyanomethyl $_{\text{maj}}$), 1.53 (9H, br. s, ^tBu 2- H_3). δ_{C} (125 MHz, CDCl_3) 156.9 (^tBu C=O), 154.2 (1-C), 143.4 (3-C), 135.8 (8-C), 135.3 (4a-C), 134.1 (7-C), 132.8 (8a-C), 129.6 (1C, d, J 25.6, 5-C), 127.0 (6-C), 118.3 (4-C), 115.9 (CN), 82.3 (^tBu 1- C_{maj}), 81.1 (^tBu 1- C_{min}), 49.3 (*N*-cyano 1-C), 35.9 (Me), 28.3 (^tBu 2-C). δ_{F} (565 MHz, CDCl_3) 65.2. ν_{max} (neat)/ cm^{-1} 3086, 2978, 2934, 1811, 1703, 1615, 1581, 1561, 1411, 1208, 1158. HRMS (ESI) $\text{C}_{17}\text{H}_{18}\text{FN}_3\text{O}_4\text{S}$ requires $[\text{M}+\text{Na}]^+$, calculated 402.0900, found 402.0885.

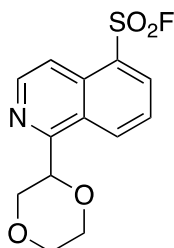
1-(2-Oxazepan-1-yl)methyl-isoquinoline-5-sulfonyl fluoride



5-8

Following the general procedure (**Section 5.2.2**), isoquinoline-8-sulfonyl fluoride (21.1 mg, 0.10 mmol) was reacted *N*-methylcaprolactam (381.6 mg, 3 mmol), following purification by Mass-Directed HPLC from a 10 minute gradient of 40 – 80% acetonitrile in water, collecting at 7.0 mins to isolate the cross coupled product, **5-8**, as a brown oil (7.3 mg, 22%). δ_{H} (500 MHz, CDCl_3) 9.03 (1H, dd, J 8.6, 2.2, 3-H), 8.70 (1H, d, J 6.2, 8-H), 8.57 (1H, dd, J 7.5, 1.2, 6-H), 8.33 (1H, br. dd, J 6.1, 1.9, 4-H), 7.82 (1H, t, J 7.6, 7-H), 5.28 (2H, s, Me H₂), 3.46 (2H, t, J 5.2, aze 7-H₂), 2.62-2.58 (2H, m, aze 3-H₂), 1.65-1.60 (4H, m, aze 4- and 6-H₂), 1.34-1.30 (2H, m, aze 5-H₂). δ_{C} (125 MHz, CDCl_3) 176.0 (C=O), 158.8 (1-C), 143.4 (8-C), 135.3 (3-C), 135.2 (6-C), 132.4 (4a-C), 129.1 (1C, d, J 24.7, 5-C), 127.4 (8a-C), 126.7 (7-C), 117.1 (4-C), 50.7 (aze 7-C), 48.2 (aze 3-C), 37.0 (Me), 29.8 (aze 6-C), 27.8 (aze 5-C), 23.3 (aze 4-C). δ_{F} (565 MHz, CDCl_3) 64.9. ν_{max} (neat)/ cm^{-1} 3088, 2932, 2857, 1635, 1543, 1408, 1205, 979. HRMS (ESI) $\text{C}_{16}\text{H}_{17}\text{FN}_2\text{O}_3\text{S}$ requires $[\text{M}+\text{H}]^+$, calculated 337.1022, found 337.1017.

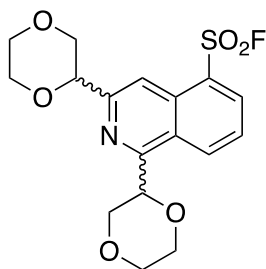
1-(1,4-Dioxan-2-yl)isoquinoline-5-sulfonyl fluoride



5-10a

Following the general procedure (Section 5.2.2), isoquinoline-8-sulfonyl fluoride (21.1 mg, 0.10 mmol) was reacted 1,4-dioxane (264.3 mg, 3 mmol), following purification by Mass-Directed HPLC from a 10 minute gradient of 40 – 50% acetonitrile in water, isolating two cross coupled products, initially collecting at 11.0 mins, **5-10a**, as a yellow amorphous solid (2.7 mg, 9%). δ_{H} (500 MHz, CDCl_3) 8.84 (1H, dt, J 8.6, 1.1, 3-H), 8.76 (1H, d, J 6.1, 8-H), 8.56 (1H, dd, J 7.5, 1.1, 6-H), 8.25 (1H, dd, J 6.1, 0.9, 4-H), 7.78 (1H, t, J 7.5, 7-H), 5.42 (1H, dd, J 9.5, 3.0, oxo 2-H), 4.21 (2H, m, oxo 3-H₂), 4.11 (2H, m, oxo 6-H₂), 3.89 (2H, m, oxo 5-H₂). δ_{C} (125 MHz, CDCl_3) 157.6 (1-C), 144.6 (3-C), 134.9 (8-C), 134.2 (7-C), 132.5 (8a-C), 129.3 (1C, d, J 24.7, 5-C), 127.1 (4a-C), 126.0 (6-C), 117.2 (4-C), 76.1 (oxo 2-C), 70.0 (oxo 3-C) 67.7 (oxo 6-C) 66.6 (oxo 5-C). δ_{F} (565 MHz, CDCl_3) 64.8. ν_{max} (neat)/ cm^{-1} 3096, 2958, 2818, 2853, 1755, 1406, 1202, 1065. HRMS (ESI) $\text{C}_{13}\text{H}_{12}\text{FNO}_4\text{S}$ requires $[\text{M}+\text{H}]^+$, calculated 298.0549, found 298.0547.

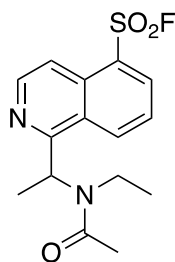
1,3-bis(1,4-Dioxan-2-yl)isoquinoline-5-sulfonyl fluoride



5-10b

Also obtained from the above reaction, isolated at 7.5 mins was **5-10b**, as a pale yellow amorphous solid (1.2 mg, 3%). δ_{H} (500 MHz, CDCl_3) 8.68 (1-H, d, J 5.9, 8-H), 8.54 (1H, d, J 8.0, 6-H), 8.36 (1H, dd, J 5.9, 2.7, 4-H), 8.23 (1H, br. d, J 8.0, 7-H), 5.70 (1H, dd, J 9.8, 2.3, oxo₁ 2-H), 5.20 (1H, t, J 5.7, oxo₃ 2-H), 4.31 (2H, appt d, J 6.2, oxo₃ 3-H₂), 4.16-4.03 (4H, m, oxo 6-H₂), 3.98-3.81 (4H, m, oxo 5-H₂), 3.40 (2H, dd, J 12.0, 9.8, oxo₁ 3-H₂). δ_{C} (125 MHz, CDCl_3) 156.0 (1-C), 145.5 (3-C), 143.1 (8-C), 134.3 (6-C), 133.7 (8a-C), 129.2 (1C, d, J 24.6, 5-C), 126.2 (7-C) 125.5 (4a-C) 117.4 (4-C). 76.6 (oxo₃ 2-C), 75.7 (oxo₁ 2-C), 73.9 (oxo₃ 3-C), 70.3 (oxo₁ 3-C), 68.0 and 67.6 (oxo_{1,3} 6-C), 66.9 and 66.4 (oxo_{1,3} 5-C). δ_{F} (565 MHz, CDCl_3) 64.5. ν_{max} (neat)/ cm^{-1} 3119, 2963, 2853, 1752, 1402, 1211, 981. HRMS (ESI) $\text{C}_{17}\text{H}_{18}\text{FNO}_6\text{S}$ requires $[\text{M}+\text{H}]^+$, calculated 384.0917, found 384.0923.

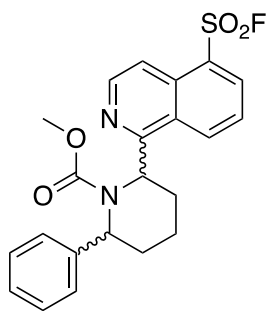
1-[1-(*N*-Ethylacetamido)ethyl]isoquinoline-5-sulfonyl fluoride



5-13

Following the general procedure (**Section 5.2.2**), isoquinoline-8-sulfonyl fluoride (21.1 mg, 0.10 mmol) was reacted *N,N*-diethylacetamide (57.6 mg, 0.5 mmol), following purification by Mass-Directed HPLC from a 10 minute gradient of 5 – 95% acetonitrile in water, collecting at 9.0 mins to isolate the cross coupled product, **5-13**, as a brown oil (2.8 mg, 8%). δ_{H} (500 MHz, CDCl_3) 8.89 (1H, dt, J 8.7, 1.1, 3-H), 8.75 (1H, d, J 6.1, 8-H), 8.55 (1H, dd, J 7.4, 1.1, 6-H), 8.30 (1H, dd, J 6.1, 2.8, 4-H), 7.80 (1H, t, J 8.1, 7-H), 6.90 (1H, q, J 6.8, Et 1-H), 3.29 (1H, m, *N*-Et 1-Ha), 3.35 (1H, m, *N*-Et 1-Hb), 2.15 (3H, s, Ac 2-H₃), 1.69 (3H, d, J 6.8, Et 2-H₃), 0.6 (3H, t, J 7.2 *N*-Et 2-H₃). δ_{C} (125 MHz, CDCl_3) 170.6 (Ac C=O), 160.9 (1-C), 144.1 (3-C), 135.0 (8-C), 134.3 (7-C), 132.2 (8a-C), 129.2 (1C, d, J 24.5, 5-C), 127.5 (4a-C), 126.7 (6-C), 116.8 (4-C), 48.9 (Et 1-C), 38.4 (*N*-Et 1-C), 21.7 (Ac 2-C), 16.6 (Et 2-C), 15.9 (*N*-Et 2-C). δ_{F} (565 MHz, CDCl_3) 64.8. ν_{max} (neat)/ cm^{-1} 3139, 2980, 2936, 1649, 1576, 1410, 1201, 978. HRMS (ESI) $\text{C}_{15}\text{H}_{17}\text{FN}_2\text{O}_3\text{S}$ requires $[\text{M}+\text{H}]^+$, calculated 325.1022, found 325.1009.

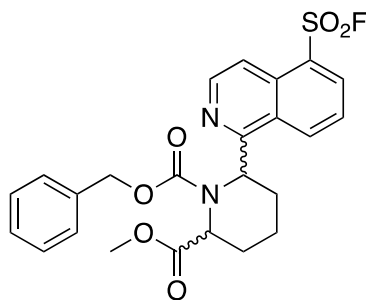
1-(*N*-Methylcarbonyl-6-phenylpiperidin-2-yl)isoquinoline-5-sulfonyl fluoride



5-16

Following the general procedure (**Section 5.2.2**), isoquinoline-8-sulfonyl fluoride (21.1 mg, 0.10 mmol) was reacted methyl 2-phenylpiperidine-1-carboxylate (109.6 mg, 0.5 mmol), following purification by Mass-Directed HPLC from a 15 minute gradient of 40 – 95% acetonitrile in water, collecting at 11.0 mins to isolate the cross coupled product, **5-16**, as a cream amorphous solid (0.4 mg, 1%). δ_{H} (500 MHz, CDCl_3) 8.80 (1H, d, J 6.2, 3-H), 8.52 (1H, d, J 7.1, 8-H), 8.38 (1H, dd, J 7.4, 1.1, 6-H), 8.26 (1H, dd, J 6.3, 2.4, 4-H), 7.67 (1H, t, J 8.1, 7-H), 7.19 (5H, m, Ph), 5.86 (1H, m, pip 2-H), 4.36 (1H, m, pip 6-H), 3.63 (3H, s, Me H_3), 2.26-2.03 (6H, m, pip 3-H, 4-H, 5- H_2). δ_{C} (125 MHz, CDCl_3) 170.5 (C=O), 157.2 (1-C), 154.8 (Ph 1-C), 141.7 (3-C), 135.0 (8-C), 136.8 (7-C), 132.8 (Ph 3- and 5-C), 131.2 (8a-C), 128.8 (Ph 4-C), 127.2 (1C, d, J 23.2, 5-C), 126.9 (4a-C), 126.3 (Ph 2- and 6-C), 125.7 (6-C), 114.1 (4-C), 59.5 (pip 2-C), 52.9 (pip 6-C), 40.0 (pip 3-C), 29.8 (Me), 26.4 (pip 5-C), 22.8 (pip 4-C). δ_{F} (565 MHz, CDCl_3) 64.5. ν_{max} (neat)/ cm^{-1} 3035, 2949, 1603, 1536, 1402, 1201, 1067. HRMS (ESI) $\text{C}_{22}\text{H}_{21}\text{FN}_2\text{O}_4\text{S}$ requires $[\text{M}+\text{H}]^+$, calculated 429.1284, found 429.1287.

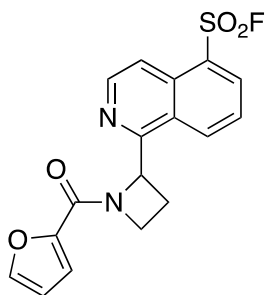
1-(*N*-Phenyl-6-methylcarbonylpiperidin-2-yl)isoquinoline-5-sulfonyl fluoride



5-17

Following the general procedure (Section 5.2.2), isoquinoline-8-sulfonyl fluoride (21.1 mg, 0.10 mmol) was reacted 2-methyl 1-phenyl piperidine-1,2-dicarboxylate (131.6 mg, 0.5 mmol), following purification by Mass-Directed HPLC from a 15 minute gradient of 5 – 95% acetonitrile in water, collecting at 14.5 mins to isolate the cross coupled product, **5-17**, as a brown oil (3.3 mg, 7%). δ_{H} (500 MHz, CDCl_3) 8.72 (1H, d, J 5.9, 3-H), 8.55 (1H, d, J 7.5, 8-H), 8.39 (1H, dd, J 7.5, 2.8, 6-H), 8.19 (1H, dd, J 6.1, 2.8, 4-H), 7.82 (1H, t, J 8.1, 7-H), 7.38 (5H, m, Cbz Ph), 5.23 (2H, s, Cbz CH_2), 5.15 (1H, m, pip 2-H), 5.09 (1H, m, pip 6-H), 3.80 (3H, s, Me), 2.26-1.89 (6H, m, pip 3-, 4- and 5-H). δ_{C} (125 MHz, CDCl_3) 172.5 (Me C=O), 171.7 (Cbz C=O), 164.0 (1-C), 144.8 (3-C), 134.8 (8-C), 133.2 (7-C), 132.4 (8a-C), 128.7 (Cbz 3- and 5-C), 128.6 (Cbz 4-C), 128.4 (1C, d, J 23.8, 5-C), 128.1 (Cbz 2- and 6-C), 126.7 (4a-C), 126.0 (6-C), 115.7 (4-C), 67.7 (Cbz CH_2), 67.0 (Me), 55.6 (pip 2-C), 42.0 (pip 6-C), 30.1 (pip 3-C), 24.8 (pip 5-C), 20.9 (pip 4-C). δ_{F} (565 MHz, CDCl_3) 63.8. ν_{max} (neat)/ cm^{-1} 3064, 2945, 2867, 1721, 1675, 1409, 1205. HRMS (ESI) $\text{C}_{24}\text{H}_{23}\text{FN}_2\text{O}_6\text{S}$ requires $[\text{M}+\text{H}]^+$, calculated 487.1339, found 487.1335.

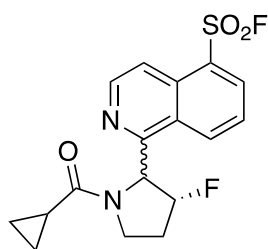
1-[N-(furan-2-carbonyl)azetidin-2-yl]isoquinoline-5-sulfonyl fluoride



5-18

Following the general procedure (**Section 5.2.2**), isoquinoline-8-sulfonyl fluoride (21.1 mg, 0.10 mmol) was reacted 1-(furan-2-carbonyl)azetidine (75.6 mg, 0.5 mmol), following purification by Mass-Directed HPLC from a 15 minute gradient of 5 – 95% acetonitrile in water, collecting at 11.0 mins to isolate the cross coupled product, **5-18**, as a brown oil (5.7 mg, 16%). δ_{H} (500 MHz, CDCl_3) 8.93 (1H, appt d, J 8.5, 3-H), 8.84 (1H, d, J 6.0, 8-H), 8.58 (1H, d, J 7.5, 6-H), 8.29 (1H, br. s, 4-H), 7.81 (1H, t, J 8.0, 7-H), 7.52 (1H, br. s, fur 3-H), 7.05 (1H, br. s, fur 5-H), 6.48 (1H, br. s, fur 4-H), 4.91 (1H, m, aze 2-H), 4.68 (2H, m, aze 4-H₂), 2.86 (2H, m, aze 3-H₂). δ_{C} (125 MHz, CDCl_3) 162.1 (C=O), 159.3 (1-C), 145.5 (3-C), 144.9 (fur 3-C), 134.8 (8-C), 133.6 (7-C), 132.3 (8a-C), 129.2 (1C, d, J 24.4, 5-C), 126.7 (4a-C), 125.8 (6-C), 116.7 (4-C), 116.2 (fur 4-C), 111.8 (fur 5-C), 60.0 (aze 2-C), 51.4 (aze 4-C), 24.1 (aze 3-C). δ_{F} (565 MHz, CDCl_3) 62.8. ν_{max} (neat)/ cm^{-1} 3100, 3014, 2966, 2933, 2893, 1747, 1624, 1411, 1204, 1135. HRMS (ESI) $\text{C}_{17}\text{H}_{13}\text{FN}_2\text{O}_4\text{S}$ requires $[\text{M}+\text{Na}]^+$, calculated 383.0478, found 383.0471.

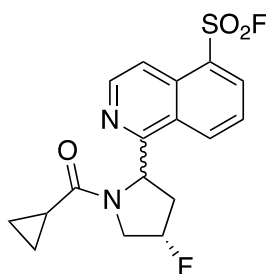
1-[(3R)-1-cyclopropanecarbonyl-3-fluoropyrrolidin-2-yl]isoquinoline-5-sulfonyl fluoride



5-19a

Following the general procedure (Section 5.2.2), isoquinoline-8-sulfonyl fluoride (21.1 mg, 0.10 mmol) was reacted (3S)-1-cyclopropanecarbonyl-3-fluoropyrrolidine (78.6 mg, 0.5 mmol), following purification by Mass-Directed HPLC from a 20 minute gradient of 20 – 60% acetonitrile in water, isolating two cross coupled products, initially collecting at 12.5 mins, **5-19a**, as a brown amorphous solid (1.0 mg, 3%, 50:50 mixture of rotamers). δ_{H} (500 MHz, CDCl_3) 8.78 (1H, appt d, J 6.3, 3-H), 8.64 (1H, d, J 8.4, 8-H), 8.60 (1H, d, J 7.3, 6-H), 8.31 (1H, br. s, 4-H), 7.83 (1H, t, J 7.9, 7-H), 6.24 (1H, m, pyrrolidinyl 2-H), 5.51 (1H, br. s, pyrrolidinyl 3- H_{Rota}), 5.40 (1H, br. s, pyrrolidinyl 3- H_{Rotb}), 4.58 (1H, m, pyrrolidinyl 5- H_a), 4.31 (1H, m, pyrrolidinyl 5- H_b), 2.86 (1H, m, pyrrolidinyl 4- H_a), 2.45 (1H, m, pyrrolidinyl 4- H_b), 1.03 (1H, m, prop 1-H), 0.91 (4H, m, prop 2- and 3- H_2). δ_{C} (125 MHz, CDCl_3) 173.0 (C=O), 160.6 (1-C), 145.4 (3-C), 134.5 (8-C), 132.8 (7-C), 131.9 (8a-C), 129.0 (1C, d, J 24.3, 5-C), 126.2 (6-C), 125.9 (4a-C), 116.3 (4-C), 92.2 (1C, d, J 179.9 3-C), 57.6 (1C, d, J 25.2, 3-C), 54.0 (5-C), 38.9 (1C, d, J 21.2, 4-C), 13.1 (prop 1-C), 8.4 and 8.3 (prop 2- or 3-C). δ_{F} (565 MHz, CDCl_3) 63.0 (SO_2F), -172.3 (pyrrolidinyl CF). ν_{max} (neat)/ cm^{-1} 3066, 2929, 1629, 1583, 1402, 1201, 1098. HRMS (ESI) $\text{C}_{17}\text{H}_{16}\text{F}_2\text{N}_2\text{O}_3\text{S}$ requires $[\text{M}+\text{Na}]^+$, calculated 389.0747, found 389.0742.

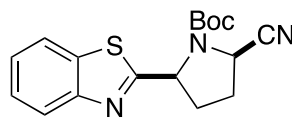
1-[(4S)-1-cyclopropanecarbonyl-4-fluoropyrrolidin-2-yl]isoquinoline-5-sulfonyl fluoride



5-19b

Also obtained from the above reaction, isolated at 15.5 mins was **5-19b**, as a brown amorphous solid (1.7 mg, 5%, 50:50 mixture of rotamers). δ_{H} (500 MHz, CDCl_3) 8.99 (1H, appt d, J 8.6, 3-H), 8.72 (1H, d, J 6.1, 8-H), 8.59 (1H, d, J 7.5, 6-H), 8.28 (1H, br. s, 4-H), 7.83 (1H, t, J 8.0, 7-H), 6.20 (1H, t, J 8.1, pyrrolidinyl 2-H), 5.63 (1H, br. s, pyrrolidinyl 4- H_{Rota}), 5.53 (1H, br. s, pyrrolidinyl 4- H_{Rotb}), 4.44 (1H, m, pyrrolidinyl 5- H_{a}), 4.29 (1H, appt dd, J 12.6, 10.5, pyrrolidinyl 5- H_{b}), 2.74 (1H, m, pyrrolidinyl 3- H_{a}), 2.60-2.55 (1H, m, pyrrolidinyl 3- H_{b}), 1.70-1.65 (1H, m, prop 1-H), 0.87-0.76 (4H, m, prop 2- and 3- H_2). δ_{C} (125 MHz, CDCl_3) 172.8 (C=O), 162.3 (1-C), 145.9 (3-C), 135.4 (8-C), 133.5 (7-C), 132.5 (8a-C), 129.3 (1C, d, J 25.2, 5-C), 127.0 (6-C), 126.3 (4a-C), 116.7 (4-C), 92.8 (1C, d, J 177.6 4-C), 56.0 (2-C), 54.2 (1C, d, J 22.5, 5-C), 31.2 (1C, d, J 21.2, 3-C), 13.0 (prop 1-C), 8.3 and 7.8 (prop 2- or 3-C). δ_{F} (565 MHz, CDCl_3) 62.8 (SO_2F), -176.2 (pyrrolidinyl CF) ν_{max} (neat)/ cm^{-1} 3086, 3061, 3003, 2977, 1629, 1402, 1200, 1087. HRMS (ESI) $\text{C}_{17}\text{H}_{16}\text{F}_2\text{N}_2\text{O}_3\text{S}$ requires $[\text{M}+\text{Na}]^+$, calculated 389.0747, found 389.0740.

2-[*N*-Boc-(2*R*)-5-cyano-pyrrolidin-2-yl]-1,3-benzothiazole

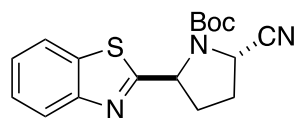


T-3a

Following the general procedure (**Section 5.2.2**), 1,3-benzothiazole (13.5 mg, 0.10 mmol) was reacted with *N*-Boc-2-cyano-pyrrolidine (98.1 mg, 0.5 mmol), following purification by Mass-Directed HPLC from a 15 minute gradient of 20 – 60% acetonitrile in water, isolating two cross coupled products, initially collecting at 11.0 mins, **T-3a**, as a pale brown amorphous solid (8.9 mg, 27%, 55:45 mixture of rotamers). δ_{H} (500 MHz, CDCl_3) 7.96 (1H, dd, J 8.2, 1.9, 7-H), 7.88 (1H, br. s, 4-H), 7.48 (1H, br. s, 6-H), 7.39 (1H, br. s, 5-H), 5.41 (1H, br. s, pyrrolidinyl 2- H_{maj})*, 5.27 (1H, br. s, pyrrolidinyl 2- H_{min})*, 4.77 (1H, br. s, pyrrolidinyl 5- H_{maj}), 4.61 (1H, br. s, pyrrolidinyl 5- H_{min}), 2.56-2.45 (4H, m, pyr, 3- and 4-H), 1.62 (9H, s, ^tBu 2- H_{min}), 1.56 (9H, s, ^tBu 2- H_{maj}). δ_{C} (125 MHz, CDCl_3) 173.4 (^tBu C=O $_{\text{min}}$), 172.7 (^tBu C=O $_{\text{maj}}$), 153.4 (2- C_{maj}), 153.3 (2- C_{min}), 152.9 (7a- C_{min}), 152.8 (7a- C_{maj}), 135.0 (3a- C_{maj}), 134.6 (3a- C_{min}), 126.5 (6- C_{min}), 126.3 (6- C_{maj}), 125.4 (5- C_{min}), 125.3 (5- C_{maj}), 123.2 (7-C), 121.9 (4- C_{min}), 121.8 (4- C_{maj}), 118.9 (CN $_{\text{maj}}$), 118.7 (CN $_{\text{min}}$), 82.9 (^tBu C $_{1\text{maj}}$), 82.5 (^tBu C $_{1\text{min}}$), 59.6 (pyrrolidinyl 5- C_{min}), 59.2 (pyrrolidinyl 5- C_{maj}), 48.4 (pyrrolidinyl 2- C_{maj}), 48.1 (pyrrolidinyl 2- C_{min}), 32.7 (pyrrolidinyl 4- C_{min}), 31.4 (pyrrolidinyl 4- C_{maj}), 29.9 (pyrrolidinyl 3- C_{maj}), 28.8 (pyrrolidinyl 3- C_{min}), 28.4 (^tBu C $_{2\text{maj}}$), 28.2 (^tBu C $_{2\text{min}}$). ν_{max} (neat)/ cm^{-1} 3042, 2993, 2921, 1722, 1409. HRMS (ESI) $\text{C}_{17}\text{H}_{19}\text{N}_3\text{O}_2\text{S}$ requires $[\text{M}+\text{H}]^+$, calculated 330.1276, found 330.1265.

*Stereochemistry assigned relative to literature similar compounds as illustrated in **Appendix H**^{173,174}.

2-[*N*-Boc-(2*S*)-5-cyano-pyrrolidin-2-yl]-1,3-benzothiazole

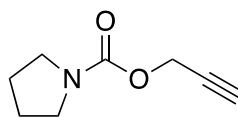


T-3b

Also obtained from the above reaction, isolated at 12.0 mins was **T-3b**, as a pale brown solid (5.3 mg, 16%, 55:45 mixture of rotamers). δ_{H} (500 MHz, CDCl_3) 7.97 (1H, d, J 8.2, 7-H), 7.84 (1H, dd, J 8.0, 7.5 4-H), 7.47 (1-H, ddd, J 8.0, 7.7, 4.3, 6-H), 7.38 (1H, ddd, J 8.0, 7.7, 4.3 5-H), 5.43 (1H, d, J 8.0, pyrrolidinyl 2- H_{maj})*, 5.32 (1H, d, J 8.0, pyrrolidinyl 2- H_{min})*, 4.85 (1H, d, J 8.1, pyrrolidinyl 5- H_{maj}), 4.74 (1H, d, J 8.1, pyrrolidinyl 5- H_{min}), 2.55-2.30 (4H, m, pyr, 3- and 4-H), 1.54 (9H, s, tBu 2- H_{maj}), 1.31 (9H, s, tBu 2- H_{min}). δ_{C} (125 MHz, CDCl_3) 173.6 (tBu C=O $_{\text{min}}$), 172.7 (tBu C=O $_{\text{maj}}$), 153.8 (2- C_{maj}), 153.5 (2- C_{min}), 153.1 (7a- C_{min}), 152.8 (7a- C_{maj}), 135.2 (3a- C_{maj}), 135.0 (3a- C_{min}), 126.4 (6- C_{min}), 126.3 (6- C_{maj}), 125.4 (5- C_{min}), 125.3 (5- C_{maj}), 123.2 (7-C), 121.9 (4- C_{min}), 121.8 (4- C_{maj}), 118.8 (CN $_{\text{maj}}$), 118.7 (CN $_{\text{min}}$), 83.1 (tBu C $_{1\text{maj}}$), 82.7 (tBu C $_{1\text{min}}$), 61.0 (pyrrolidinyl 5- C_{min}), 60.3 (pyrrolidinyl 5- C_{maj}), 48.2 (pyrrolidinyl 2- C_{maj}), 48.1 (pyrrolidinyl 2- C_{min}), 32.7 (pyrrolidinyl 4- C_{min}), 31.4 (pyrrolidinyl 4- C_{maj}), 29.9 (pyrrolidinyl 3- C_{maj}), 28.8 (pyrrolidinyl 3- C_{min}), 28.4 (tBu C $_{2\text{maj}}$), 28.2 (tBu C $_{2\text{min}}$). ν_{max} (neat)/ cm^{-1} 3078, 2985, 2942, 1698, 1412. HRMS (ESI) $\text{C}_{17}\text{H}_{19}\text{N}_3\text{O}_2\text{S}$ requires $[\text{M}+\text{H}]^+$, calculated 330.1276, found 330.1264.

*Stereochemistry assigned relative to literature similar compounds as illustrated in **Appendix H**^{173,174}.

Poc-pyrrolidine



03

Pyrrolidine (1.00 g, 14.08 mmol) was dissolved in dry DCM (20 mL) and cooled to 0 °C on ice, to which triethylamine (2.15 mL, 15.36 mmol) was added and the solution stirred. Propargyl chloroformate (1.25 mL, 12.80 mmol) was added dropwise to the solution, and stirred for 1 hour before warming to room temperature overnight, until consumption of the chloroformate was shown by TLC. The reaction mixture was then washed with brine (2 × 10 mL) and water (2 × 10 mL), dried with Na₂SO₄ and concentrated *in vacuo*. The crude product was purified through a silica plug, eluting with DCM to give Poc-pyrrolidine¹⁷², **03** as a colourless oil (2.15 g, 98%). δ_H (500 MHz, CDCl₃) 4.69 (2H, t, *J* 1.5, poc 1-H₂), 3.37 (4H, dt, *J* 15.4, 6.7, 2- and 5-H₂), 2.44 (1H, t, *J* 1.5, poc 3-H), 1.86 (4H, m, 3- and 4-H₂). δ_C (125 MHz, CDCl₃) 154.1 (poc C=O), 79.0 (poc 2-C), 74.3 (poc 3-C), 52.6 (poc 1-C), 46.5 and 46.0 (2- and 5-C), 25.9 and 25.0 (3- and 4-C). *R*_F 0.42 (DCM). ν_{max} (neat)/cm⁻¹ 3310, 3299, 2965, 2744, 1701.

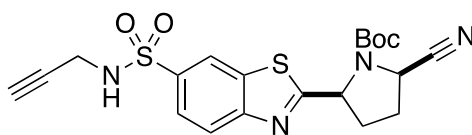
6-(*N*-Poc-pyrrolidin-2-yl)pyridine-3-sulfonyl fluoride



3-1 Alkyne

A deprotection of 6-(*N*-Boc-pyrrolidin-2-yl)pyridine-3-sulfonyl fluoride, **3-1**, (4 mg, 0.012 mmol) was carried out using TFA (20% in DCM), stirring for 2 hours at room temperature. The solution was concentrated *in vacuo* to remove excess TFA, before resuspending in DCM (1 mL). The solution was cooled to 0 °C, and the propargyl chloride (2 μ L, 0.024 mmol) and triethylamine (4 μ L, 0.026 mmol) were added dropwise. The reaction was allowed to warm to room temperature and left to stir overnight. The mixture was concentrated *in vacuo*, dissolved in acetonitrile, and purified via Mass-Directed HPLC with acetonitrile to water as a gradient of 5-95%, the eluted samples were lyophilised to give the pure product **3-1 Alkyne**, as a brown oil (1.6 mg, 42%, 60:40 mixture of rotamers). δ_{H} (500 MHz, CDCl_3) 9.13 (1H, s, 2-H), 8.22 (1H, m, 5-H), 7.49 (1H, appt dd, J 8.4, 12.7, 4H), 5.10 (1H, appt td, J 3.5, 8.4, pyrrolidinyl 2-H), 4.68 (1H, appt qd, J 2.0, 12.2, 5- H_{maj}), 4.55 (1H, appt qd, J 2.0, 12.2, 5- H_{min}), 3.71 (2H, m, poc 1- H_2), 2.47 (1H, t, J 2.6, poc- 3-H), 2.39 (2H, m, pyrrolidinyl 3- and 4- H_a), 2.03 (2H, m, pyrrolidinyl 3- and 4- H_b). δ_{C} (125 MHz, CDCl_3) 170.6 (poc C=O $_{\text{min}}$), 169.9 (poc C=O $_{\text{maj}}$), 154.4 (6- C_{maj}), 153.9 (6- C_{min}), 149.1 (2-C), 136.8 (4-C), 128.5 (1C, d, J 25.4, 3-C), 121.4 (5- C_{maj}), 120.8 (5- C_{min}), 78.4 (poc 2- C_{maj}), 78.1 (poc 2- C_{min}), 74.8 (poc 3- C_{maj}), 74.6 (poc 3- C_{min}), 63.0 (pyrrolidinyl 2- C_{maj}), 62.6 (pyrrolidinyl 2- C_{min}), 53.2 (pyrrolidinyl 5- C_{maj}), 52.9 (pyrrolidinyl 5- C_{min}), 48.0 (poc 1- C_{min}), 47.6 (poc 1- C_{maj}), 34.2 (pyrrolidinyl 3- C_{min}), 33.0 (pyrrolidinyl 3- C_{maj}), 24.3 (pyrrolidinyl 4- C_{maj}), 23.3 (pyrrolidinyl 4- C_{min}). δ_{F} (565 MHz, CDCl_3) 68.7. ν_{max} (neat)/ cm^{-1} 3104, 3054, 2938, 2214, 1749, 1619, 1409, 1221, 1153. HRMS (ESI) $\text{C}_{13}\text{H}_{13}\text{FN}_2\text{O}_4\text{S}$ requires $[\text{M}+\text{H}]^+$, calculated 313.0658, found 313.0650.

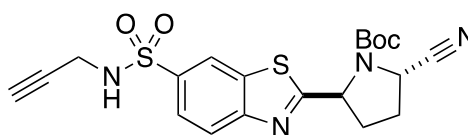
2-[N-Boc-(2R)-5-cyano-pyrrolidin-2-yl]-5-(prop-2-yl-1-yl)sulfamoyl-1,3-benzothiazole



1-3a Alkyne

A portion of 2-[N-Boc-(2R)-5-cyano-pyrrolidin-2-yl]-1,3-benzothiazole-6-sulfonyl fluoride, **1-3a** (10 mg, 0.024 mmol) was reacted with a 50% solution of propargyl amine in acetone (5ml) at room temperature overnight, until consumption of starting material was shown by LC-MS. The mixture was concentrated *in vacuo*, dissolved in acetonitrile, and purified via Mass-Directed HPLC with acetonitrile to water as a gradient of 20-60% over 20 minutes, collecting at 15.0 mins. The eluted samples were lyophilised to give the pure product **1-3a Alkyne** as a brown oil (6.8 mg, 63%, 55:45 mixture of rotamers). δ_{H} (500 MHz, CDCl_3) 8.47 (1H, br. s, 7-H), 8.09 (1H, dd, *J* 8.6, 0.6, 4-H), 7.98 (1H, br. s, 5-H), 5.41 (1H, br. s, pyrrolidinyl 2- H_{maj}), 5.28 (1H, br. s, pyrrolidinyl 2- H_{min}), 4.80 (1H, br. s, pyrrolidinyl 5- H_{maj}), 4.71 (1H, br. s, NH), 4.64 (1H, br. s, pyrrolidinyl 5- H_{min}), 3.90 (2H, s, prop 1- H_2), 2.61-2.43 (4H, m, pyrrolidinyl 3- and 4- H_2), 2.06 (1H, s, prop 3-H), 1.62 (9H, s, ^tBu 2- $\text{H}_{3\text{min}}$), 1.56 (9H, s, ^tBu 2- $\text{H}_{3\text{maj}}$). δ_{C} (125 MHz, CDCl_3) 179.0 (^tBu C=O), 170.9 (2-C), 156.3 (7a-C) 153.1 (3a-C), 136.4 (6-C), 125.2 (7-C), 123.8 (4-C), 122.4 (5-C), 118.6 (CN $_{\text{maj}}$), 83.5 (^tBu 1- C_{maj}), 83.0 (^tBu 1- C_{min}), 77.9 (prop 2-C), 73.5 (prop 3-C), 61.0 (pyrrolidinyl 5- C_{min}), 60.4 (pyrrolidinyl 5- C_{maj}), 48.3 (pyrrolidinyl 2-C), 33.1 (pyrrolidinyl 4- C_{min}), 31.9 (pyrrolidinyl 4- C_{maj}), 30.6 (pyrrolidinyl 3- C_{maj}), 30.1 (pyrrolidinyl 3- C_{min}), 33.1 (^tBu 1-C), 28.3 (^tBu 2-C). ν_{max} (neat)/ cm^{-1} 3268, 2977, 2905, 2024, 1708, 1337, 1121. HRMS (ESI) $\text{C}_{20}\text{H}_{22}\text{N}_4\text{O}_4\text{S}_2$ requires $[\text{M}+\text{Na}]^+$, calculated 469.0980, found 469.0976.

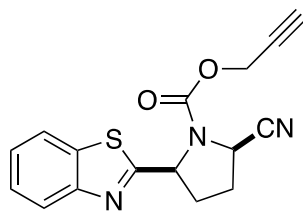
2-[N-Boc-(2s)-5-cyano-pyrrolidin-2-yl]-5-(prop-2-yl-1-yl)sulfamoyl-1,3-benzothiazole



1-3b Alkyne

A portion of 2-[N-Boc-(2S)-5-cyano-pyrrolidin-2-yl]-1,3-benzothiazole-6-sulfonyl fluoride, **1-3b** (15 mg, 0.036 mmol) was reacted with a 50% solution of propargyl amine in acetone (5ml) at room temperature overnight, until consumption of starting material was shown by LC-MS. The mixture was concentrated *in vacuo*, dissolved in acetonitrile, and purified via Mass-Directed HPLC with acetonitrile to water as a gradient of 20-60% over 20 minutes, collecting at 16.0 mins, **1-3b Alkyne** as a brown oil (11.6 mg, 71%, 55:45 mixture of rotamers). δ_{H} (500 MHz, CDCl_3) 8.44 (1H, d, J 7.0, 7-H), 8.07 (1H, d, J 7.0, 4-H), 7.97 (1H, m, 5-H), 5.47 (1H, d, J 8.5, pyrrolidinyl 2- H_{maj}), 5.35 (1H, d, J 8.5, pyrrolidinyl 2- H_{min}), 4.87 (1H, d, J 7.5, pyrrolidinyl 2- H_{min}), 4.75 (1H, d, J 7.5, pyrrolidinyl 2- H_{min}), 3.91 (2H, m, prop 1- $\text{H}_{2\text{min}}$), 3.88 (2H, m, prop 1- $\text{H}_{2\text{maj}}$), 3.32 (1H, br. s, NH), 2.75-2.33 (4H, m, pyrrolidinyl 3- and 4- H_2), 2.07 (1H, m, prop 3- H_{maj}), 2.03 (1H, m, prop 3- H_{min}), 1.55 (9H, s, ^tBu 2- $\text{H}_{3\text{maj}}$), 1.31 (9H, s, ^tBu 2- $\text{H}_{3\text{min}}$). δ_{C} (125 MHz, CDCl_3) 178.4 (^tBu C=O $_{\text{min}}$), 177.9 (^tBu C=O $_{\text{maj}}$), 155.8 (2- C_{maj}), 155.7 (2- C_{min}), 152.9 (7a- C_{maj}), 152.7 (7a- C_{min}), 136.8 (3a- C_{min}), 136.5 (3a- C_{maj}), 135.3 (6- C_{maj}), 134.8 (6- C_{min}), 125.4 (5- C_{min}), 125.2 (5- C_{maj}), 123.8 (7-C), 122.3 (4-C), 118.6 (CN $_{\text{maj}}$), 118.4 (CN $_{\text{min}}$), 83.5 (^tBu 1- C_{maj}), 82.9 (^tBu 1- C_{min}), 77.9 (prop 2- C_{min}), 77.8 (prop 2- C_{maj}), 73.5 (prop 3- C_{maj}), 73.3 (prop 3- C_{min}), 59.6 (pyrrolidinyl 5- C_{min}), 59.3 (pyrrolidinyl 5- C_{maj}), 48.5 (pyrrolidinyl 2- C_{maj}), 48.2 (pyrrolidinyl 2- C_{min}), 33.1 (prop 1-C), 32.6 (pyrrolidinyl 4- C_{min}), 31.4 (pyrrolidinyl 4- C_{maj}), 29.9 (pyrrolidinyl 3- C_{maj}), 28.8 (pyrrolidinyl 3- C_{min}), 28.4 (^tBu 2- C_{maj}), 28.2 (^tBu 2- C_{min}). ν_{max} (neat)/ cm^{-1} 3274, 2978, 2121. 1705, 1368, 1162. HRMS (ESI) $\text{C}_{20}\text{H}_{22}\text{N}_4\text{O}_4\text{S}_2$ requires $[\text{M}+\text{H}]^+$, calculated 447.1161, found 447.1157

2-[*N*-Poc-(2*R*)-5-cyano-pyrrolidin-2-yl]-1,3-benzothiazole



T-3a Alkyne

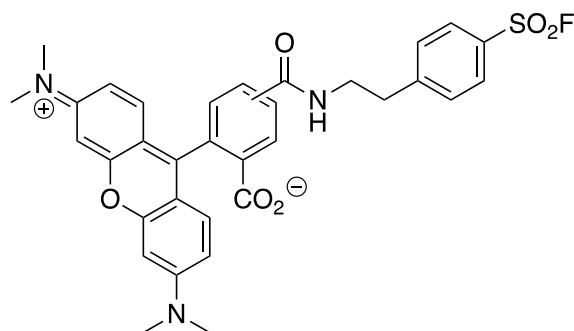
A deprotection of 2-[*N*-Boc-(2*R*)-5-cyano-pyrrolidin-2-yl]-1,3-benzothiazole, **T-3a**, (13.5 mg, 0.041 mmol) was carried out using TFA (20% in DCM), stirring for 2 hours at room temperature. The solution was concentrated *in vacuo* to remove excess TFA, before resuspending in DCM (5 mL). The solution was cooled to 0 °C, and the propargyl chloride (6 μ L, 0.08 mmol) and triethylamine (13 μ L, 0.09 mmol) were added dropwise. The reaction was allowed to warm to room temperature and left to stir overnight. The mixture was concentrated *in vacuo*, dissolved in acetonitrile, and purified via Mass-Directed HPLC with acetonitrile to water as a gradient of 20-60% over 20 minutes, collecting at 9.5 mins, **T-3 alkyne** as a brown oil (4.9 mg, 38%, 50:50 mixture of rotamers). δ_{H} (500 MHz, CDCl₃) 8.00 (1H, appt ddd, *J* 8.2, 1.2, 0.6, 7-H), 7.88 (1H, br. s, 4-H), 7.49 (1H, br. s, 6-H), 7.40 (1H, br. s, 5-H), 5.47 (1H, br. s, pyrrolidinyl 2-*H*_{RotA}), 5.42 (1H, br. s, pyrrolidinyl 2-*H*_{RotB}), 4.91 (1H, br. s, pyrrolidinyl 2-*H*_{min}), 4.78 (2H, br. s, Poc 1-*H*₂), 4.65 (1H, br. s, pyrrolidinyl 2-*H*_{min}), 2.62-2.39 (5H, br. m, pyrrolidinyl 3- and 4-*H*₂ and Poc 3-*H*). δ_{C} (125 MHz, CDCl₃) 172.8 (Poc C=O_{RotA}), 172.8 (Poc C=O_{RotB}), 153.6 (2-C), 151.0 (7a-C), 135.2 (3a-C), 126.4 (6-C), 125.5 (5-C), 123.3 (7-C), 122.1 (4-C), 118.1 (CN), 76.6 (Poc 2-*C*_{RotB}), 75.8 (Poc 3-*C*_{RotA}), 75.6 (Poc 3-*C*_{RotB}), 61.1 (pyrrolidinyl 2-*C*_{RotA}), 60.8 (pyrrolidinyl 2-*C*_{RotB}), 54.3 (Poc 1-*C*_{RotA}), 54.2 (Poc 1-*C*_{RotB}), 48.7 (pyrrolidinyl 5-*C*_{RotA}), 48.2 (pyrrolidinyl 5-*C*_{RotB}), 33.4 (pyrrolidinyl 2-*C*_{RotA}), 32.1 (pyrrolidinyl 4-*C*_{RotB}), 30.8 (pyrrolidinyl 3-*C*_{maj}), 29.8 (pyrrolidinyl 3-*C*_{min}). ν_{max} (neat)/cm⁻¹ 3287, 3067, 2956, 2130, 1717, 1311, 1160. HRMS (ESI) C₁₆H₁₃N₃O₂S requires [M+Na]⁺, calculated 334.0626, found 334.0620.

4-(2-(Hex-5-ynamido)ethyl)benzene-1-sulfonyl fluoride



6-Hexynoic acid (50.0 mg, 0.40 mmol) was added to dry DCM (10 mL), to which DIPEA (138 μ L, 0.80 mmol), oxyma pure (62.5 mg, 0.44 mmol) and DIC (68.9 μ L, 0.44 mmol) were added and the solution was stirred. 4-Aminoethylbenzenesulfonyl fluoride (95 mg, 0.40 mmol) was added portionwise and the reaction left to stir over night at room temperature, until consumption of starting material was observed by LC-MS. The mixture was *concentrated in vacuo*, dissolved in acetonitrile, and purified via Mass-Directed HPLC with acetonitrile to water as a gradient of 20-95% over 10 minutes, eluted at 7.5 mins. The samples were lyophilised to give the pure sulfonyl fluoride alkyne¹⁰⁵, **SF-Alkyne** as a colourless fluffy solid (17.8 mg, 30%). δ_{H} (500 MHz, CDCl_3) 7.95 (2H, d, J 10.0, 2- and 6-H), 7.47 (2H, d, J 10.0, 3- and 5-H), 5.55 (1H, br. s, NH), 3.56 (2H, appt q, J 8.5, Et 2-H₂), 2.97 (2H, t, J 8.5, Et 1-H₂), 2.30 (2H, t, J 8.5, Hex 2-H₂), 2.23 (2H, td, J 8.5, 3.4, Hex 4-H₂), 1.96 (1H, t, J 3.4, Hex 6-H), 1.84 (2 H, p, J 8.5, Hex 3-H₂). δ_{C} (125 MHz, CDCl_3) 172.5 (C=O), 147.7 (5-C), 130.1 (3- and 5-C), 129.5 (2- and 6-C), 128.8 (1C, d, J 25.6, 1-C), 83.3 (5-C), 69.4 (Hex 6-C), 40.1 (Et 2-C), 35.9 (Et 1-C), 34.9 (Hex 2-C), 24.0 (Hex 3-C), 17.7 (Hex 4-C). δ_{F} (375 MHz, CDCl_3) 66.2. ν_{max} (neat)/ cm^{-1} 3270, 2918, 1675, 1410, 1218, 1102. HRMS (ESI) $\text{C}_{17}\text{H}_{16}\text{FN}_2\text{O}_3\text{S}$ requires $[\text{M}+\text{Na}]^+$, calculated 389.0747, found 389.0742.

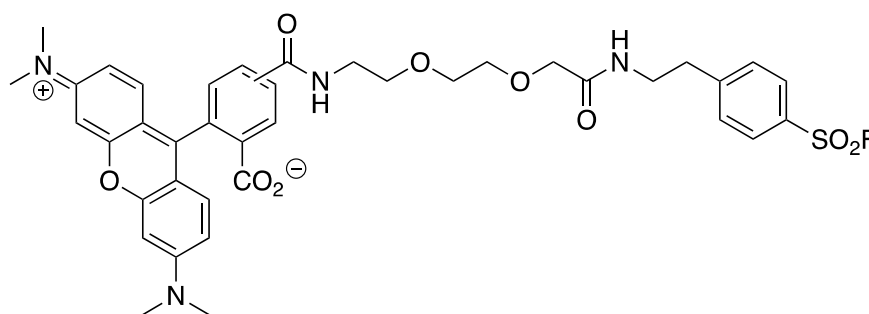
4-[2-(5(6)-Carboxy-tetramethyl-rhodamine)ethyl]benzene-1-sulfonyl fluoride



Rh-SF

5(6)-Carboxy-tetramethyl-rhodamine (20.0 mg, 0.046 mmol) was dissolved in DCM (1 mL) and coupled with 4-(2-aminoethyl)benzenesulfonyl fluoride hydrochloride (5.0 mg, 0.021 mmol) using DIPEA (16.2 μ L, 0.092 mmol), oxyma pure (7 mg, 0.051 mmol) and DIC (7 μ L, 0.051 mmol). The reaction mixture was stirred overnight, in the dark, at room temperature and product formation was confirmed by LC-MS. The mixture was concentrated *in vacuo*, dissolved in acetonitrile, and purified via Mass-Directed HPLC with acetonitrile to water as a gradient of 5-50% over a 20-minute gradient, eluting at 19.0 minutes. The purity confirmed by analytical HPLC, and the eluted samples were lyophilised to give the **Rhodamine-sulfonyl fluoride probe**¹⁰⁵ as a purple amorphous solid (5.3 mg, 41%, Purity: 80%). HRMS (ESI) $C_{33}H_{30}FN_3O_6S$ requires $[M+H]^+$, calculated 616.1912, found 616.1936.

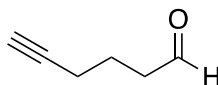
4-[2-(2-(5(6)-Carboxy-tetramethyl-rhodamine)aminoethoxy)ethoxyacetamido)ethyl]benzene-1-sulfonyl fluoride



Rh-Peg-SF

4-(2-Aminoethyl)benzenesulfonyl fluoride hydrochloride (100 mg, 0.41 mmol) was suspended in DCM (2 mL) with DIPEA (72 μ L, 0.41 mmol). To this, Boc-NH-(PEG) acid DCHA salt was added along with oxyma pure (68 mg, 0.45 mmol) and DIC (76 μ L, 0.45 mmol). The reaction mixture was stirred overnight at room temperature and product formation was confirmed by LC-MS. The reaction was concentrated *in vacuo* to afford an orange solid. The crude product was resuspended in a solution of 20% TFA in DCM and stirred for 1 hour until Boc deprotection shown by LC-MS, the mixture was concentrated *in vacuo*. An aliquot of the deprotected product (~7.5 mg) was dissolved in DCM (1 mL) to which 5(6)-Carboxy-tetramethyl-rhodamine (20 mg, 0.046 mmol) was added and coupled using DIPEA (16.2 μ L, 0.092 mmol), oxyma pure (7 mg, 0.051 mmol) and DIC (7 μ L, 0.051 mmol). The reaction mixture was stirred overnight, in the dark, at room temperature and product formation was confirmed by LC-MS. The mixture was concentrated *in vacuo*, dissolved in acetonitrile, and purified via Mass-Directed HPLC with acetonitrile to water as a gradient of 20-40% over a 10 minute gradient to elute at 9.5 mins, The purity confirmed by analytical HPLC and the eluted samples were lyophilised to give the **Rhodamine-PEG-sulfonyl fluoride probe** as a purple amorphous solid (3.0 mg, 19%, Purity: 85%). HRMS (ESI) C₃₉H₄₁FN₄O₉S requires [M+H]⁺, calculated 761.2651, found 761.2682.

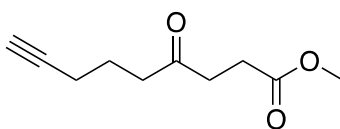
5-Hexyn-1-al



Hexyn-1-ol (2.0 mL, 18.10 mmol), was added to dry DCM (40 mL), with DMSO (5.8 mL, 81.60 mmol) and triethylamine (11.4 mL, 81.60 mmol) before cooling to 0 °C. Sulphur trioxide pyridine (13.0g, 81.60 mmol) was added portion-wise, and the solution stirred. Once dissolved, the solution was warmed to room temperature, and stirred for 2 hours, monitoring by TLC until completion, visualising with *p*-anisaldehyde stain. The reaction mixture was quenched with HCl, (1M, 40 mL) and the organic layer diluted in diethyl ether (200 mL) to help prevent product loss during evaporation. The solution was concentrated *in vacuo*, with a maximum temperature of 20 °C, and pressure control of 400 mbar, due to compounds volatility*. The crude product was purified by column chromatography in pentane: diethyl ether from 0 – 10% to elute the pure product, concentrated *in vacuo* to 5 mL, 5-hexyn-1-al¹⁷⁵⁻¹⁷⁷ was isolated in a solution of diethyl ether, due to compound volatility. δ_{H} (500 MHz, CDCl₃) 9.68 (1H, t, *J* 1.4, 1-H), 2.49 (2H, td, *J* 8.8, 1.7, 2-H₂), 2.15 (2H, td, *J* 8.8, 1.7, 4-H₂), 1.89 (1H, t, *J* 3.4, 6-H), 1.73 (2H, p, *J* 8.8, 3-H₂). δ_{C} (125 MHz, CDCl₃) 201.4 (1-C), 83.1 (5-C), 69.3 (6-C), 42.4 (2-C), 20.7 (3-C), 17.6 (4-C). ν_{max} (neat)/cm⁻¹ 3292, 2943, 2727, 2117, 1709. *R*_F 0.69 (80:20 Hexane–EtOAc). HRMS (ESI) C₆H₈O requires [2M+Na]⁺, calculated 215.1048, found 215.1021.

*Purification was attempted via distillation but was unable to separate from DCM.

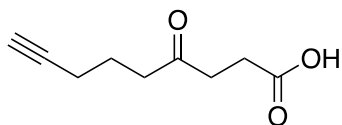
Methyl 4-oxonon-8-ynoate



A solution of 5-hexyn-1-ol in diethyl ether (~ 1.00 g, 10.40 mmol) was added to a crimped vial, with dioxane (10.0 mL), methyl acrylate (4.60 mL, 52.0 mmol), triethylamine (1.00 mL, 7.30 mmol). The 3-Benzyl-5-(2-hydroxyethyl)-4-methylthiazolium chloride catalyst (392 mg, 1.46 mmol) was added, and the flask briefly flushed with nitrogen. The reaction was heated to 80 °C for 24 hours, monitoring by TLC until consumption of the starting material was observed. The reaction mixture was concentrated *in vacuo* and purified by column chromatography, eluting in hexane: EtOAc from 0 – 20% to give the methyl 4-oxonon-8-ynoate^{175,176} as a colourless oil (312 mg, 20%*) δ_{H} (500 MHz, CDCl₃) 3.66 (3H, s, OMe), 2.70 (2H, td, *J* 6.8, 1.4, 5-H₂), 2.59 (2H, m, 3-H₂), 2.57 (2H, m, 2-H₂), 2.21 (2H, td, *J* 6.8, 1.7, 7-H₂), 1.95 (1H, t, *J* 2.7, 9-H), 1.79 (2H, p, *J* 6.8, 6-H₂). δ_{C} (125 MHz, CDCl₃) 208.3 (4-C), 173.3 (1-C), 83.6 (8-C), 69.2 (9-H), 51.9 (OMe), 41.2 (2-C), 37.3 (5-C), 27.7 (3-C), 22.3 (6-C), 17.8 (7-C). ν_{max} (neat)/cm⁻¹ 3290, 2923, 1703. *R_F* 0.32 (80:20 Hexane–EtOAc). HRMS (ESI) C₁₀H₁₄O₃ requires [M+Na]⁺, calculated 205.0841, found 205.0831.

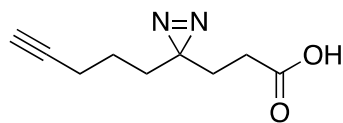
*Combined yield of oxidation and acrylate coupling

4-Oxonon-8-ynoic acid



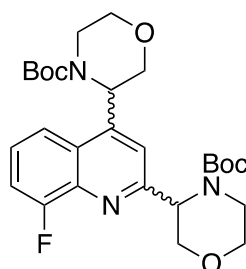
Methyl 4-oxonon-8-ynoate (850 mg, 4.67 mmol) was dissolved in methanol (20 mL) with lithium hydroxide (559 mg, 23.25 mmol) and water (427 μ L, 23.72 mmol) and the solution stirred at room temperature for 24 hours. The reaction mixture was diluted in diethyl ether (30 mL) and washed with HCl (1M, 30 mL). The aqueous layer was then extracted with ether (2 \times 20 mL) and the organic layers combined, dried over Na₂SO₄ and concentrated *in vacuo* to afford 4-oxonon-8-ynoic acid^{175,176} as a colourless oil (600 mg, 76%). δ_{H} (500 MHz, CDCl₃) 5.33 (1H, br. s, OH), 2.70 (2H, t, *J* 6.8, 5-H₂), 2.57 (2H, t, *J* 6.8, 3-H₂), 2.55 (2H, t, *J* 6.8, 2-H₂), 2.17 (2H, td, *J* 6.8, 4.0, 7-H₂), 1.95 (1H, t, *J* 2.7, 9-H), 1.79 (2H, p, *J* 6.8, 6-H₂). δ_{C} (125 MHz, CDCl₃) 208.2 (4-C), 178.3 (1-C), 83.6 (8-C), 69.3 (9-H), 41.1 (2-C), 37.1 (5-C), 27.8 (3-C), 22.3 (6-C), 17.9(7-C). ν_{max} (neat)/cm⁻¹ 3284, 2953, 2115, 1734, 1713. HRMS (ESI) C₉H₁₂O₃ requires [M+Na]⁺, calculated 191.1818, found 191.1773.

4-(4H-diazirin-4-yl)non-8-ynoic acid



Liquid ammonia (40 mL) was generated by condensation in dry ice/ acetone at $-78\text{ }^{\circ}\text{C}$. 4-Oxonon-8-ynoic acid (600 mg, 4.26 mmol) was added and the solution allowed to warm to reflux for 4 hours. HOSA (553 mg, 4.89 mmol) was added as a solution in anhydrous methanol (5 mL) and the reaction mixture was allowed to slowly warm to room temperature and stirred for 16 hours. Nitrogen gas was bubbled through the reaction mixture for 1 hour to remove residual ammonia, and the solution was filtered and concentrated to give a crude oil. The solution was redissolved in dry methanol (15 mL) and cooled to $0\text{ }^{\circ}\text{C}$ with triethylamine (890 μL , 6.36 mmol). iodine_(s) was added portion-wise, until the solutions purple colour remained. The solution was then diluted in DCM (10 mL) and washed with HCl (1M, 10 mL), Na₂S₂O₃ solution (10%, 10 mL) and NaCl (Sat., 10 mL) before drying over Na₂SO₄ and concentrated *in vacuo*. The crude product was purified by column chromatography, eluting in a gradient of Hex:EtOAc from 75:25 – 33:66% with 1 % acetic acid to afford the diazirine product^{175,176} as an orange oil (283 mg, 44%). δ_{H} (500 MHz, CDCl₃) 2.17 (4H, m, 2- and 7-H₂), 1.95 (1H, t, *J* 2.8, 9-H), 1.76 (2H, t, *J* 8.8, 3-H₂), 1.55 (2H, m, 7-H₂), 1.33 (2H, p, *J* 8.8, 6-H₂). δ_{C} (125 MHz, CDCl₃) 177.9 (1-C), 83.4 (8-C), 69.2 (9-C), 31.7 (5-C), 28.3 (2-C), 28.1 (3-C), 27.8 (4-C), 22.7 (6-C), 18.0 (7-C). ν_{max} (neat)/cm⁻¹ 3097, 2935, 1708, 1584. *R*_F 0.46 (50:50 Hexane–EtOAc). HRMS (ESI) C₉H₁₂N₂O₂ requires [M+Na]⁺, calculated 203.0796, found 203.0809.

2,4-Bis(Boc-morpholin-3-yl)-8-Fluoroquinoline



11 and 12

To a LC-MS vial as stock solutions, 8-fluoroquinoline (200 μ L, 1.5 M) and *N*-Boc-morpholine (333 μ L, 1.5 M) were mixed with TFA (100 μ L of a 2 M stock), the organocatalyst 4-CzIPN (100 μ L, 0.05 M), and *t*-butyl peracetate (159 μ L of a 50% w/v solution) were added along with acetone (107 μ L) to a total volume of 1 mL, to give final amounts of 8-fluoroquinoline (14.8 mg, 0.1 mmol), *N*-Boc-morpholine (93.6 mg, 0.5 mmol), TFA (200 mM), catalyst (5 mM) and *t*-butyl peracetate (500 mM). The reaction vials were sealed and stirred on a fan cooled HepatoChem lightbox with irradiation under a Kessil A160 WE LED Tuna Blue lamp for 24 hrs⁴¹. The mixtures were concentrated under air to give the crude product. The crude reaction mixture was dissolved in acetonitrile and purified via Mass-Directed HPLC with acetonitrile to water with a gradient between 80-95% for 20 mins, eluting two cross coupled products, **11** and **12** as separable diastereomers of unknown configurations as yellow oils (5.65 and 7.12 mg, 25%).

Diastereomer A (**11**), Isolated at 10.0 mins:

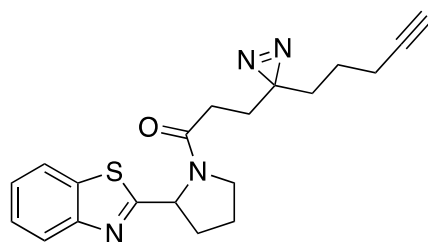
δ_{H} (500 MHz, CDCl_3) 7.91 (1H, d, J 8.5, 5-H), 7.69 (1H br. s, 3-H), 7.47 (1H, m, 6-H), 7.37 (1H, m, 7-H), 5.69 (1H, br. s, morph₂ or 4 3-H), 5.29 (1H, br. s, morph₂ or 4 2-H_a) 4.92 (1H, br. s, morph₂ or 4 2-H_a), 4.29 (1H, br. d, J 12.0, morph₂ or 4 3-H) 4.04 (1H, dd, J 12.0, 4.2, morph₂ or 4 6-H_a), 3.91 (3H, m, morph₂ and 4 2-H_b and morph₂ or 4 6-H_a), 3.82 (2H, appt br. d, J 12.9, morph₂ and 4 6-H_b), 3.62 (2H, m, morph₂ and 4 5-H_a) 3.38 (2H, br. m, morph₂ and 4 5-H_b), 1.56 (18H, s, morph₂ and 4 *t*Bu 2-H_{3min}). δ_{C} (125 MHz, CDCl_3) 159.6 (morph₂ or 4 C=O), 157.6 (morph₂ or 4 C=O), 154.7 (1C, d, J 139.0, 8-C), 139.1 (4a- or 8a-C), 127.2 (4a- or 8a-C), 126.3 (6-C), 126.2 (2- or 4-C), 119.2 (5-C), 113.6 (2-C), 113.5 (2- or 4-C), 81.1 and 80.6 (^tBu C₁), 69.4 (morph 2-C), 69.1 (morph 6-C), 67.1 (morph 3-C), 66.8 (morph 5-C), 28.4 (^tBu C₃). δ_{F} (375 MHz, CDCl_3) -123.4. ν_{max} (neat)/ cm^{-1} 2975, 2930,

2859, 1696, 1404, 1366. HRMS (ESI) $C_{27}H_{36}FN_3O_6$ requires $[M+H]^+$, calculated 518.2666, found 518.2688.

Diastereomer B (12), Isolated at 10.5 mins:

δ_H (500 MHz, $CDCl_3$) 7.96 (1H, d, J 8.5, 5-H), 7.80 (1H br. s, 3-H), 7.46 (1H, m, 6-H), 7.37 (1H, m, 7-H), 5.71 (1H, br. s, morph₂ or 4 3-H), 5.30 (1H, br. s, morph₂ or 4 2-H_a) 4.90 (1H, br. s, morph₂ or 4 2-H_a), 4.26 (1H, br. d, J 12.0, morph₂ or 4 3-H) 4.03 (1H, dd, J 12.0, 4.2, morph₂ or 4 6-H_a), 3.92 (3H, m, morph₂ and 4 2-H_b and morph₂ or 4 6-H_a), 3.82 (2H, appt br. m, morph₂ and 4 6-H_b), 3.62 (2H, m, morph₂ and 4 5-H_a) 3.22 (2H, br. m, morph₂ and 4 5-H_b), 1.56 (18H, s, morph₂ and 4 tBu 2-H_{3min}). δ_C (125 MHz, $CDCl_3$) 159.6 (morph₂ or 4 C=O), 157.6 (morph₂ or 4 C=O), 154.6 (1C, d, J 138.0, 8-C), 139.0 (4a- or 8a-C), 127.3 (4a- or 8a-C), 126.2 (6-C), 126.1 (2- or 4-C), 119.3 (5-C), 113.6 (2-C), 113.4 (2- or 4-C), 81.2 and 80.6 (^tBu C₁), 69.4 (morph 2-C), 69.1 (morph 6-C), 67.2 (morph 3-C), 66.9 (morph 5-C), 28.5 (^tBu C_{3min}). δ_F (375 MHz, $CDCl_3$) -123.6. ν_{max} (neat)/ cm^{-1} 2975, 2928, 2857, 1693, 1406, 1366. HRMS (ESI) $C_{27}H_{36}FN_3O_6$ requires $[M+H]^+$, calculated 518.2666, found 518.2693.

2-[N-(4-(4H-dizirin-4-yl)non-8-ynamide)-pyrrolidin-2-yl]-1,3-benzothiazole



T-1 Probe

A deprotection of 2-(*N*-Boc-pyrrolidin-2-yl)-1,3-benzothiazole, **T-1**, (40.0 mg, 0.13 mmol) was carried out using TFA (20% in DCM), stirring for 2 hours at room temperature. The solution was concentrated *in vacuo* to remove excess TFA, before resuspending in DMF (10 mL) and cooling to 0 °C and stirred. To this 4-(4H-dizirin-4-yl)non-8-ynoic acid (17.0 mg, 0.11) was added along with the coupling agents EDC (20.0 mg, 0.13 mmol) and HOBT (15.0 mg, 0.11 mmol). Triethylamine (31 μ L, 0.22 mmol) was added slowly and the reaction stirred for 1 hour, before warming to room temperature overnight. The mixture was concentrated *in vacuo*, dissolved in acetonitrile, and purified via Mass-Directed HPLC with acetonitrile to water as a gradient of 35-95% over a 15 mins, the eluted samples collected at 9.0 mins, and were lyophilised to give the **T-1 probe** as a pale-yellow oil (10.88 mg, 23%, 65:35 mixture of rotamers). δ_{H} (500 MHz, CDCl_3) 8.03 (1H, appt d, J 8.2, 7- H_{min}), 7.96 (1H, appt d, J 8.2, 7- H_{maj}), 7.90 (1H, appt d, J 8.5, 7.5 4- H_{min}), 7.81 (1H, appt d, J 8.5, 7.5 4- H_{maj}), 7.62 (1H, dt, J 7.2, 1.3, 6- H_{min}), 7.45-7.40 (1H, m, 6- H_{maj} and 5- H_{min}), 7.34 (1H, dt, J 7.2, 1.3, 5- H_{maj}), 5.65 (1H, dd, J 8.0, 2.1, pyrrolidinyl 2- H_{maj}), 5.40 (1H, dd, J 8.0, 2.1, pyrrolidinyl 2- H_{min}), 3.93-3.61 (2H, m, pyrrolidinyl 5- H_2), 2.55-2.31 (2H, m, pyrrolidinyl 3- H_2), 2.22-2.02 (8H, m, pyrrolidinyl 4- H_2 , non 2- and 3- $\text{H}_{2\text{maj}}$, non 7- H_2), 1.93 (1H, t, J 2.7, non 9- H_{min}), 1.86 (1H, t, J 2.7, non 9- H_{min}), 1.82-1.66 (4H, m, non 2- and 3- $\text{H}_{2\text{min}}$), 1.56-1.53 (2H, m, non 5- $\text{H}_{2\text{maj}}$), 1.42-1.39 (2H, m, non 5- $\text{H}_{2\text{min}}$), 1.34 (2H, p, J 7.5, non 6- $\text{H}_{2\text{maj}}$), 1.31 (2H, p, J 7.5, non 6- $\text{H}_{2\text{min}}$). δ_{C} (125 MHz, CDCl_3) 174.4 (non C=O $_{\text{min}}$), 173.8 (non C=O $_{\text{min}}$), 171.1 (2- C_{min}), 170.7 (2- C_{maj}), 153.7 (7a- C_{min}), 153.5 (7a- C_{min}), 135.1 (3a- C_{maj}), 134.8 (3a- C_{min}), 126.6 (6- C_{min}), 126.0 (6- C_{maj}), 125.6 (5- C_{min}), 125.0 (5- C_{maj}), 123.3 (7- C_{min}), 123.1 (7- C_{maj}), 122.0 (4- C_{min}), 121.2 (7- C_{maj}), 83.4 (non 8- C_{maj}), 83.5 (non 8- C_{min}), 69.1 (non 9- C_{maj}), 69.0 (non 9- C_{min}), 60.4 (pyrrolidinyl 2- C_{min}), 59.2 (pyrrolidinyl 2- C_{maj}), 47.3 (pyrrolidinyl 5- C_{maj}), 47.0 (pyrrolidinyl 5- C_{min}), 35.1 (pyrrolidinyl 3- C_{min}), 32.1 (pyrrolidinyl 3- C_{maj}), 32.0 (non 5- C_{maj}), 31.9 (non 5- C_{min}), 28.8 (non 2- C_{min}), 28.7 (non 2- C_{maj}), 28.2 (non 3- C_{min}),

28.1 (non 3-C_{maj}), 28.1 (4-C_{min}), 27.7 (4-C_{maj}), 24.5 (pyrrolidinyl 4-C_{maj}), 22.9 (non 6-C_{maj}), 22.8 (non 6-C_{min}), 22.4 (pyrrolidinyl 4- C_{min}), 18.0 (non 7-C_{maj}), 17.9 (non 7-C_{min}).
v_{max} (neat)/cm⁻¹ 3023, 2945, 1684, 1583,1470, 1458, 1432. HRMS (ESI) C₂₀H₂₂N₄OS requires [M+Na]⁺, calculated 367.1593, found 367.1595.

References

- 1 CDC, Parasites - About Parasites, <https://www.cdc.gov/parasites/about.html>, (accessed 4 February 2019).
- 2 D. G. Baker, *Lab. Rat*, 2006, 453–478.
- 3 D. C. Bartholomeu, S. M. R. Teixeira and N. M. A. El-Sayed, *Am. Trypanos. Chagas Dis.*, 2017, 429–454.
- 4 D. T. John, W. A. Petri, E. K. Markell, M. Voge and E. K. Markell, *Medical Parasitology*, Saunders Elsevier, 7th Edition., 2006.
- 5 L. Peacock, C. Kay, M. Bailey and W. Gibson, *PLoS Pathog.*, 2018, **14**, e1007043.
- 6 NA, Human African trypanosomiasis, https://www.who.int/trypanosomiasis_african/en/, (accessed 5 February 2019).
- 7 NA, Chagas disease (American trypanosomiasis), <https://www.who.int/chagas/en/>, (accessed 5 February 2019).
- 8 H. M. James, D. M., Gilles, *Human Anti Parasitic Drugs: Pharmacology and Usage*, John Wiley & Sons, Ltd, 1985.
- 9 CDC, African Trypanosomiasis, <https://www.cdc.gov/parasites/sleepingsickness/>, (accessed 5 February 2019).
- 10 W. H. Organization, *Sustaining the Drive to Overcome the Global Impact of Neglected Tropical Diseases : Second WHO Report on Neglected Tropical Diseases.*, World Health Organization, 2013.
- 11 J. Lukes, Trypanosomatida, <http://tolweb.org/Trypanosomatida/98015>, (accessed 5 February 2019).
- 12 J. Lukes, I. L. Mauricio, G. Schönian, J.-C. Dujardin, K. Soteriadou, J.-P. Dedet, K. Kuhls, K. W. Q. Tintaya, M. Jirků, E. Chocholová, C. Haralambous, F. Pratlong, M. Oborník, A. Horák, F. J. Ayala and M. A. Miles, *Proc. Natl. Acad. Sci. U. S. A.*, 2007, **104**, 9375–80.
- 13 M. P. Barrett, D. W. Boykin, R. Brun and R. R. Tidwell, *Br. J. Pharmacol.*, 2007, **152**, 1155–1171.
- 14 N. Baker, H. P. de Koning, P. Mäser and D. Horn, *Trends Parasitol.*, 2013, **29**, 110–118.
- 15 A. Y. Sokolova, S. Wyllie, S. Patterson, S. L. Oza, K. D. Read and A. H. Fairlamb, *Antimicrob. Agents Chemother.*, 2010, **54**, 2893–2900.
- 16 G. Eperon, M. Balasegaram, J. Potet, C. Mowbray, O. Valverde and F. Chappuis, *Expert Rev. Anti. Infect. Ther.*, 2014, **12**, 1407–1417.
- 17 T. Burki, *Lancet Infect. Dis.*, 2019, **19**, 30–31.

- 18 M. P. Pollastri, *Trends Parasitol.*, 2018, **34**, 178–179.
- 19 E. Torreale, B. B. Trunz, D. Tweats, M. Kaiser, R. Brun, G. Mazué, M. A. Bray and B. Pécoul, *PLoS Negl. Trop. Dis.*, 2010, **4**, 1–15.
- 20 V. K. B. K. Mesu, W. M. Kalonji, C. Bardonneau, O. V. Mordt, S. Blesson, F. Simon, S. Delhomme, S. Bernhard, W. Kuziena, J. P. F. Lubaki, S. L. Vuvu, P. N. Ngima, H. M. Mbembo, M. Ilunga, A. K. Bonama, J. A. Heradi, J. L. L. Solomo, G. Mandula, L. K. Badibabi, F. R. Dama, P. K. Lukula, D. N. Tete, C. Lumbala, B. Scherrer, N. Strub-Wourgaft and A. Tarral, *Lancet*, 2018, **391**, 144–154.
- 21 H. Burrell-Saward, A. J. Harris, R. de LaFlor, H. Sallam, M. S. Alavijeh, T. H. Ward and S. L. Croft, *Int. J. Antimicrob. Agents*, 2017, **50**, 203–209.
- 22 NA, Sleeping sickness elimination progresses in 2021 despite COVID-19, <https://www.who.int/news/item/30-05-2022-sleeping-sickness-elimination-progresses-in-2021-despite-covid-19>, (accessed 21 March 2023).
- 23 R. Diaz, S. A. Luengo-Arratta, J. D. Seixas, E. Amata, W. Devine, C. Cordon-Obras, D. I. Rojas-Barros, E. Jimenez, F. Ortega, S. Crouch, G. Colmenarejo, J. M. Fiandor, J. J. Martin, M. Berlanga, S. Gonzalez, P. Manzano, M. Navarro and M. P. Pollastri, *PLoS Negl. Trop. Dis.*, 2014, **8**, e3253.
- 24 A. Woodland, S. Thompson, L. A. T. Cleghorn, N. Norcross, M. De Rycker, R. Grimaldi, I. Hallyburton, B. Rao, S. Norval, L. Stojanovski, R. Brun, M. Kaiser, J. A. Frearson, D. W. Gray, P. G. Wyatt, K. D. Read and I. H. Gilbert, *ChemMedChem*, 2015, **10**, 1809–1820.
- 25 E. R. Sharlow, T. A. Lyda, H. C. Dodson, G. Mustata, M. T. Morris, S. S. Leimgruber, K.-H. Lee, Y. Kashiwada, D. Close, J. S. Lazo and J. C. Morris, *PLoS Negl. Trop. Dis.*, 2010, **4**, e659.
- 26 I. H. Gilbert, *Parasitology*, 2014, **141**, 28–36.
- 27 I. H. Gilbert, *J. Med. Chem.*, 2013, **56**, 7719–7726.
- 28 D. C. Swinney, *Clin. Pharmacol. Ther.*, 2013, **93**, 299–301.
- 29 R. M. Reguera, E. Calvo-Álvarez, R. Álvarez-Velilla and R. Balaña-Fouce, *Int. J. Parasitol. Drugs Drug Resist.*, 2014, **4**, 355.
- 30 R. C. Mohs and N. H. Greig, *Alzheimer's Dement. Transl. Res. Clin. Interv.*, 2017, **3**, 651–657.
- 31 D. G. Brown and H. J. Wobst, *J. Med. Chem.*, 2019.
- 32 F. S. Buckner, A. Buchynskyy, P. Nagendar, D. A. Patrick, J. Robert Gillespie, Z. Herbst, R. R. Tidwell and M. H. Gelb, 2020, **5**, 1–18.
- 33 H. Kakeya, *Nat. Prod. Rep.*, 2016, **33**, 648–654.

- 34 N. Aulner, A. Danckaert, J. E. Ihm, D. Shum and S. L. Shorte, *Trends Parasitol.*, 2019, 35, 559–570.
- 35 S. Wyllie, M. Thomas, S. Patterson, S. Crouch, M. De Rycker, R. Lowe, S. Gresham, M. D. Urbaniak, T. D. Otto, L. Stojanovski, F. R. C. Simeons, S. Manthri, L. M. MacLean, F. Zuccotto, N. Homeyer, H. Pflaumer, M. Boesche, L. Sastry, P. Connolly, S. Albrecht, M. Berriman, G. Drewes, D. W. Gray, S. Ghidelli-Disse, S. Dixon, J. M. Fiandor, P. G. Wyatt, M. A. J. Ferguson, A. H. Fairlamb, T. J. Miles, K. D. Read and I. H. Gilbert, *Nature*, 2018, **560**, 192–197.
- 36 M. H. Wright and S. A. Sieber, *Nat. Prod. Rep.*, 2016, 33, 681–708.
- 37 J. L. Siqueira-Neto, O. R. Song, H. Oh, J. H. Sohn, G. Yang, J. Nam, J. Jang, J. Cechetto, C. B. Lee, S. Moon, A. Genovesio, E. Chatelain, T. Christophe and L. H. Freitas-Junior, *PLoS Negl. Trop. Dis.*, 2010, **4**, e675.
- 38 J. L. Siqueira-Neto, S. Moon, J. Jang, G. Yang, C. Lee, H. K. Moon, E. Chatelain, A. Genovesio, J. Cechetto and L. H. Freitas-Junior, *PLoS Negl. Trop. Dis.*, 2012, **6**, e1671.
- 39 J. Müller and A. Hemphill, *New Approaches for the Identification of Drug Targets in Protozoan Parasites*, Academic Press, 2013.
- 40 T. W. J. Cooper, I. B. Campbell and S. J. F. Macdonald, *Angew. Chemie Int. Ed.*, 2010, **49**, 8082–8091.
- 41 J. Dong, Q. Xia, X. Lv, C. Yan, H. Song, Y. Liu and Q. Wang, *Org. Lett.*, 2018, **20**, 5661–5665.
- 42 J. P. Hughes, S. S. Rees, S. B. Kalindjian and K. L. Philpott, *Principles of early drug discovery*, Wiley-Blackwell, 2011, vol. 162.
- 43 A. Nadin, C. Hattotuwigama and I. Churcher, *Angew. Chemie - Int. Ed.*, 2012, **51**, 1114–1122.
- 44 S. D. Roughley and A. M. Jordan, *J. Med. Chem.*, 2011, **54**, 3451–3479.
- 45 G. Karageorgis, S. Warriner and A. Nelson, *Nat. Chem.*, 2014, **6**, 872–876.
- 46 K. M. Backus, B. E. Correia, K. M. Lum, S. Forli, B. D. Horning, G. E. González-Páez, S. Chatterjee, B. R. Lanning, J. R. Teijaro, A. J. Olson, D. W. Wolan and B. F. Cravatt, 2016, **534**, 570–574.
- 47 A. Keeley, L. Petri, P. Ábrányi-Balogh and G. M. Keserű, *Drug Discov. Today*, 2020, **25**, 983–996.
- 48 E. Resnick, A. Bradley, J. Gan, A. Douangamath, T. Krojer, R. Sethi, P. P. Geurink, A. Aimon, G. Amitai, D. Bellini, J. Bennett, M. Fairhead, O. Fedorov, R. Gabizon, J. Gan, J. Guo, A. Plotnikov, N. Reznik, G. F. Ruda, L. Díaz-Sáez, V. M.

- Straub, T. Szommer, S. Velupillai, D. Zaidman, Y. Zhang, A. R. Coker, C. G. Dowson, H. M. Barr, C. Wang, K. V. M. Huber, P. E. Brennan, H. Ovaa, F. Von Delft and N. London, *J. Am. Chem. Soc.*, 2019, **141**, 8951–8968.
- 49 R. Grainger, T. D. Heightman, S. V. Ley, F. Lima and C. N. Johnson, *Chem. Sci.*, 2019, **10**, 2264–2271.
- 50 C. Remeur, C. B. Kelly, N. R. Patel and G. A. Molander, *ACS Catal.*, 2017, **7**, 6065–6069.
- 51 Z. Li and C. J. Li, *J. Am. Chem. Soc.*, 2005, **127**, 6968–6969.
- 52 F. D. Lewis and T. Ho, *Am. Chem. Soc.*, 1980, **102**, 1751–1752.
- 53 J. Singh, R. C. Petter, T. A. Baillie and A. Whitty, *Nat. Rev. Drug Discov.*, 2011, **10**, 307–317.
- 54 D. S. Johnson, E. Weerapana and B. F. Cravatt, *Future Med. Chem.*, 2010, **2**, 949–964.
- 55 M. H. Potashman and M. E. Duggan, *J. Med. Chem.*, 2009, **52**, 1231–1246.
- 56 R. Lagoutte, R. Patouret and N. Winssinger, *Curr. Opin. Chem. Biol.*, 2017, **39**, 54–63.
- 57 J. G. Robertson, *Biochemistry*, 2005, **44**, 5561–5571.
- 58 R. R. Yocum, D. J. Waxman, J. R. Rasmussen and J. L. Strominger, *Proc. Natl. Acad. Sci. U. S. A.*, 1979, **76**, 2730–2734.
- 59 J. R. Vane and R. M. Botting, in *Thrombosis Research*, Elsevier Ltd, 2003, vol. 110, pp. 255–258.
- 60 S. Parmar, K. Patel and J. Pinilla-Ibarz, *P T*, 2014, **39**, 483.
- 61 Enzymes Can Be Inhibited by Specific Molecules - Biochemistry - NCBI Bookshelf, <https://www.ncbi.nlm.nih.gov/books/NBK22530/>, (accessed 23 April 2020).
- 62 C. C. Wang, *J. Cell. Biochem.*, 1991, **45**, 49–53.
- 63 R. Poulin, L. Lu, B. Ackermann, P. Bey and A. E. Pegg, *J. Biol. Chem.*, 1992, **267**, 150–158.
- 64 N. V. Grishin, A. L. Osterman, H. B. Brooks, M. A. Phillips and E. J. Goldsmith, *Biochemistry*, 1999, **38**, 15174–15184.
- 65 I. M. Serafimova, M. A. Pufall, S. Krishnan, K. Duda, M. S. Cohen, R. L. Maglathlin, J. M. McFarland, R. M. Miller, M. Frödin and J. Taunton, *Nat. Chem. Biol.*, 2012, **8**, 471–476.
- 66 Z. Zhao and P. E. Bourne, *Drug Discov. Today*, 2018, **23**, 727–735.
- 67 E. H. Krenske, R. C. Petter and K. N. Houk, *J. Org. Chem.*, 2016, **2016**, 11726–

- 11733.
- 68 C. G. Jakob, A. K. Upadhyay, P. L. Donner, E. Nicholl, S. N. Addo, W. Qiu, C. Ling, S. M. Gopalakrishnan, M. Torrent, S. P. Cepa, J. Shanley, A. R. Shoemaker, C. C. Sun, A. Vasudevan, K. R. Woller, J. Brad Shotwell, B. Shaw, Z. Bian and J. E. Hutti, *J. Med. Chem.*, 2018, **61**, 6647–6657.
- 69 J. K. Eaton, L. Furst, L. L. Cai, V. S. Viswanathan and S. L. Schreiber, *Bioorg. Med. Chem. Lett.*, 2020, **30**, 127538.
- 70 M. G. Quesne, R. A. Ward and S. P. de Visser, *Front. Chem.*, 2013, **1**, 39.
- 71 A. Hinman, H. H. Chuang, D. M. Bautista and D. Julius, *Proc. Natl. Acad. Sci. U. S. A.*, 2006, **103**, 19564–19568.
- 72 J. C. Powers, J. L. Asgian, O. Zlem Dogan, D. Ekici and K. E. James, *Chem. Rev.*, 2002, **102**, 4639–4750.
- 73 D. Greenbaum, K. F. Medzihradzky, A. Burlingame and M. Bogyo, *Chem. Biol.*, 2000, **7**, 569–581.
- 74 L. A. Crawford and E. Weerapana, *Mol. Biosyst.*, 2016, **12**, 1768–1771.
- 75 K. X. Chen, C. A. Lesburg, B. Vibulbhan, W. Yang, T. Y. Chan, S. Venkatraman, F. Velazquez, Q. Zeng, F. Bennett, G. N. Anilkumar, J. Duca, Y. Jiang, P. Pinto, L. Wang, Y. Huang, O. Selyutin, S. Gavalas, H. Pu, S. Agrawal, B. Feld, H. C. Huang, C. Li, K. C. Cheng, N. Y. Shih, J. A. Kozlowski, S. B. Rosenblum and F. G. Njoroge, *J. Med. Chem.*, 2012, **55**, 2089–2101.
- 76 W. Chen, J. Dong, L. Plate, D. E. Mortenson, G. J. Brighty, S. Li, Y. Liu, A. Galmozzi, P. S. Lee, J. J. Hulce, B. F. Cravatt, E. Saez, E. T. Powers, I. A. Wilson, K. B. Sharpless and J. W. Kelly, *J. Am. Chem. Soc.*, 2016, **138**, 7353–7364.
- 77 D. E. Mortenson, G. J. Brighty, L. Plate, G. Bare, W. Chen, S. Li, H. Wang, B. F. Cravatt, S. Forli, E. T. Powers, K. B. Sharpless, I. A. Wilson and J. W. Kelly, *J. Am. Chem. Soc.*, 2018, **140**, 200–210.
- 78 A. Narayanan and L. H. Jones, *Chem. Sci.*, 2015, **6**, 2650–2659.
- 79 M. Gehringer and S. A. Laufer, *J. Med. Chem.*, 2019, **62**, 5673–5724.
- 80 S. Sommer, N. D. Weikart, U. Linne and H. D. Mootz, *Bioorganic Med. Chem.*, 2013, **21**, 2511–2517.
- 81 R. M. Lopachin and T. Gavin, *Chem. Res. Toxicol.*, 2014, **27**, 1081–1091.
- 82 M. H. Larraufie, W. S. Yang, E. Jiang, A. G. Thomas, B. S. Slusher and B. R. Stockwell, *Bioorganic Med. Chem. Lett.*, 2015, **25**, 4787–4792.
- 83 D. A. Erlanson, A. C. Braisted, D. R. Raphael, M. Randal, R. M. Stroud, E. M. Gordon and J. A. Wells, *Proc. Natl. Acad. Sci. U. S. A.*, 2000, **97**, 9367–9372.

- 84 Y. Liu, Z. Xie, D. Zhao, J. Zhu, F. Mao, S. Tang, H. Xu, C. Luo, M. Geng, M. Huang and J. Li, *J. Med. Chem.*, 2017, **60**, 2227–2244.
- 85 D. J. Augeri, J. A. Robl, D. A. Betebenner, D. R. Magnin, A. Khanna, J. G. Robertson, A. Wang, L. M. Simpkins, P. Taunk, Q. Huang, S.-P. Han, B. Abboa-Offei, M. Cap, L. Xin, L. Tao, E. Tozzo, G. E. Welzel, D. M. Egan, J. Marcinkeviciene, S. Y. Chang, S. A. Biller, M. S. Kirby, R. A. Parker and L. G. Hamann, *J. Am. Chem. Soc.*, 2005, **48**, 5025–5037.
- 86 V. Bonatto, R. F. Lameiro, F. R. Rocho, J. Lameira, A. Leitão and C. A. Montanari, *RSC Med. Chem.*, 2023, **2023**, 201–217.
- 87 S. Ray, D. F. Kreitler, A. M. Gulick and A. S. Murkin, *ACS Chem. Biol.*, 2018, **13**, 56.
- 88 P. Martín-Gago, E. K. Fansa, M. Winzker, S. Murarka, P. Janning, C. Schultz-Fademrecht, M. Baumann, A. Wittinghofer and H. Waldmann, *Cell Chem. Biol.*, 2017, **24**, 589-597.e5.
- 89 G. Palermo, D. Branduardi, M. Masetti, A. Lodola, M. Mor, D. Piomelli, A. Cavalli and M. De Vivo, *J. Med. Chem.*, 2011, **54**, 6612–6623.
- 90 A. Buvailo, New Opportunities In Covalent Inhibition: Targeting Lysine - Blog - Enamine, <https://enamine.net/en-blog/new-opportunities-in-covalent-inhibition-targeting-lysine>, (accessed 16 July 2020).
- 91 P. Cal, J. Vicente, E. Pires, A. Coelho, L. Veiros, C. Cordeiro and P. Gois, *J. Am. Chem. Soc.*, 2012, **134**, 10299–10305.
- 92 J. Adams and M. Kauffman, *Cancer Invest.*, 2004, **22**, 304–311.
- 93 U. P. Dahal, A. M. Gilbert, R. S. Obach, M. E. Flanagan, J. M. Chen, C. Garcia-Irizarry, J. T. Starr, B. Schuff, D. P. Uccello and J. A. Young, *Cite this Med. Chem. Commun.*, 2014, **7**, 864.
- 94 S. Lin, X. Yang, S. Jia, A. M. Weeks, M. Hornsby, P. S. Lee, R. V. Nichiporuk, A. T. Iavarone, J. A. Wells, F. D. Toste and C. J. Chang, *Science (80-.)*, 2017, **355**, 597–602.
- 95 G. Nicola, J. Tomberg, R. F. Pratt, R. A. Nicholas and C. Davies, *Biochemistry*, 2010, **49**, 8094–8104.
- 96 R. L. Tennyson, G. S. Cortez, H. J. Galicia, C. R. Kreiman, C. M. Thompson and D. Romo, *J. Am. Chem. Soc.*, 1999, **121**, 1731–1736.
- 97 C. Wang, D. Abegg, B. G. Dwyer and A. Adibekian, *ChemBioChem*, 2019, **20**, 2212–2216.
- 98 T. E. J. Chavas, M. J. Fuchter and P. A. Dimaggio, *ACS Chem. Biol.*, 2018, **13**,

- 2897–2907.
- 99 P. R. A. Zanon, F. Yu, P. Z. Musacchio, L. Lewald, M. Zollo, K. Krauskopf, D. Mrdović, P. Raunft, T. E. Maher, M. Cigler, C. J. Chang, K. Lang, F. D. Toste, A. I. Nesvizhskii and S. M. Hacker, .
- 100 R. Lonsdale and R. A. Ward, *Chem. Soc. Rev.*, 2018, **47**, 3816–3830.
- 101 T. K. Smith, A. Crossman, J. S. Brimacombe and M. A. J. Ferguson, 2004, **23**, 4701–4708.
- 102 J. S. Brimacombe, S. Cottaz, R. A. Field, S. W. Homans, M. J. McConville, A. Mehlert, K. G. Milne, J. E. Ralton, Y. A. Roy, P. Schneider and N. Zitzmann, *Parasitology*, 1994, **108**, 45–54.
- 103 M. L. S. Güther and M. A. J. Ferguson, *EMBO J.*, 1995, **14**, 3080–3093.
- 104 K. E. Gilbert, A. Vuorinen, A. Aatkar, P. Pogány, J. Pettinger, E. K. Grant, J. M. Kirkpatrick, K. Rittinger, D. House, G. A. Burley and J. T. Bush, *ACS Chem. Biol.*, 2023, **18**, 285–295.
- 105 D. A. Shannon, C. Gu, C. J. Mclaughlin, M. Kaiser, R. A. L. van der Hoorn and E. Weerapana, *ChemBioChem*, 2012, **13**, 2327–2330.
- 106 K. S. Yang, S. Z. Leeuwon, S. Xu and W. R. Liu, *J. Med. Chem.*, 2022, **65**, 8686–8698.
- 107 A. Bandyopadhyay and J. Gao, *Curr. Opin. Chem. Biol.*, 2016, **34**, 110–116.
- 108 W. J. Metzler, J. Yanchunas, C. Weigelt, K. Kish, H. E. Klei, D. Xie, Y. Zhang, M. Corbett, J. K. Tamura, B. He, L. G. Hamann, M. S. Kirby and J. Marcinkeviciene, *Protein Sci.*, 2008, **17**, 240–250.
- 109 C. D. O’Conner and R. B. Hames, *Proteomics*, Scion Publishing LTD, 2008.
- 110 R. Markus, M. H. Wright and E. W. Tate, *Parasitology*, 2018, **145**, 157–174.
- 111 S. V. Frye, *Nat. Chem. Biol.*, 2010, **6**, 159–161.
- 112 M. Fonović, *Mol. Cell. Proteomics*, 2007, **6**, 1761–1770.
- 113 K. A. Kalesh, D. S. B. Sim, J. Wang, K. Liu, Q. Lin and S. Q. Yao, *Chem. Commun.*, 2010, **46**, 1118–1120.
- 114 Y.-L. L. Hsu, C.-C. C. Yang, T.-C. C. Chou, C.-H. H. Tai, L.-Y. Y. Chen, S.-L. L. Fu, J.-J. J. Lin and L.-C. C. Lo, *Tetrahedron*, 2016, **72**, 58–68.
- 115 D. J. Lapinsky, *Bioorg. Med. Chem.*, 2012, **20**, 6237–6247.
- 116 E. Smith and I. Collins, *Future Med. Chem.*, 2015, **7**, 159–183.
- 117 C. Iacobucci, M. Gö, C. Piotrowski, C. Arlt, A. Rehkamp, C. Ihling, C. Hage and A. Sinz, *Anal. Chem.*, 2018, **10**, 21.
- 118 L. Dubinsky, B. P. Krom and M. M. Meijler, *Bioorg. Med. Chem.*, 2012, **20**, 554–

- 570.
- 119 G. D. Prestwich, G. Dormán, J. T. Elliott, D. M. Marecak and A. Chaudhary, *Photochem. Photobiol.*, 1997, **65**, 222–234.
- 120 G. W. Preston and A. J. Wilson, *Chem. Soc. Rev.*, 2013, **42**, 3289.
- 121 J. Brunner, S. H. Serin and F. M. Richards, *J. Biol. Chem.*, 1980, **255**, 3313–3318.
- 122 A. L. MacKinnon and J. Taunton, *Curr. Protoc. Chem. Biol.*, 2009, **1**, 55–73.
- 123 R. Neelarapu, D. L. Holzle, S. Velaparthi, H. Bai, M. Brunsteiner, S. Y. Blond and P. A. Petukhov, *J. Med. Chem.*, 2011, **54**, 4350–4364.
- 124 K. Lang and J. W. Chin, *ACS Chem. Biol.*, 2014, **9**, 16–20.
- 125 C. P. Ramil and Q. Lin, *Chem. Commun.*, 2013, **49**, 11007–22.
- 126 F. Himo, T. Lovell, R. Hilgraf, V. V. Rostovtsev, L. Noodleman, K. B. Sharpless and V. V. Fokin, *Am. Chem. Soc.*, 2005, **127**, 210–216.
- 127 M. L. Blackman, M. Royzen and J. M. Fox, *J. Am. Chem. Soc.*, 2008, **130**, 13518–13519.
- 128 F. L. Lin, H. M. Hoyt, H. Van Halbeek, R. G. Bergman, C. R. Bertozzi, H. van Halbeek, R. G. Bergman and C. R. Bertozzi, *J. Am. Chem. Soc.*, 2005, **127**, 2686–2695.
- 129 J. E. Hein and V. V. Fokin, *Chem. Soc. Rev.*, 2010, **39**, 1302.
- 130 A. Makarem, R. Berg and B. F. Straub, *Angew. Chem., Int. Ed*, 2015, **54**, 7431–7435.
- 131 J. Lehmann, M. H. Wright and S. A. Sieber, *Chem. - A Eur. J.*, 2016, **22**, 4666–4678.
- 132 L. Zhu, C. J. Brassard, X. Zhang, P. M. Guha and R. J. Clark, *Chem. Rec.*, 2016, **16**, 1501–1517.
- 133 Y. Zhang, B. R. Fonslow, B. Shan, M. C. Baek and J. R. Yates, *Chem. Rev.*, 2013, **113**, 2343.
- 134 B. Bogdanov and R. D. Smith, *Mass Spectrom. Rev.*, 2005, **24**, 168–200.
- 135 N. L. Kelleher, H. Y. Lin, G. A. Valaskovic, D. J. Aaserud, E. K. Fridriksson and F. W. McLafferty, *J. Am. Chem. Soc.*, 1999, **121**, 806–812.
- 136 J. D. Tipton, J. C. Tran, A. D. Catherman, D. R. Ahlf, K. R. Durbin and N. L. Kelleher, *J. Biol. Chem.*, 2011, **286**, 25451–25458.
- 137 L. A. Webster, M. Thomas, M. Urbaniak, S. Wyllie, H. Ong, M. Tinti, A. H. Fairlamb, M. Boesche, S. Ghidelli-Disse, G. Drewes and I. H. Gilbert, *ACS Infect. Dis.*, 2018, **4**, 1475–1486.
- 138 B. J. W. P., *Cancer Cell*, 2017, **32**, 9–25.

- 139 G. R. P. E, *Cell Chem. Biol.*, 2016, **23**, 10–17.
- 140 L. B. Tulloch, S. K. Menzies, A. L. Fraser, E. R. Gould, E. F. King, M. K. Zacharova, G. J. Florence and T. K. Smith, 2017, **11**, 5886.
- 141 E. L. Meredith, A. Kumar, A. Konno, J. Szular, S. Alsford, K. Seifert, D. Horn and S. R. Wilkinson, *Mol. Microbiol.*, 2017, **106**, 207–222.
- 142 T. L. Riss, R. A. Moravec, A. L. Niles, S. Duellman, H. A. Benink, T. J. Worzella and L. Minor, *Cell Viability Assays*, Eli Lilly & Company and the National Center for Advancing Translational Sciences, 2004.
- 143 S. H. Grimm, B. Gagestein, J. F. Keijzer, N. Liu, R. H. Wijdeven, E. B. Lenselink, A. W. Tuin, A. M. C. H. van den Nieuwendijk, G. J. P. van Westen, C. A. A. van Boeckel, H. S. Overkleeft, J. Neefjes and M. van der Stelt, *Bioorganic Med. Chem.*, 2019, **27**, 692–699.
- 144 J. Dong, L. Krasnova, M. G. Finn and K. Barry Sharpless, *Angew. Chemie - Int. Ed.*, 2014, **53**, 9430–9448.
- 145 H. J. Reich, Fluorine NMR,
<https://organicchemistrydata.org/hansreich/resources/nmr/?page=nmr-content%2F>, (accessed 30 July 2020).
- 146 J. Sloop, *Reports Org. Chem.*, 2013, **2013**, 1–12.
- 147 K. J. Padiya, S. Gavade, B. Kardile, M. Tiwari, S. Bajare, M. Mane, V. Gaware, S. Varghese, D. Harel and S. Kurhade, *Org. Lett.*, 2012, **14**, 2814–2817.
- 148 T. Nasr Allah, ne Savourey, J. ean-Claude Berthet, E. Nicolas and and Thibault Cantat, *Angew. Chemie*, 2019, **131**, 11000–11003.
- 149 C. R. Ganellin, P. B. Bishop, R. B. Bambal, S. M. T. T. Chan, B. Leblond, A. N. J. J. Moore, L. Zhao, P. Bourgeat, C. Rose, F. Vargas and J.-C. C. Schwartz, *J. Med. Chem.*, 2005, **48**, 7333–7342.
- 150 M. L. S. Güther, W. J. Masterson and M. A. J. Ferguson, *J. Biol. Chem.*, 1994, **269**, 18694–18701.
- 151 NA, Chemicalize - Instant Cheminformatics Solutions,
<https://chemicalize.com/welcome>, (accessed 3 November 2022).
- 152 L. H. Jones and J. W. Kelly, *RSC Med. Chem.*, 2020, **11**, 10.
- 153 BioRad, *DC Protein Assay Instruction Manual*, .
- 154 Y. Jung, N. Noda, J. Takaya, M. Abo, K. Toh, K. Tajiri, C. Cui, L. Zhou, S. I. Sato and M. Uesugi, *ACS Chem. Biol.*, 2022, **17**, 340–347.
- 155 Y. Liu, M. P. Patricelli and B. F. Cravatt, *Proc. Natl. Acad. Sci. U. S. A.*, 1999, **96**, 14694–14699.

- 156 E. W. McConnell, A. L. Smythers and L. M. Hicks, *J. Am. Soc. Mass Spectrom.*, 2020, **31**, 1697–1705.
- 157 M. K. Dennehy, K. A. M. Richards, G. R. Wernke, Y. Shyr and D. C. Liebler, *Chem. Res. Toxicol.*, 2006, **19**, 20–29.
- 158 H. L. Wong and D. C. Liebler, *Chem. Res. Toxicol.*, 2008, **21**, 796–804.
- 159 N. Sakai, R. Komatsu, N. Uchida, R. Ikeda and T. Konakahara, *Org. Lett.*, 2010, **12**, 1300–1303.
- 160 J. Hou, A. Ee, W. Feng, J. H. Xu, Y. Zhao and J. Wu, *J. Am. Chem. Soc.*, 2018, **140**, 5257–5263.
- 161 J. D. Bell and J. A. Murphy, *Chem. Soc. Rev.*, 2021, **50**, 9540–9685.
- 162 J. L. Reymond, *Acc. Chem. Res.*, 2015, **48**, 722–730.
- 163 G. J. Brighty, R. C. Botham, S. Li, L. Nelson, D. E. Mortenson, G. Li, C. Morisseau, H. Wang, B. D. Hammock, K. B. Sharpless and J. W. Kelly, *Nat. Chem.*, 2020, **12**, 906.
- 164 A. L. Borne, J. W. Brulet, K. Yuan and K. L. Hsu, *RSC Chem. Biol.*, 2021, **2**, 322–337.
- 165 F. Sutanto, S. Shaabani, C. G. Neochoritis, T. Zarganes-Tzitzikas, P. Patil, E. Ghonchepour and A. Dömling, *Sci. Adv.*, 2021, **7**, 9307–9318.
- 166 A. Galmozzi, E. Dominguez, B. F. Cravatt and E. Saez, *Methods Enzymol.*, 2014, **538**, 151.
- 167 J. Rayo, N. Amara, P. Krief and M. M. Meijler, *J. Am. Chem. Soc.*, 2011, **133**, 7469–7475.
- 168 Q. Zheng, J. Dong and K. B. Sharpless, *J. Org. Chem.*, 2016, **81**, 11360–11362.
- 169 C. Lee, N. D. Ball and G. M. Sammis, *Chem. Commun.*, 2019, **55**, 14753–14756.
- 170 M. Magre and J. Cornella, *J. Am. Chem. Soc.*, 2021, **143**, 21497–21502.
- 171 M. J. Girgis, L. E. Kuczynski, S. M. Berberena, C. A. Boyd, P. L. Kubinski, M. L. Scherholz, D. E. Drinkwater, X. Shen, S. Babiak and B. G. Lefebvre, *Org. Process Res. Dev.*, 2008, **12**, 1209–1217.
- 172 T. D. Aicher, R. C. Anderson, J. Gao, S. S. Shetty, G. M. Coppola, J. L. Stanton, D. C. Knorr, D. M. Sperbeck, L. J. Brand, C. C. Vinluan, E. L. Kaplan, C. J. Dragland, H. C. Tomaselli, A. Islam, R. J. Lozito, X. Liu, W. M. Maniara, W. S. Fillers, D. Delgrande, R. E. Walter and W. R. Mann, *J. Med. Chem.*, 2000, **43**, 236–249.
- 173 B. M. Trost and F. Miege, *J. Am. Chem. Soc.*, 2014, **136**, 3016–3019.
- 174 Y. Takahashi, R. Yoshii, T. Sato and N. Chida, *Org. Lett.*, 2018, **20**, 5705–5708.

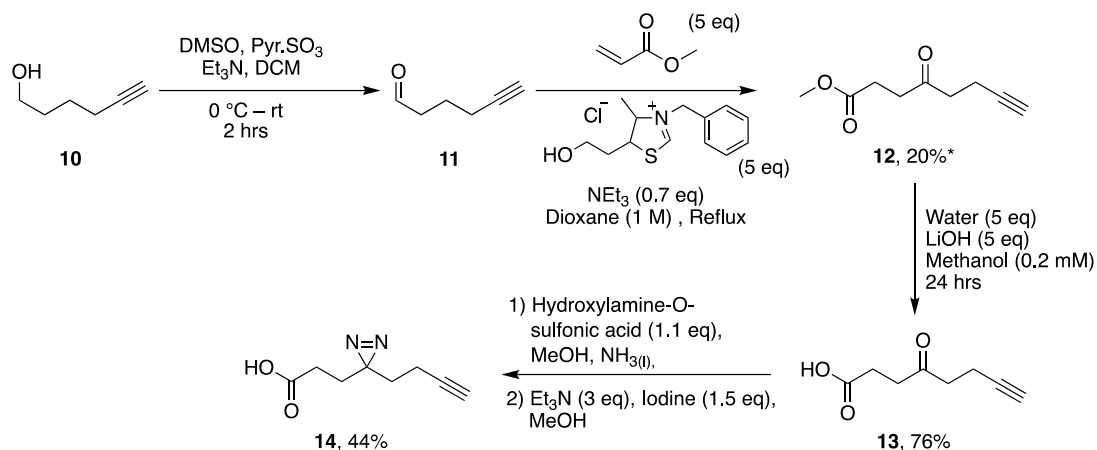
- 175 Z. Li, P. Hao, L. Li, C. Y. J. Tan, X. Cheng, G. Y. J. Chen, S. K. Sze, H. M. Shen, S. Q. Yao and P. D. S. Q. Y. Dr. Zhengqiu Li, Piliang Hao, Dr. Lin Li, Chelsea Y. J. Tan, Xiamin Cheng, Grace Y. J. Chen, Prof. Dr. Siu Kwan Sze, Prof. Dr. Han-Ming Shen, *Angew. Chemie - Int. Ed.*, 2013, **52**, 8551–8556.
- 176 P. Kleiner, W. Heydenreuter, M. Stahl, V. S. Korotkov, S. A. Sieber and P. D. S. A. S. M. Sc. Philipp Kleiner, Dr. Wolfgang Heydenreuter, M. Sc. Matthias Stahl, Dr. Vadim S. Korotkov, *Angew. Chemie - Int. Ed.*, 2016, **56**, 1396–1401.
- 177 D. Ma and X. Lu, *Tetrahedron*, 1990, **46**, 6319–6330.

Appendices

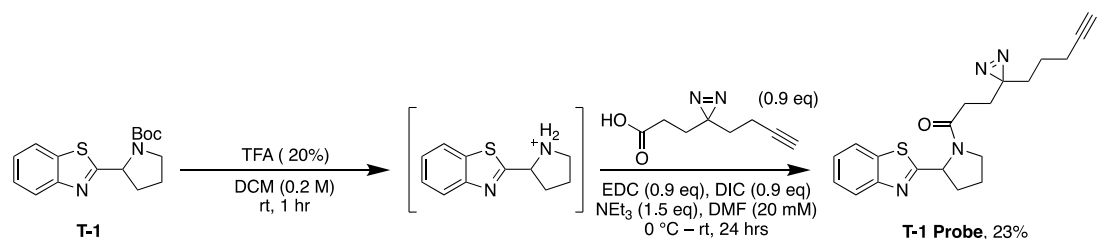
Appendix A

Design and Synthesis of a Photoaffinity-Based Probe: Previous work within the group by Dr Gomm and Dr Griggs led to the discovery of several potent anti-trypanosomal compounds when screened against *T. brucei brucei* (**Figure 1.9**). An investigation to identify these compounds mode of action was initiated by synthesising photoaffinity probe analogues of these active compounds.

Initially, a ‘minimalist terminal alkyne-diazirine’ linker was synthesised, previously reported by *Li et al*^{1,2}, the protocol was optimised for use in house, working with volatile chemicals.



Due to the ease of synthesis and time constraints a photoaffinity probe was synthesised based around the compound **01**, later referred to in this work as **T-1**. **T-1 Probe** was synthesised by direct modification of the parent compound as previously utilised in probe synthesis (**3.3.1**). initially deprotecting the Boc-amine using TFA (20% in DCM), before an amide coupling using EDC and DIC to append the diazirine-alkyne linker.

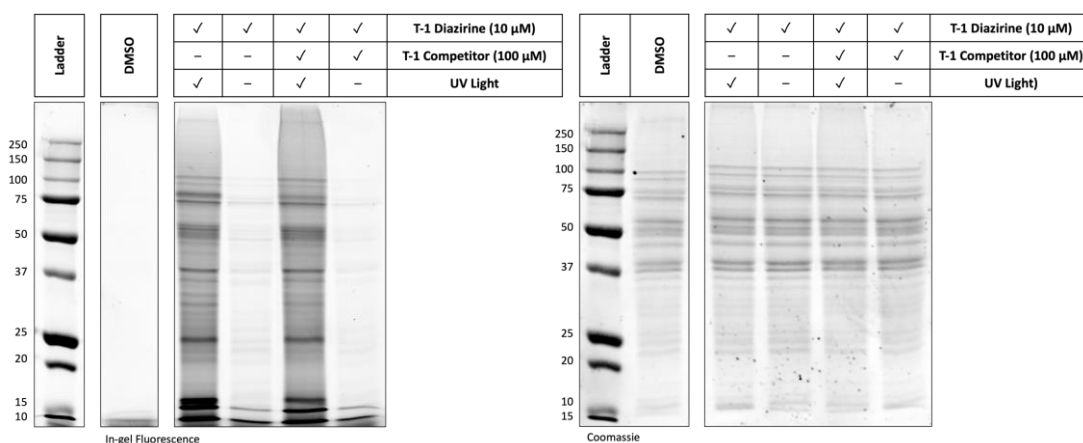


¹ *Angew. Chemie - Int. Ed.*, 2013, **52**, 8551–8556.

² *Angew. Chemie - Int. Ed.*, 2016, **56**, 1396–1401.

The probe is currently being screened in St. Andrews to test for anti-trypanosomal activity, aiming to retain the toxicity seen from the parent compound. The probe can then be used to explore the protein targets of the active compound by incubation with cell lysate and enrichment with a biotin tag to identify the proteins by MS/MS.

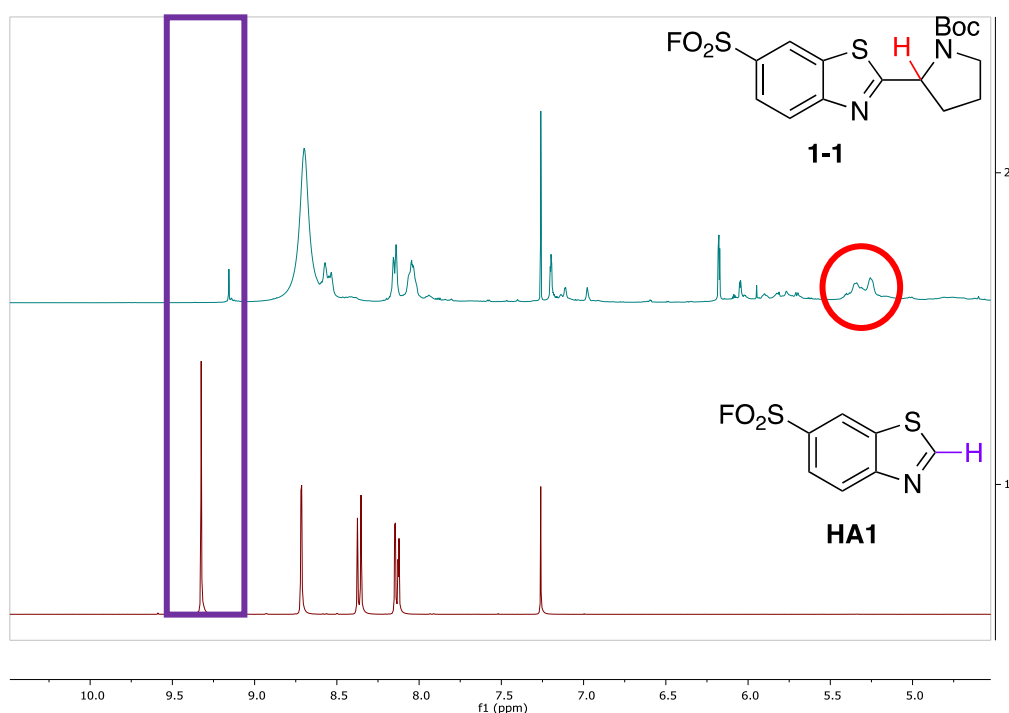
The reactive profile of **T-1 Probe** was explored by in-gel fluorescence incubating with *T. brucei brucei* lysate and attaching a rhodamine fluorophore. This probe shows broad labelling across the *T. brucei* proteome under these conditions. There was also no observed competition when pre-incubating with the parent compound **T-1**.



Appendix B

Determining Reaction Success: A workflow to screen these photoredox reactions for success was necessary to streamline library generation, with the limiting factor being purification of all reactions. The reactions were screened for intermolecular product formation by fluorine and proton NMR and LC-MS to determine which reactions should be purified.

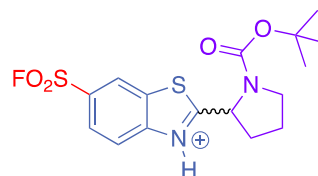
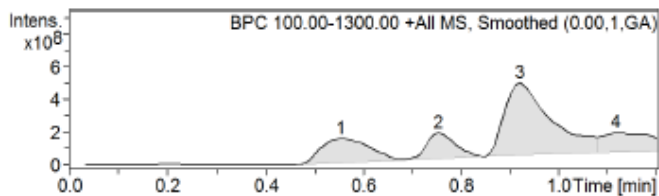
^1H NMR can be used to identify characteristic proton changes to show product formation. The dehydrogenative coupling reaction occurs with the proton next to a heteroatom in both the hydrogen donor and heteroarene. The removal of this aromatic proton can be observed (purple). A characteristic proton of the product can be found between 5–6 ppm, on the carbon next to both a heteroatom, and the aromatic system. This peak (red) presents as a broad doublet due to rotamer formation, caused by slow rotation of the amide bond of the Boc protecting group.



LC-MS analysis is also useful to identify intermolecular products. But due to their acid sensitivity, Boc protecting groups have been shown to fragment under the chromatography conditions. For example, the reaction between *N*-Boc-pyrrolidine and 1,3-benzothiazole-6-sulfonyl fluoride, the expected mass of the ionised compound, 387, is not observed, instead we see a $-\text{tBu}$ mass, 331, and a $-\text{Boc}$ mass, 287. This is also

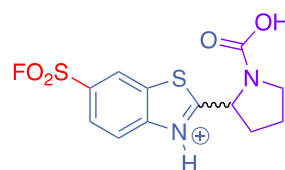
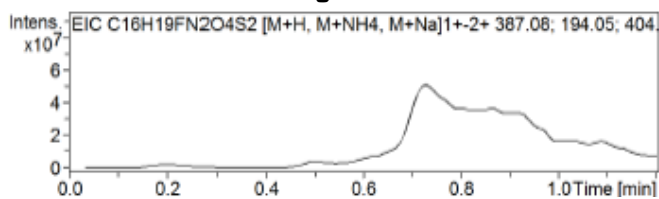
observed in the HPLC-MS, meaning Boc protected products are collected via a pseudo peak of the deprotected products to be purified. With this information, each mass adduct should be tested, to identify the strongest signal for purification.

UV Trace



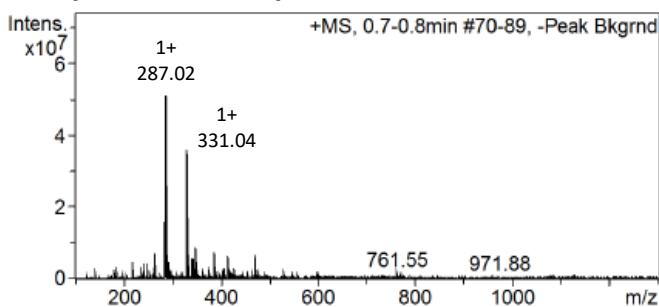
Molecular Weight: 387.4639

Extracted Ion Chromatogram



Molecular Weight: 331.3559

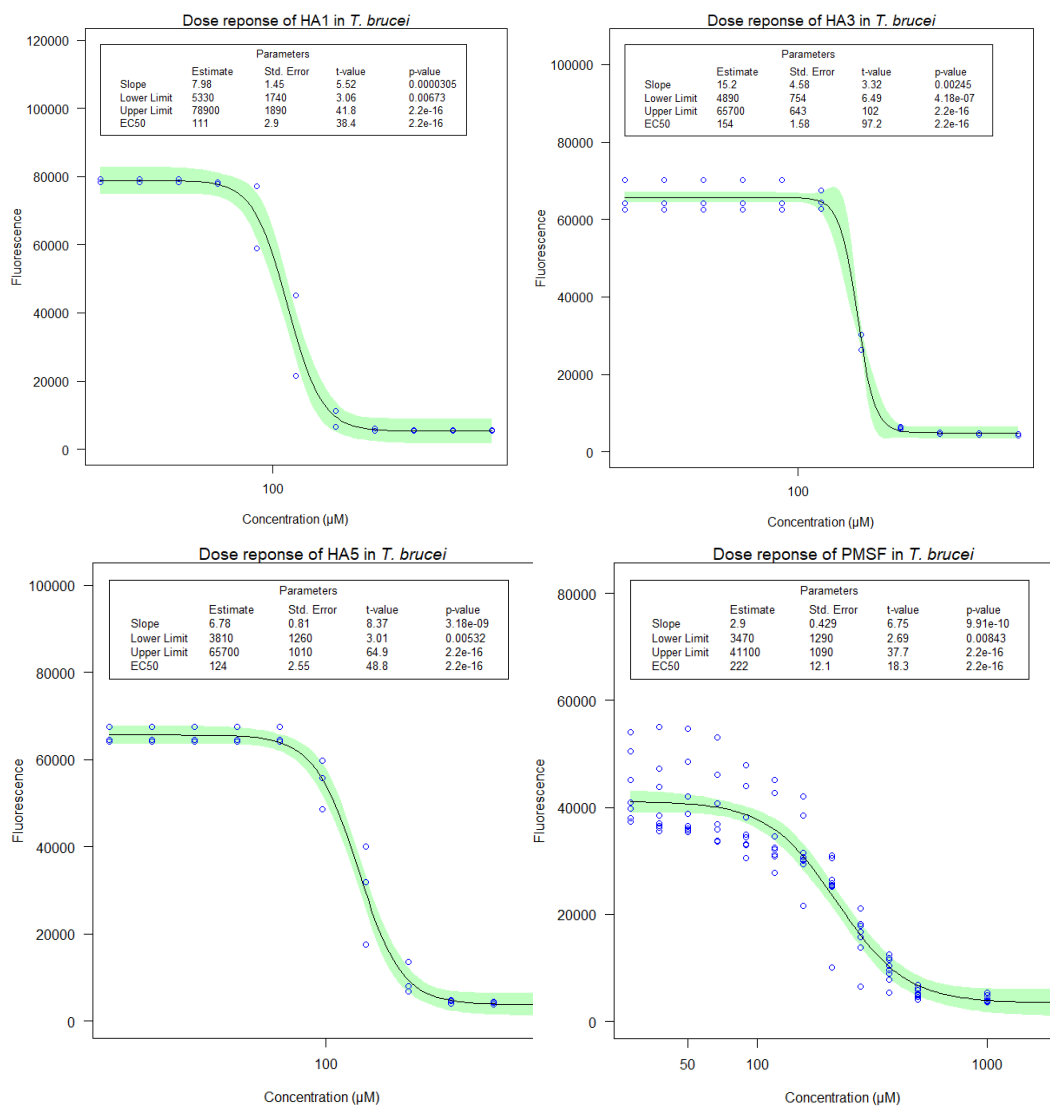
Compound 2 Mass Spectrum



Molecular Weight: 287.3469

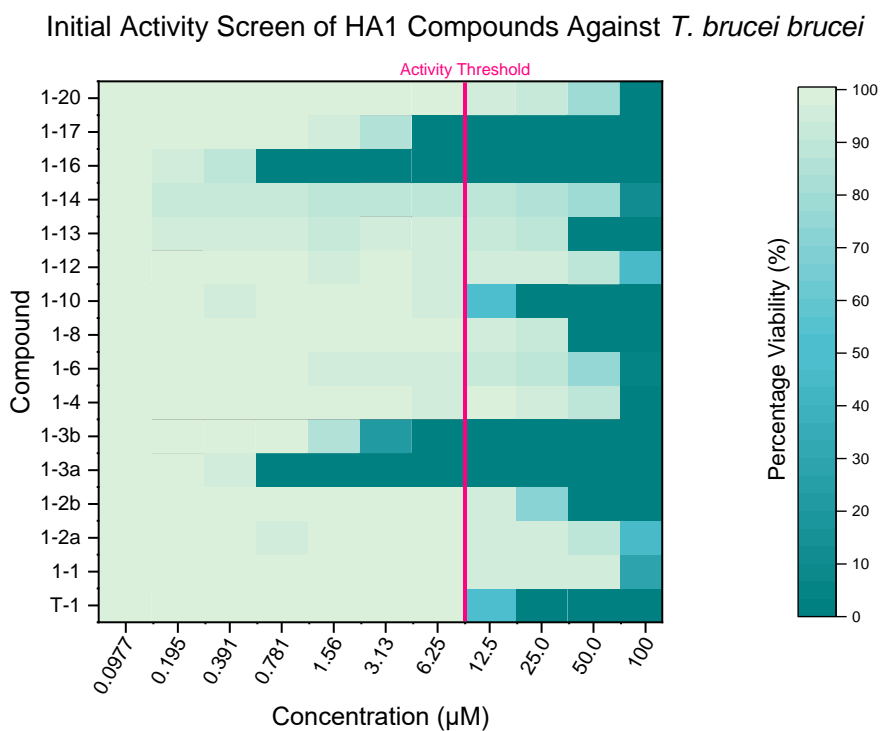
Appendix C

Screening Hetarene Cores: An initial screen was carried out to investigate baseline activity of the hetarene cores before functionalisation, compared to a known trypanocidal compound, PMSF, a protease inhibitor. The hetarenes were incubated with *T. brucei brucei*, to determine cell viability using the resazurin based viability assay following the general procedure (5.3). The screen was carried out in triplicate, and the dose response plotted to calculate an EC₅₀ value using the software R, fitting a sigmoidal dose response via the LL.4() logarithmic fitting function. Each core showed an activity of greater than 100 µM, so screening the library compounds at lower concentrations can be used to highlight where functionalisation of these cores improves activity.

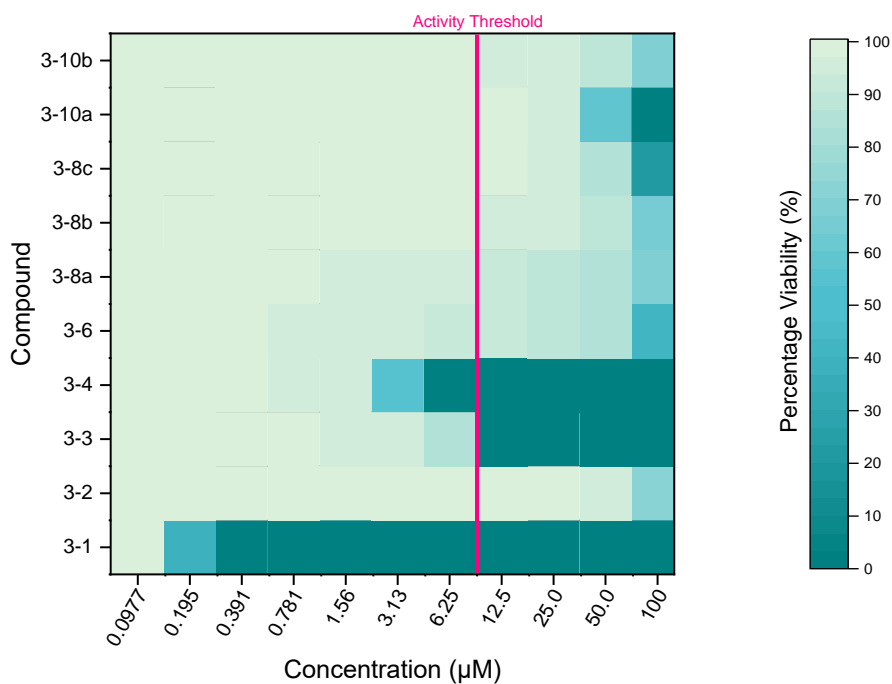


Appendix D

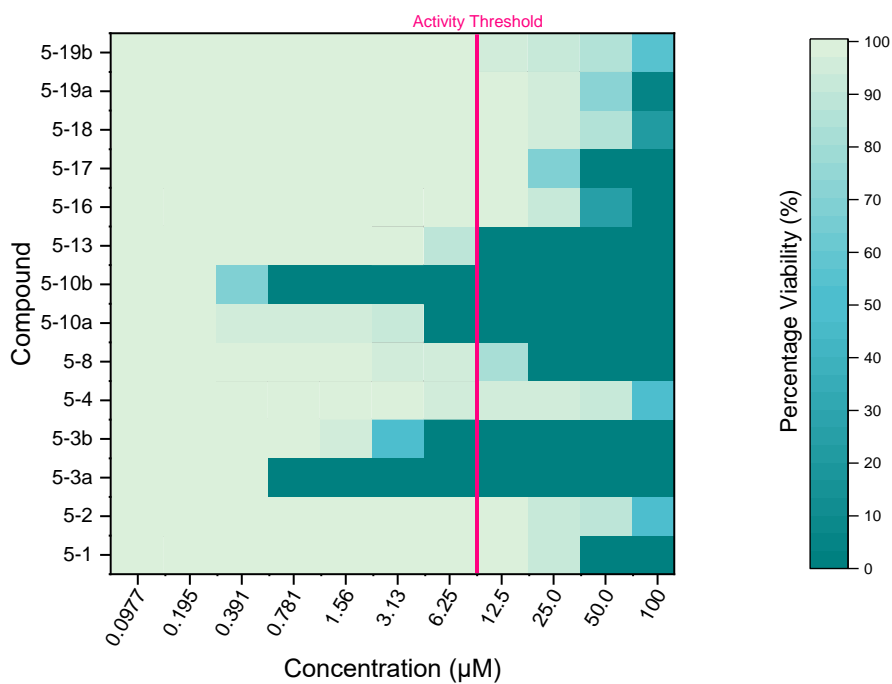
Heat Map of Initial Screen: An initial screen was carried out across the compound library against *T. brucei brucei*, using the resazurin based viability assay, screening in a 11-point serial dilution from 100 – 0.1 μM . The fluorescence response was normalised as percentage against the positive control, pentamidine (100 nM) and plotted as a heat map. The screen was carried out as a single replicate to gain a provisional insight into which compounds to pursue. A hit was characterised as having an EC_{50} less than 20 μM (red), the active 15 compounds were taken forward for further investigation. The resazurin based viability assays were carried out following the general procedure (5.3).



Initial Activity Screen of HA3 Compounds Against *T. brucei brucei*

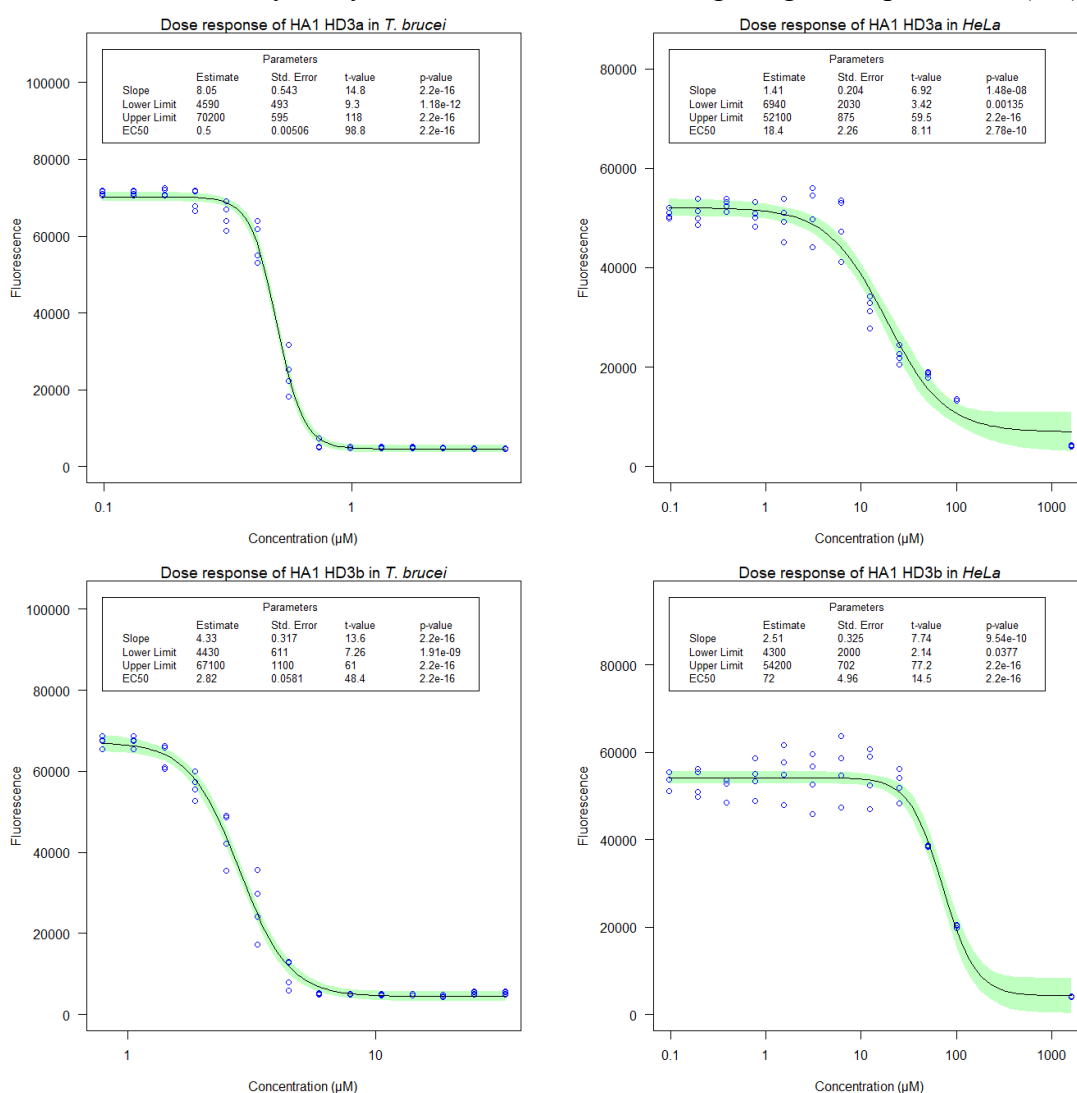


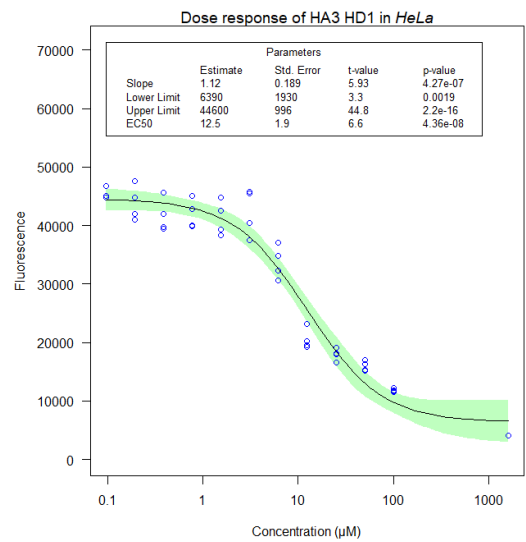
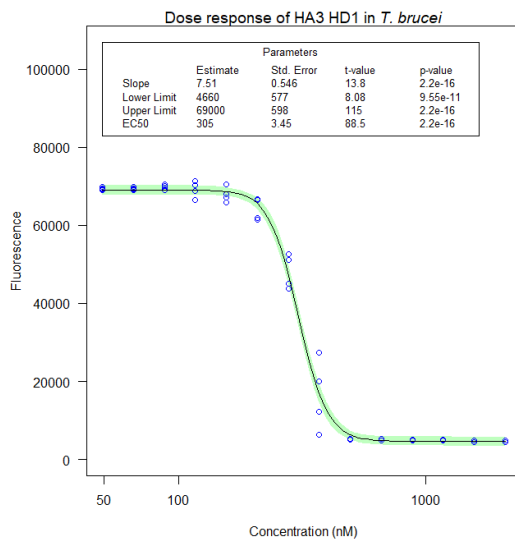
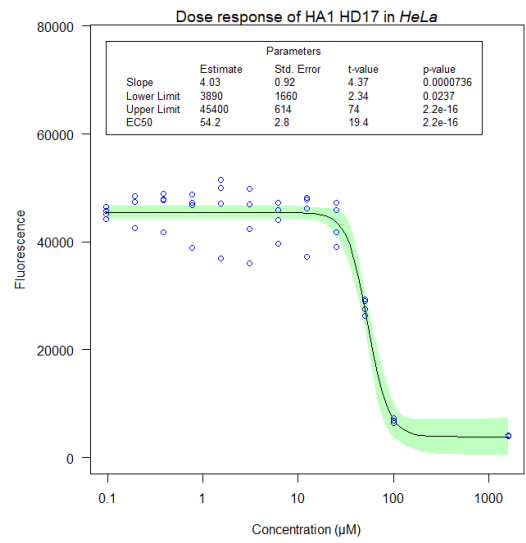
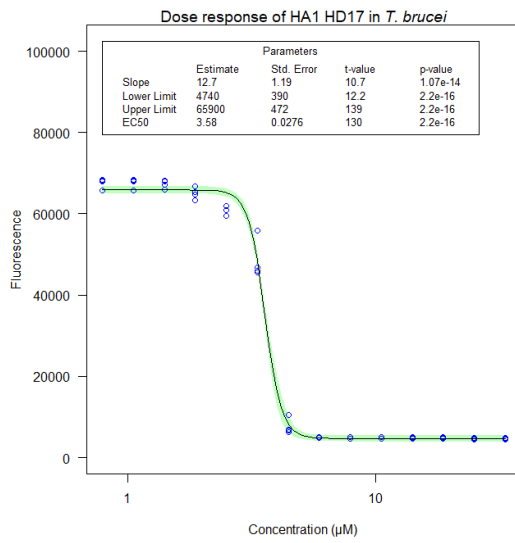
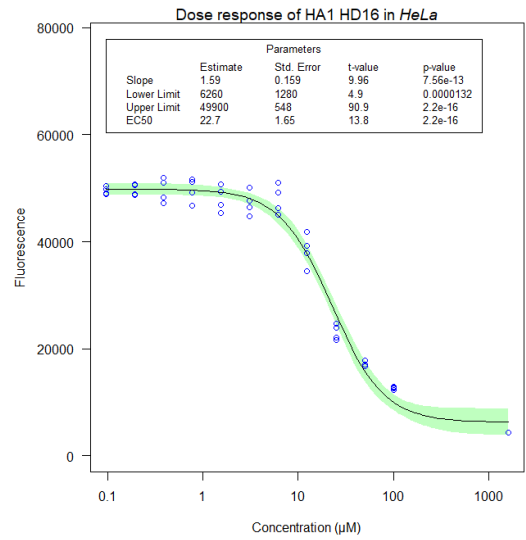
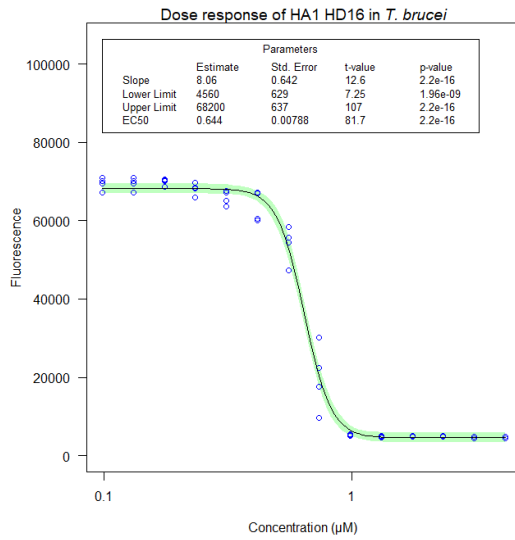
Initial Activity Screen of HA5 Compounds Against *T. brucei brucei*

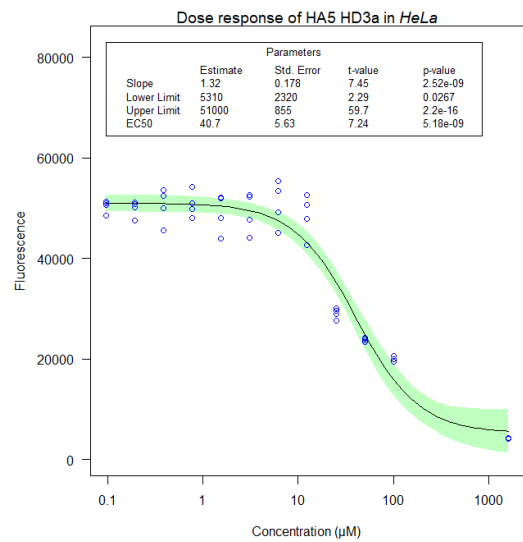
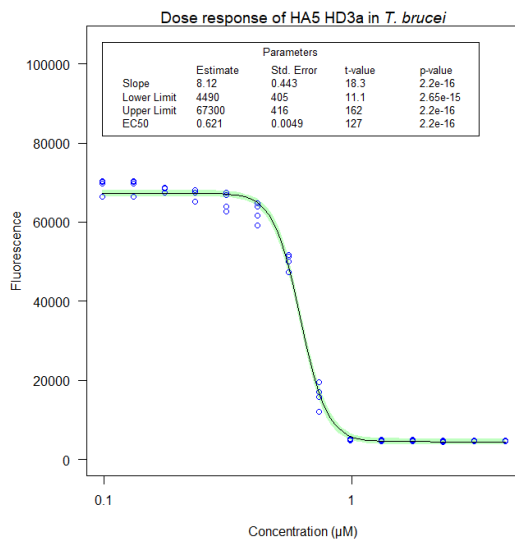
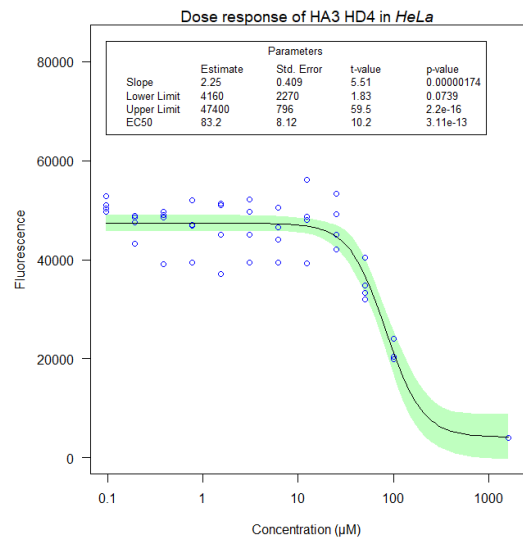
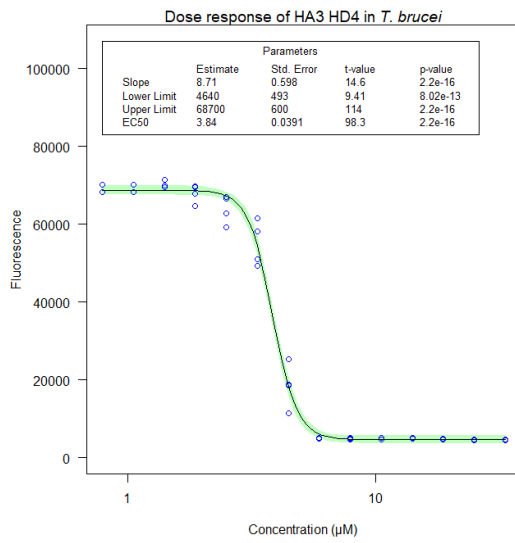
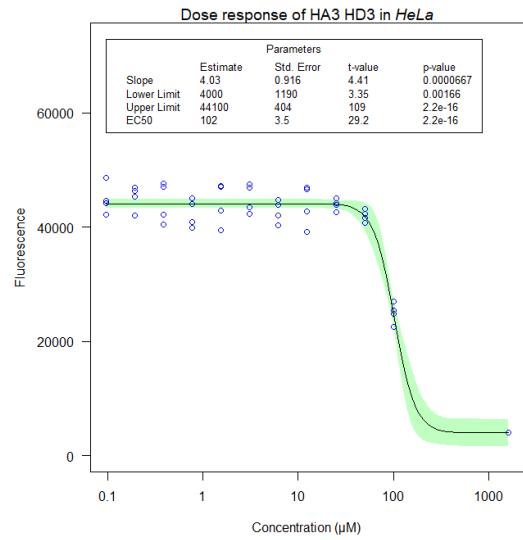
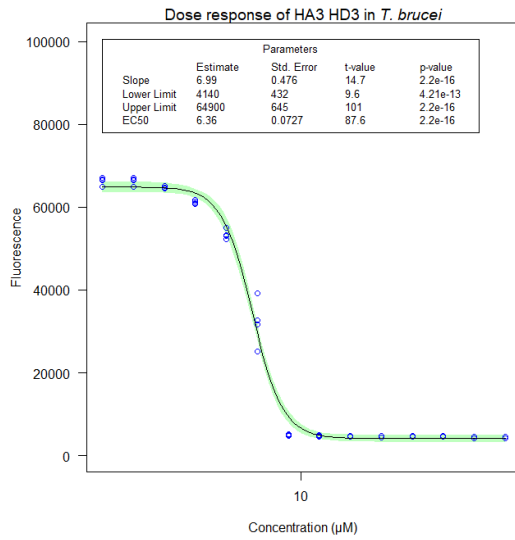


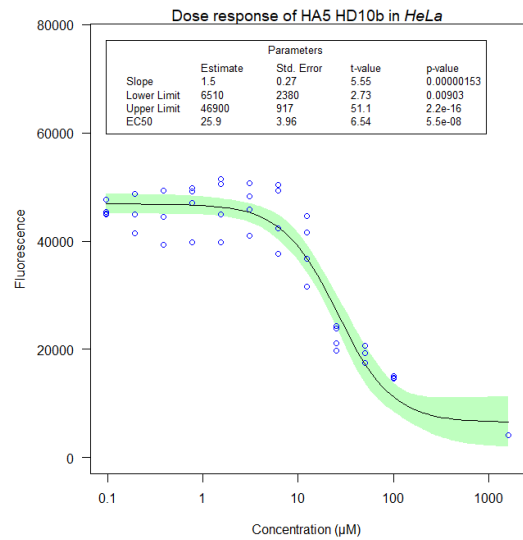
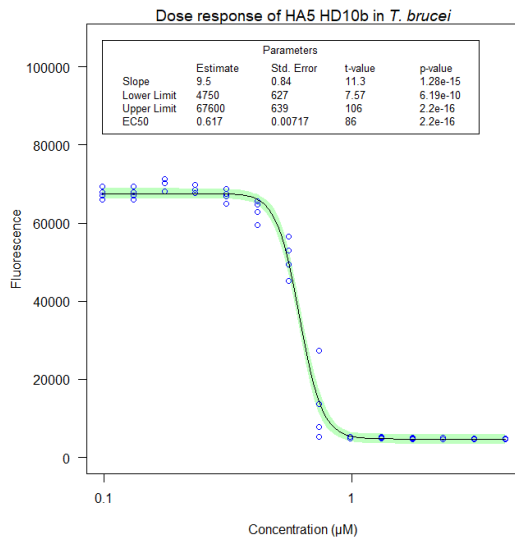
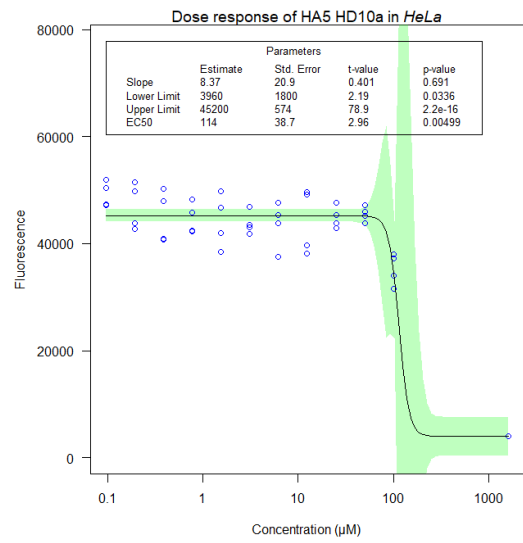
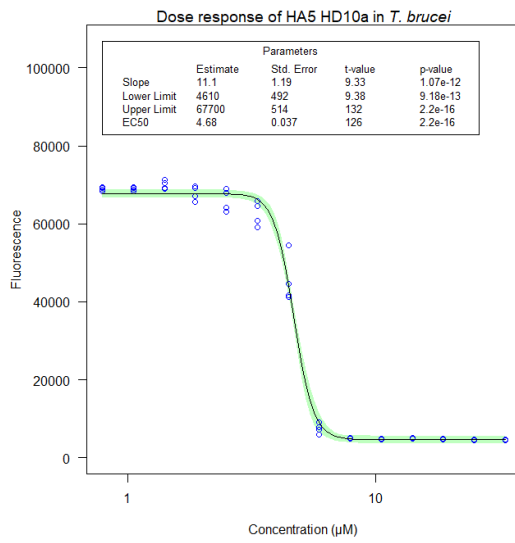
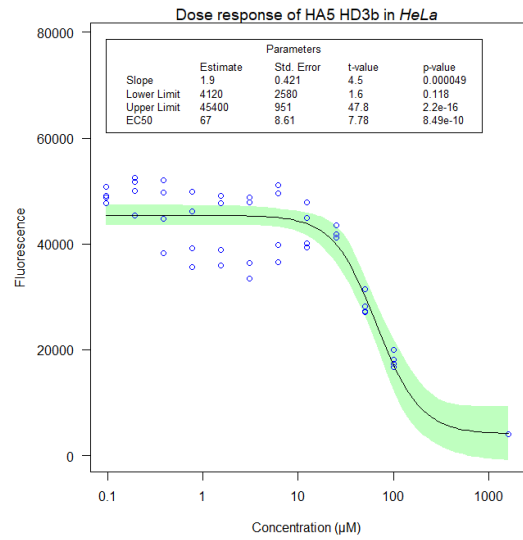
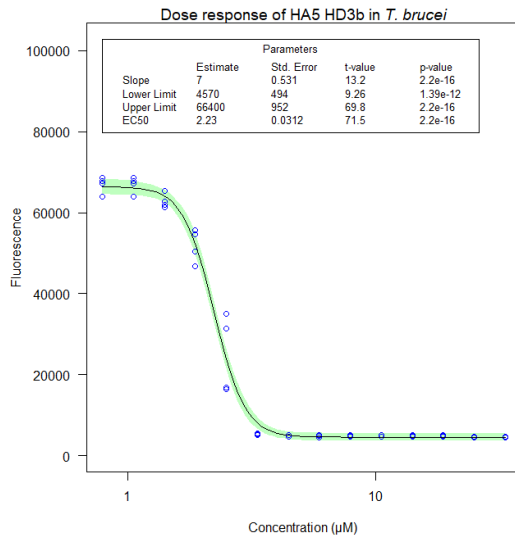
Appendix E

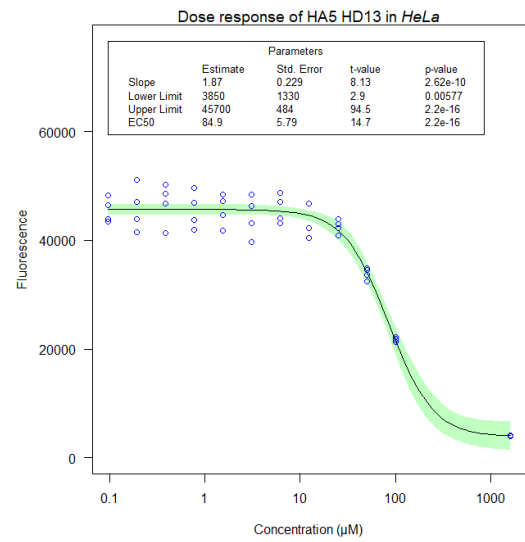
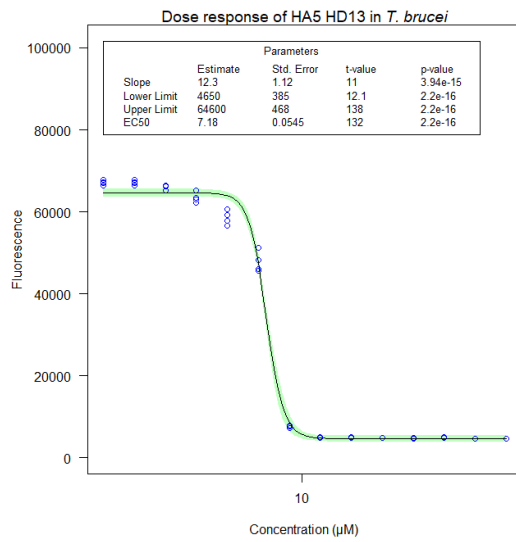
Active Compound Screening Data: Preliminary data identified 12 compounds with less than 10 μM activity. These were taken forward for further investigation to gain an accurate EC_{50} value, as well as determining their selectivity for the parasite against human cells. The compounds were screened in quadruplicate, at a narrower screening concentration, around the EC_{50} identified from the initial screen. Their EC_{50} values were calculated using the sigmoidal logarithmic fitting function in R. these values were then compared to EC_{50} values against human, HeLa cells, to determine selectivity. The resazurin based viability assays were carried out following the general procedure (5.3).





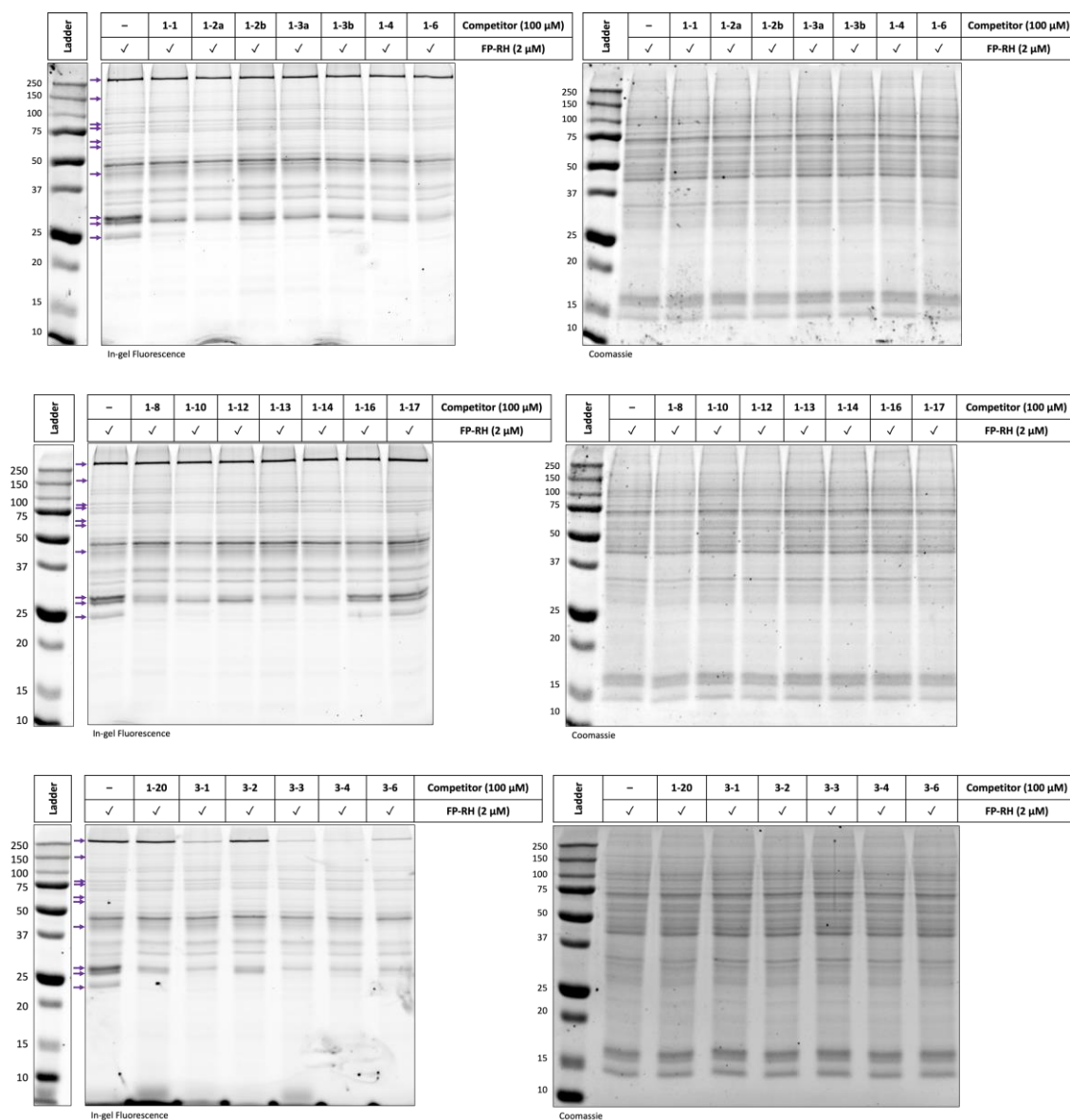


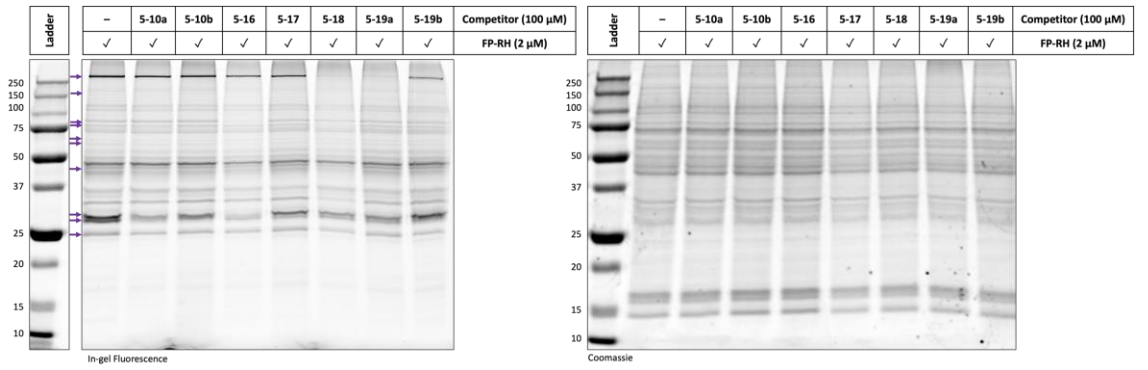
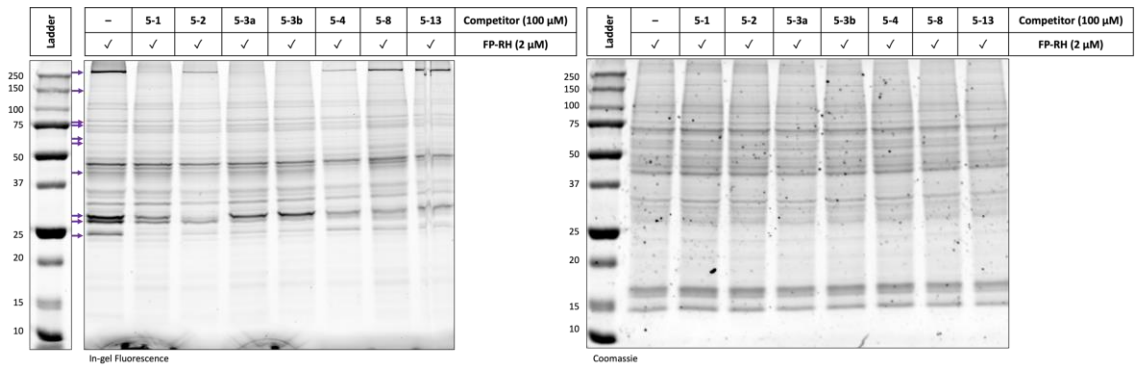
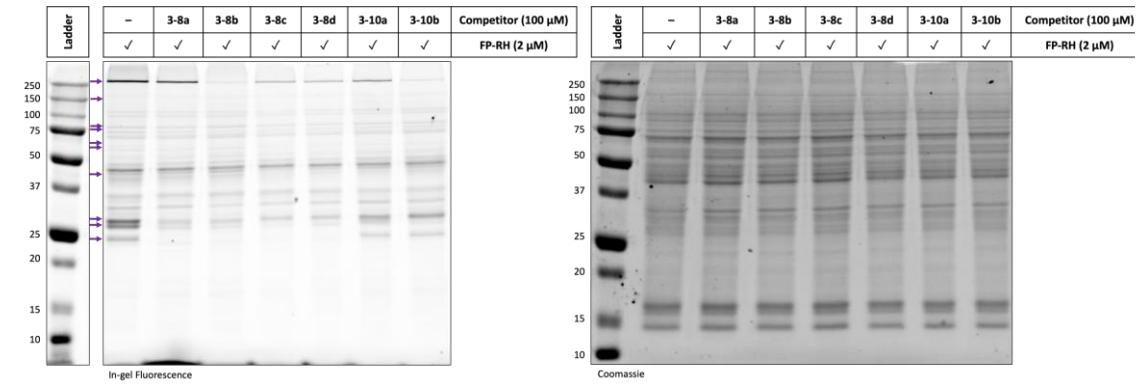




Appendix F

Competitive Profiling Against FP-RH on HeLa Lysate: In-gel fluorescence analysis of competition the fluorophosphonate rhodamine probe, **FP-RH**, against the library of electrophilic ligands. Lysate was incubated with the competitor compound (100 μM) for 30 minutes, before adding **FP-RH** (2 μM) for a further 30 min. Following the standard protocol (5.4), the samples were precipitated in acetone (4 volumes), washed, and prepared for gel loading. Running on a 12% SDS-PAGE gel for 40 minutes at 180 V. Any observed competing bands are highlighted in the control by a purple arrow, and the degree of competition quantified using densitometry, calculated using the software 'Image Lab' to output a percentage of competition for each key protein band (*Figure 3.6*).

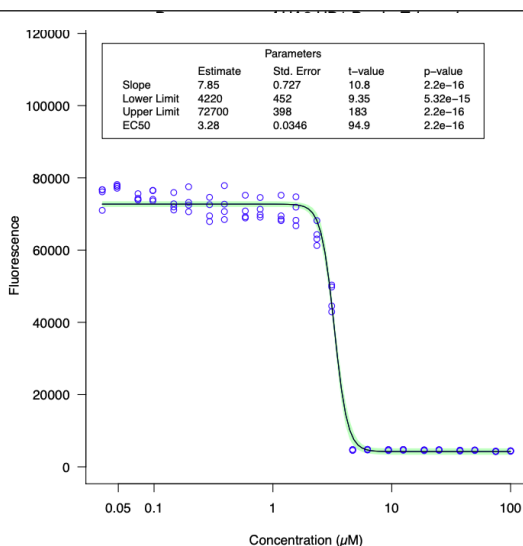




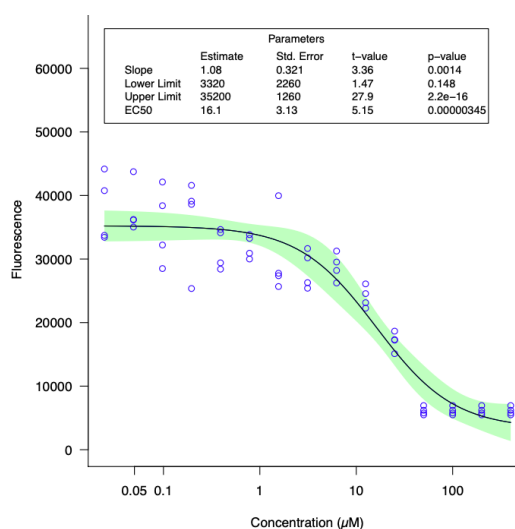
Appendix G

Alkyne Analogue Screening Data: Activity screening of the four chemical probes synthesised based on active compounds, in the resazurin-based phenotypic assay. The compounds were screened in quadruplicate against *T. brucei brucei*, incubating for 72 hours at concentrations between 100 μM – 50 nM. Following the general procedure(5.3). The fluorescence response was normalised against a positive control and plotted to calculate a dose response in the software R, fitting a sigmoidal dose response via the LL.4() logarithmic fitting function to calculate the compounds EC50 for comparison to the parent compounds.

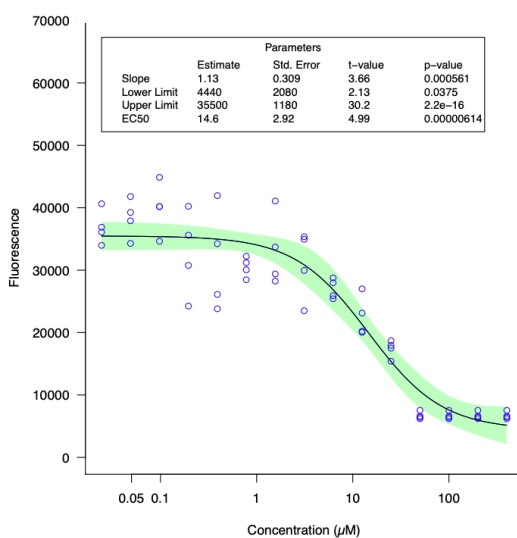
Dose Response of 3-1 Poc in *T. brucei brucei*



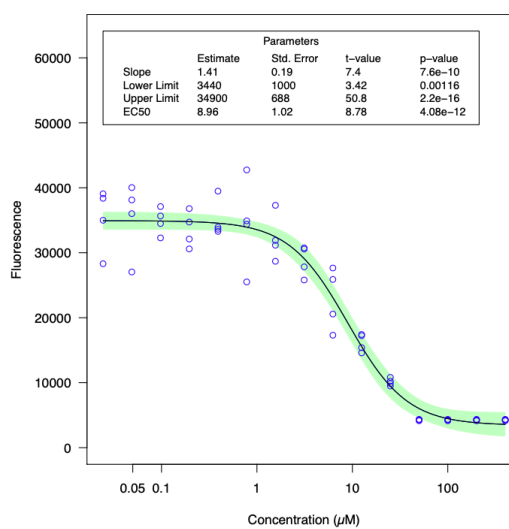
Dose Response of T-3a Alkyne in *T. brucei brucei*



Dose Response of 1-3a Alkyne in *T. brucei brucei*

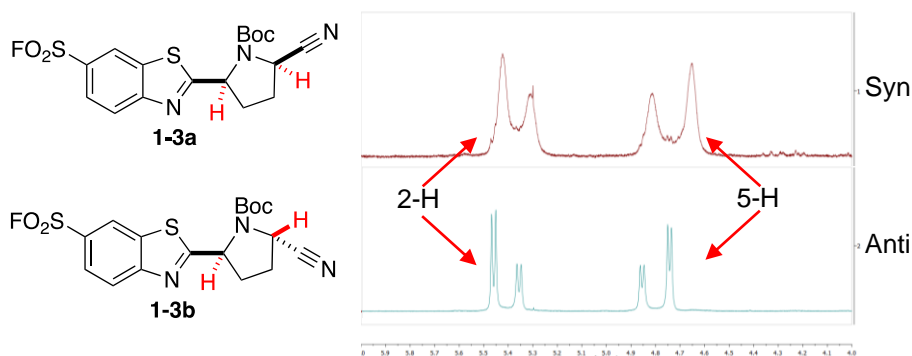


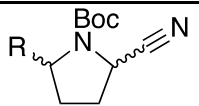
Dose Response of 1-3b Alkyne in *T. brucei brucei*



Appendix H

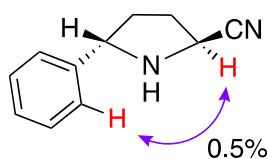
Assigning Stereochemistry of HD3 Containing Compounds: The diastereomers pairs of compounds **T-3**, **1-3** and **5-3** were isolated by mass-directed HPLC. Analysis of these proton NMR's showed clear trends between the pairs, in the chemical shifts and broadness of the peaks between 4 – 6 ppm, for pyrrolidine protons 2- and 5-H, with proton 5-H was distinguishable from HMBC coupling between it and the nitrile carbon.



	Syn		Anti	
	2-H (ppm)	5-H (ppm)	2-H (ppm)	5-H (ppm)
R = HAT	5.41 (maj) 5.27 (min)	4.77 (maj) 4.61 (min)	5.43 (maj) 5.32 (min)	4.85 (maj) 4.74 (min)
R = HA1	5.42 (maj) 5.31 (min)	4.81 (maj) 4.65 (min)	5.46 (maj) 5.35 (min)	4.85 (maj) 4.74 (min)
R = HA5	5.95 (maj) 5.75 (min)	4.87 (min) 4.75 (maj)	5.99 (maj) 5.87 (min)	5.06 (min) 4.97 (maj)

Trends	<ul style="list-style-type: none"> • Lower chemical shift • Broad multiplet or singlet peaks 	<ul style="list-style-type: none"> • Higher chemical shift • Sharp peaks, apparent doublets
--------	----------------------------------------------------------------------------------------------------------------------	---------------------------------------------------------------------------------------------------------------------

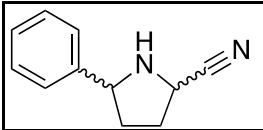
The relative stereochemistry of these compounds was then assigned by comparison to literature compounds, containing an electron withdrawing nitrile group and aromatic ring with α -protons. The stereochemistry of these compounds was assigned though an NOE experiment, highlighting a weak interaction between the α -phenyl protons and pyrrolidine 5-H, only present in the syn confirmation due to proximal interactions in space³.



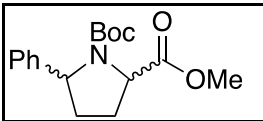
These compounds also contained the same trends in proton NMR's, with the anti-

³ B. M. Trost and F. Miege, *J. Am. Chem. Soc.*, 2014, **136**, 3016–3019.

diastereomer having higher chemical shifts and sharper peaks.

	Syn		Anti	
	2-H (ppm)	5-H (ppm)	2-H (ppm)	5-H (ppm)
	4.43	4.30	4.28	4.18
Trends	<ul style="list-style-type: none"> • Lower chemical shift • Broad multiplet peaks 		<ul style="list-style-type: none"> • Higher chemical shift • Sharp peaks, apparent doublets 	

These trends are also observed for similar compounds containing the Boc- protecting group, as seen in the below example, containing an aromatic ring and an electron withdrawing ester group, having similar electronic properties to a nitrile. Although not a direct comparison to **HD3**, The presence of a bulky Boc- protecting group validates these trends in the presence of rotameric compounds⁴.

	Syn		Anti	
	2-H (ppm)	5-H (ppm)	2-H (ppm)	5-H (ppm)
	4.98 (maj) 4.74 (min)	4.35 (min) 4.49 (maj)	5.20 (maj) 5.03 (min)	4.64 (min) 4.52 (maj)
Trends	<ul style="list-style-type: none"> • Lower chemical shift • Broad multiplet peaks 		<ul style="list-style-type: none"> • Higher chemical shift • Sharp peaks, apparent doublets 	

⁴ Y. Takahashi, R. Yoshii, T. Sato and N. Chida, *Org. Lett.*, 2018, **20**, 5705–5708.